

POLITECNICO DI MILANO

Scuola di Ingegneria Civile, Ambientale e Territoriale

**Corso di Laurea Magistrale in INGEGNERIA PER L'AMBIENTE E IL  
TERRITORIO - ENVIRONMENTAL AND LAND PLANNING ENGINEERING**



**Retrieval of parameters and variables of a hydrological water  
and energy balance model from satellite images**

Case studies of Barrax and Foggia

Supervisor: Chiar.mo Prof. Marco MANCINI

Co-supervisor: Ing. Chiara CORBARI

Master thesis by:

Marco STANGANELLI

837896

Academic year 2015 – 2016



# CONTENTS

1. INTRODUCTION.....	3
2. MeTHODOLOGY: REMOTE SENSING DATA ANALYSIS .....	5
2.1 Landsat 7.....	5
2.2 Landsat 8.....	7
2.3 Correction to physical parameters .....	9
2.3.1 About Landsat 7 .....	10
2.3.2 About Landsat 8 .....	12
2.4 The vegetation parameters and the Land Surface Temperature (LST) variable..	14
2.4.1 The Normalized Difference Vegetation Index (NDVI) .....	14
2.4.2 The Fractional Vegetation Cover (FVC).....	15
2.4.3 The Leaf Area Index (LAI) .....	15
2.4.4 Albedo (ALB) .....	16
2.4.5 Land Surface Temperature (LST) retrieval methods from Landsat .....	17
3. CASE STUDIES .....	20
3.1 Barrax.....	20
3.2 Foggia .....	22
4. DATA ANALYSIS .....	24
4.1 Statistical analyses .....	24
4.1.1 L7 SLC failure.....	25
4.1.2 Clouds problem .....	26
4.1.3 Barrax .....	27
4.1.4 Foggia.....	40
4.2 Analysis of the relationship LST-VIs .....	53
4.2.1 Barrax .....	55

4.2.2 Foggia.....	59
4.3 Comparison analyses with in situ retrieved data .....	63
4.3.1 Barrax.....	64
4.3.2 Foggia.....	70
5 Land use classification .....	<b>Errore. Il segnalibro non è definito.</b>
5.1 Barrax.....	75
5.1.1 Barrax, 28 <sup>th</sup> of May and 13 <sup>th</sup> of June 2012.....	75
5.1.2 Barrax, 4 <sup>th</sup> of June 2014 .....	78
5.1.3 Barrax, 7 <sup>th</sup> of June 2015 .....	82
5.2 Foggia .....	91
5.2.1 Foggia, 27 <sup>th</sup> of January 2016.....	91
5.2.2 Foggia, 19 <sup>th</sup> of May 2016.....	94
6 MODELLING: WATER AND ENERGY FLUXES (BARRAX) .....	98
6.1 Introduction to FEST-EWB hydrological model.....	99
6.2 Input parameters .....	99
6.3 Output parameters.....	105
6.3.1 Comparison LST output, 24 <sup>th</sup> of July.....	106
6.3.2 Comparison LST output, 25 <sup>th</sup> of July.....	108
6.3.3 Comparison le output, 24 <sup>th</sup> of July .....	110
6.3.4 Comparison le output, 25 <sup>th</sup> of July .....	112
6.3.5 Output comparison with punctual data.....	114
6.4 Root Mean Square Error (RMSE) .....	126
6.4.1 RMSE input.....	126
6.4.2 RMSE output.....	127
Bibliography .....	129

# LIST OF FIGURES

FIGURE 1. SLC OPERATION SYSTEM.....	6
FIGURE 2. SLC LANDSAT 7 FAILURE IN THE IMAGERY OF THE 10 <sup>TH</sup> MAY 2011 IN BARRAX AREA .....	7
FIGURE 3. BANDPASS WAVELENGTH FOR L8 OLI AND TIRS SENSOR COMPARED TO L7 EMT+ SENSOR.....	8
FIGURE 4. EXAMPLE OF USED ATMOSPHERIC CORRECTIONS .....	18
FIGURE 5. BARRAX SITE FROM GOOGLE MAPS (GOOGLE).....	20
FIGURE 6. BARRAX SITE FROM L8 IMAGERY .....	21
FIGURE 7. FOGGIA SITE FROM GOOGLE MAPS (GOOGLE).....	22
FIGURE 8. FOGGIA SITE FROM L8 .....	23
FIGURE 9. BEFORE AND AFTER LANDSAT_GAPFILL CORRECTION ON THE NDVI DATA OF THE 10 <sup>TH</sup> OF MAY 2011 IN BARRAX.....	25
FIGURE 10. BEFORE AND AFTER LANDSAT_GAPFILL CORRECTION ON THE ALBEDO DATA OF THE 10 <sup>TH</sup> OF MAY 2011 IN BARRAX.....	25
FIGURE 11. BUILDING A ROI NOT CONSIDERING CLOUDY PIXELS ON THE 13 <sup>TH</sup> OF SEPTEMBER 2016 IN BARRAX .....	26
FIGURE 12. L8 IMAGERY ON THE 24 <sup>TH</sup> OF MAY 2016, JD 145 PATH 199, ROW 33.....	27
FIGURE 13. L8 IMAGERY ON THE 31 <sup>ST</sup> OF MAY 2016, JD 152 PATH 200, ROW 33 .....	28
FIGURE 14. L8 ZOOMED IMAGERIES ON JD 145(LEFT) AND 152(RIGHT) ON BARRAX AREA STUDY.....	28
FIGURE 15. BARRAX, JD 145, LST MAP .....	29
FIGURE 16. BARRAX, JD 145, LST HISTOGRAM.....	29
FIGURE 17. BARRAX, JD 145, NDVI MAP.....	30
FIGURE 18. BARRAX, JD 145, NDVI HISTOGRAM.....	30
FIGURE 19. BARRAX, JD 145, FVC MAP.....	31
FIGURE 20. BARRAX, JD 145, FVC HISTOGRAM.....	31
FIGURE 21. BARRAX, JD 145, LAI MAP.....	32
FIGURE 22. BARRAX, JD 145, LAI HISTOGRAM .....	32
FIGURE 23. BARRAX, JD 145, ALBEDO MAP .....	33
FIGURE 24. BARRAX, JD 145, ALBEDO HISTOGRAM .....	33
FIGURE 25. BARRAX, PLOT OF RETRIEVED LST MEAN VALUES	
FIGURE 26. BARRAX, PLOT OF RETRIEVED FVC MEAN VALUES	
FIGURE 27. BARRAX, PLOT OF RETRIEVED LAI MEAN VALUES .....	37
FIGURE 28. BARRAX, PLOT OF RETRIEVED ALBEDO MEAN VALUES .....	38
FIGURE 29. BARRAX, PLOT OF COMPARED FVC – LAI VALUES.....	39
FIGURE 30. FOGGIA, L8 IMAGERY ON THE 31 <sup>ST</sup> OF MARCH 2016, JD 091.....	40
FIGURE 31. FOGGIA L8 ZOOMED IMAGERY ON THE 31 <sup>ST</sup> OF MARCH 2016 AREA STUDY, JD 091 .....	41
FIGURE 32. FOGGIA, JD 091 USED ROI FOR STATISTICAL ANALYSIS.....	41
FIGURE 33. FOGGIA, JD 091, LST MAP.....	42
FIGURE 34. FOGGIA, JD 091, LST HISTOGRAM.....	42
FIGURE 35. FOGGIA, JD 091, NDVI MAP.....	43

FIGURE 36. FOGGIA, JD 091, NDVI HISTOGRAM .....	43
FIGURE 37. FOGGIA, JD 091, FVC MAP .....	44
FIGURE 38. FOGGIA, JD 091, FVC HISTOGRAM .....	44
FIGURE 39 FOGGIA, JD 091, LAI MAP .....	45
FIGURE 40. FOGGIA, JD 091, LAI HISTOGRAM .....	45
FIGURE 41. FOGGIA, JD 091, ALBEDO MAP .....	46
FIGURE 42. FOGGIA, JD 091, ALBEDO HISTOGRAM .....	46
FIGURE 43. FOGGIA, PLOT OF RETRIEVED LST MEAN VALUES.....	50
FIGURE 44. FOGGIA, PLOT OF RETRIEVED FVC MEAN VALUES .....	50
FIGURE 45. FOGGIA, PLOT OF RETRIEVED LAI MEAN VALUES .....	51
FIGURE 46. FOGGIA, PLOT OF RETRIEVED ALBEDO MEAN VALUES .....	51
FIGURE 47. FOGGIA, PLOT OF COMPARED FVC – LAI VALUES .....	52
FIGURE 48. THEORY OF THE TRIANGLE .....	53
FIGURE 49 . BARRAX, COMPARISON LST-FVC, 2011.....	55
FIGURE 50. BARRAX, COMPARISON LST-FVC, 2012 .....	56
FIGURE 51. BARRAX, COMPARISON LST-FVC, 2013 .....	56
FIGURE 52. BARRAX, COMPARISON LST-FVC, 2014 .....	57
FIGURE 53. BARRAX, COMPARISON LST-FVC, 2015 .....	57
FIGURE 54. BARRAX, COMPARISON LST-FVC, 2016 .....	58
FIGURE 55. FOGGIA, COMPARISON LST-FVC, 2011.....	59
FIGURE 56. FOGGIA, COMPARISON LST-FVC, 2012.....	60
FIGURE 57. FOGGIA, COMPARISON LST-FVC, 2013.....	60
FIGURE 58. FOGGIA, COMPARISON LST-FVC, 2014.....	61
FIGURE 59. FOGGIA, COMPARISON LST-FVC, 2015.....	61
FIGURE 60. FOGGIA, COMPARISON LST-FVC, 2016.....	62
FIGURE 61. BARRAX, COMPARISON LST: SATELLITE – IN SITU DATA BY THE FIELD CAMPAIGN OF 2012.....	64
FIGURE 62. BARRAX, PLOT OF THE COMPARISON L7 DATA – EL CRUCE DATA .....	65
FIGURE 63. BARRAX, PLOT OF THE COMPARISON LST: L8 DATA – EL CRUCE DATA .....	66
FIGURE 64. BARRAX, PLOT OF THE COMPARISON LST: LANDSAT WHOLE DATA – EL CRUCE DATA .....	66
FIGURE 65. BARRAX, PLOT OF THE COMPARISON ALBEDO: L7 DATA – EL CRUCE DATA .....	68
FIGURE 66. BARRAX, PLOT OF THE COMPARISON ALBEDO: L8 DATA – EL CRUCE DATA .....	68
FIGURE 67. BARRAX, PLOT OF THE COMPARISON ALBEDO: LANDSAT WHOLE DATA – EL CRUCE DATA.....	69
FIGURE 68. FOGGIA, PLOT OF THE COMPARISON LST: L7 DATA – IN SITU DATA.....	71
FIGURE 69. FOGGIA, PLOT OF THE COMPARISON LST: L8 DATA – IN SITU DATA.....	71
FIGURE 70. FOGGIA, PLOT OF THE COMPARISON LST: LANDSAT WHOLE DATA – IN SITU DATA .....	72
FIGURE 71. FOGGIA, PLOT OF THE COMPARISON ALBEDO: L7 DATA – IN SITU DATA .....	72
FIGURE 72. FOGGIA, PLOT OF THE COMPARISON ALBEDO: L8 DATA – IN SITU DATA .....	73
FIGURE 73. FOGGIA, PLOT OF THE COMPARISON ALBEDO LANDSAT WHOLE DATA – IN SITU DATA .....	73
FIGURE 74. BARRAX LANDUSE MAP 2011 -2012 IN LAS TIESAS FARM .....	75

FIGURE 75. BARRAX, TRAINING ROI, JD 149 (LEFT) AND (RIGHT)JD 165, 2012 .....	76
FIGURE 76. BARRAX, CLASSIFIED IMAGE, JD 149 (LEFT) AND (RIGHT) JD 165, 2012 .....	77
FIGURE 77. BARRAX, SPECTRA OF REFORESTATION AND CAMELINA .....	77
FIGURE 78. BARRAX LANDUSE MAP 2013 -2014 IN LAS TIESAS FARM (C. LATORRE 2014) .....	78
FIGURE 79. BARRAX, TRAINING ROI, JD 155 2014 (LEFT) AND CLASSIFIED IMAGE, JD 155 2014 (RIGHT)..	79
FIGURE 80. BARRAX, SPECTRA OF USED ROIS, JD 155 2014.....	81
FIGURE 81. BARRAX, SPECTRA OF POPPY ROI, JD 139 (LEFT), 155 (RIGHT)AND 194 (DOWN)2014 .....	81
FIGURE 82. BARRAX LANDUSE MAP 2014 -2015 IN LAS TIESAS FARM .....	82
FIGURE 83. BARRAX, TRAINING ROI, JD 158 2015. WITH ENTIRE BARLEY ROIS (LEFT), AND WITHOUT A BARLEY ROI(RIGHT).....	83
FIGURE 84. BARRAX, CLASSIFIED IMAGE, JD 158 2015. CLASSIFICATION MADE WITH ENTIRE BARLEY ROIS (LEFT), AND WITHOUT A BARLEY ROI(RIGHT) .....	83
FIGURE 85. BARRAX, SPECTRUM OF BARLEY ROI, JD 158 2015 .....	84
FIGURE 86. BARRAX, SPECTRUM OF BITTER VETCH ROI, JD 158 2015.....	85
FIGURE 87. BARRAX, SPECTRUM OF CORN ROI, JD 158 2015 .....	85
FIGURE 88. BARRAX, SPECTRUM OF FALLOW ROI, JD 158 2015.....	86
FIGURE 89. BARRAX, SPECTRUM OF GARLIC ROI, JD 158 2015 .....	86
FIGURE 90. BARRAX, SPECTRUM OF POPPY ROI, JD 158 2015 .....	87
FIGURE 91. BARRAX, SPECTRUM OF BARLEY ROI, JD 158 2015 .....	87
FIGURE 92. BARRAX, SPECTRUM OF REFORESTATION ROI, JD 158 2015 .....	88
FIGURE 93. BARRAX, SPECTRUM OF SUNFLOWER ROI, JD 158 2015.....	88
FIGURE 94. BARRAX, SPECTRUM OF VINEYARD ROI, JD 158 2015 .....	89
FIGURE 95. BARRAX, SPECTRUM OF URBAN ROI, JD 158 2015.....	89
FIGURE 96. BARRAX, SPECTRUM OF WALNUT AND PISTACHO ROI, JD 158 2015 .....	90
FIGURE 97. BARRAX, STATISTICS OF THE SPECTRUM OF WHEAT ROI, JD 158 2015 .....	90
FIGURE 98. FOGGIA, SHAPE FILE CONTAINING 2016 LANDUSE INFORMATION, PLOTTED ON GOOGLE EARTH IMAGE.....	91
FIGURE 99. FOGGIA, SPECTRA OF ASPARAGUS, LEAF BEET AND SPINACH .....	92
FIGURE 100. FOGGIA, TRAINING ROIS, JD 027 .....	93
FIGURE 101. FOGGIA, ZOOM ON TRAINING ROIS, JD 027.....	93
FIGURE 102. FOGGIA, CLASSIFIED IMAGE JD 027 .....	94
FIGURE 103. FOGGIA, TRAINING ROIS, JD 139 .....	95
FIGURE 104. FOGGIA, ZOOM ON TRAINING ROIS, JD 139.....	95
FIGURE 105. FOGGIA, CLASSIFIED IMAGE, JD 139.....	96
FIGURE 106. FOGGIA VALIDATION, ZOOM ON THE CLASSIFIED IMAGE AREA WITHOUT PART OF WHEAT ROI (LEFT) AND THE CLASSIFIED AREA WITH ENTIRE ROI (RIGHT), JD 139 2016.....	96
FIGURE 107. FOGGIA VALIDATION, CLASSIFIED IMAGE WITHOUT PART OF WHEAT ROI, JD 139 2016 .....	97
FIGURE 108. FEST-EWB PROCESS .....	98
FIGURE 109. COMPARISON AMONG L7 206-AHS 207 RETRIEVED DATA .....	101

FIGURE 110. INPUT COMPARISON .....	104
FIGURE 111. COMPARISON LST OUTPUT, 24 <sup>TH</sup> OF JULY .....	107
FIGURE 112. COMPARISON LST OUTPUT, 25 <sup>TH</sup> OF JULY .....	109
FIGURE 113. COMPARISON LE OUTPUT, 24 <sup>TH</sup> OF JULY .....	111
FIGURE 114. COMPARISON LE OUTPUT, 25 <sup>TH</sup> OF JULY .....	113
FIGURE 115. MAP OF THE STATIONS USED FOR OUTPUT COMPARISONS .....	114
FIGURE 116. VINEYARD, PUNCTUAL OUTPUT GRAPHICS.....	117
FIGURE 117. REFORESTATION, PUNCTUAL OUTPUT GRAPHICS .....	119
FIGURE 118. CAMELINA, PUNCTUAL OUTPUT GRAPHICS .....	122
FIGURE 119. AHS-SIMULATIONS PUNCTUAL COMPARISON ON 25 <sup>TH</sup> AND 26 <sup>TH</sup> OF JULY .....	125



## LIST OF TABLES

TABLE 1. LANDSAT 7 TECHNICAL FEATURES .....	6
TABLE 2. LANDSAT 8 TECHNICAL FEATURES .....	8
TABLE 3. L7 <i>Esun</i> VALUES .....	11
TABLE 4. L7 EARTH – SUN DISTANCE VALUES .....	11
TABLE 5. BARRAX, JD 145, LST BASIC STATISTICS .....	29
TABLE 6. BARRAX, JD 145, NDVI BASIC STATISTICS .....	30
TABLE 7. BARRAX, JD 145, FVC BASIC STATISTICS .....	31
TABLE 8. BARRAX, JD 145, LAI BASIC STATISTICS .....	32
TABLE 9. BARRAX, JD 145, ALBEDO BASIC STATISTICS .....	33
TABLE 10. BARRAX 2011 RETRIEVED MEAN VALUES .....	34
TABLE 11. BARRAX 2012 RETRIEVED MEAN VALUES .....	34
TABLE 12. BARRAX 2013 RETRIEVED MEAN VALUES .....	35
TABLE 13. BARRAX 2014 RETRIEVED MEAN VALUES .....	35
TABLE 14. BARRAX 2015 RETRIEVED MEAN VALUES .....	36
TABLE 15. BARRAX 2016 RETRIEVED MEAN VALUES .....	36
TABLE 16. FOGGIA, JD 091, LST BASIC STATISTICS .....	42
TABLE 17. FOGGIA, JD 091, NDVI BASIC STATISTICS .....	43
TABLE 18. FOGGIA, JD 091, FVC BASIC STATISTICS.....	44
TABLE 19. FOGGIA, JD 091, LAI BASIC STATISTICS.....	45
TABLE 20. FOGGIA, JD 091, ALBEDO BASIC STATISTICS .....	46
TABLE 21. FOGGIA 2011 RETRIEVED MEAN VALUES .....	47
TABLE 22. FOGGIA 2012 RETRIEVED MEAN VALUES .....	47
TABLE 23. FOGGIA 2013 RETRIEVED MEAN VALUES .....	48
TABLE 24. FOGGIA 2014 RETRIEVED MEAN VALUES .....	48
TABLE 25. FOGGIA 2015 RETRIEVED MEAN VALUES .....	48
TABLE 26. FOGGIA 2016 RETRIEVED MEAN VALUES .....	49
TABLE 27. BARRAX, COMPARISON LST: SATELLITE – IN SITU DATA BY THE STATION EL CRUCE.....	65
TABLE 28. BARRAX, COMPARISON ALBEDO: L7 – IN SITU DATA BY THE STATION EL CRUCE.....	67
TABLE 29. FOGGIA, COMPARISON LST AND ALBEDO: LANDSAT DATA – IN SITU DATA .....	70
TABLE 30. BARRAX ROIS FOR IMAGE OF JD 149 (LEFT) AND JD 165 (RIGHT), BASED ON LANDUSE MAP 2012 .....	76
TABLE 31. BARRAX ROIS FOR IMAGE OF JD 155 2014.....	79
TABLE 32. BARRAX ROIS FOR IMAGE OF JD 158 2015.....	83
TABLE 33. BARRAX, STATISTICS OF THE SPECTRUM OF BARLEY ROI, JD 158 2015 .....	84
TABLE 34. BARRAX, STATISTICS OF THE SPECTRUM OF BITTER VETCH ROI, JD 158 2015.....	85
TABLE 35. BARRAX, STATISTICS OF THE SPECTRUM OF CORN ROI, JD 158 2015 .....	85
TABLE 36. BARRAX, STATISTICS OF THE SPECTRUM OF FALLOW ROI, JD 158 2015.....	86

TABLE 37. BARRAX, STATISTICS OF THE SPECTRUM OF GARLIC ROI, JD 158 2015 .....	86
TABLE 38. BARRAX, STATISTICS OF THE SPECTRUM OF POPPY ROI, JD 158 2015 .....	87
TABLE 39. BARRAX, STATISTICS OF THE SPECTRUM OF BARLEY ROI, JD 158 2015 .....	87
TABLE 40. BARRAX, STATISTICS OF THE SPECTRUM OF REFORESTATION ROI, JD 158 2015 .....	88
TABLE 41. BARRAX, STATISTICS OF THE SPECTRUM OF SUNFLOWER ROI, JD 158 2015 .....	88
TABLE 42. BARRAX, STATISTICS OF THE SPECTRUM OF VINEYARD ROI, JD 158 2015 .....	89
TABLE 43. BARRAX, STATISTICS OF THE SPECTRUM OF URBAN ROI, JD 158 2015 .....	89
TABLE 44. BARRAX, STATISTICS OF THE SPECTRUM OF WALNUT AND PISTACHO ROI, JD 158 2015 .....	90
TABLE 45. BARRAX, STATISTICS OF THE SPECTRUM OF WHEAT ROI, JD 158 2015.....	90
TABLE 46. FOGGIA ROIS, BASED ON INFORMATIONAL SHAPE FILE, JD 027. WHERE CAVOLO=CABBAGE, SPINACI=SPINACH, RUCOLA=ROCKET SALAD, ERBETTE=LEAF BEET, COSTE=SWISS CHARD, CAVOLO NERO=BLACK CABBAGE, FINOCCHI=FENNEL, ASPARAGI=ASPARAGUS, PREZZEMOLO=PARSLEY, VERZE=SAVOY CABBAGE, CIME DI RAPA=TURNIP GREENS, VIGNA=VINEYARDS, ULIVI=OLIVE GROVES, PARCO NATURALE=NATURAL PARK, IS A WOODLAND. ....	92
TABLE 47. FOGGIA ROIS, BASED ON INFORMATIONAL SHAPE FILE, JD 139. WHERE POMODORO=TOMATOES, ASPARAGI=ASPARAGUS, VIGNA=VINEYARDS, ULIVI=OLIVE GROVES, GRANO=WHEAT, PARCO NATURALE=NATURAL PARK, IS A WOODLAND. ....	94
TABLE 48. CONFIGURATIONS OF THE SIMULATIONS .....	100
TABLE 49. STATISTICAL COMPARISON AMONG L7 206-AHS 207 RETRIEVED DATA.....	102
TABLE 50. INPUT STATISTICAL COMPARISON .....	105
TABLE 51. OUTPUT STATISTICAL COMPARISON LST 24 <sup>TH</sup> OF JULY .....	107
TABLE 52. OUTPUT STATISTICAL COMPARISON LST 25 <sup>TH</sup> OF JULY .....	109
TABLE 53. OUTPUT STATISTICAL COMPARISON LE 24 <sup>TH</sup> OF JULY .....	111
TABLE 54. OUTPUT STATISTICAL COMPARISON LE 25 <sup>TH</sup> OF JULY .....	113

## ABSTRACT

The purpose of this thesis is studying, processing, and analyzing the best resolution satellite images free of costs available to civil users, in order to assess the vegetation parameters and variables usable as input to a hydrological model.

Processing satellite images, we analysed the spectra of the cultures present in the study area, checking the vegetation growth of the plants over the time by the vegetation indices. Moreover, knowing the spectra of the specific cultures present in the fields, we classified a region, recognizing and identifying the different spectra present in a large area.

Using the retrieved data in conjunction to in field campaigns data, we computed the FEST-EWB, (Flash-flood Event-based Spatially distributed rainfall-runoff Transformation-Energy Water Balance), a distributed hydrological energy water balance model, to test the quality of retrieved images in the model process.

The algorithms used returns good results in order to retrieve the vegetation indices and variables used to classify areas, and promising results were obtained using these parameters in input to the hydrological model.

## SOMMARIO

Lo scopo di questo elaborato di laurea è lo studio, l'elaborazione, e l'analisi delle immagini satellitari, con la miglior risoluzione disponibile agli utenti civili, al fine di ricavare parametri di vegetazione e variabili utilizzabili come input a un modello idrologico.

Elaborando immagini satellitari, abbiamo analizzato gli spettri delle colture presenti nelle aree di studio, controllando la crescita delle piante nel tempo grazie agli indici di vegetazione. Inoltre, conoscendo gli spettri delle colture specifiche presenti nei campi, è stato possibile classificare un'area più vasta, riconoscendo e identificando i diversi spettri presenti nel territorio, associando gli spettri agli ortaggi coltivati in quel dato luogo.

Utilizzando i dati satellitari in unione ai dati ottenuti da campagne di misura, abbiamo verificato la bontà dei dati satellitari in utilizzo come input al modello idrologico distribuito FEST-EWB, (Flash-flood Event-based Spatially distributed rainfall-runoff Transformation-Energy Water Balance).

Gli algoritmi utilizzati hanno assicurato buoni risultati nella stima degli indici di vegetazione e delle variabili utilizzate per classificare aree, inoltre, sono stati riscontrati promettenti risultati nell'utilizzo dei parametri in input al modello idrologico.

# 1. INTRODUCTION

A hydrological model (like FEST-EWB) requires in input vegetation parameters that could be retrieved with remote sensing, provides distributed information continuous in time, after an accurate calibration with *in situ* data. Moreover, also state variables of hydrological models can be retrieved from remote sensing, e.g. Land Surface Temperature (LST) and Soil Moisture(SM).

Today, the maximum resolution available from the satellites is 30m from Landsat 7 and Landsat 8; is it enough for the analyses? Obviously, the answer depends from the scale of the area considered, from the type of analyses and from the precision of the result that we want to obtain. Anyhow, this is the best resolution still usable and it permits to retrieve Vegetation Indices, Albedo and Land Surface Temperature.

The objective of this thesis is the retrieval of these data from remote sensing from 2011 to 2016 for two agricultural area in Italy and Spain, in order to perform hydrological simulations.

In the second chapter is described the theoretical part of the remote sensing, introducing the technical characteristics of the satellites used, Landsat 7 and Landsat 8, the algorithms implemented in the process of the data and the parameters assessed: Normalized Difference Vegetation Index (NDVI), Fractional Vegetation Cover (FVC), Leaf Area Index (LAI), Albedo and Land Surface Temperature (LST).

In the third chapter are introduced the case studies: two agriculture areas in Barrax (Valencia, Spain) and in Foggia (Puglia, Italy).

All the analyses realized on the data can be found in the fourth chapter, where there are three different analyses: a statistical analysis on the data, examine mean retrieved values over the time; a comparison with *in situ* data, comprehensive of the tables with the data used and the errors of the estimated data in relation to the observed ones; and a comparison among LST and Vis, analysing the correlation between the parameters.

The fifth chapter presents classified images of land use. Starting from the knowledge of land use maps, specific spectra of cultures are identified, allowing to research in the area similar spectra. It is possible to detect a particular spectrum from remote and classify the entire surrounding area, and to follow the growth of the plants in the time. The classifications are done on different images, validating the processing with control operations.

The last step of this thesis is the use of the retrieved data in the hydrological model FEST-EWB for the case study of Barrax. The objective of this chapter is to understand how the errors are propagated into the hydrological model. In particular, the effect of input parameters (FVC, LAI, Albedo), from different satellites and dates, will be analysed on FEST-EWB estimates of LST and latent heat flux. This is achieved with the idea of using Landsat 5, 7, 8 and Sentinel 2 and 3 data.

Thesis data are then discussed observing the entire results of this document.

## ***2. METHODOLOGY: REMOTE SENSING DATA ANALYSIS***

### ***2.1 LANDSAT 7***

The Landsat 7 satellite was successfully launched from Vandenberg Air Force Base on April 15, 1999 from NASA.

Landsat 7 is a 5000 poundclass satellite designed for a 705 km, sun synchronous, earth mapping orbit with a 16-day repeat cycle. Its payload is a single nadirpointing instrument, the Enhanced Thematic Mapper Plus (ETM+). The Landsat program is the longest-running enterprise for acquisition of satellite imagery of Earth and its images find applications in agriculture, cartography, geology, forestry and regional planning.

The instruments on the Landsat satellites have acquired millions of images. The images, archived in the United States and at Landsat receiving stations around the world, are a unique resource for global change research and applications in agriculture, cartography, geology, forestry, regional planning, surveillance and education, and can be viewed through the United States Geological Survey USGS Earthexplorer website (USGS, <http://earthexplorer.usgs.gov/>).

All the data elaborated in this thesis were downloaded from Earthexplorer website.

Landsat ETM+ Whisk-Broom sensor images consist of eight spectral bands with a spatial resolution of 30 meters for Bands 1 to 7. The resolution for Band 8 (panchromatic) is 15 meters. All bands can collect one of two gain settings (high or low) for increased radiometric sensitivity and dynamic range, while Band 6, the thermal infrared band, collects both high and low gain for all scenes. Landsat 7 ETM+ band is acquired at 60 meter resolution, but is resampled to 30 meter in delivered data product. Approximate scene size is 170 km north-south by 183 km east-west.

Enhanced Thematic Mapper Plus (ETM+)	Landsat 7	Wavelength (micrometers)	Resolution (meters)
	Band 1	0.45-0.52	30
	Band 2	0.52-0.60	30
	Band 3	0.63-0.69	30
	Band 4	0.77-0.90	30
	Band 5	1.55-1.75	30
	Band 6	10.40-12.50	60 * (30)
	Band 7	2.09-2.35	30
	Band 8	.52-.90	15

TABLE 1. LANDSAT 7 TECHNICAL FEATURES

On May 31, 2003, the Scan Line Corrector (SLC) in the ETM+ instrument failed. The SLC consists of a pair of small mirrors that rotate about an axis in tandem with the motion of the main ETM+ scan mirror.

The purpose of the SLC is to compensate for the forward motion (along-track) of the spacecraft so that the resulting scans are aligned parallel to each other. Without the effects of the SLC, the instrument images the Earth in a "zig-zag" fashion, resulting in some areas that are imaged twice and others that are not imaged at all.

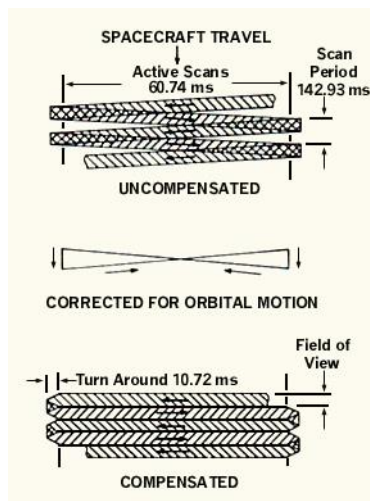


FIGURE 1. SLC OPERATION SYSTEM

The net effect is that approximately 22% of the data in a Landsat 7 scene is missing when acquired without a functional SLC.

The SLC problem is mechanical and permanent in nature; since that time, L7 has continued to acquire useful image data in the "SLC-off" mode.



Data products are available with the missing data.



FIGURE 2. SLC LANDSAT 7 FAILURE IN THE IMAGERY OF THE 10<sup>TH</sup> MAY 2011 IN BARRAX AREA

In 2013, Landsat 7 was joined by Landsat 8.

## 2.2 LANDSAT 8

On 11 February 2013 took place the launch of Landsat 8, from Space Launch Complex 3E at Vandenberg Air Force Base. Landsat 8 Operational Land Imager (OLI) and Thermal Infrared Sensor (TIRS) images consist of nine spectral bands with a spatial resolution of 30 meters for Bands 1 to 7 and 9. New band 1 (ultra-blue) is useful for coastal and aerosol studies. New band 9 is useful for cirrus cloud detection. The resolution for Band 8 (panchromatic) is 15 meters. Thermal bands 10 and 11 are useful in providing more accurate surface temperatures and are collected at 100 meters but are resampled to 30 meter in delivered data product. Approximate scene size is 170 km north-south by 183 km east-west. Landsat 8 carries two Push-Broom instruments: OLI sensor and TIRS sensor. The main difference between the new TIRS and previous TM/ETM sensors is the presence of two TIR bands in the atmospheric window between 10 and 12  $\mu\text{m}$ , which represents an advancement over the single thermal band present on TM and ETM sensors.

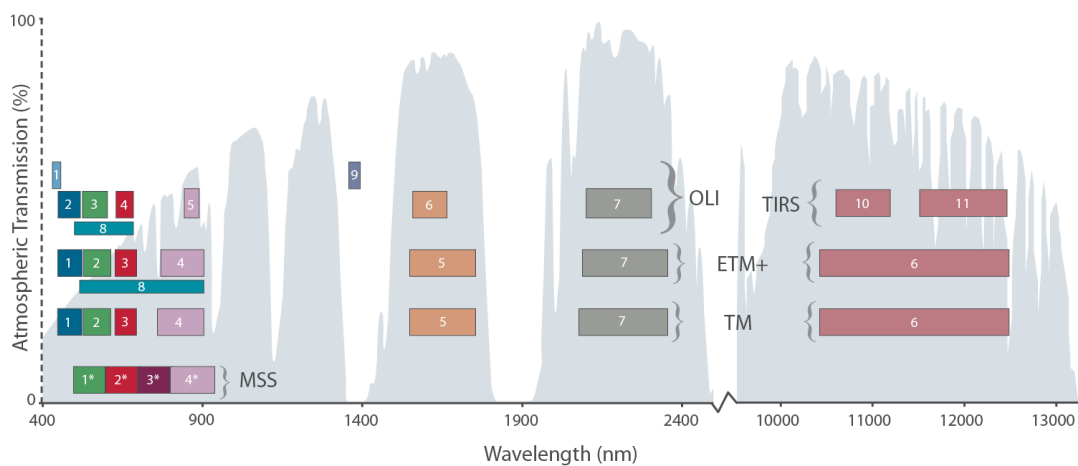
<b>Landsat 8 Operational Land Imager (OLI) and Thermal Infrared Sensor (TIRS)</b>  <b>Launched February 11, 2013</b>	<b>Bands</b>	<b>Wavelength (micrometers)</b>	<b>Resolution (meters)</b>
	Band 1 - Coastal aerosol	0.43 - 0.45	30
	Band 2 - Blue	0.45 - 0.51	30
	Band 3 - Green	0.53 - 0.59	30
	Band 4 - Red	0.64 - 0.67	30
	Band 5 - Near Infrared (NIR)	0.85 - 0.88	30
	Band 6 - SWIR 1	1.57 - 1.65	30
	Band 7 - SWIR 2	2.11 - 2.29	30
	Band 8 - Panchromatic	0.50 - 0.68	15
	Band 9 - Cirrus	1.36 - 1.38	30
	Band 10 - Thermal Infrared (TIRS) 1	10.60 - 11.19	100 * (30)
	Band 11 - Thermal Infrared (TIRS) 2	11.50 - 12.51	100 * (30)

**TABLE 2. LANDSAT 8 TECHNICAL FEATURES**

The Landsat 8 satellite images the entire Earth every 16 days in an 8-day offset from Landsat 7.

The sensors both provide improved signal-to-noise (SNR) radiometric performance quantized over a 12-bit dynamic range. Improved signal to noise performance enable better characterization of land cover state and condition.

Landsat 8 images have a large file size, at approximately 1 GB compressed.



\* MSS bands 1-4 were known as bands 4-7, respectively, on Landsats 1-3

**FIGURE 3. BANDPASS WAVELENGTH FOR L8 OLI AND TIRS SENSOR COMPARED TO L7 ETM+ SENSOR**

## *2.3 CORRECTION TO PHYSICAL PARAMETERS*

Standard Landsat data products consist of quantized and calibrated scaled Digital Numbers (DN) representing multispectral image data acquired by both the Operational Land Imager and Thermal Infrared Sensor.

The products are delivered in 16-bit unsigned integer format and can be rescaled to the Top Of Atmosphere (TOA) reflectance and/or radiance using radiometric rescaling coefficients provided in the product metadata file (MTL file). The MTL file also contains the thermal constants needed to convert TIRS data to the at-satellite brightness temperature.

Since the launch of Landsat 8 in 2013, thermal energy from outside the normal field of view (stray light) has affected the data collected in TIRS Bands 10 and 11. This can vary throughout each scene and depends upon radiance outside the instrument field of view, which users cannot correct in the Landsat Level 1 data product. Band 11 is significantly more contaminated by stray light than Band 10. It is recommended from the United States Geological Survey (USGS) that users refrain from using Band 11 data in quantitative analysis including use of Band 11 in Split-Window surface temperature retrieval algorithms. (USGS, [http://landsat.usgs.gov/Landsat8\\_Using\\_Product.php](http://landsat.usgs.gov/Landsat8_Using_Product.php)  
[http://landsat.usgs.gov/Landsat8\\_Using\\_Product.php](http://landsat.usgs.gov/Landsat8_Using_Product.php))

This is why, in this thesis, is used only Single Channel surface temperature retrieval algorithm.

### 2.3.1 ABOUT LANDSAT 7

ETM+ band data can be converted to TOA spectral radiance using the radiance rescaling factors provided in the metadata file:

$$L_{sensor,i} = a_{0,i} + a_{1,i}DN_i$$

Where  $L_{sensor,i}$  is the at-sensor radiance or Top Of Atmospheric calculated for each band  $i$ ,  $a_{0,i}$  is the offset, the band-specific additive rescaling factor from the metadata,  $a_{1,i}$  is the gain, the band-specific multiplicative rescaling factor from the metadata, meanwhile  $DN_i$  are the quantized and calibrated standard product pixel values. The coefficients  $a_{0,i}$  and  $a_{1,k}$  can be found in the MTL file, the first one is `RADIANCE_ADD_BAND_x`, the second one is `RADIANCE_MULT_BAND_x`, where  $x$  is the number. The values of radiance coefficients for each Landsat 7 file are:

```

RADIANCE_MULT_BAND_1 = 1.181
RADIANCE_MULT_BAND_2 = 1.210
RADIANCE_MULT_BAND_3 = 0.943
RADIANCE_MULT_BAND_4 = 0.640
RADIANCE_MULT_BAND_5 = 0.191
RADIANCE_MULT_BAND_6_VCID_1 = 0.067
RADIANCE_MULT_BAND_6_VCID_2 = 0.037
RADIANCE_MULT_BAND_7 = 0.066
RADIANCE_MULT_BAND_8 = 0.976
RADIANCE_ADD_BAND_1 = -7.38071
RADIANCE_ADD_BAND_2 = -7.60984
RADIANCE_ADD_BAND_3 = -5.94252
RADIANCE_ADD_BAND_4 = -5.73976
RADIANCE_ADD_BAND_5 = -1.19122
RADIANCE_ADD_BAND_6_VCID_1 = -0.06709
RADIANCE_ADD_BAND_6_VCID_2 = 3.16280
RADIANCE_ADD_BAND_7 = -0.41650
RADIANCE_ADD_BAND_8 = -5.67559

```

Assuming that the land surface has a Lambertian behavior,  $L_{sensor,i}$  is a solar irradiance function:

$$L_{sensor,i} = \frac{E_{sun} \cos \theta_i \rho_i}{D\pi}$$

Where  $E_{sun}$  is the solar irradiance on the top of the atmosphere (for that spectrum band), known from solar tables,  $\rho_i$  is the apparent reflectivity of the cover in the band  $i$ ;  $\theta$  is the zenithal angle of the incident flux, and  $D$  is a factor of correction of the distance Earth - Sun,  $D$  varies between 0.983 and 1.014 and depends by the day of the year.

ETM+ Band	$E_{sun}$ values
<b>1</b>	1970
<b>2</b>	1840
<b>3</b>	1547
<b>4</b>	1044
<b>5</b>	225.7
<b>7</b>	82.06
<b>8</b>	1369

TABLE 3. L7  $E_{sun}$  VALUES

JD	Distance	JD	Distance	JD	Distance	JD	Distance	JD	Distance
<b>1</b>	0.98331	<b>74</b>	0.99446	<b>152</b>	1.01403	<b>227</b>	1.01281	<b>305</b>	0.99253
<b>15</b>	0.98365	<b>91</b>	0.99926	<b>166</b>	1.01577	<b>242</b>	1.00969	<b>319</b>	0.98916
<b>32</b>	0.98536	<b>106</b>	1.00353	<b>182</b>	1.01667	<b>258</b>	1.00566	<b>335</b>	0.98608
<b>46</b>	0.98774	<b>121</b>	1.00756	<b>196</b>	1.01646	<b>274</b>	1.00119	<b>349</b>	0.98426
<b>60</b>	0.99084	<b>135</b>	1.01087	<b>213</b>	1.01497	<b>288</b>	0.99718	<b>365</b>	0.98333

TABLE 4. L7 EARTH – SUN DISTANCE VALUES

Finally, the apparent reflectivity can be calculated from a simple formula:

$$\rho_i = \frac{D\pi L_{sensor,i}}{E_{0,i} \cos \theta_i}$$

This reflectivity is considered apparent because needs atmospheric corrections.

### 2.3.2 ABOUT LANDSAT 8

OLI and TIRS band data can be converted to TOA spectral radiance using the radiance rescaling factors provided in the metadata file, exactly in the same way of Landsat 7:

$$L_{sensor,i} = a_{0,i} + a_{1,i}DN_i$$

The values of radiance coefficients for each Landsat 8 file are:

```
RADIANCE_MULT_BAND_1 = 1.2639E-02
RADIANCE_MULT_BAND_2 = 1.2942E-02
RADIANCE_MULT_BAND_3 = 1.1926E-02
RADIANCE_MULT_BAND_4 = 1.0057E-02
RADIANCE_MULT_BAND_5 = 6.1544E-03
RADIANCE_MULT_BAND_6 = 1.5305E-03
RADIANCE_MULT_BAND_7 = 5.1587E-04
RADIANCE_MULT_BAND_8 = 1.1382E-02
RADIANCE_MULT_BAND_9 = 2.4053E-03
RADIANCE_MULT_BAND_10 = 3.3420E-04
RADIANCE_MULT_BAND_11 = 3.3420E-04
RADIANCE_ADD_BAND_1 = -63.19491
RADIANCE_ADD_BAND_2 = -64.71235
RADIANCE_ADD_BAND_3 = -59.63188
RADIANCE_ADD_BAND_4 = -50.28496
RADIANCE_ADD_BAND_5 = -30.77189
RADIANCE_ADD_BAND_6 = -7.65269
RADIANCE_ADD_BAND_7 = -2.57937
RADIANCE_ADD_BAND_8 = -56.90874
RADIANCE_ADD_BAND_9 = -12.02635
RADIANCE_ADD_BAND_10 = 0.10000
RADIANCE_ADD_BAND_11 = 0.10000
```

OLI band data can also be converted to TOA planetary reflectance using reflectance rescaling coefficients provided in the product metadata file (MTL file). The following equation is used to convert DN values to TOA reflectance for OLI data as follows:

$$\rho\lambda' = a_{2,i} + a_{3,i}DN_i$$

Where  $\rho\lambda'$  is the TOA planetary reflectance, without correction for solar angle. Note that  $\rho\lambda'$  does not contain a correction for the sun angle,  $a_{2,i}$  is the offset, the band-specific additive rescaling factor from the metadata,  $a_{3,i}$  is the gain, band-specific multiplicative rescaling factor from the metadata, meanwhile  $DN_i$  are the quantized and calibrated standard product pixel values.

The coefficients  $a_{2,i}$  and  $a_{3,i}$  can be find in the MTL file, the first one is REFLECTANCE\_ADD\_BAND\_x, the second one is REFLECTANCE\_MULT\_BAND\_x, where x is the number.

The values of reflectance coefficients for each Landsat 8 file are:

```

REFLECTANCE_MULT_BAND_1 = 2.0000E-05
REFLECTANCE_MULT_BAND_2 = 2.0000E-05
REFLECTANCE_MULT_BAND_3 = 2.0000E-05
REFLECTANCE_MULT_BAND_4 = 2.0000E-05
REFLECTANCE_MULT_BAND_5 = 2.0000E-05
REFLECTANCE_MULT_BAND_6 = 2.0000E-05
REFLECTANCE_MULT_BAND_7 = 2.0000E-05
REFLECTANCE_MULT_BAND_8 = 2.0000E-05
REFLECTANCE_MULT_BAND_9 = 2.0000E-05
REFLECTANCE_ADD_BAND_1 = -0.100000
REFLECTANCE_ADD_BAND_2 = -0.100000
REFLECTANCE_ADD_BAND_3 = -0.100000
REFLECTANCE_ADD_BAND_4 = -0.100000
REFLECTANCE_ADD_BAND_5 = -0.100000
REFLECTANCE_ADD_BAND_6 = -0.100000
REFLECTANCE_ADD_BAND_7 = -0.100000
REFLECTANCE_ADD_BAND_8 = -0.100000
REFLECTANCE_ADD_BAND_9 = -0.100000

```

TOA reflectance with a correction for the sun angle is then:

$$\rho\lambda = \frac{\rho\lambda'}{\cos \theta_{sz}} = \frac{\rho\lambda'}{\sin \theta_{se}}$$

Where  $\rho\lambda$  is the TOA planetary reflectance,  $\theta_{sz}$  is the local sun elevation angle, the scene centre sun elevation angle in degrees is provided in the MTL file with the name SUN\_ELEVATION, and  $\theta_{se}$  is the local solar zenith angle, where the relation between the angles is:

$$\theta_{sz} = 90^\circ - \theta_{se}$$

## *2.4 THE VEGETATION PARAMETERS AND THE LAND SURFACE TEMPERATURE (LST) VARIABLE*

A Vegetation Index (VI) is a spectral transformation of two or more bands designed to enhance the contribution of vegetation properties and allows reliable spatial and temporal inter-comparisons of terrestrial photosynthetic activity and canopy structural variations (Wikipedia).

In this thesis are retrieved different VIs for the use in the hydrological. The VIs calculated from the images are the Normalized Difference Vegetation Index (NDVI), the Fractional Vegetation Cover (FVC), the Leaf Area Index (LAI). Moreover, two variables are also computed: Albedo (ALB) and Land Surface Temperature (LST).

### *2.4.1 THE NORMALIZED DIFFERENCE VEGETATION INDEX (NDVI)*

The NDVI is a simple indicator that can be used to analyse remote sensing measurements and assess whether the target being observed contains live green yellow, red vegetation or not.

The NDVI is an index of plant “greenness” or photosynthetic activity, and is one of the most commonly used vegetation indices. Vegetation indices are based on the observation that different surfaces reflect different types of light differently. Photosynthetically active vegetation, in particular, absorbs most of the red light that hits it while reflecting much of the near infrared light. Vegetation that is dead or stressed reflects more red light and less near infrared light. Likewise, non-vegetated surfaces have a much more even reflectance across the light spectrum.

NDVI is calculated as:

$$NDVI = \frac{NIR - Red}{NIR + Red}$$



Where NIR is the Near InfraRed band (Band 5 for Landsat 8 and Band 4 for Landsat7), Red is the red band (Band 4 for Landsat 8 and Band 3 for Landsat 7). The output of NDVI is a new image file. Values of NDVI can range from -1.0 to +1.0, but values less than zero typically do not have any ecological meaning, so the range of the index is truncated to 0.0 to +1.0. Higher values signify a larger difference between the red and near infrared radiation recorded by the sensor - a condition associated with highly photosynthetically-active vegetation. Low NDVI values mean there is little difference between the red and NIR signals. This happens when there is little photosynthetic activity, or when there is just very little NIR light reflectance (i.e., water reflects very little NIR light).

### **2.4.2 THE FRACTIONAL VEGETATION COVER (FVC)**

The FVC is a useful parameter for many environmental and climate-related applications that, for each image, would tell us the fraction of the total pixel that is covered by the trees.

The method used to derive the fractional cover is an empirical method (Ana ANDREU 2015):

$$FVC = \left( \frac{NDVI - NDVI_{min}}{NDVI_{max} - NDVI_{min}} \right)$$

Where  $NDVI_{min}$  used is equal to 0.15,  $NDVI_{max}$  used is equal to 0.90.

The output of FVC is a new image file. In accord of our script, the values of FVC can range from 0.0 to +1.0. High values signify a large area covered by vegetation. On the other side, low FVC values mean the opposite.

### **2.4.3 THE LEAF AREA INDEX (LAI)**

The LAI is a different vegetation index, which is used for the computation of evapotranspiration, an important variable for numerous processes in various disciplines of bio-and geosciences. *In situ* measurements are the most accurate source of LAI among

the LAI measuring methods, but they have the limitation of being labour, intensive and site specific. For this reason, spatial-explicit applications (from regional to continental scales), satellite remote sensing is a promising source for obtaining LAI with different spatial resolutions. However, satellite-derived LAI measurements using empirical models require calibration and validation with the *in situ* campaign measurements.

LAI is calculated in this way (Muhammad Ali 2015 ):

$$LAI = \frac{-\ln(1 - FVC)}{k(\theta)}$$

Here,  $k(\theta)$  is the light extinction coefficient for a given solar zenith angle. The solar zenith angle ( $\theta$ ) depends on terrain geometry, solar declination, solar elevation angle, latitudinal location and day of the year. The light extinction coefficient is a measure of attenuation of radiation in the canopy. In ours cases it was estimated equal to 0.5.

#### **2.4.4 ALBEDO (ALB)**

Albedo is the fraction of shortwave radiation reflected from the Earth back into space. It is a measure of the reflectivity of the earth's surface.

We can obtain this parameter in a different way for Landsat 7 and Landsat 8, because of the differences of the two sensors. Albedo is calculated as the integration of at-surface reflectance across the shortwave spectrum as shown (Yinghai Ke 2016 ):

$$\text{Landsat 7 ETM+: } 0.254r_1 + 0.149r_2 + 0.147r_3 + 0.311r_4 + 0.103r_5 + 0.036r_7$$

$$\text{Landsat 8 OLI: } 0.130r_1 + 0.115r_2 + 0.143r_3 + 0.180r_4 + 0.281r_5 + 0.108r_6 + 0.042r_7$$

Where  $r$  is the surface reflectance for each different band, and the coefficients are representative of the surface solar radiation fraction within the spectral range for each band.

## 2.4.5 LAND SURFACE TEMPERATURE (LST) RETRIEVAL METHODS FROM LANDSAT

The Land Surface Temperature (LST) is an index of the equilibrium thermodynamic state resulting from the energy balance of the fluxes between the atmosphere, surface and subsurface soil, so knowledge of LST is of great interest in many applications such as assessing water and energy budgets at the surface/atmosphere interface, evapotranspiration estimation, General Circulation Models (GCM) and the greenhouse effect.

The LST retrieved from high to medium spatial resolution remote sensing data for many environmental studies, particularly the applications related to water resources management over agricultural sites, was a key factor for the final decision of including a thermal infrared instrument on board the Landsat 8.

As already mentioned, this new sensor includes two TIR bands in the atmospheric window between 10 and 12  $\mu\text{m}$ , thus allowing the application of split-window (SW) algorithms in addition to single-channel (SC) algorithms or direct inversions of the radiative transfer equation used in Landsat 7 sensor ETM+, with only one TIR band, but in this thesis, is use just SC due to Band 11 problem.

Methods for LST retrieval are based on the Radiative Transfer Equation(RTE), which can be written in the thermal infrared region as (Juan C. Jiménez-Muñoz 2004):

$$L_{sensor,i} = [\varepsilon_i B_i(T_s) + (1 - \varepsilon_i) L_{atm,i}^\downarrow] \tau_i + L_{atm,i}^\uparrow$$

Where  $L_{sensor,i}$  as already mentioned, is the at-sensor radiance or Top Of Atmospheric radiance, i.e., the radiance measured by the sensor after radiance corrections;  $\varepsilon_i$  is the land surface emissivity,  $B_i(T_s)$  is the blackbody radiance given by the Planck's law and  $T_s$  is the LST,  $L_{atm,i}^\downarrow$  is the downwelling atmospheric radiance,  $\tau_i$  is the total atmospheric transmissivity between the surface and the sensor and  $L_{atm,i}^\uparrow$  is the upwelling atmospheric radiance.

The atmospheric parameters  $\tau$ ,  $L_{atm}^{\downarrow}$ ,  $L_{atm}^{\uparrow}$  can be downloaded from NASA website (NASA <http://atmcorr.gsfc.nasa.gov/>) where a calculator of atmospheric correction computes the parameters for each precise day, hour, longitude and latitude of a precise place in the world obtain with a specific satellite.

```

Date (yyyy-mm-dd):          2011-05-10
Input Lat/Long:             38.901/  -2.707
GMT Time:                   10:43
L7 Spectral Response Curve from handbook
Mid-latitude winter standard atmosphere
User input surface conditions
Surface altitude (km):      -999.000
Surface pressure (mb):      -999.000
Surface temperature (C):    -999.000
Surface relative humidity (%): -999.000

Band average atmospheric transmission:  0.90
Effective bandpass upwelling radiance:  0.78 W/m^2/sr/um
Effective bandpass downwelling radiance: 1.31 W/m^2/sr/um

```

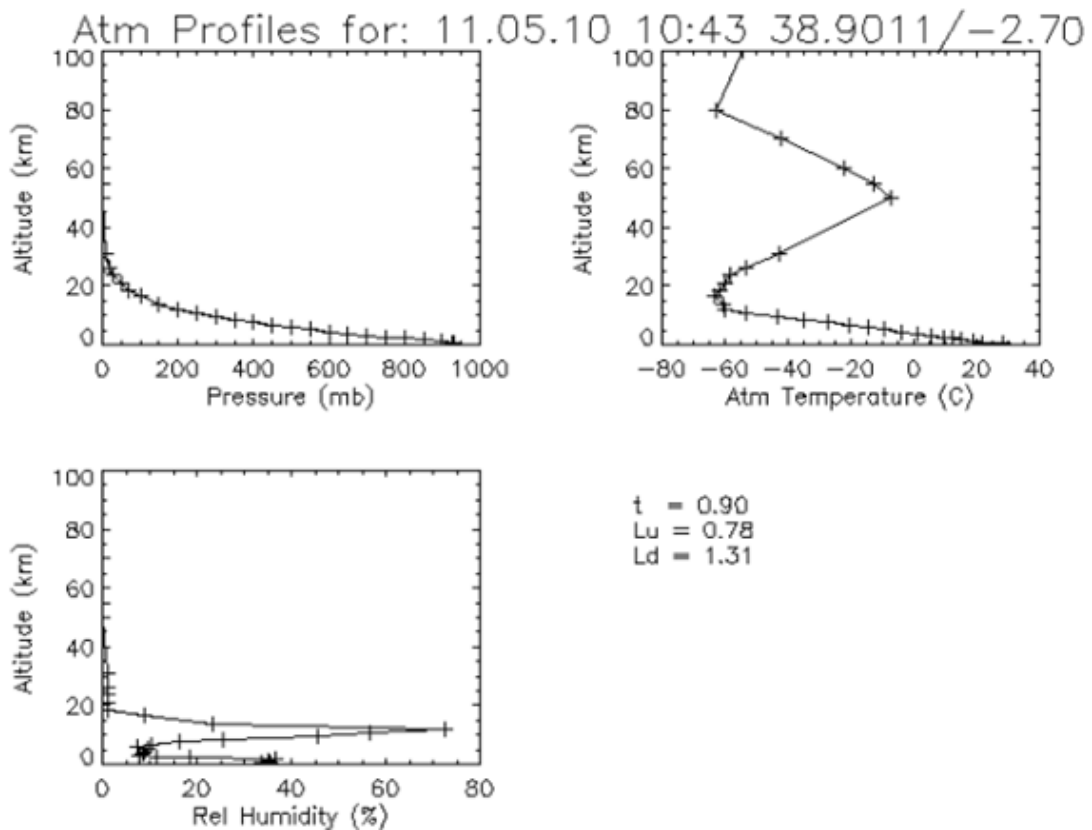


FIGURE 4. EXAMPLE OF USED ATMOSPHERIC CORRECTIONS

### 2.4.5.1 THE SINGLE-CHANNEL ALGORITHM (SC)

SC methods retrieve LST only from one thermal band, this algorithm is based on the solving for the Planck radiance according to the equations already seen. (Jiménez-Muñoz 2006)

$$B_i(T_s) = \frac{L_{sensor,i} - L_{atm,i}^{\uparrow}}{\varepsilon_i \tau_i} - \frac{(1 - \varepsilon_i)L_{atm,i}^{\downarrow}}{\varepsilon_i}$$

LST can be finally retrieved by inversion of the Planck's law:

$$T_s = \frac{c_2}{\lambda_i} \left[ \ln \left( \frac{c_1}{\lambda_i^5 B_i} + 1 \right) \right]^{-1}$$

Where  $\lambda$  is the spectral filter for the response function,  $c_1$  and  $c_2$ , which are the constants in the Planck's function, for Landsat 7, have the values:  $c_1 = 1.19104 \cdot 10^8 W \mu m^4 m^{-2} sr^{-1}$ , and  $c_2 = 14287.7 \mu m K$ .

Meanwhile, for Landsat 8,  $c_1 = 1.19104 \cdot 10^8 W \mu m^4 m^{-2} sr^{-1}$ , and  $c_2 = 14387.7 \mu m K$ .

The surface emissivity used for Landsat 7 and Landsat 8, is retrieved with the same equation, even if the band is different. The band used for Landsat 7 is, the thermal infrared one, is the band 6, for Landsat 8 is the band 10 from OLI sensor.

$\varepsilon$  is calculated as:

$$\varepsilon = 0.971(1 - FVC) + 0.982FVC$$

According to (Jiménez-Muñoz 2006).

## 3. CASE STUDIES

Two case studies are analysed in Italy and Spain.

### 3.1 BARRAX

The first study area is an agricultural area in Barrax, a municipality in the province of Albacete in the center of Spain which belongs to the Autonomous Community of Castilla-La Mancha (39°02'31 "N, 2°04'56" W, 698m above sea level), characterized by an alternation of irrigated and dry cultivated area.

The soils of the area are Inceptisols in terms of soil taxonomy. About 65% of cultivated lands at Barrax are dryland (67% winter cereals; 33% fallow) and 35% irrigated land (75% corn; 15% barley/sunflower; 5% alfalfa; 5% onions and vegetables).



FIGURE 5. BARRAX SITE FROM GOOGLE MAPS (GOOGLE)

The area has been selected in many other ESA experiments due to its flat terrain, minimising the complications introduced by variable lighting geometry, and the presence of large and uniform land-use units, suitable for validating moderate resolution satellite image products.

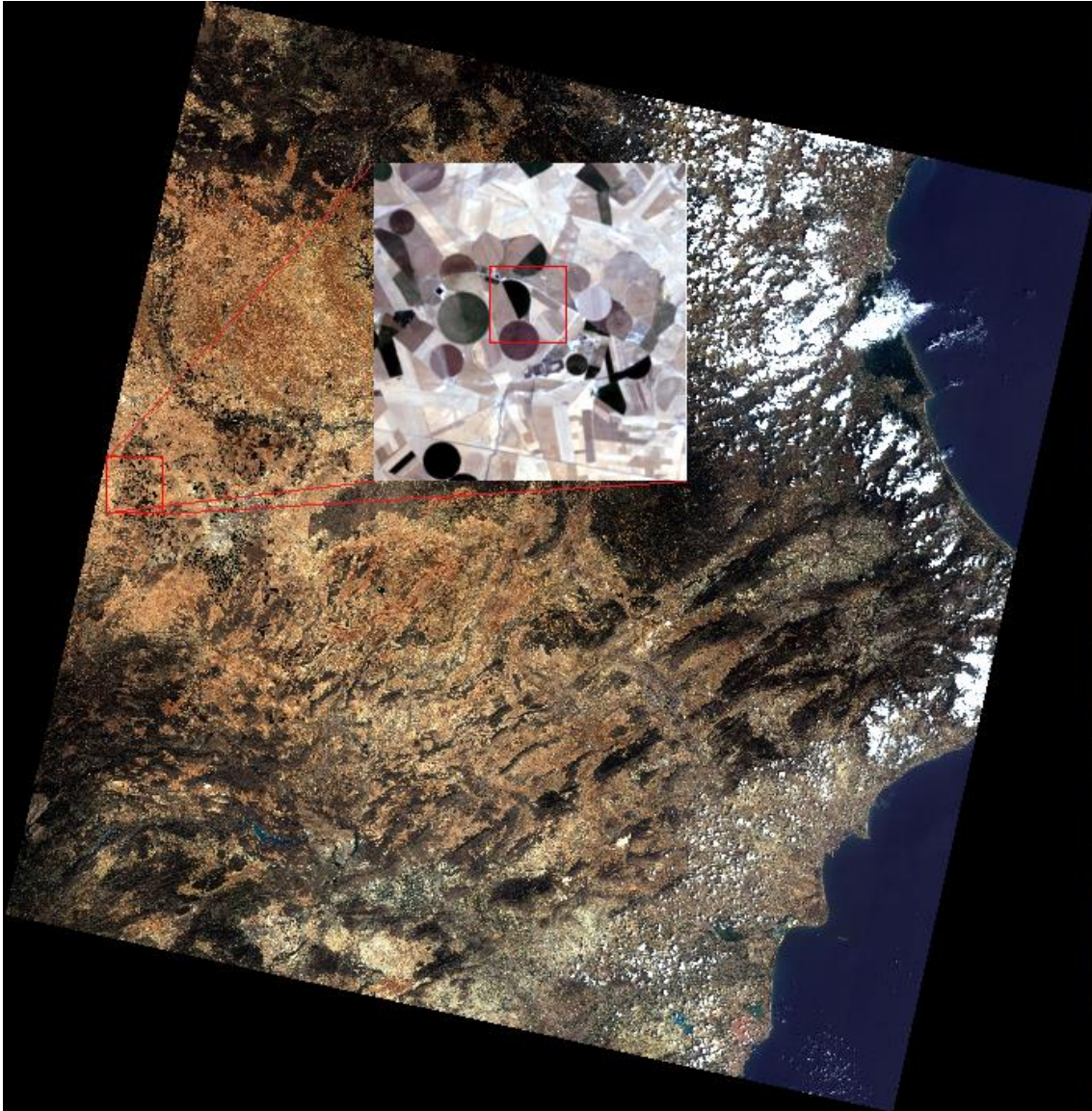


FIGURE 6. BARRAX SITE FROM L8 IMAGERY

The fields in this area are managed by the Instituto Técnico Agronómico Provincial de Albacete (ITAP). The basic purpose of the ITAP is the transfer of technology, disseminating knowledge and technical advances, as a way of bridge and connection between the scientific world and everyday activities agrifood.

Each imagery processed contains more than 40000 pixels.

### 3.2 FOGGIA

The second study area is a site near Foggia (41°27'39.32"N, 15°33'21.67"E, 76m above sea level), a municipality of Puglia, in southern Italy, capital of the province of Foggia.



FIGURE 7. FOGGIA SITE FROM GOOGLE MAPS (GOOGLE)

Foggia is the main city of a plain called Tavoliere, also known as the "granary of Italy", due to the quantity of wheat fields. In winter there are a lot of green vegetables fields, like spinach, asparagus, cabbages and leaf beet. With the warmer seasons, the main fields are wheat and tomatoes fields.

In this site, there are other cities like Lucera, San Severo and Torremaggiore, a little artificial lake called "Invaso del Celone", and a hilly area.



The studied considers only the fields present in the surroundings of these zones, which are part of the fields of the irrigation consortium (<http://consorzio.fg.it/>) “Consorzio per la bonifica della Capitanata”, which has an extension of 441.000 ha.

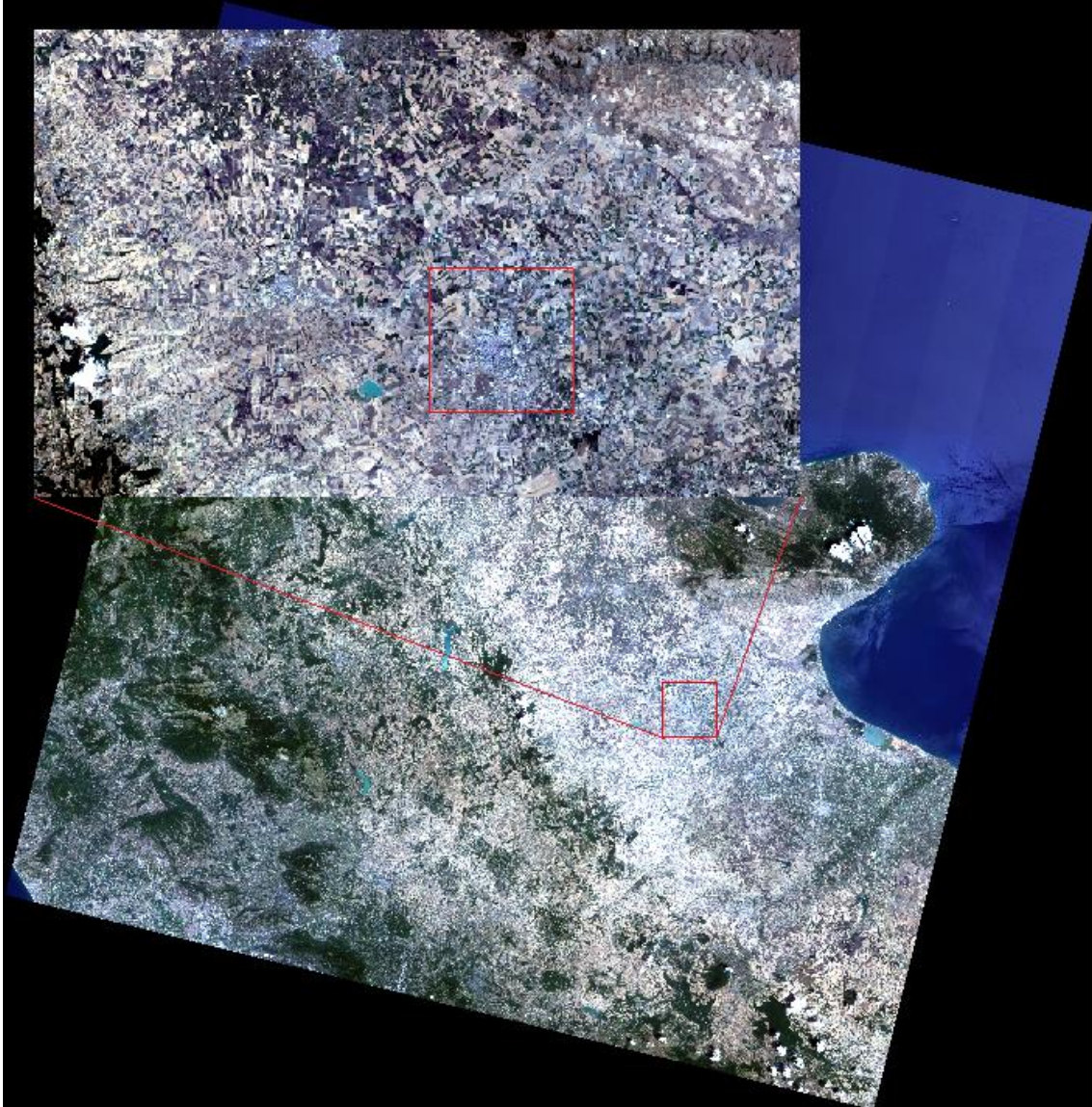


**FIGURE 8. FOGGIA SITE FROM L8**

The area considered is composed by more than 2500000 pixels.

## **4. DATA ANALYSIS**

In this chapter, the images are analysed and for each of them are retrieved parameters and variables for the two case studies. A statistical analysis is performed over the whole image to identify the consistencies among data. Moreover, a local validation of the retrieved parameters is performed.

The main program used for the data elaboration is ENVI, a useful software for processing and analysing geospatial imagery; ENVI combines spectral image processing and image analysis technology with a user-friendly interface so users can get meaningful information from imagery. The scientific programming language correlated to ENVI is IDL.

### **4.1 STATISTICAL ANALYSES**

The first analysis deals with the estimates of the different parameters and then with the evolution of the mean and standard deviation of each parameter, examining the time series, the comparison among correlated indices FVC and LAI and the relationship between LST and FVC. The steps in this analysis have been the following:

- download all the utilizable data, from the beginning of 2011 to September 2016, for Barrax and Foggia
- download all the relative atmospheric corrections for each data from NASA website
- run the IDL code obtaining ALBEDO, NDVI, FVC, LAI and LST
- crop the area of interest of each product
- obtain the mean and standard deviation of the values contained in each pixel for each image produced

The historical series in this thesis consider the temporal period January 2011 – September 2016 and the data used are the ones of Landsat 7 archive for the years 2011, 2012, and beginning 2013, meanwhile for the rest of 2013 and for 2014, 2015, 2016 are used mostly the ones of Landsat 8 archive.

#### 4.1.1 L7 SLC FAILURE

The main problem in the image processing has been the presence of the black stripes due to SLC failure in Landsat 7. An attempt to correct this problem has been done using the software ENVI. The imageries have been processed with a specific correction applied to create an image without stripes, taking advantage of an interpolation that can be implemented with an ENVI extension called *Landsat\_gapfill*.

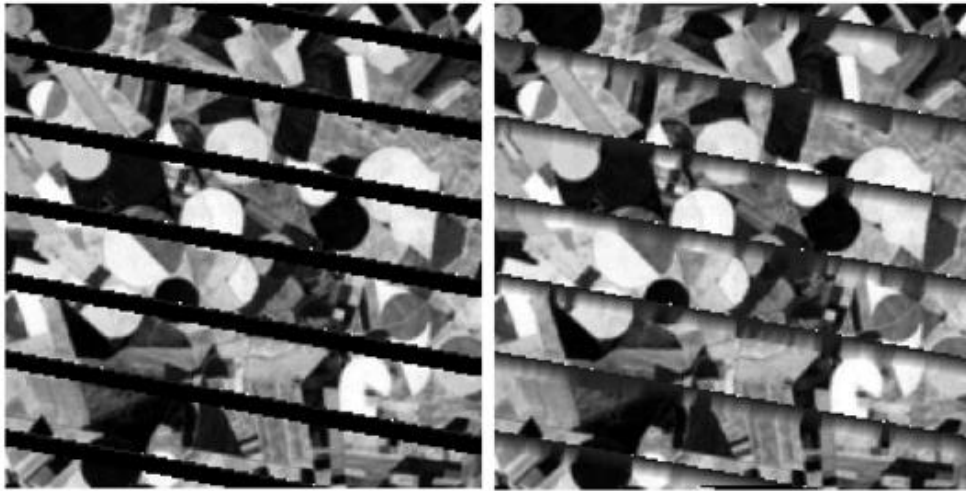


FIGURE 9. BEFORE AND AFTER LANDSAT\_GAPFILL CORRECTION ON THE NDVI DATA OF THE 10<sup>TH</sup> OF MAY 2011 IN BARRAX

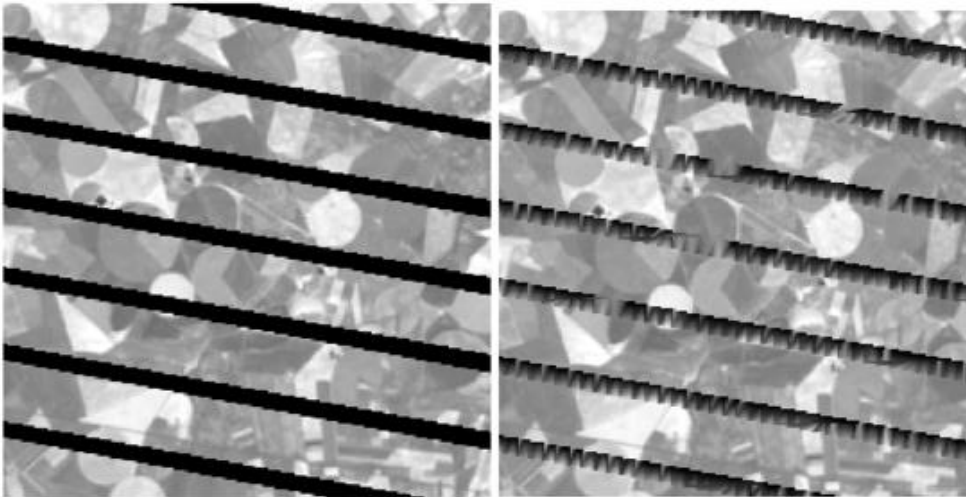


FIGURE 10. BEFORE AND AFTER LANDSAT\_GAPFILL CORRECTION ON THE ALBEDO DATA OF THE 10<sup>TH</sup> OF MAY 2011 IN BARRAX

Nevertheless, the outputs haven't been considered good enough for our purpose, so, in this thesis, are used only the imageries with *Nan* value on the stripes obtained with the realized code in IDL, due to the presence of high variability.

### 4.1.2 CLOUDS PROBLEM

Another important problem are the clouds. When the sky is completely covered by the clouds is impossible to work with the data, so the images with cloudy weather are useless, but when the clouds are small and sporadic, is possible to not consider only the pixels with the clouds, creating a Region Of Interest (ROI) with the software, and computing the data without clouds.

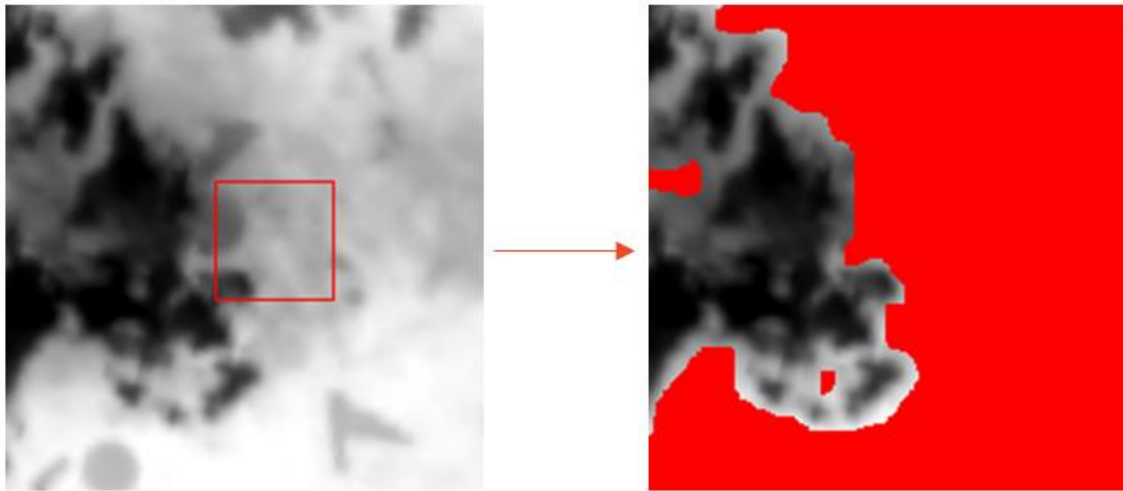


FIGURE 11. BUILDING A ROI NOT CONSIDERING CLOUDY PIXELS ON THE 13<sup>TH</sup> OF SEPTEMBER 2016 IN BARRAX

The problem of the clouds in Barrax is almost irrelevant, considering the position of the area, in the middle of Spain, away from mountain with sun almost all the year; instead in Foggia the situation is completely different, there are large period of the years in which is not possible to have images with no clouds, because of the geographical position.

This problem, in Foggia, limits the image availability.

### 4.1.3 BARRAX

The imageries processed in Barrax area are 111 from 2011 to 2016, the imageries used for the analysis in Barrax are 84, have been excluded the cloudy ones and has been decided to work only with Landsat 8 for the years 2014, 2015 and 2016. Landsat 8 images have a large file size, at approximately 1 GB compressed, Landsat 7 approximately 0.3 GB compressed.

Barrax is located between two overlapping of the Landsat overpasses, this means that we can have an imagery of Barrax each 8 days for L7 and one each 8 days for L8. As we can see in the following image, we have an image of Landsat in path 199 and 200, the row is always the number 33, in the Julian Day (JD) 145 and 152. In the red box the ITAP experimental field Las Tiesas is identified.

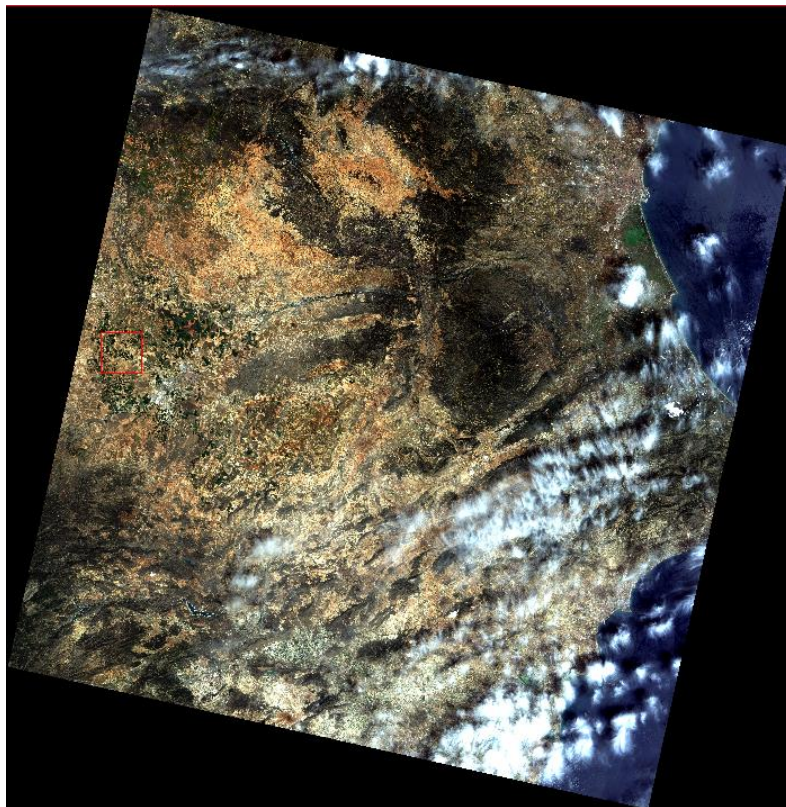


FIGURE 12. L8 IMAGERY ON THE 24TH OF MAY 2016, JD 145 PATH 199, ROW 33

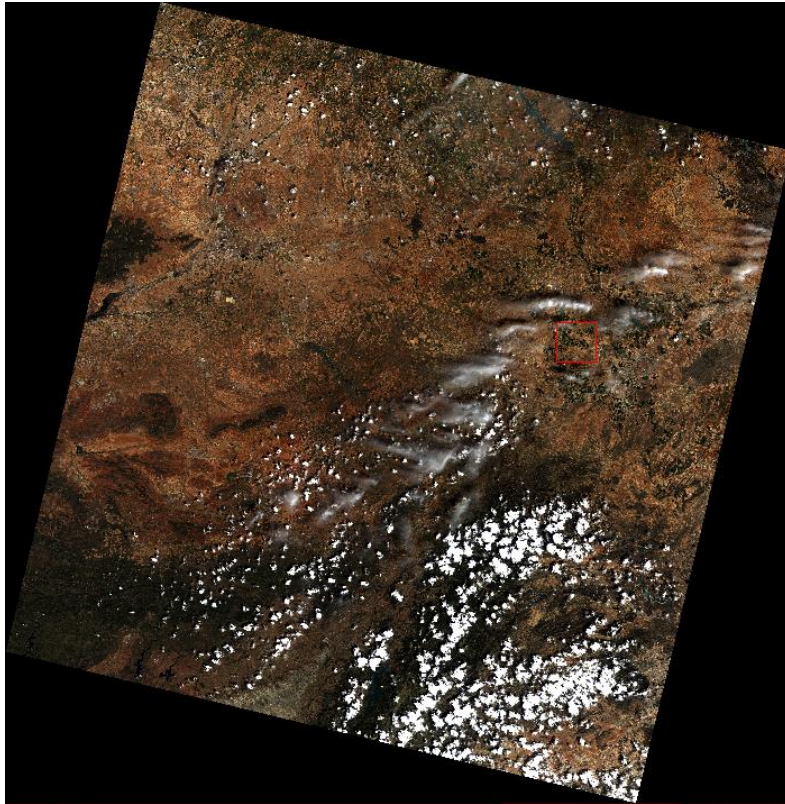


FIGURE 13. L8 IMAGERY ON THE 31ST OF MAY 2016, JD 152 PATH 200, ROW 33

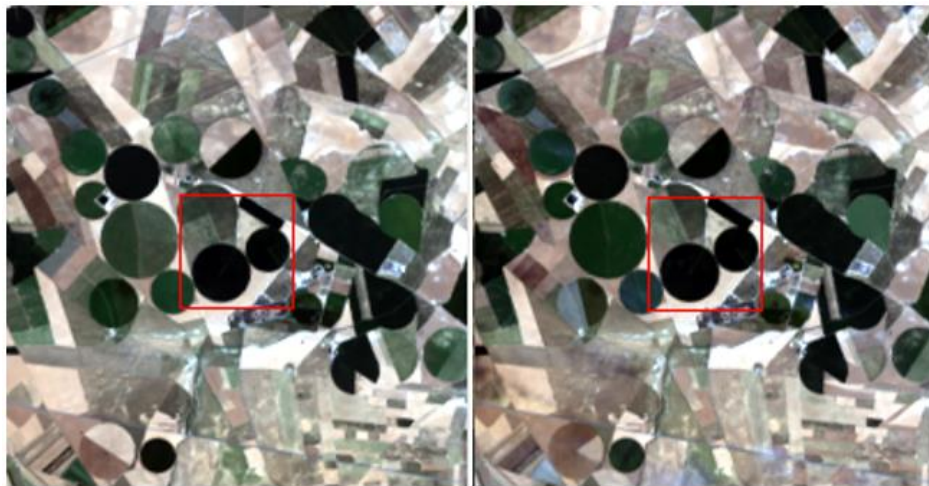


FIGURE 14. L8 ZOOMED IMAGERIES ON JD 145 (LEFT) AND 152 (RIGHT) ON BARRAX AREA STUDY

For each imagery are retrieved the mean values of LST, NDVI, FVC, LAI and Albedo. In the next images is possible to see an example of the processing result of 1 of the 84 imageries elaborated, Julian Day 145. For each datum is plotted the map in .tiff format, the histogram of the data values and the basics statistics. The spatial resolution is of 100m, in fact the shape of the fields is less defined than for the 30m parameters.

- LST

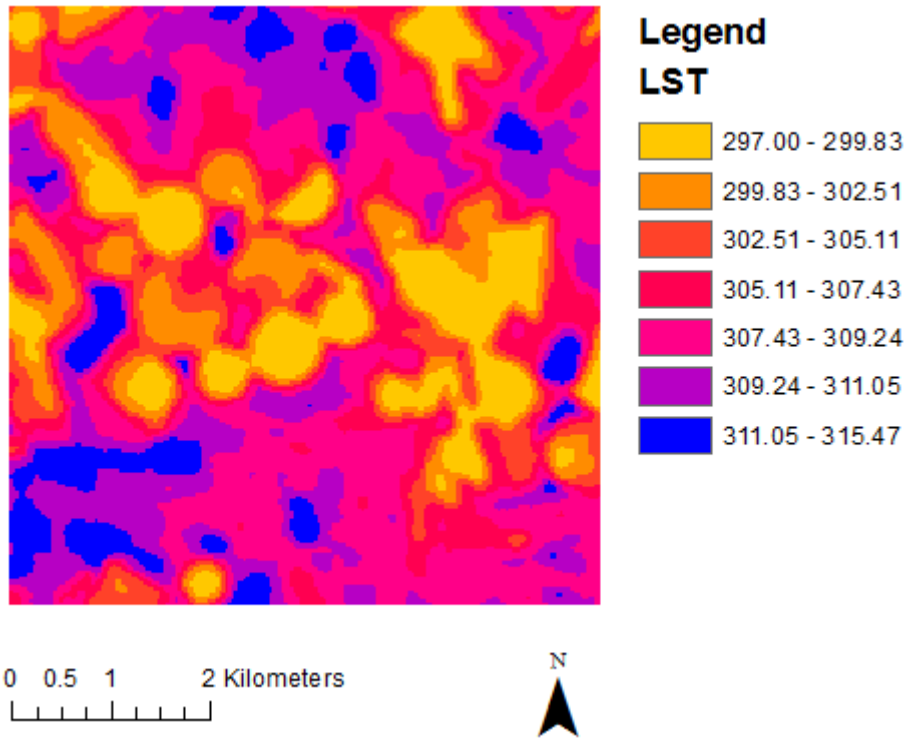


FIGURE 15. BARRAX, JD 145, LST MAP

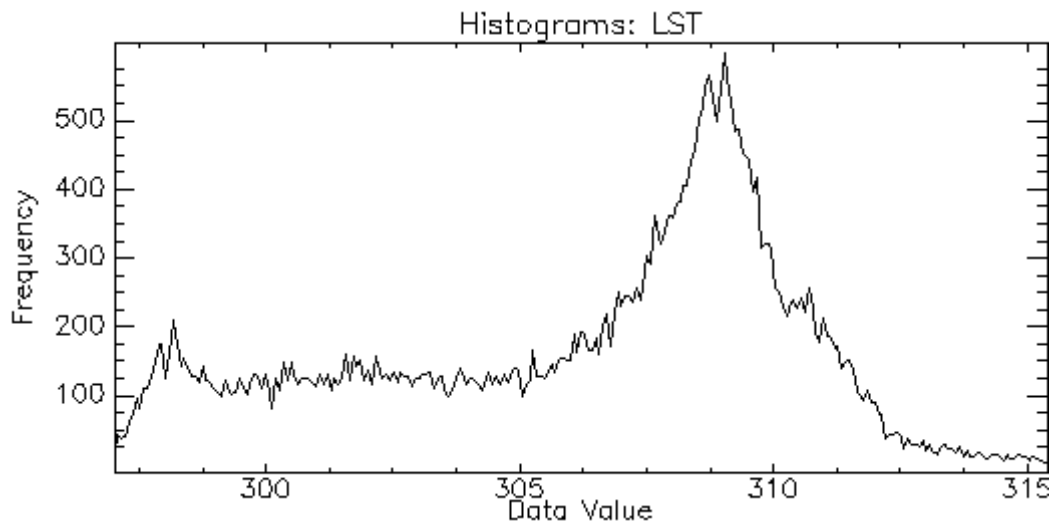


FIGURE 16. BARRAX, JD 145, LST HISTOGRAM

Basic Stats	Min	Max	Mean	Stdev
Data Value [K]	297.01	315.47	306.27	4.12

TABLE 5. BARRAX, JD 145, LST BASIC STATISTICS

- NDVI

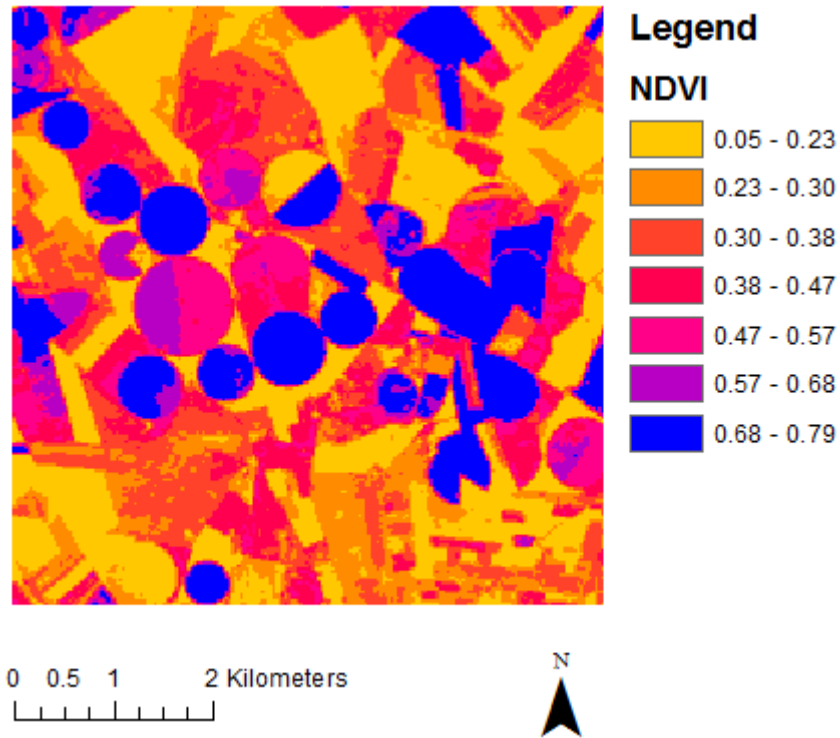


FIGURE 17. BARRAX, JD 145, NDVI MAP

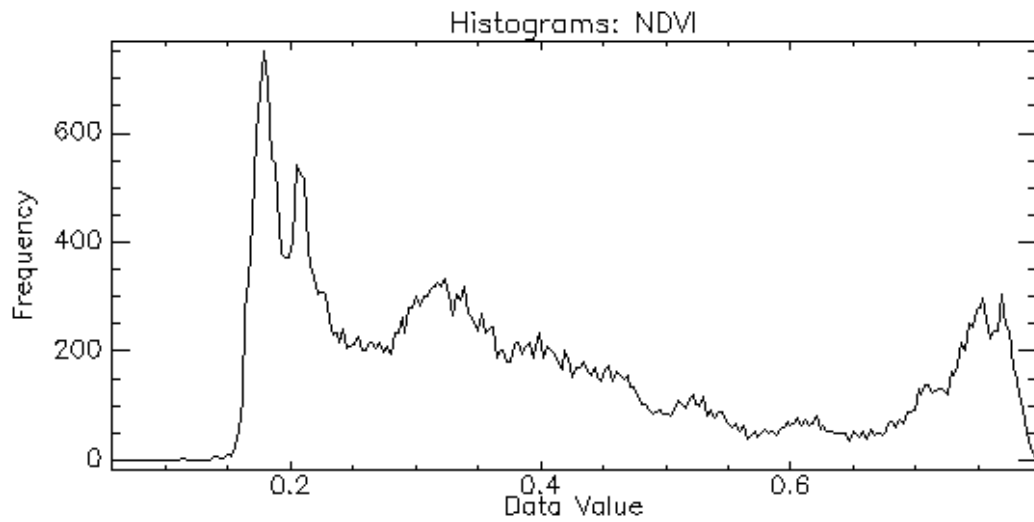


FIGURE 18. BARRAX, JD 145, NDVI HISTOGRAM

Basic Stats	Min	Max	Mean	Stdev
Data Value	0.06	0.80	0.39	0.19

TABLE 6. BARRAX, JD 145, NDVI BASIC STATISTICS



- FVC

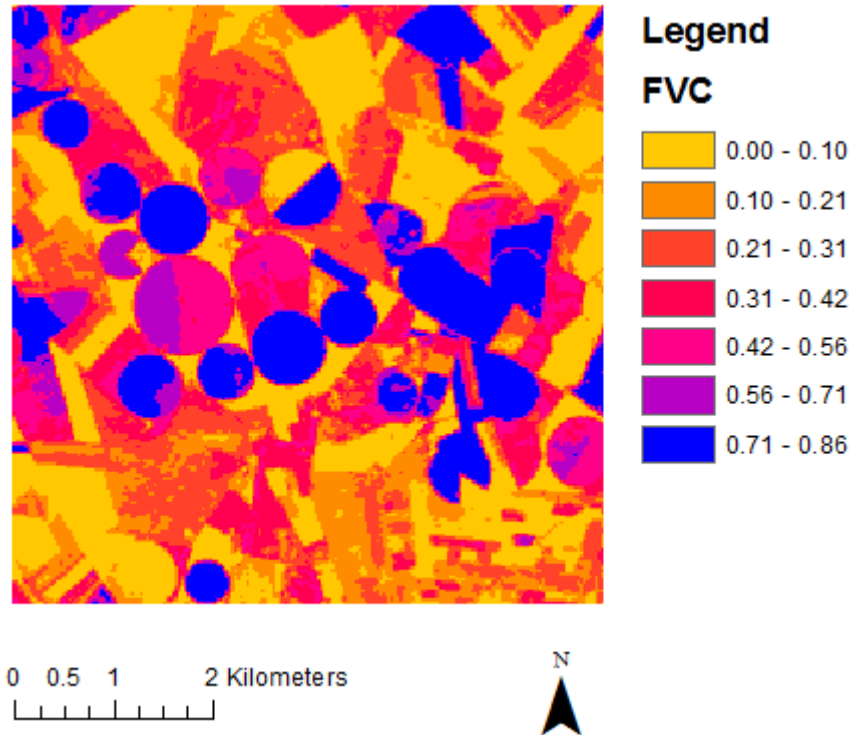


FIGURE 19. BARRAX, JD 145, FVC MAP

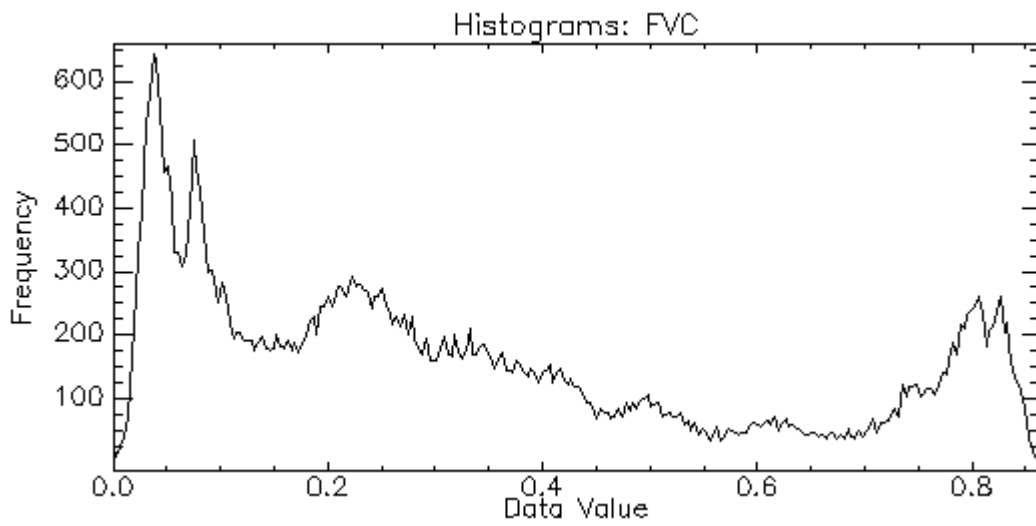


FIGURE 20. BARRAX, JD 145, FVC HISTOGRAM

Basic Stats	Min	Max	Mean	Stdev
Data Value	0.00	0.86	0.33	0.26

TABLE 7. BARRAX, JD 145, FVC BASIC STATISTICS

- LAI

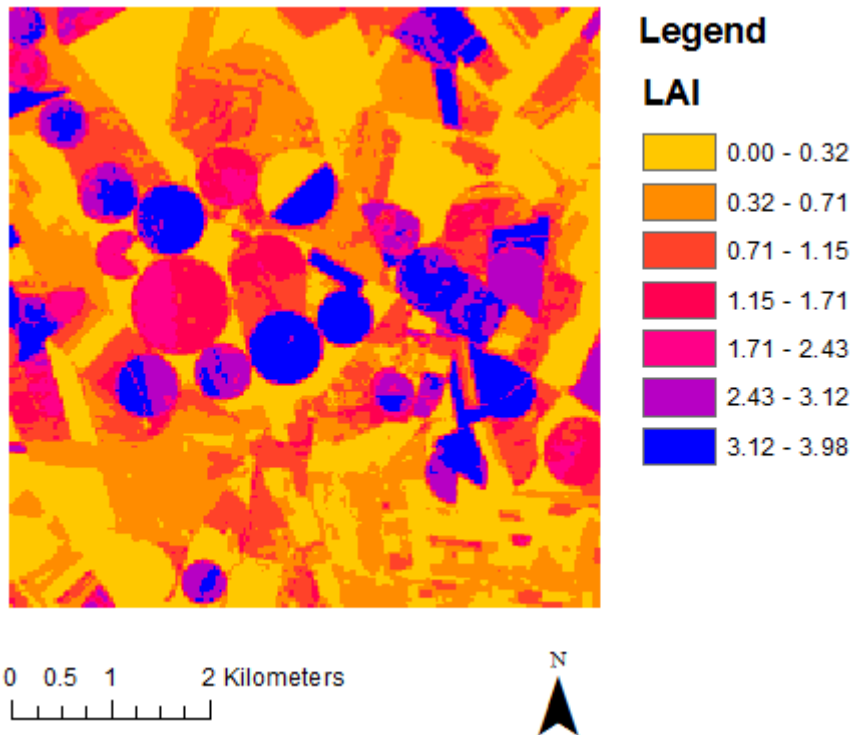


FIGURE 21. BARRAX, JD 145, LAI MAP

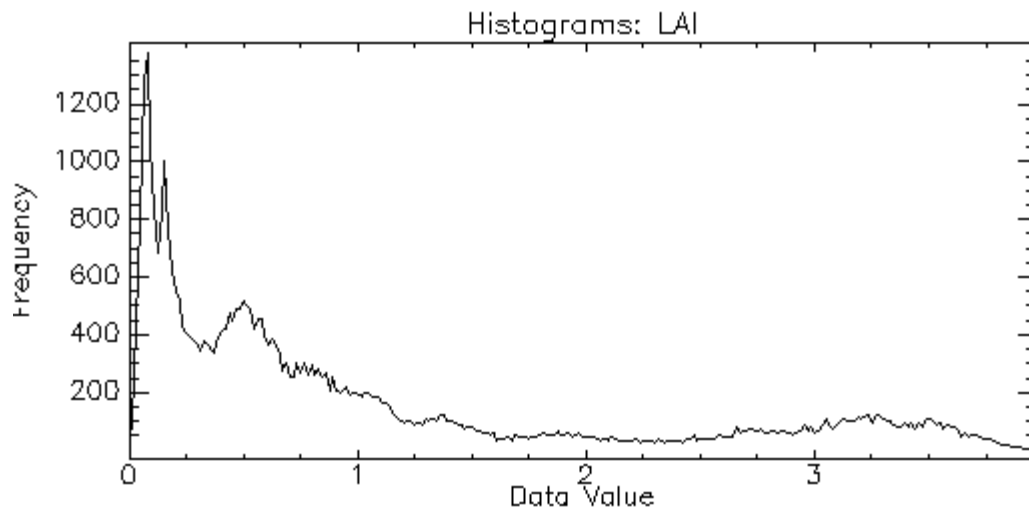


FIGURE 22. BARRAX, JD 145, LAI HISTOGRAM

Basic Stats	Min	Max	Mean	Stdev
Data Value	0.00	3.99	1.01	1.06

TABLE 8. BARRAX, JD 145, LAI BASIC STATISTICS

- Albedo

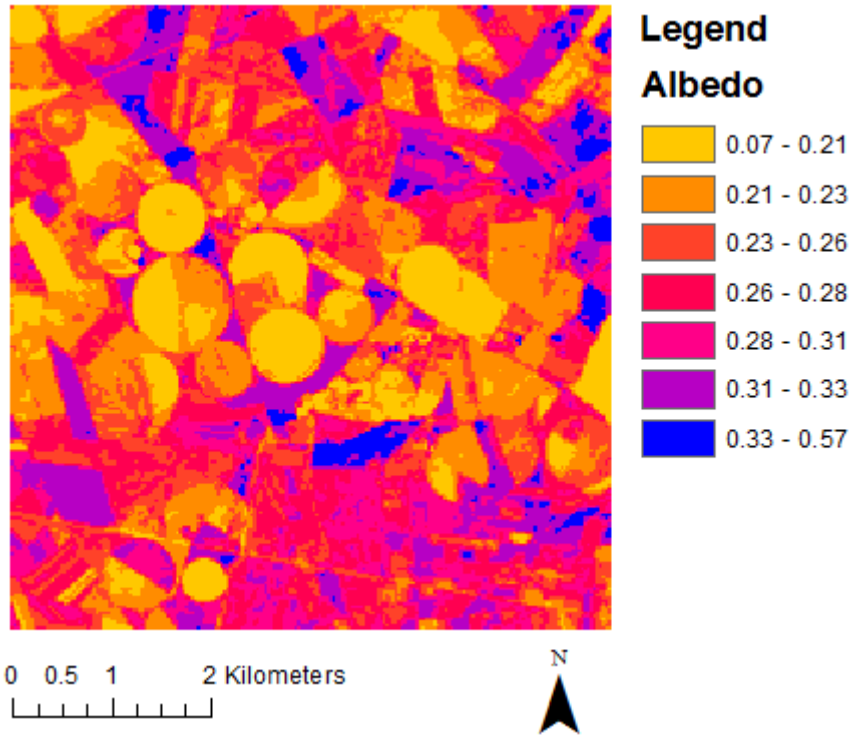


FIGURE 23. BARRAX, JD 145, ALBEDO MAP

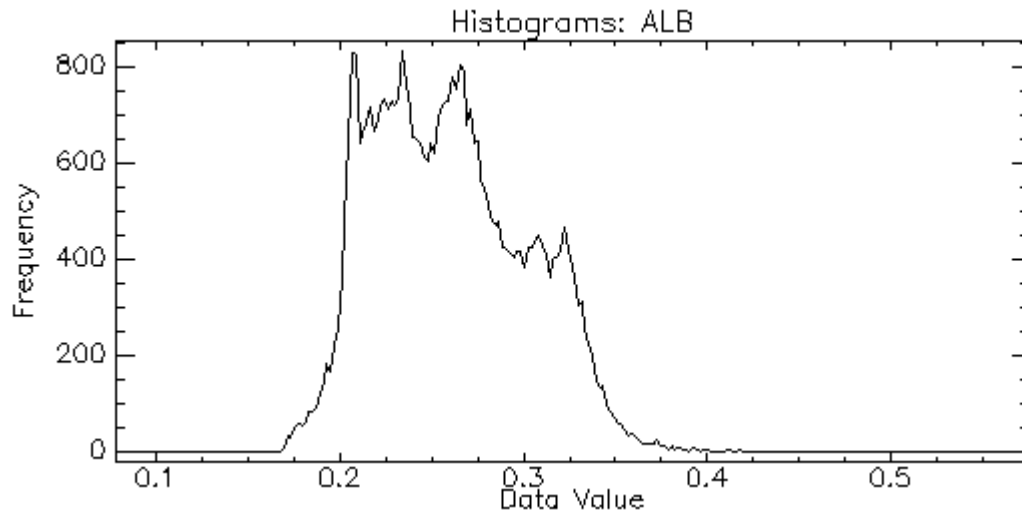


FIGURE 24. BARRAX, JD 145, ALBEDO HISTOGRAM

Basic Stats	Min	Max	Mean	Stdev
Data Value	0.08	0.58	0.26	0.04

TABLE 9. BARRAX, JD 145, ALBEDO BASIC STATISTICS

The areas with higher values of Albedo are urban or bare soil areas.

In the following tables are analysed the measured mean values of the area of Barrax, about LST, NDVI, LAI, FVC and Albedo; in the first column is indicated the Julian Day (JD) of the measures.

<b>2011</b>						
<b>JD</b>	<b>LST K</b>	<b>LST °C</b>	<b>NDVI</b>	<b>LAI</b>	<b>FVC</b>	<b>ALB</b>
<b>34</b>	283.92	10.77	0.22	0.21	0.10	0.17
<b>66</b>	290.30	17.15	0.24	0.28	0.12	0.19
<b>98</b>	301.23	28.08	0.42	1.00	0.35	0.20
<b>130</b>	298.84	25.69	0.47	1.43	0.43	0.19
<b>219</b>	320.44	47.29	0.20	0.56	0.18	0.23
<b>235</b>	319.68	46.53	0.19	0.43	0.15	0.23
<b>251</b>	318.13	44.98	0.19	0.36	0.12	0.21
<b>258</b>	309.97	36.82	0.17	0.25	0.10	0.21
<b>283</b>	305.87	32.72	0.15	0.22	0.09	0.20
<b>315</b>	294.64	21.49	0.15	0.20	0.08	0.17
<b>338</b>	285.86	12.71	0.18	0.19	0.08	0.13

TABLE 10. BARRAX 2011 RETRIEVED MEAN VALUES

<b>2012</b>						
<b>JD</b>	<b>LST K</b>	<b>LST °C</b>	<b>NDVI</b>	<b>LAI</b>	<b>FVC</b>	<b>ALB</b>
<b>5</b>	286.62	13.47	0.19	0.18	0.08	0.16
<b>30</b>	279.74	6.59	0.20	0.19	0.08	0.17
<b>46</b>	284.61	11.46	0.20	0.17	0.08	0.17
<b>69</b>	297.72	24.57	0.21	0.23	0.10	0.19
<b>78</b>	292.19	19.04	0.21	0.28	0.11	0.21
<b>101</b>	296.84	23.69	0.30	0.71	0.24	0.22
<b>149</b>	309.49	36.34	0.32	0.78	0.26	0.20
<b>165</b>	310.20	37.05	0.28	0.60	0.21	0.22
<b>190</b>	331.56	58.41	0.23	0.57	0.18	0.24
<b>206</b>	313.45	40.30	0.21	0.70	0.23	0.25
<b>213</b>	317.67	44.52	0.22	0.48	0.16	0.24
<b>238</b>	313.29	40.14	0.20	1.21	0.36	0.24
<b>277</b>	294.55	21.40	0.18	0.33	0.13	0.19
<b>302</b>	285.03	11.88	0.22	0.23	0.10	0.15
<b>334</b>	279.85	6.70	0.27	0.40	0.16	0.16

TABLE 11. BARRAX 2012 RETRIEVED MEAN VALUES

2013						
JD	LST K	LST °C	NDVI	LAI	FVC	ALB
32	287.68	14.53	0.21	0.22	0.10	0.19
55	282.28	9.13	0.24	0.29	0.12	0.19
80	287.37	14.22	0.29	0.47	0.19	0.20
96	283.77	10.62	0.36	0.86	0.29	0.17
104	298.29	25.14	0.42	1.15	0.36	0.24
143	300.77	27.62	0.45	1.43	0.40	0.22
152	301.54	28.39	0.41	1.12	0.35	0.25
175	309.56	36.41	0.31	0.62	0.22	0.23
200	318.47	45.32	0.27	0.50	0.16	0.28
223	316.93	43.78	0.27	0.58	0.16	0.26
248	308.24	35.09	0.25	0.43	0.14	0.26
255	303.90	30.75	0.26	0.44	0.15	0.23
328	283.20	10.05	0.22	0.23	0.09	0.21

TABLE 12. BARRAX 2013 RETRIEVED MEAN VALUES

2014						
JD	LST K	LST °C	NDVI	LAI	FVC	ALB
50	285.34	12.19	0.26	0.39	0.15	0.22
75	297.09	23.94	0.32	0.64	0.22	0.24
82	291.87	18.72	0.35	0.86	0.27	0.23
123	305.27	32.12	0.37	1.01	0.30	0.25
130	313.48	40.33	0.37	0.94	0.30	0.24
139	303.16	30.01	0.34	0.75	0.25	0.28
146	305.85	32.70	0.35	0.96	0.27	0.25
155	310.08	36.93	0.32	0.71	0.22	0.26
162	303.73	30.58	0.29	0.50	0.19	0.26
171	304.80	31.65	0.27	0.40	0.16	0.28
178	309.65	36.50	0.26	0.46	0.15	0.26
194	317.21	44.06	0.25	0.44	0.14	0.27
203	320.40	47.25	0.25	0.49	0.14	0.29
219	325.26	52.11	0.24	0.41	0.13	0.29
226	307.31	34.16	0.25	0.39	0.13	0.28
235	320.24	47.09	0.25	0.44	0.13	0.28
242	310.82	37.67	0.25	0.45	0.13	0.26
251	318.81	45.66	0.23	0.27	0.10	0.27

TABLE 13. BARRAX 2014 RETRIEVED MEAN VALUES

2015						
JD	LST K	LST °C	NDVI	LAI	FVC	ALB
5	282.46	9.31	0.24	0.34	0.13	0.20
53	282.69	9.54	0.25	0.36	0.14	0.24
69	298.00	24.85	0.31	0.63	0.22	0.23
110	292.29	19.14	0.47	1.35	0.43	0.25
126	305.56	32.41	0.45	1.43	0.40	0.25
142	307.56	34.41	0.37	0.98	0.30	0.27
158	312.88	39.73	0.32	0.69	0.23	0.28
181	314.83	41.68	0.25	0.36	0.13	0.27
190	316.85	43.70	0.24	0.34	0.12	0.29
213	317.83	44.68	0.24	0.38	0.12	0.28
245	314.39	41.24	0.24	0.38	0.12	0.26
302	285.37	12.22	0.22	0.18	0.10	0.25
350	278.06	4.91	0.17	0.07	0.03	0.22

TABLE 14. BARRAX 2015 RETRIEVED MEAN VALUES

2016						
JD	LST K	LST °C	NDVI	LAI	FVC	ALB
24	288.48	15.33	0.24	0.31	0.13	0.20
33	286.47	13.32	0.23	0.26	0.11	0.20
65	285.41	12.26	0.30	0.55	0.20	0.22
72	291.77	18.62	0.29	0.54	0.18	0.23
145	306.27	33.12	0.39	1.01	0.33	0.26
152	306.17	33.02	0.39	1.13	0.33	0.25
161	316.88	43.73	0.34	0.73	0.25	0.27
184	318.65	45.50	0.27	0.46	0.16	0.26
193	323.32	50.17	0.25	0.36	0.13	0.28
200	314.04	40.89	0.25	0.38	0.13	0.27
209	321.04	47.89	0.25	0.43	0.14	0.29
225	313.06	39.91	0.24	0.38	0.13	0.28
241	319.81	46.66	0.24	0.30	0.12	0.28
257	303.94	30.79	0.21	0.14	0.08	0.32

TABLE 15. BARRAX 2016 RETRIEVED MEAN VALUES

It is possible to plot the data, having a graphical vision of the mean values retrieved. LST data seems to be consistent from the different years with similar mean values. This is also true for FVC and LAI showing that the vegetation seasons were the same over the years.

Albedo has a small variability over the year between summer and winter.

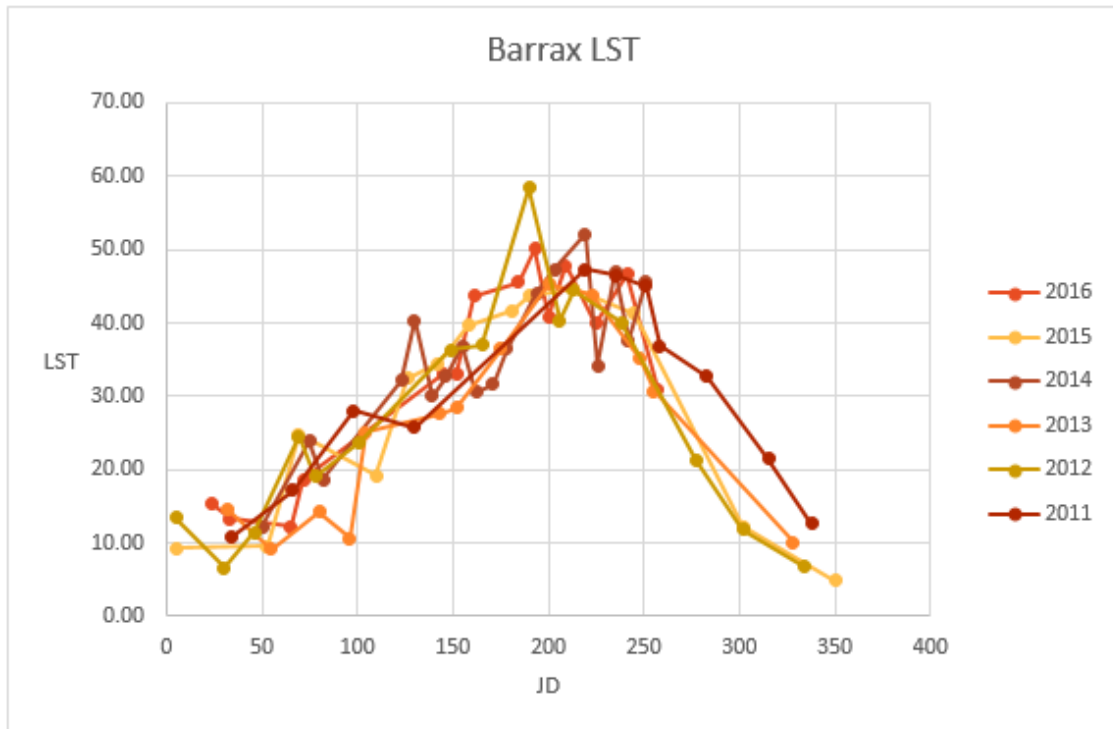


FIGURE 25. BARRAX, PLOT OF RETRIEVED LST MEAN VALUES

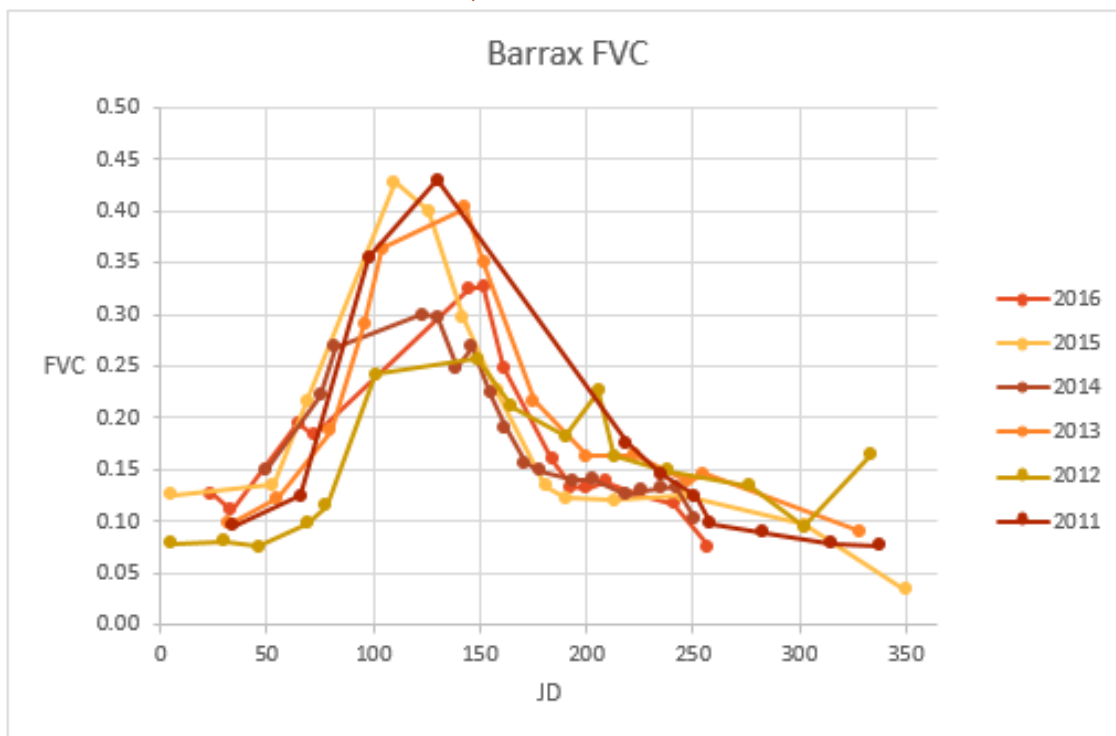


FIGURE 26. BARRAX, PLOT OF RETRIEVED FVC MEAN VALUES

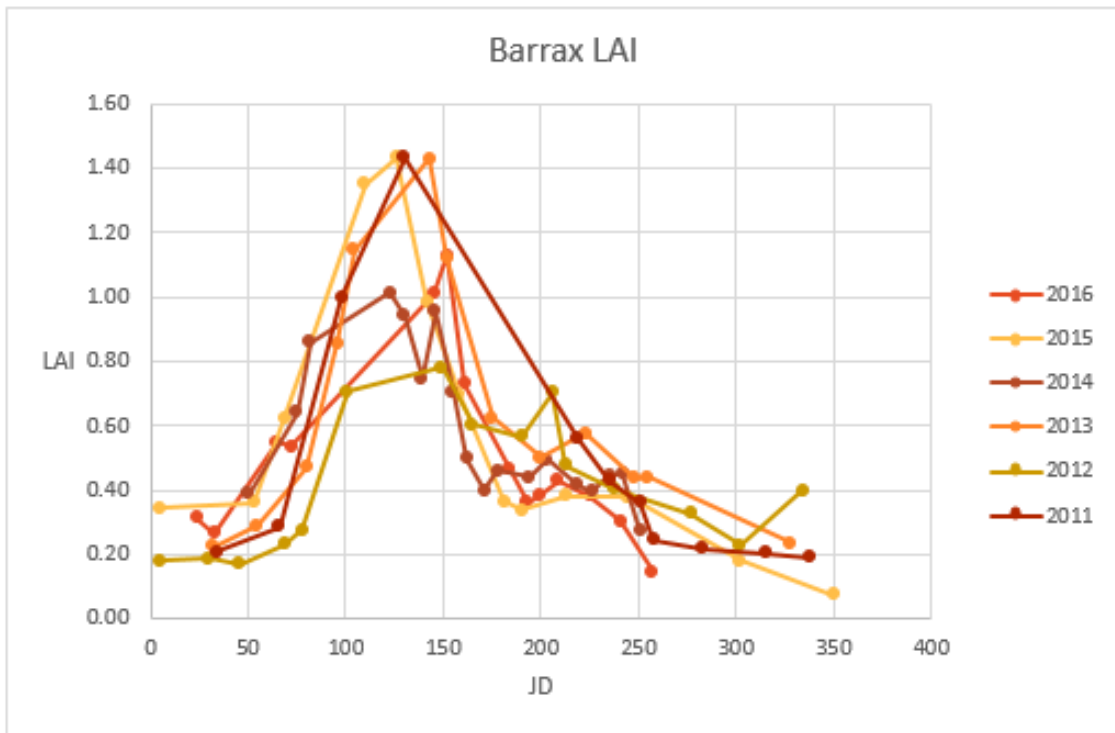


FIGURE 27. BARRAX, PLOT OF RETRIEVED LAI MEAN VALUES

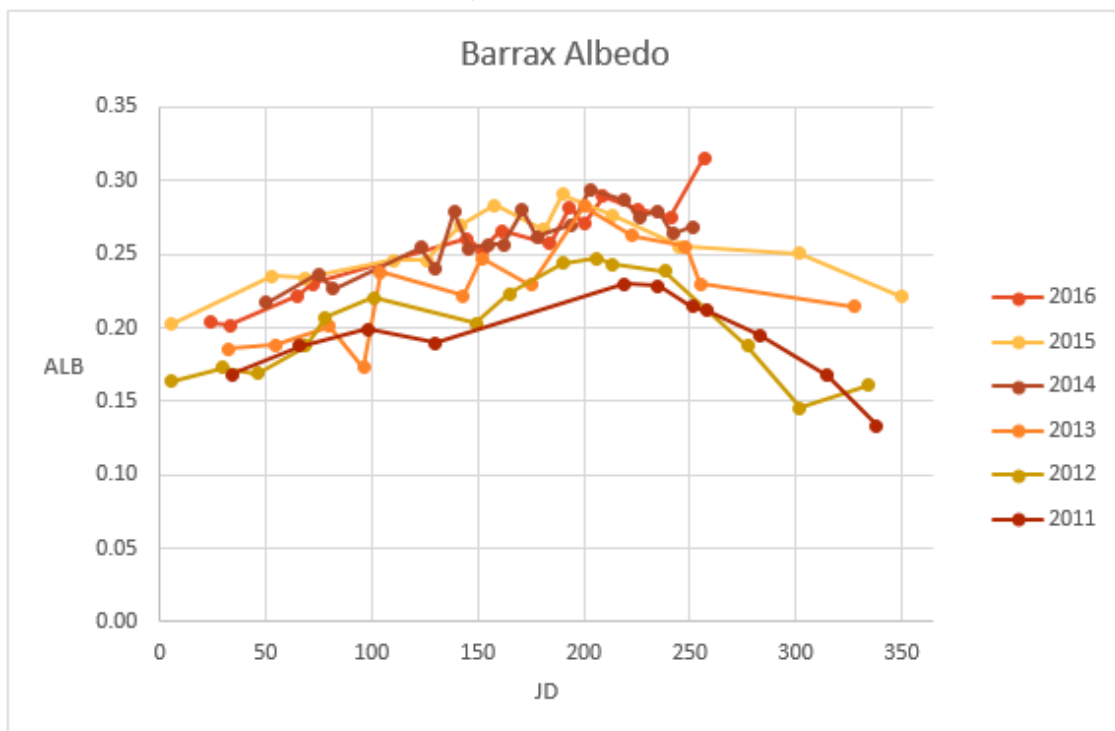


FIGURE 28. BARRAX, PLOT OF RETRIEVED ALBEDO MEAN VALUES



As mentioned in the first chapter, LAI index depends from FVC index, in the following graphs is possible to see the correlation among the two indices, where the operator  $R^2$  is always closer to 1, indicating a good linear correlation.

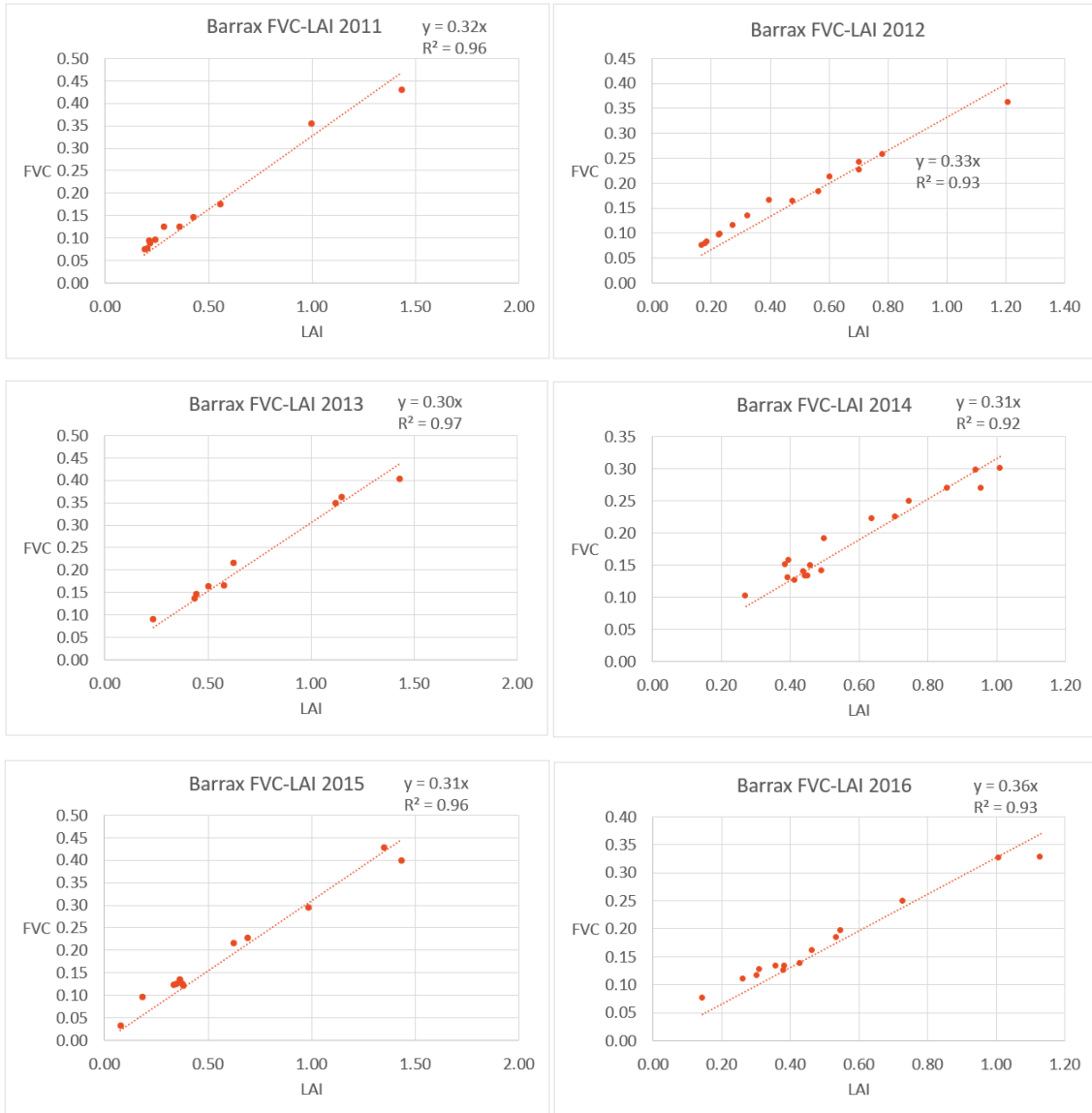


FIGURE 29. BARRAX, PLOT OF COMPARED FVC - LAI VALUES

#### 4.1.4 Foggia

The imageries processed in Foggia's area are 87, the imageries used for the analysis in Foggia are 53, have been excluded the cloudy ones and has been decided to work only with Landsat 8 for the year 2015. Landsat 8 images have a large file size, at approximately 1 GB compressed, Landsat 7 approximately 0.3 GB compressed.



FIGURE 30. FOGGIA, L8 IMAGERY ON THE 31ST OF MARCH 2016, JD 091

In this area, there are not only field, like in Barrax's area, but there are some urban areas, a little lake, and other zones that are not considerable for our analysis.

For this reason, is necessary to build a Region Of Interest and not consider in the analysis the "infesting" pixel.

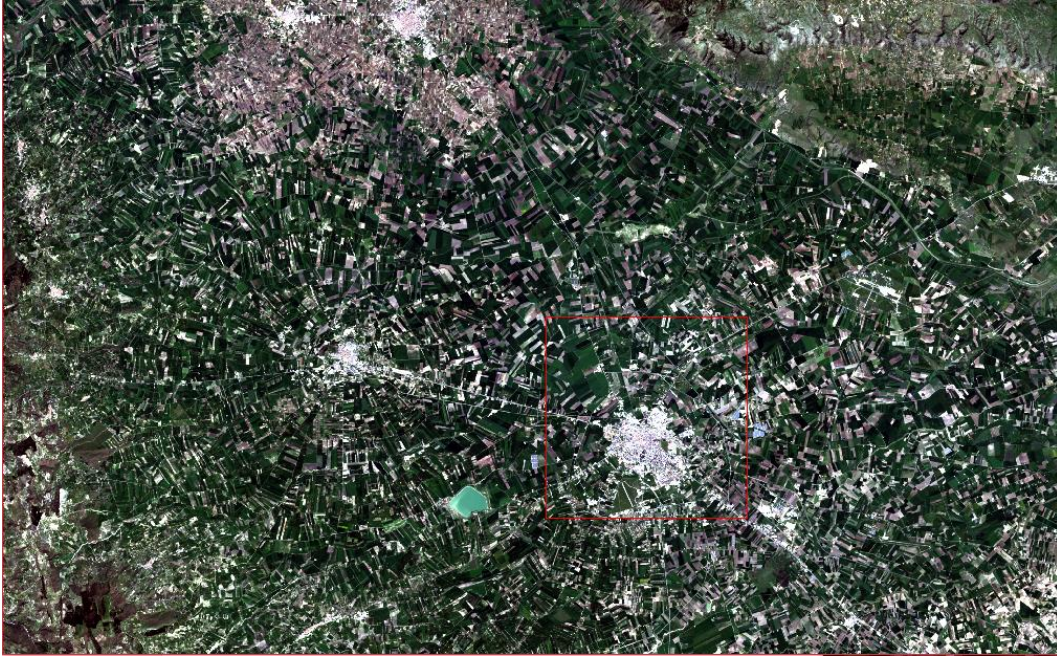


FIGURE 31. FOGGIA L8 ZOOMED IMAGERY ON THE 31ST OF MARCH 2016 AREA STUDY, JD 091

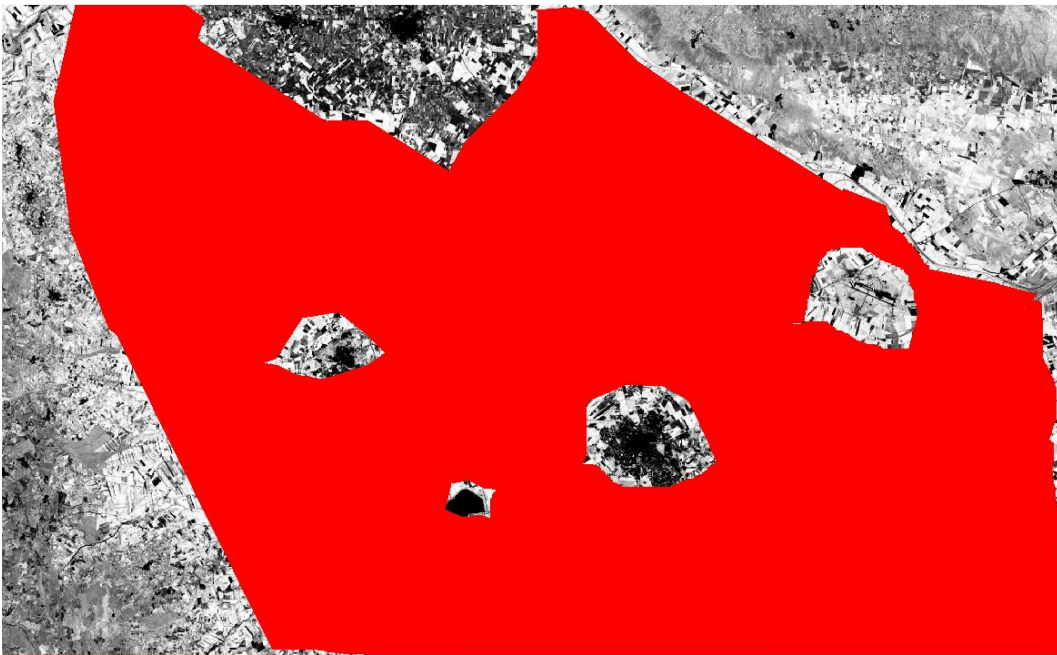


FIGURE 32. FOGGIA, JD 091 USED ROI FOR STATISTICAL ANALYSIS

Analysing the pixels inside the ROI is possible to obtain the mean values of LST, NDVI, FVC, LAI and Albedo. In the next images is possible to see an example of the processing result of 1 of the 53 imageries elaborated, about the image of Julian Day 091, 31<sup>st</sup> of March 2016. For each datum is plotted the map in .tiff format, the histogram of the data values and the basics statistics.

- LST

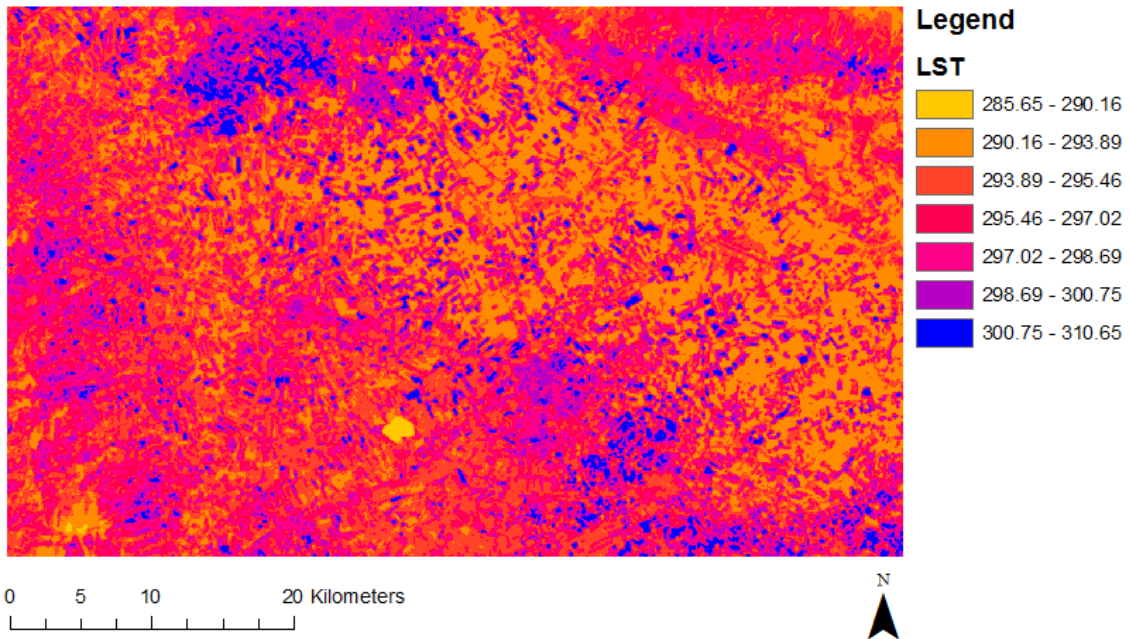


FIGURE 33. FOGGIA, JD 091, LST MAP

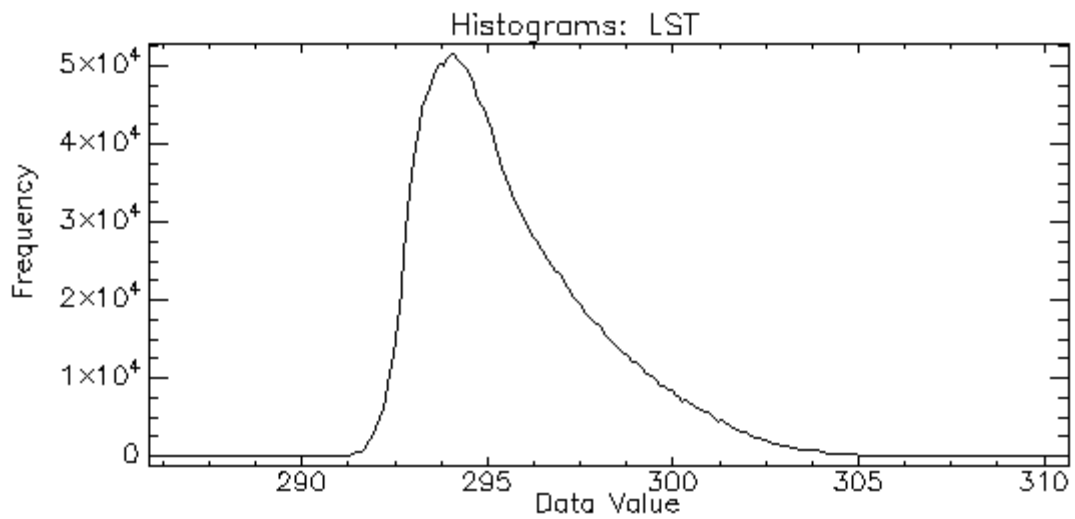


FIGURE 34. FOGGIA, JD 091, LST HISTOGRAM

Basic Stats	Min	Max	Mean	Stdev
Data Value [K]	285.86	310.65	295.69	2.33

TABLE 16. FOGGIA, JD 091, LST BASIC STATISTICS

- NDVI

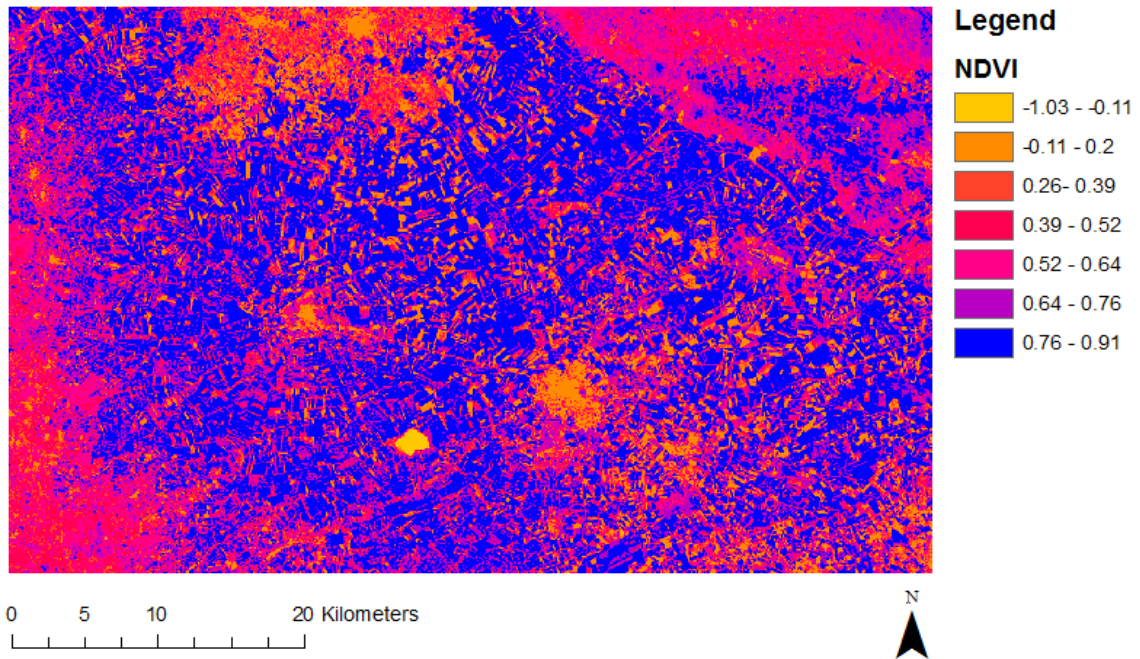


FIGURE 35. FOGGIA, JD 091, NDVI MAP

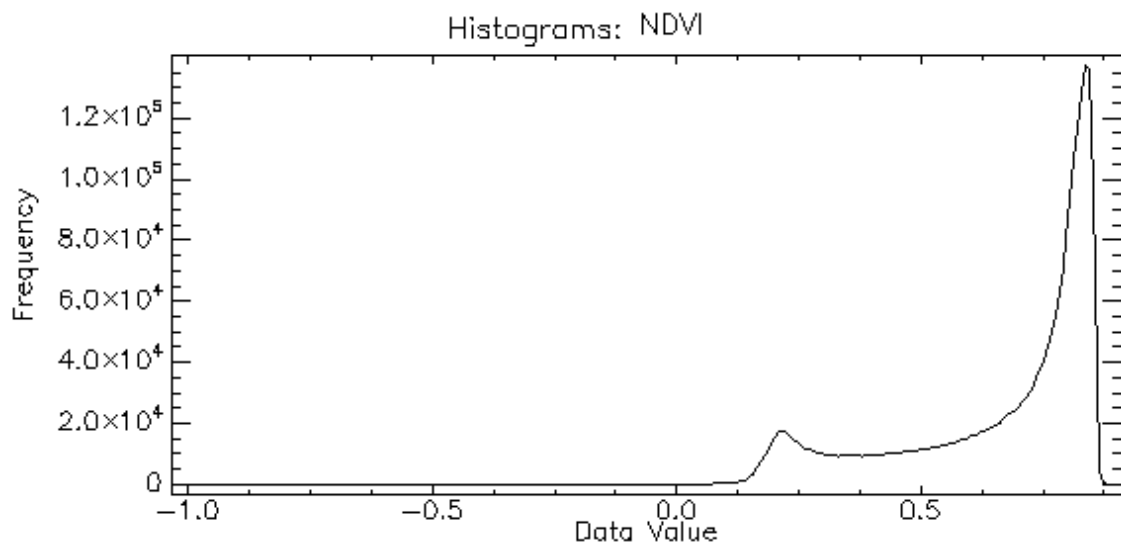


FIGURE 36. FOGGIA, JD 091, NDVI HISTOGRAM

Basic Stats	Min	Max	Mean	Stdev
Data Value	-1.03	0.91	0.67	0.20

TABLE 17. FOGGIA, JD 091, NDVI BASIC STATISTICS

- FVC

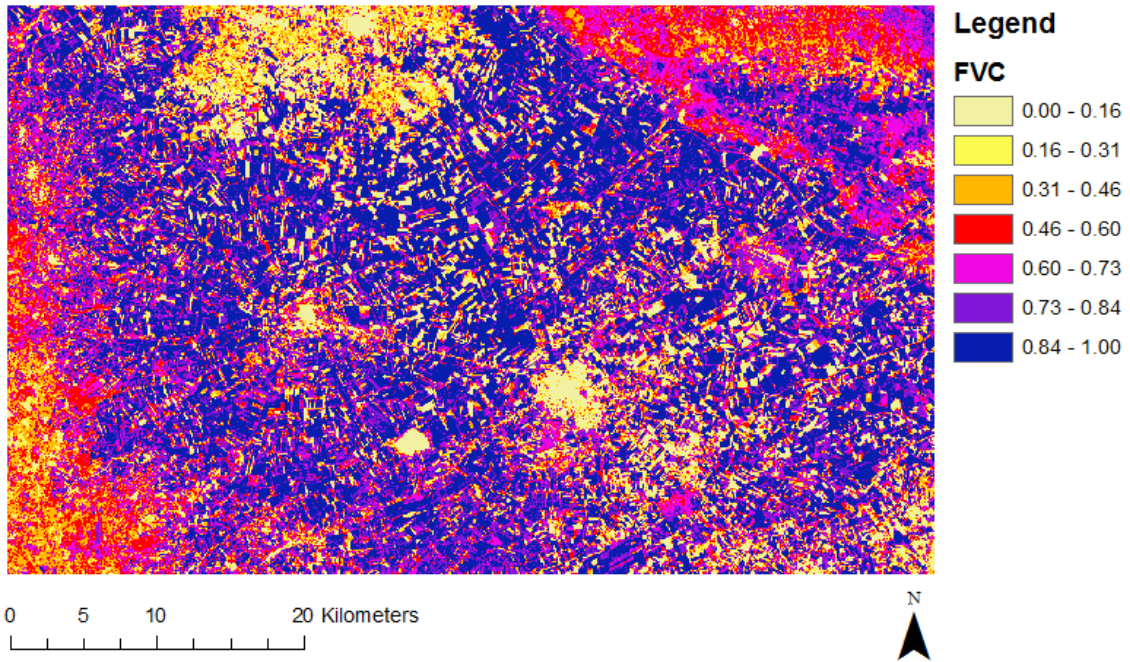


FIGURE 37. FOGGIA, JD 091, FVC MAP

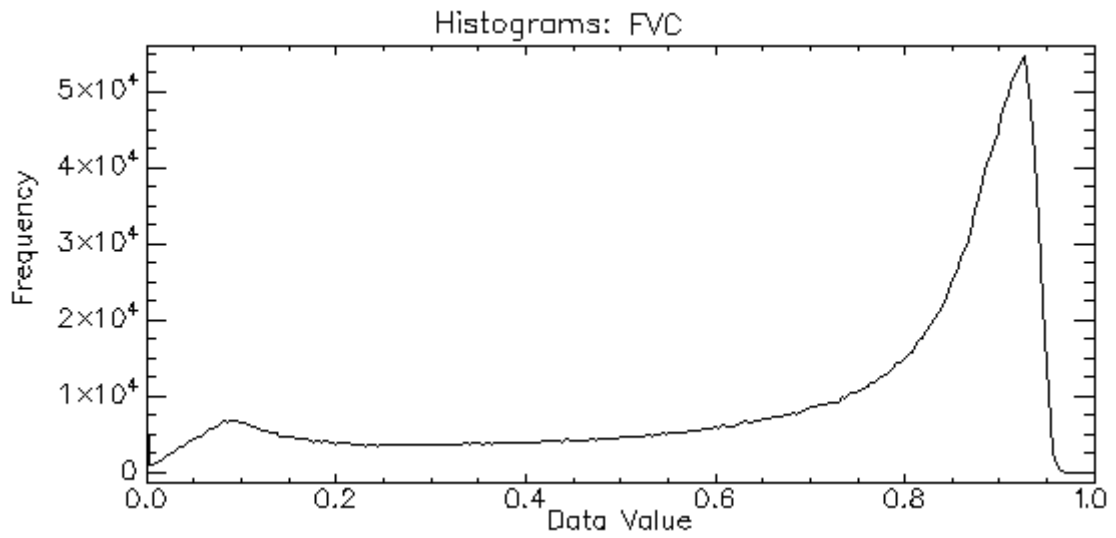


FIGURE 38. FOGGIA, JD 091, FVC HISTOGRAM

Basic Stats	Min	Max	Mean	Stdev
Data Value	0.00	1.00	0.69	0.27

TABLE 18. FOGGIA, JD 091, FVC BASIC STATISTICS

- LAI

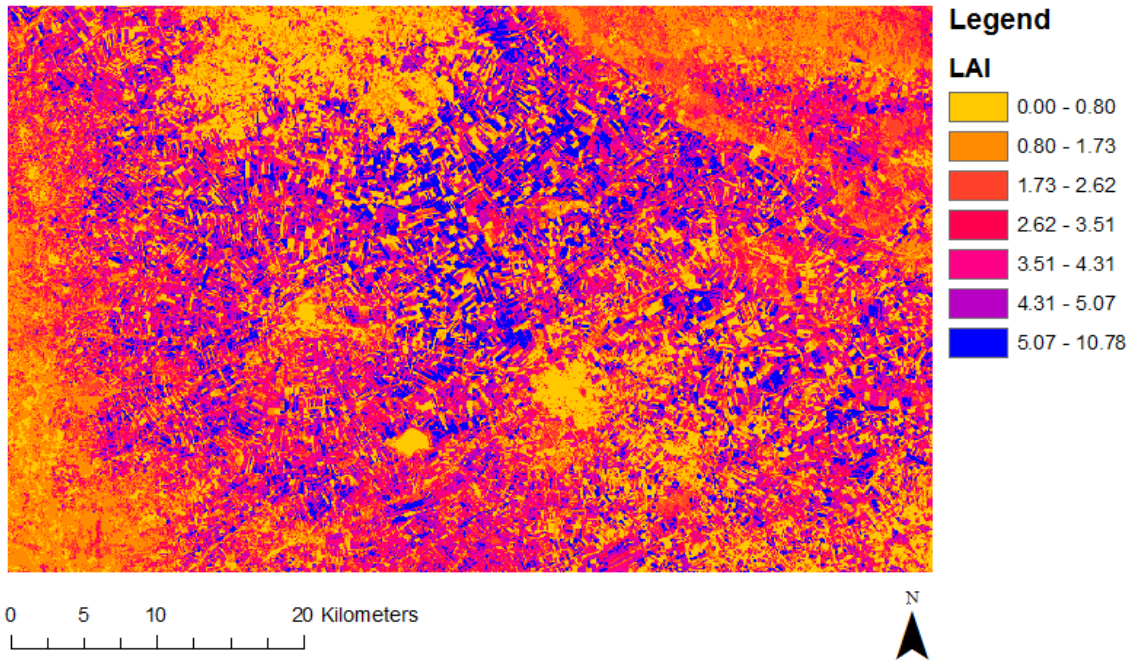


FIGURE 39 FOGGIA, JD 091, LAI MAP

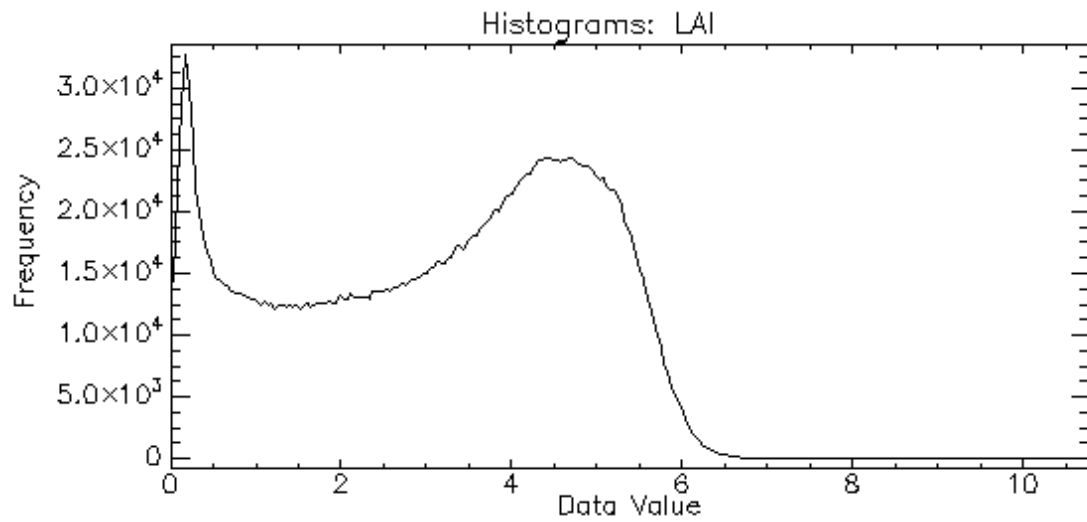


FIGURE 40. FOGGIA, JD 091, LAI HISTOGRAM

Basic Stats	Min	Max	Mean	Stdev
Data Value	0.00	10.78	3.13	1.74

TABLE 19. FOGGIA, JD 091, LAI BASIC STATISTICS

- Albedo

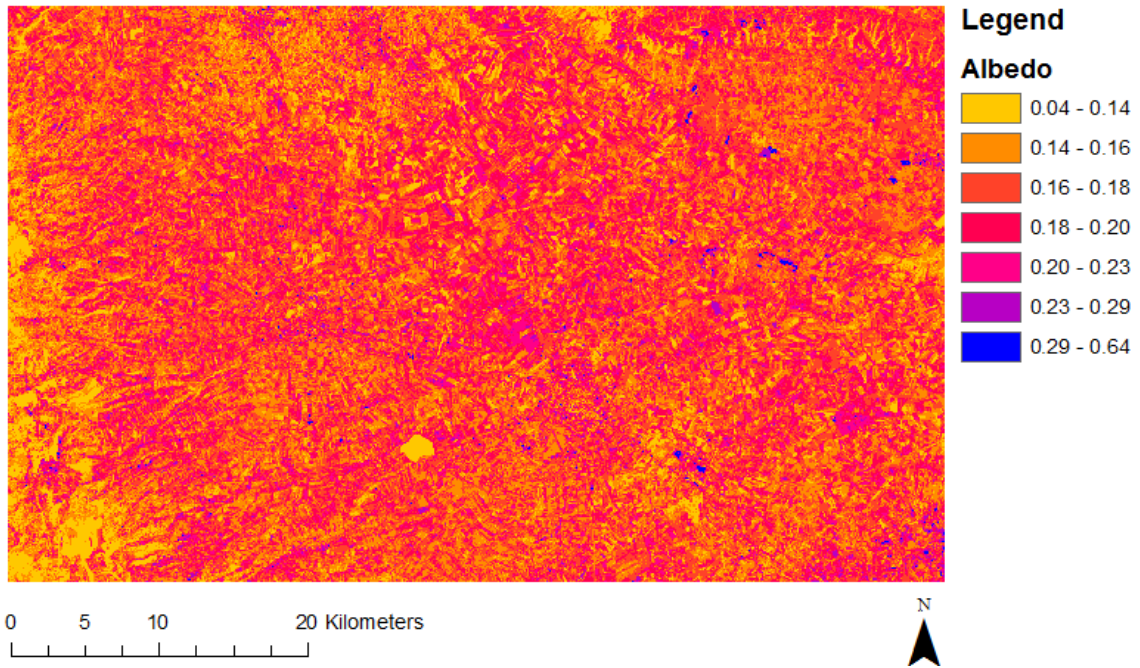


FIGURE 41. FOGGIA, JD 091, ALBEDO MAP

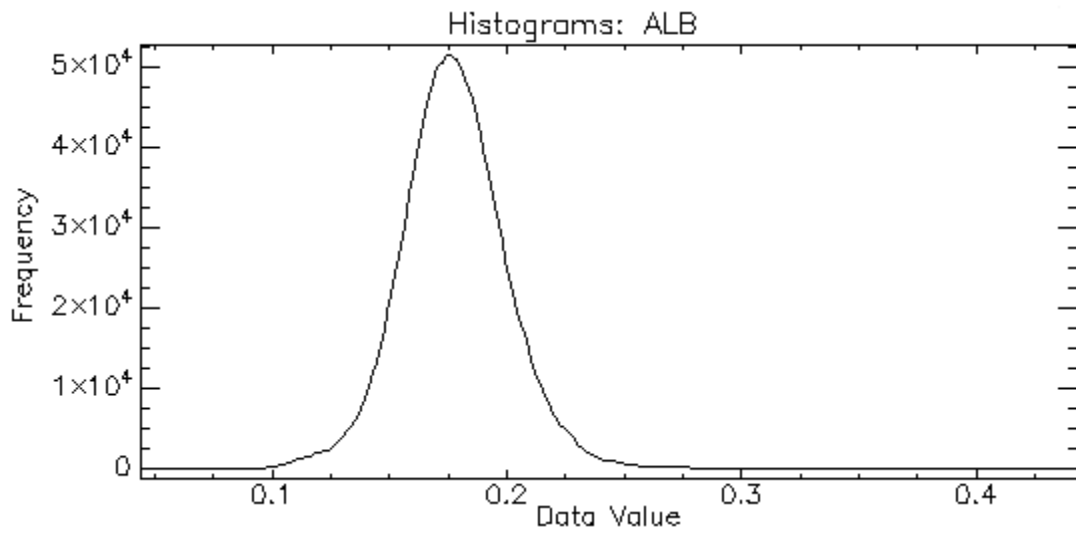


FIGURE 42. FOGGIA, JD 091, ALBEDO HISTOGRAM

Basic Stats	Min	Max	Mean	Stdev
Data Value	0.04	0.45	0.18	0.02

TABLE 20. FOGGIA, JD 091, ALBEDO BASIC STATISTICS



In the following tables is possible to take a look of the measured mean values of the area of Foggia, about LST, NDVI, LAI, FVC and Albedo; in the first column is indicated the Julian Day (JD) of the measures.

<b>2011</b>						
<b>JD</b>	<b>LST K</b>	<b>LST °C</b>	<b>NDVI</b>	<b>LAI</b>	<b>FVC</b>	<b>ALB</b>
<b>37</b>	288.52	15.37	0.40	0.94	0.34	0.14
<b>69</b>	287.67	14.52	0.50	1.47	0.47	0.15
<b>85</b>	291.30	18.15	0.54	1.65	0.52	0.16
<b>101</b>	297.34	24.19	0.60	2.16	0.60	0.17
<b>229</b>	316.30	43.15	0.19	0.47	0.18	0.16
<b>245</b>	318.25	45.10	0.17	0.37	0.15	0.16
<b>261</b>	314.76	41.61	0.17	0.38	0.16	0.15
<b>277</b>	307.58	34.43	0.18	0.44	0.17	0.14
<b>341</b>	288.70	15.55	0.21	0.45	0.18	0.11

TABLE 21. FOGGIA 2011 RETRIEVED MEAN VALUES

<b>2012</b>						
<b>JD</b>	<b>LST K</b>	<b>LST °C</b>	<b>NDVI</b>	<b>LAI</b>	<b>FVC</b>	<b>ALB</b>
<b>88</b>	297.89	24.74	0.51	1.57	0.48	0.16
<b>152</b>	306.71	33.56	0.25	0.38	0.16	0.20
<b>168</b>	318.87	45.72	0.23	0.31	0.12	0.22
<b>184</b>	324.71	51.56	0.19	0.33	0.13	0.22
<b>200</b>	316.84	43.69	0.19	0.50	0.18	0.20
<b>216</b>	322.92	49.77	0.18	0.60	0.22	0.19
<b>232</b>	315.94	42.79	0.17	0.48	0.18	0.18
<b>280</b>	310.22	37.07	0.19	0.44	0.18	0.15
<b>296</b>	302.63	29.48	0.18	0.48	0.19	0.14

TABLE 22. FOGGIA 2012 RETRIEVED MEAN VALUES

2013						
JD	LST K	LST °C	NDVI	LAI	FVC	ALB
106	299.25	26.10	0.66	2.89	0.68	0.17
194	317.56	44.41	0.27	0.42	0.16	0.22
210	326.27	53.12	0.25	0.35	0.14	0.21
226	317.60	44.45	0.23	0.31	0.11	0.20
290	292.75	19.60	0.19	0.25	0.09	0.19
362	286.03	12.88	0.22	0.52	0.21	0.11

TABLE 23. FOGGIA 2013 RETRIEVED MEAN VALUES

2014						
JD	LST K	LST °C	NDVI	LAI	FVC	ALB
45	280.99	7.84	0.34	0.92	0.33	0.19
77	296.77	23.62	0.60	2.21	0.60	0.16
125	294.07	20.92	0.55	1.75	0.54	0.16
141	306.07	32.92	0.41	1.00	0.36	0.14
157	312.17	39.02	0.27	0.41	0.17	0.16
173	315.14	41.99	0.23	0.44	0.17	0.17
197	307.26	34.11	0.31	0.56	0.21	0.21
221	312.45	39.30	0.25	0.45	0.18	0.16
261	307.01	33.86	0.27	0.42	0.17	0.18
293	303.09	29.94	0.24	0.41	0.14	0.15
325	291.61	18.46	0.24	0.41	0.14	0.13

TABLE 24. FOGGIA 2014 RETRIEVED MEAN VALUES

2015						
JD	LST K	LST °C	NDVI	LAI	FVC	ALB
8	280.00	6.75	0.29	0.48	0.19	0.16
88	276.67	3.42	0.44	1.15	0.38	0.23
152	311.23	37.98	0.32	0.56	0.23	0.18
184	316.93	43.68	0.26	0.39	0.15	0.23
200	329.24	55.99	0.26	0.39	0.15	0.22
216	316.82	43.57	0.26	0.39	0.15	0.21
264	294.12	20.87	0.23	0.30	0.11	0.16
312	288.13	14.88	0.26	0.39	0.15	0.18

TABLE 25. FOGGIA 2015 RETRIEVED MEAN VALUES

2016						
JD	LST K	LST °C	NDVI	LAI	FVC	ALB
91	295.69	22.54	0.67	3.13	0.69	0.18
131	303.29	30.14	0.53	1.61	0.51	0.16
139	299.77	26.62	0.51	1.52	0.48	0.15
147	309.34	36.19	0.36	0.77	0.29	0.15
163	298.69	25.54	0.23	0.32	0.13	0.18
187	318.39	45.24	0.29	0.50	0.19	0.21
195	315.26	42.11	0.25	0.40	0.16	0.19
203	317.82	44.67	0.30	0.54	0.20	0.21
227	313.65	40.50	0.28	0.58	0.22	0.17
243	318.67	45.52	0.24	0.46	0.19	0.16

TABLE 26. FOGGIA 2016 RETRIEVED MEAN VALUES

Is possible to plot the data, having a graphical vision of the mean values retrieved.

LST follows a season shape with higher temperatures in summer than winter, as expected. 2015, 2013, 2012 have hotter values.

FVC and LAI have higher values during winter till the beginning of April, as expected this period is the most intensive cultivation time.

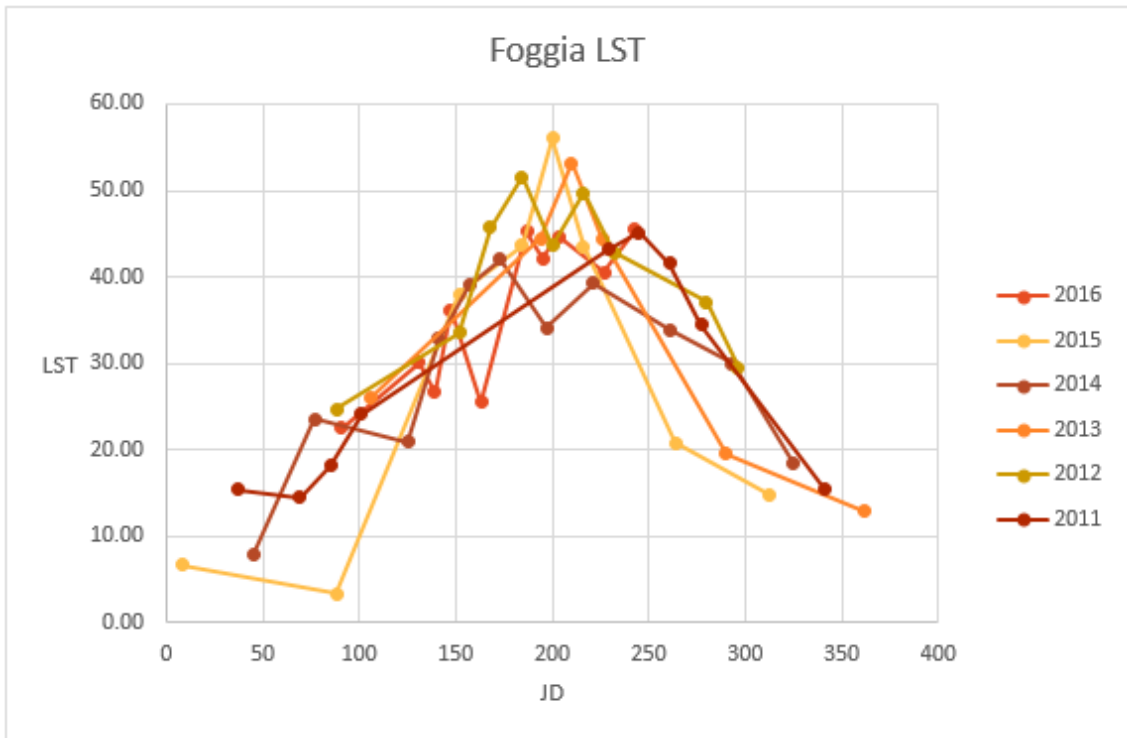


FIGURE 43. FOGGIA, PLOT OF RETRIEVED LST MEAN VALUES

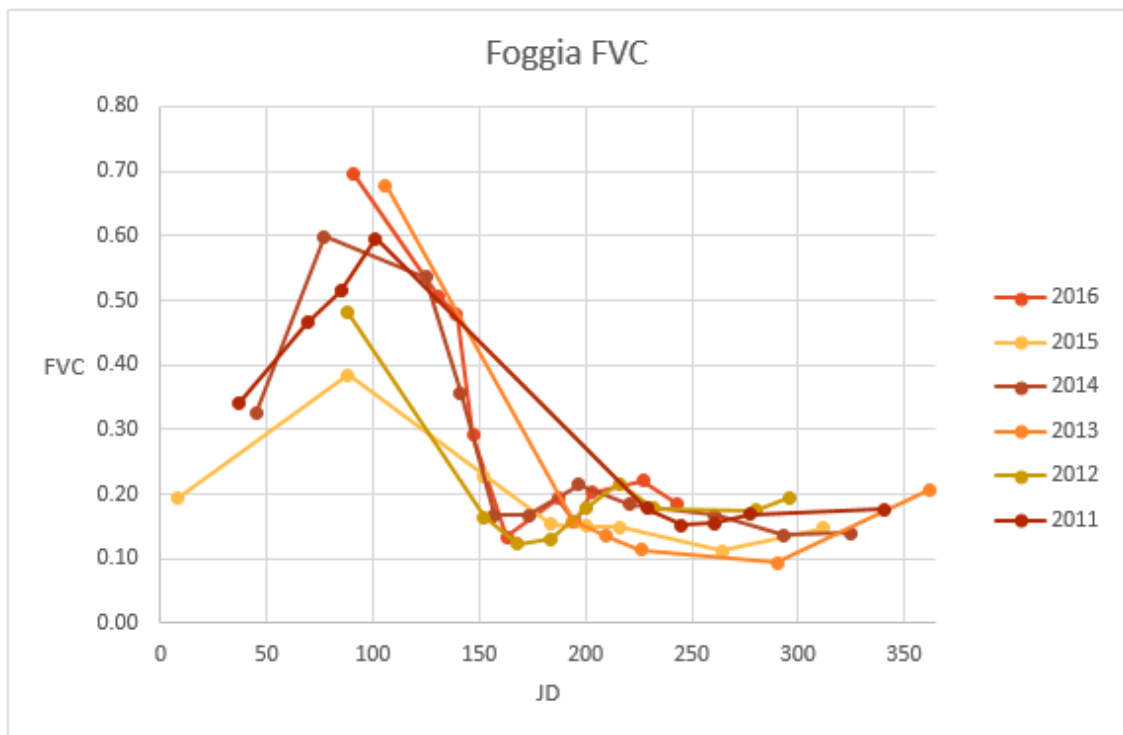


FIGURE 44. FOGGIA, PLOT OF RETRIEVED FVC MEAN VALUES

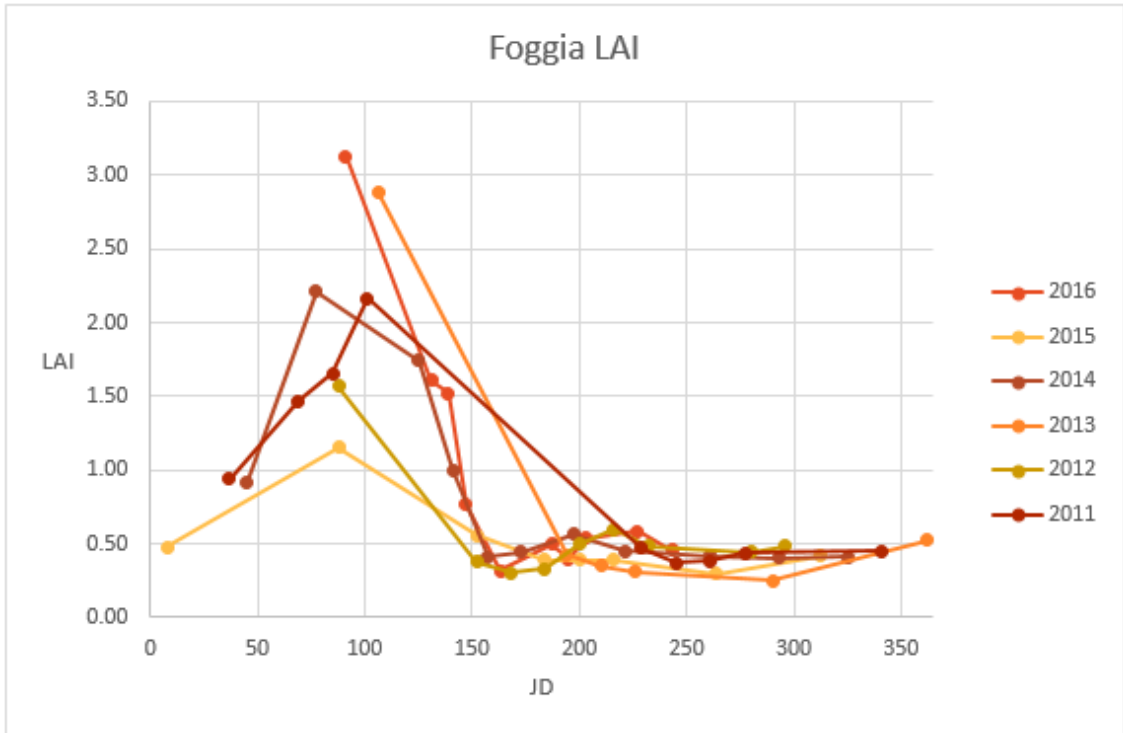


FIGURE 45. FOGGIA, PLOT OF RETRIEVED LAI MEAN VALUES

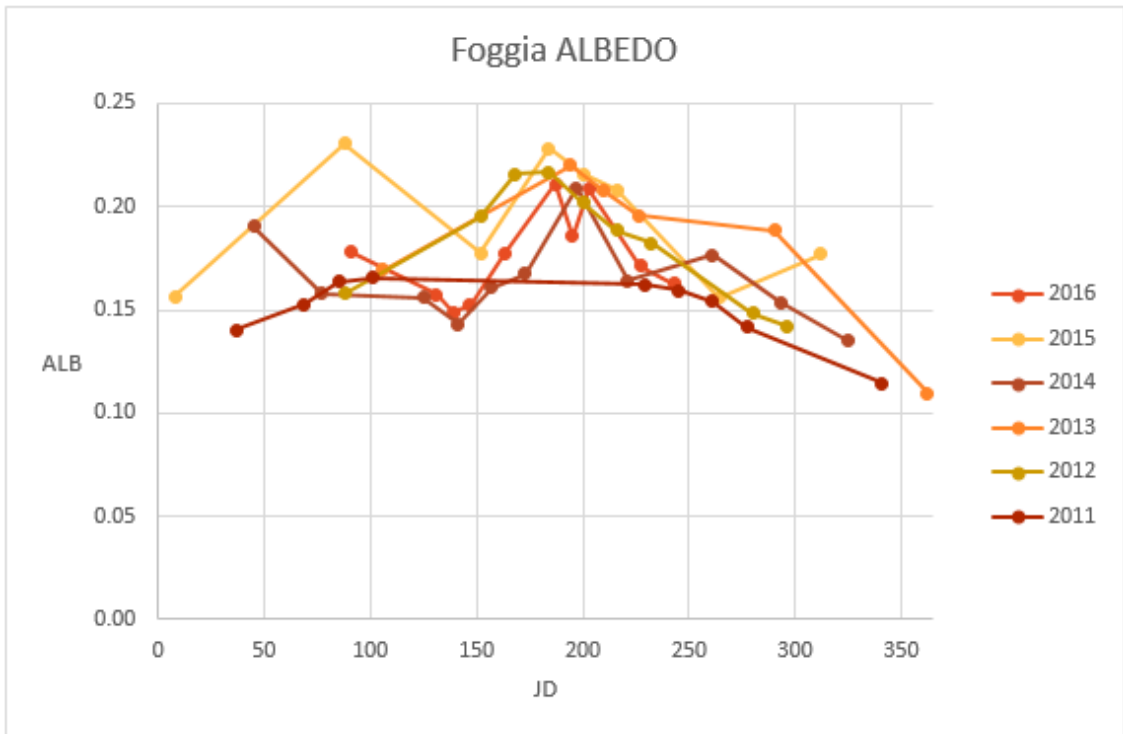


FIGURE 46. FOGGIA, PLOT OF RETRIEVED ALBEDO MEAN VALUES

As mentioned in the first chapter, LAI index depends from FVC index, in the following graphs is possible to see the correlation among the two indices, where the operator  $R^2$  is always closer to 1, indicating a good linear correlation.

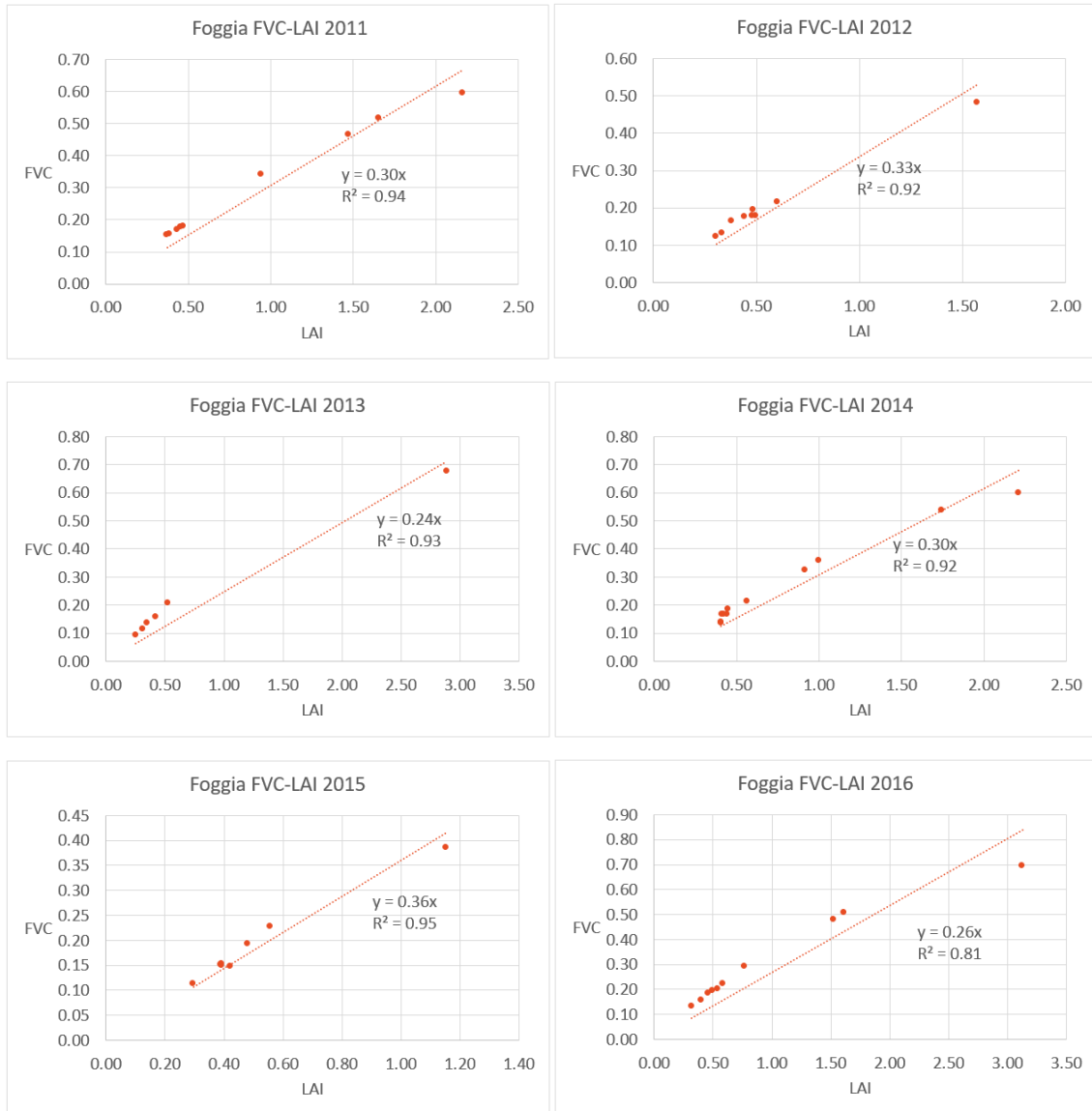


FIGURE 47. FOGGIA, PLOT OF COMPARED FVC – LAI VALUES

## 4.2 ANALYSIS OF THE RELATIONSHIP LST-VIs

The relationship between LST and a VI, in particular with FVC, is also analysed, which is of interest in hydrological estimates. The shape in the LST – VI feature space results to be a triangle (or trapezoid), because of the low sensitivity of LST to soil moisture variations over vegetated areas, and an increased sensitivity (and thus greater spatial variation) over areas of bare soil.

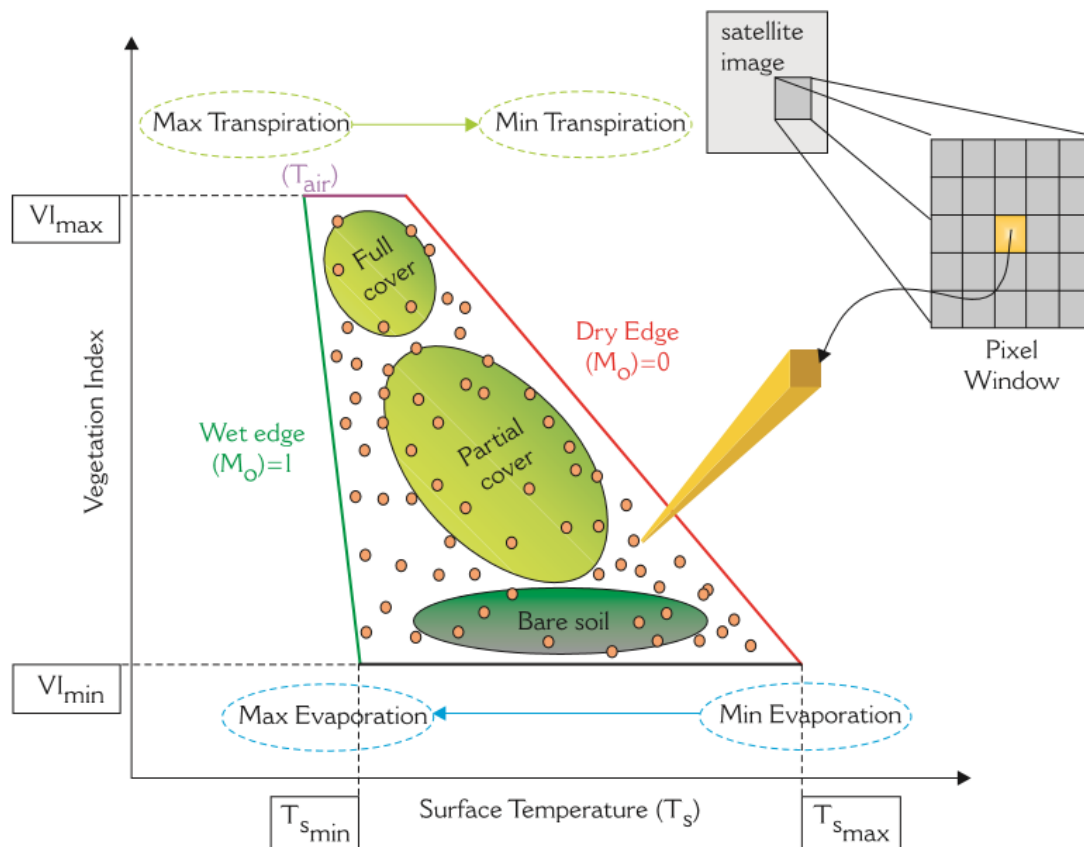


FIGURE 48. THEORY OF THE TRIANGLE

“Referring back to Figure 48, the right-hand border of the triangle (or trapezoid) (the so called ‘dry edge or warm edge’) is defined by the locus of points of highest temperature but which contain differing amounts of bare soil and vegetation, and is assumed to represent conditions of limited surface soil moisture.

Likewise, the left-hand edge (the so-called ‘wet edge or cold edge’) corresponds to the set of cooler pixels that have varying amounts of vegetation cover and have the maximum

soil water content. Variation along the lower edge (i.e., the ‘base’) of the triangle (or trapezoid), is assumed to reflect the combined effects of soil water content and topography variations across areas of bare soil,

while the triangle’s (or trapezoid’s) apex equates to the status of full vegetation cover (expressed by the highest VI value). The remaining points within the triangular space correspond to pixels with varying vegetation cover, somewhere between bare soil and dense vegetation. For data points having the same VI, LST can range markedly. When well supplied with water, transpiration acts to cool vegetation very effectively, but as vegetation undergoes water stress the plant tends to close its stomata, with the resulting transpiration decrease leading to an increase in leaf temperature.

Thus, for pixels with the same VI, those with minimum LST represent the case of the strongest evaporative cooling, while those with maximum LST represent those with the weakest evaporative cooling. In this way, the triangle’s (or trapezoid’s) ‘dry edge’ is considered to represent the upper limit of evaporation for the different vegetation conditions found within the scene, whereas the reverse is implied for the ‘cold edge’. The presence of a trapezoidal rather than perfectly triangular feature space plot is produced by LST increasing when the VI remains at the maximum value, and is interpreted to result from variations in soil thermal inertia with changing soil water content (which affects the soil heat storage and therefore the soil temperature. The relatively narrow vertex of the triangular envelope expresses the comparatively low sensitivity of leaf temperature to changes in soil water content when compared to bare soil, the much greater sensitivity of which is evidenced by the triangle’s much wider base.” (T.N. Carlson 2009)

For this type of analyses are plotted the data of 4 days per year, electing the vernal imageries available, the VI chose for this analysis is FVC, plotted in axis x, with LST in axis y. Note that the following images have inverted axis respect to Figure 48.



### 4.2.1 BARRAX

The data used are those related to JD:

- 2011: 098, 130, 219, 235
- 2012: 101, 149, 165, 190
- 2013: 104, 143, 152, 175
- 2014: 139, 146, 155, 162
- 2015: 126, 142, 158, 181
- 2016: 145, 152, 161, 184

For each year, the images are plotted in box of four images. Not always the shape is a triangle or a trapezoid, it depends from the variability of cultures, from the quantity of water present in the soil, closely linked to the period of life cycle in which the plants are. Taller is the column of data with low FVC values and more LST values, the base along the y axis, greater is the presence of bare soil.

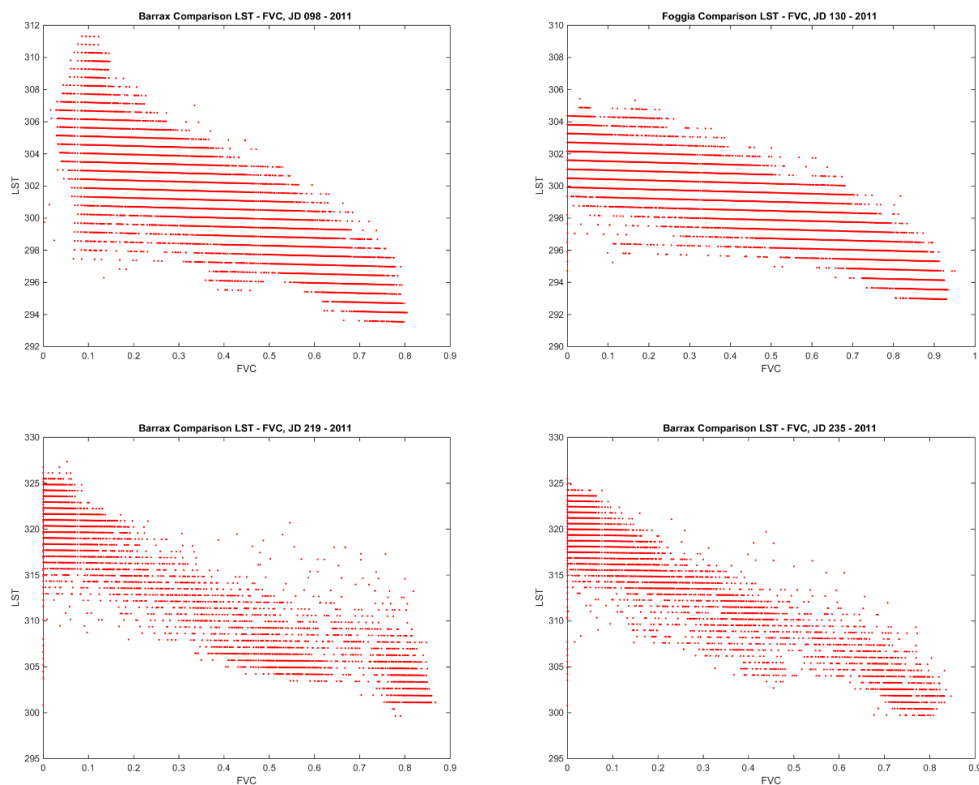


FIGURE 49 . BARRAX, COMPARISON LST-FVC, 2011

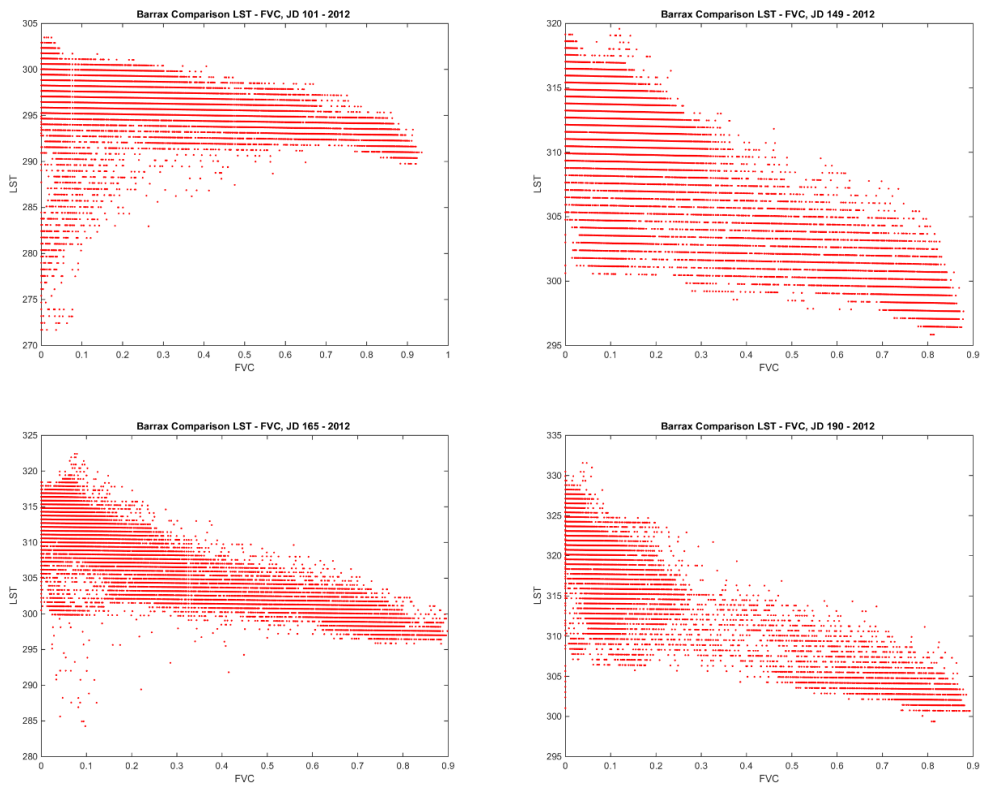


FIGURE 50. BARRAX, COMPARISON LST-FVC, 2012

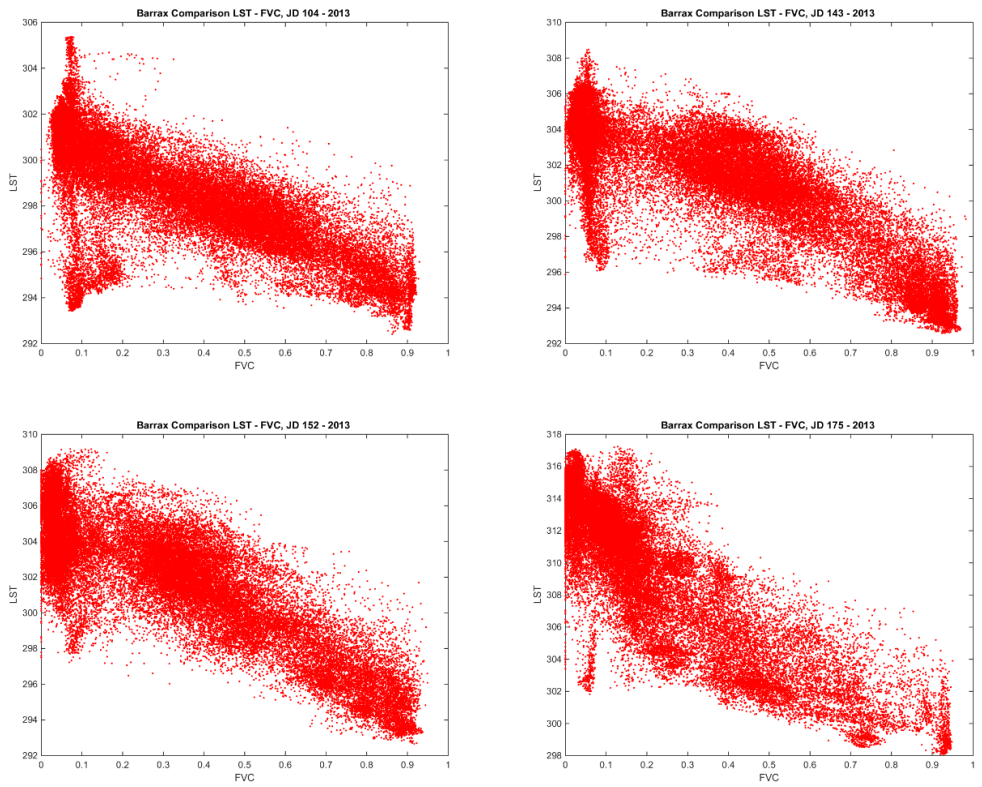


FIGURE 51. BARRAX, COMPARISON LST-FVC, 2013

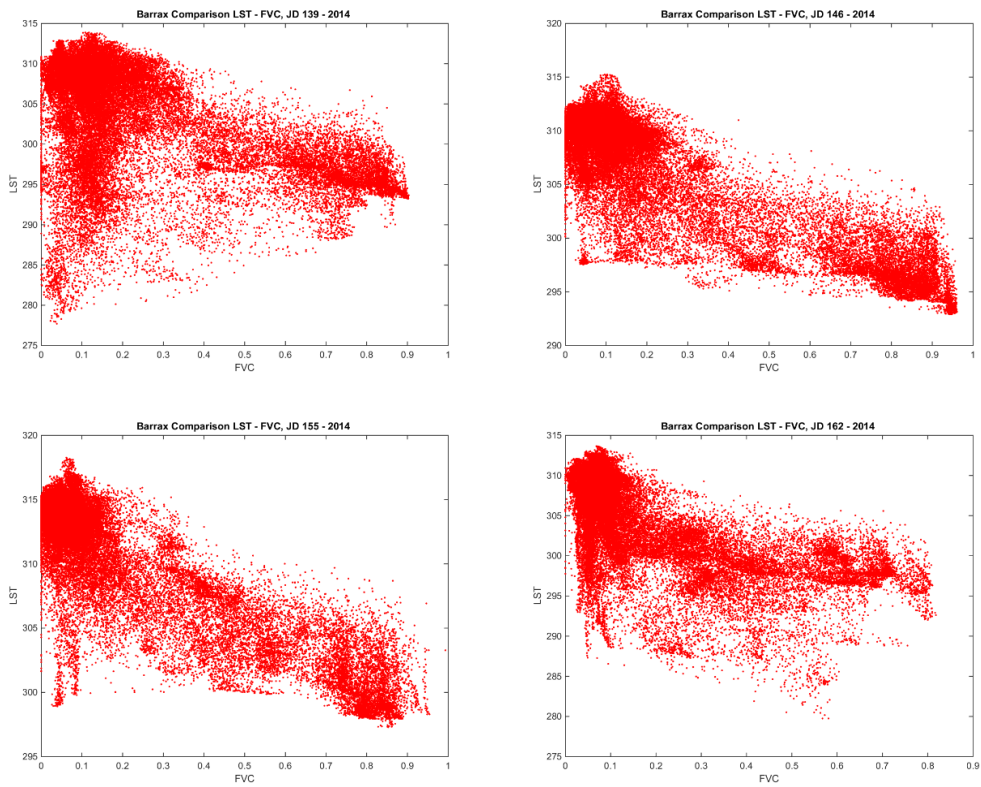


FIGURE 52. BARRAX, COMPARISON LST-FVC, 2014

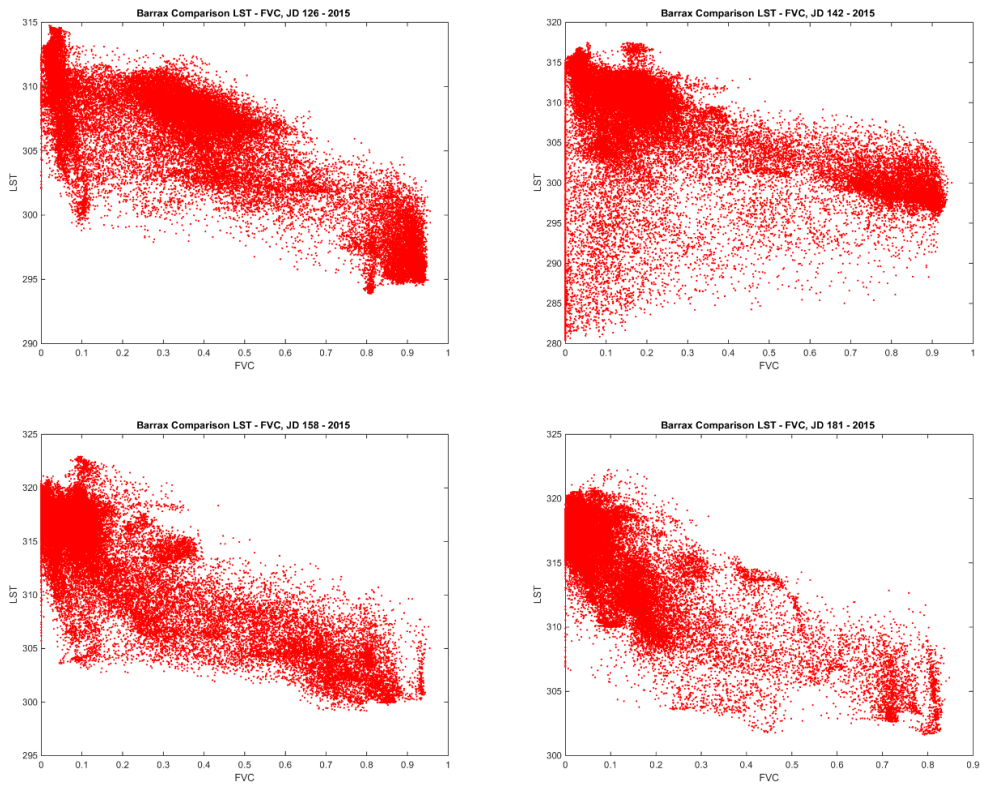


FIGURE 53. BARRAX, COMPARISON LST-FVC, 2015

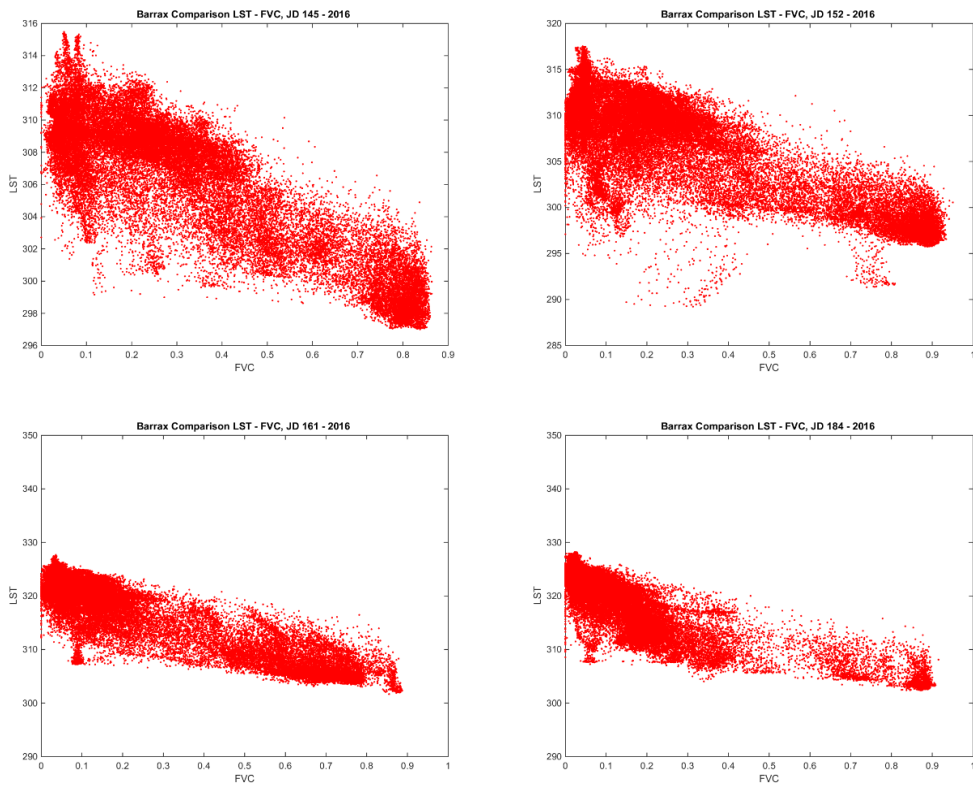


FIGURE 54. BARRAX, COMPARISON LST-FVC, 2016

It is possible to notice that Landsat 7 images have systematic linear gaps; this means that probably the algorithm used discretizes the values of the retrieved data, creating a gap of 0.5 K among clusters of data.

## 4.2.2 FOGGIA

The data used are those related to JD:

- 2011: 085, 101, 219, 245
- 2012: 088, 152, 168, 184
- 2013: 106, 194, 210, 226
- 2014: 125, 141, 157, 173
- 2015: 120, 152, 184, 200
- 2016: 131, 139, 163, 187

For each year, the images are plotted in box of four images. In comparison to Barrax, the shape of the relationship LST-FVC in Foggia is different. In this analysis the urban area and the little lake closer to Foggia are included, this is why there is the presence of lower LST.

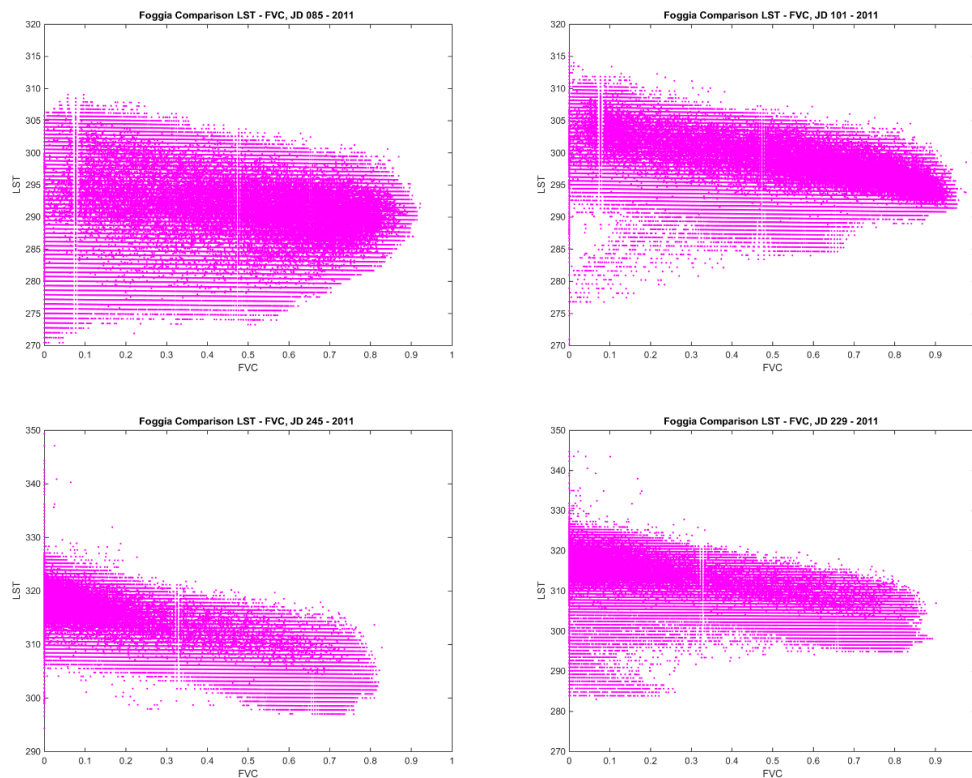


FIGURE 55. FOGGIA, COMPARISON LST-FVC, 2011

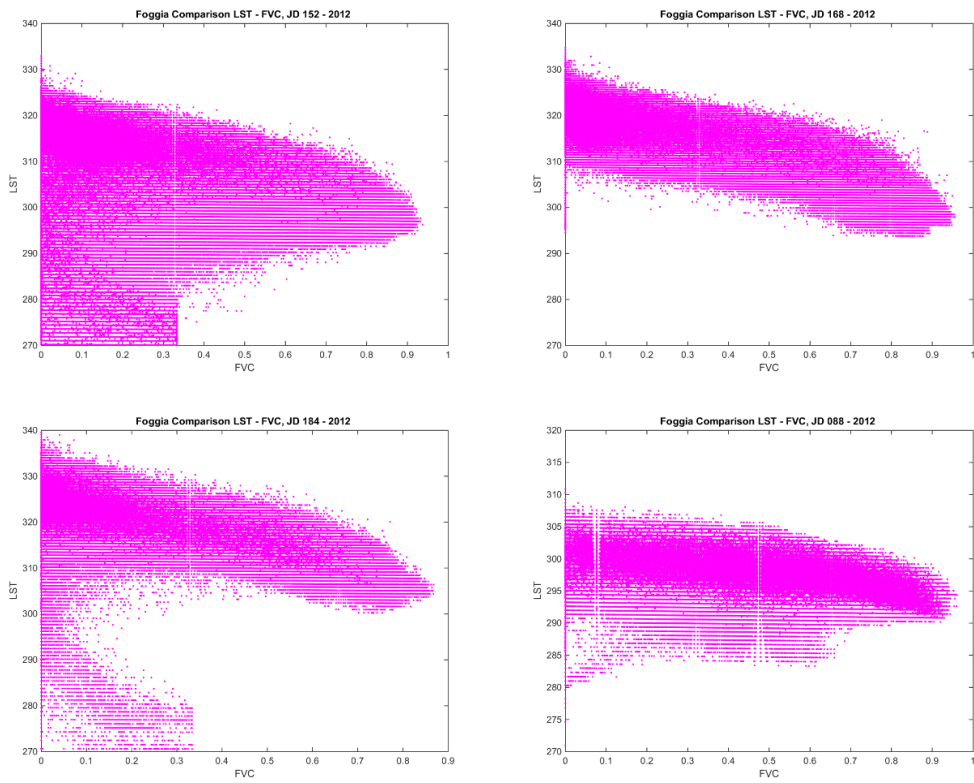


FIGURE 56. FOGGIA, COMPARISON LST-FVC, 2012

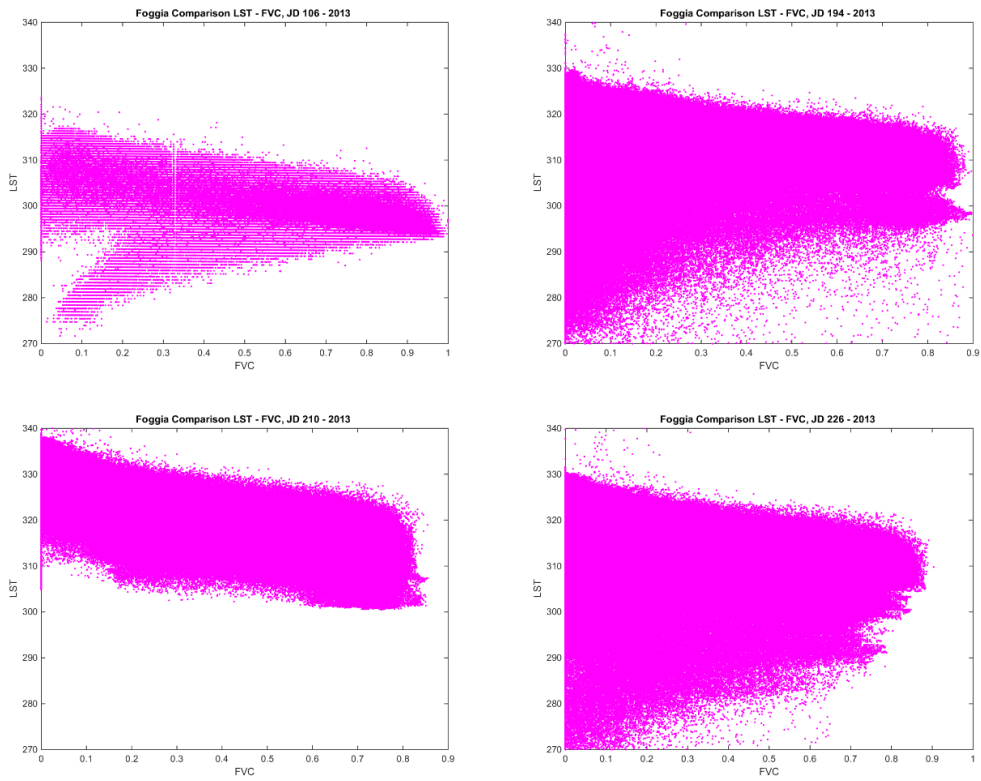


FIGURE 57. FOGGIA, COMPARISON LST-FVC, 2013

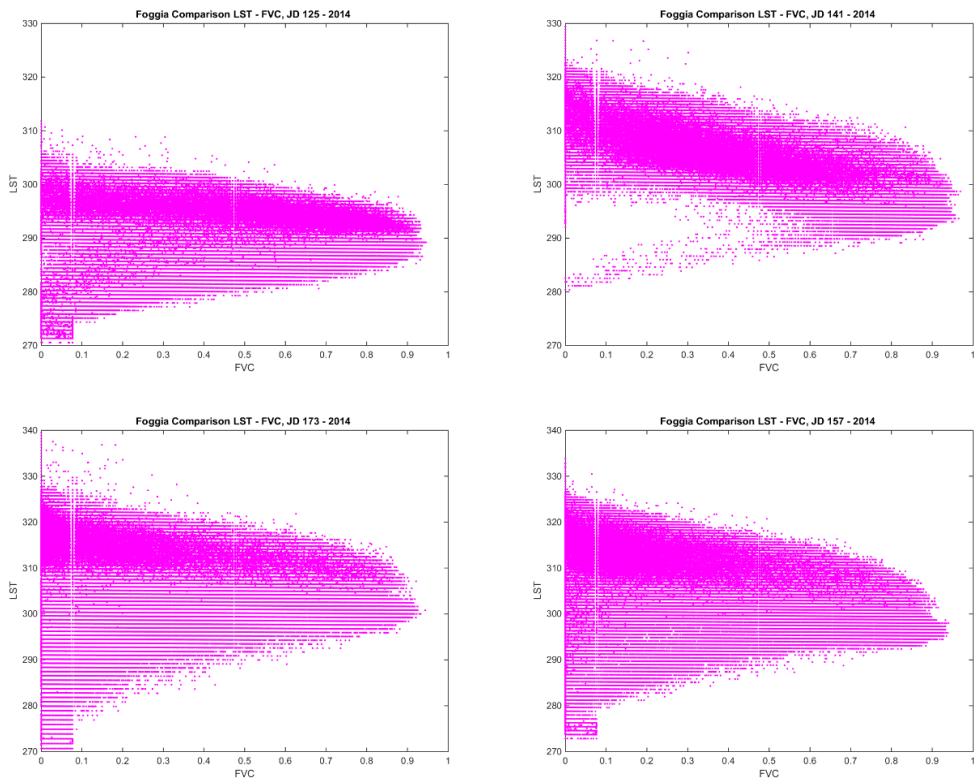


FIGURE 58. FOGGIA, COMPARISON LST-FVC, 2014

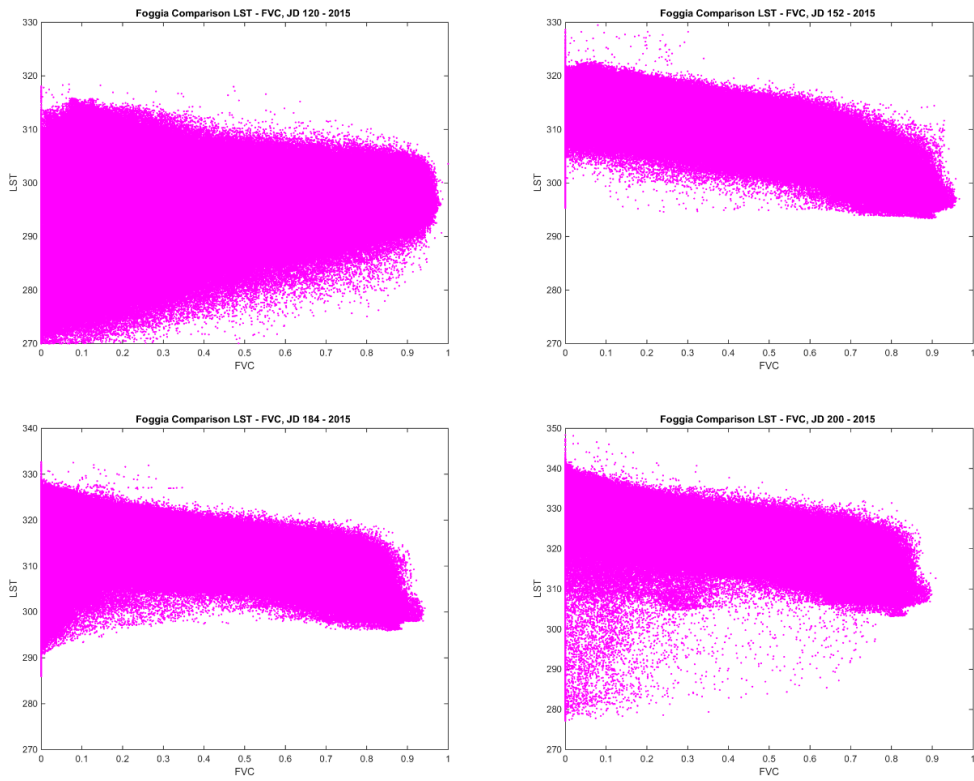
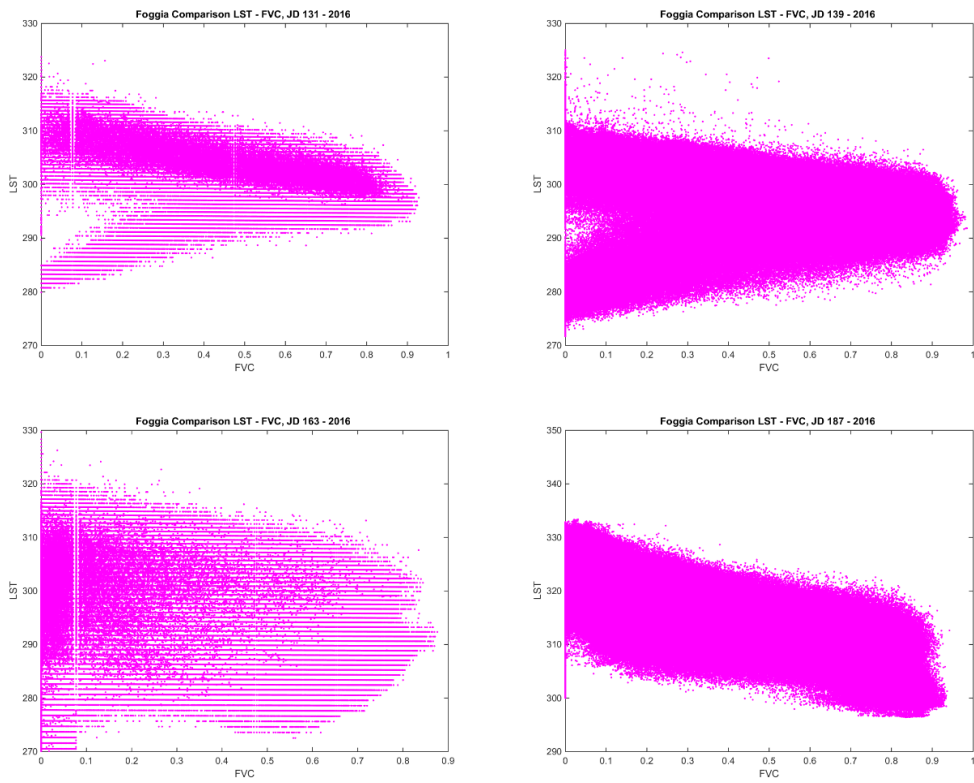


FIGURE 59. FOGGIA, COMPARISON LST-FVC, 2015



**FIGURE 60. FOGGIA, COMPARISON LST-FVC, 2016**

Like for Barrax, also in this case, Landsat 7 images present a linear gap referred to LST retrieval. In this case the dispersion of the data is higher and the trapezoid shape isn't so clear, due to the larger spectra variability.



### 4.3 COMPARISON ANALYSES WITH IN SITU RETRIEVED DATA

The second performed analysis performed, is a comparison with *in situ* data, linking pixel values, obtained with Landsat, with precise values given by eddy covariance stations, which measures several meteorological variables, among which the four components of the net radiation.

In particular, the incoming and outgoing longwave radiations are used for LST and albedo retrieval:

$$LST = \sqrt[4]{\frac{RS_{out}}{\varepsilon\sigma}}$$

Where  $\varepsilon$  represents the emissivity,  $\sigma = 5.670367 \cdot 10^{-8} W m^{-2}K^{-4}$  is the Stefan-Boltzmann constant and  $RS_{out}$  is the outgoing longwave radiations.

Is possible obtain albedo with the simple ratio of reflected solar radiation ( $RS_{out}$ ) and global solar radiation ( $RS_{in}$ ):

$$ALB = \frac{RS_{out}}{RS_{in}}$$

The main obstacle in this type of analysis is given by the resolution of satellite imagery; the comparison presented in this thesis is between a punctual data, retrieved with outgoing radiometers that have a field of view of  $150^\circ$ , which means a mean area of measurements of about  $2-5m^2$  according its instrument height, and the value of a pixel of 30m resolution. Thus, this implies the strong hypothesis that *in situ* data have the same homogenous values in the closers 30m, independently from the conditions of the closer area.

This is the main problem of the analysis and this is why the results are not expected to be perfect.

### 4.3.1 BARRAX

In Barrax different types data are used for this analysis are 2.

#### 4.3.1.1 COMPARISON BARRAX – FIELD CAMPAIGN SUMMER 2012

The first one is a comparison with the field campaign performed in summer 2012 by a group of international university among which Politecnico di Milano and Universitat de Valencia (Corbari 2012).

Unfortunately, about the first analysis, only one satellite data matches with the data retrieved by the *in situ* campaign developed in summer 2012. The data is a LST measure from the station positioned in the area with coordinates 39335100 N, -2513488 E:

2012			
JD	LST sat °C	LST in situ °C	Error [%]
138	45.37	42.74	0.06

FIGURE 61. BARRAX, COMPARISON LST: SATELLITE – IN SITU DATA BY THE FIELD CAMPAIGN OF 2012

#### 4.3.1.2 COMPARISON BARRAX – “EL CRUCE” STATION DATA

The second one is a comparison with the assessed data by the station called “El Cruce”, which is placed in a grass area with coordinates 39.060528 N, -2.099806 E, from 2011 until 2014.

This time the comparison involves LST and ALB data.

Year	JD	LST °C sat	LST °C in situ	Error [%]
2011	219	38.09	30	0.26
2011	235	38.24	33.9	0.12
2011	258	30.70	26	0.18
2011	315	19.62	22.8	0.13
2011	338	12.90	14.8	0.12
2012	5	12.65	15.3	0.17
2012	30	7.25	14.4	0.49
2012	46	11.55	18.3	0.36
2012	69	20.62	22.8	0.09

2012	190	38.12	38	0.00
2012	213	38.34	38.3	0.00
2012	238	35.24	31	0.14
2012	302	13.02	14.4	0.1
2012	334	7.36	7.5	0.02
2013	200	40.51	31.46	0.29
2013	223	39.46	31.11	0.27
2013	248	32.75	31.86	0.03
2013	255	32.12	30.87	0.04
2013	328	9.33	13.63	0.32
2014	50	12.98	18.91	0.31

TABLE 27. BARRAX, COMPARISON LST: SATELLITE - IN SITU DATA BY THE STATION EL CRUCE

The mean error is equal to 0.17.

It is possible to plot the data, having a graphical vision of the mean values retrieved.

Are plotted:

- The comparison between Landsat 7 and *in situ* data
- The comparison between Landsat 8 and *in situ* data
- The comparison between the entire Landsat data and *in situ* data

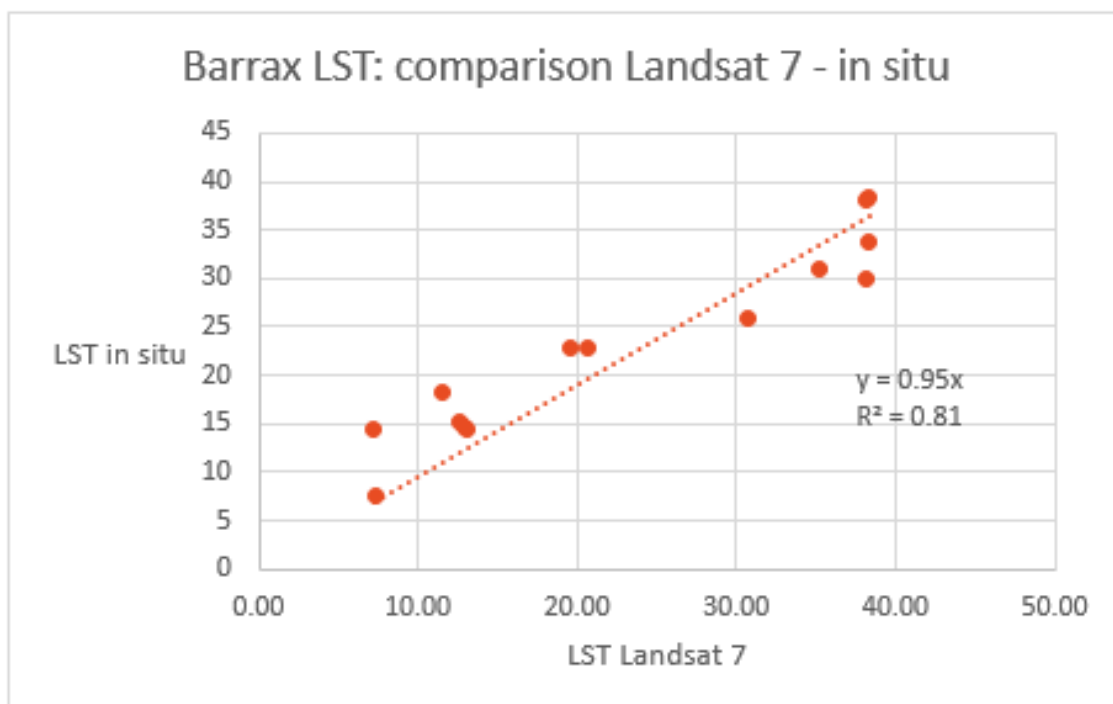


FIGURE 62. BARRAX, PLOT OF THE COMPARISON L7 DATA - EL CRUCE DATA

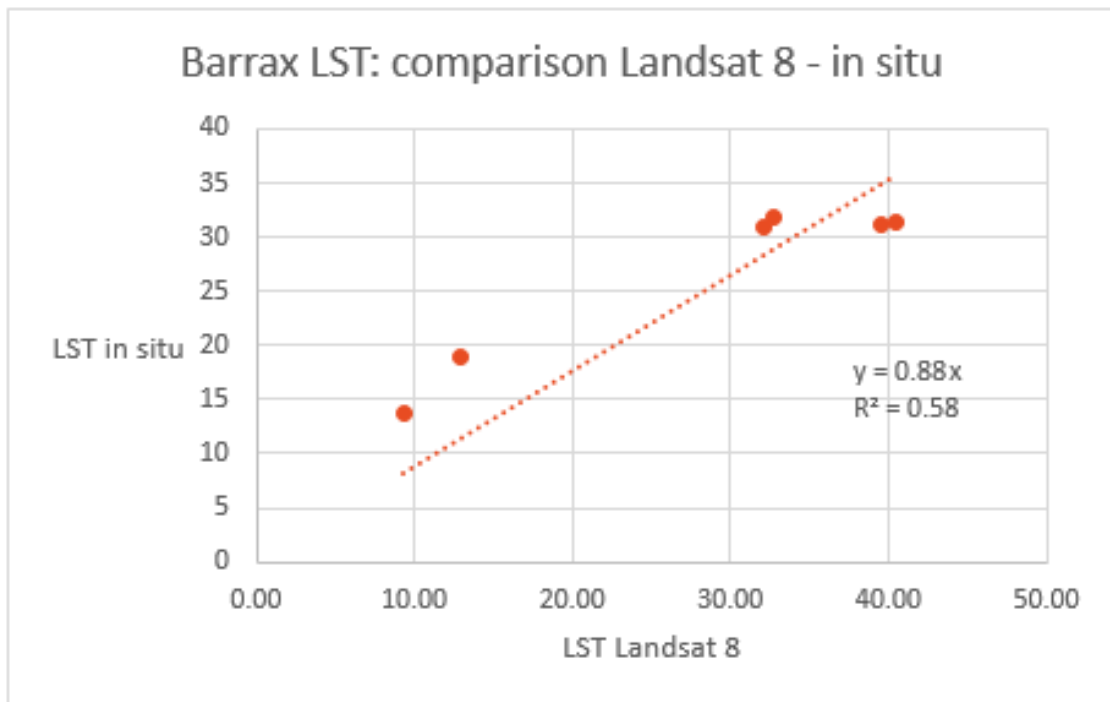


FIGURE 63. BARRAX, PLOT OF THE COMPARISON LST: L8 DATA - EL CRUCE DATA

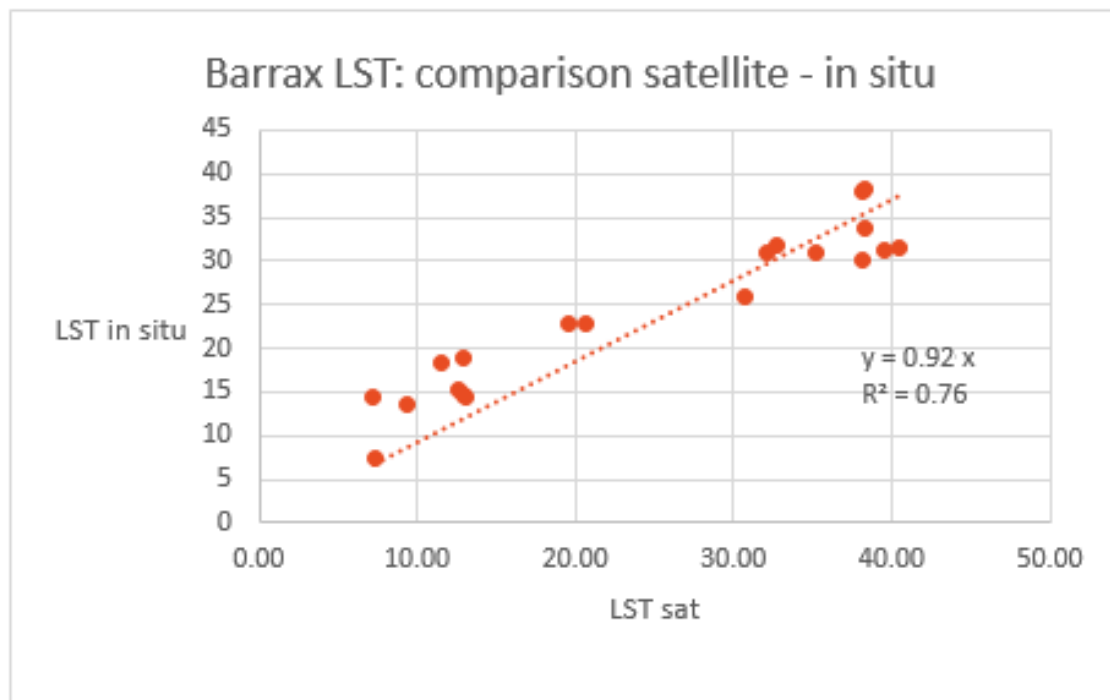


FIGURE 64. BARRAX, PLOT OF THE COMPARISON LST: LANDSAT WHOLE DATA - EL CRUCE DATA

The correlation between the different types of data is almost linear, as is possible to deduced from the equation of the line, even if the dispersion index  $R^2$  is not closer to 1, but is considerate acceptable. In the following the comparison between in situ and satellite albedo is reported:

Year	JD	ALB	ALB in situ	Error [%]	Year	JD	ALB	ALB in situ	Error [%]
2011	219	0.20	0.21	0.04	2014	146	0.22	0.21	0.02
2011	235	0.21	0.23	0.08	2014	155	0.23	0.21	0.10
2011	251	0.22	0.23	0.03	2014	162	0.22	0.20	0.08
2011	258	0.20	0.24	0.17	2014	171	0.24	0.21	0.14
2011	315	0.18	0.25	0.27	2014	178	0.21	0.20	0.06
2011	338	0.17	0.25	0.31	2014	194	0.21	0.19	0.09
2012	5	0.19	0.27	0.30	2014	203	0.23	0.21	0.07
2012	30	0.20	0.25	0.20	2014	219	0.22	0.21	0.04
2012	46	0.21	0.26	0.18	2014	226	0.22	0.22	0.01
2012	69	0.22	0.24	0.08	2014	235	0.21	0.22	0.04
2012	190	0.20	0.18	0.11	2014	242	0.20	0.23	0.12
2012	213	0.21	0.17	0.22	2014	251	0.21	0.23	0.08
2012	238	0.20	0.18	0.10	2015	5	0.22	0.32	0.29
2012	302	0.18	0.22	0.18	2015	53	0.24	0.28	0.14
2012	334	0.18	0.23	0.19	2015	69	0.22	0.26	0.16
2013	200	0.23	0.20	0.13	2015	110	0.21	0.22	0.04
2013	223	0.21	0.21	0.01	2015	126	0.21	0.21	0.03
2013	248	0.22	0.22	0.01	2015	142	0.23	0.21	0.13
2013	255	0.20	0.22	0.09	2015	158	0.22	0.20	0.13
2013	328	0.21	0.29	0.26	2015	181	0.22	0.22	0.00
2014	50	0.20	0.25	0.20	2015	190	0.23	0.21	0.11
2014	75	0.22	0.23	0.07	2015	213	0.22	0.21	0.01
2014	82	0.20	0.22	0.11	2015	245	0.21	0.24	0.09
2014	123	0.22	0.19	0.13	2015	302	0.24	0.26	0.09
2014	130	0.21	0.22	0.02	2015	350	0.22	0.30	0.27

TABLE 28. BARRAX, COMPARISON ALBEDO: L7 - IN SITU DATA BY THE STATION EL CRUCE

The mean error is 0.12.

From the following figures it is possible to note that the angular coefficient is almost 1, while  $R^2$  is very low, showing a large instability in the albedo retrieval.

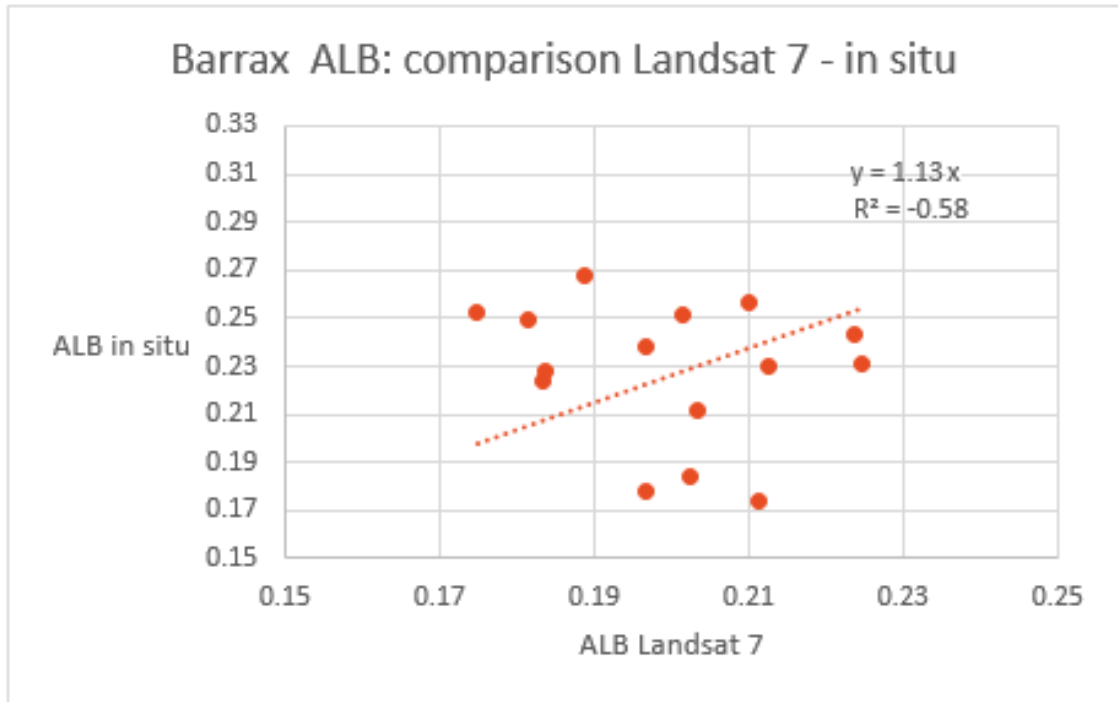


FIGURE 65. BARRAX, PLOT OF THE COMPARISON ALBEDO: L7 DATA - EL CRUCE DATA

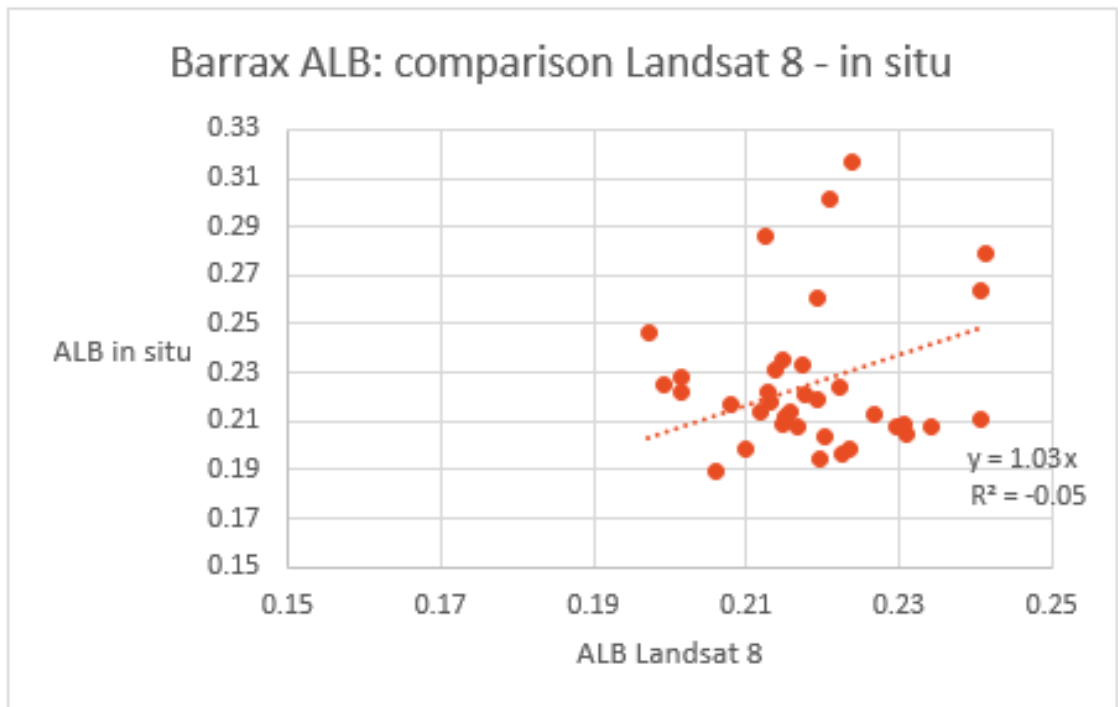


FIGURE 66. BARRAX, PLOT OF THE COMPARISON ALBEDO: L8 DATA - EL CRUCE DATA

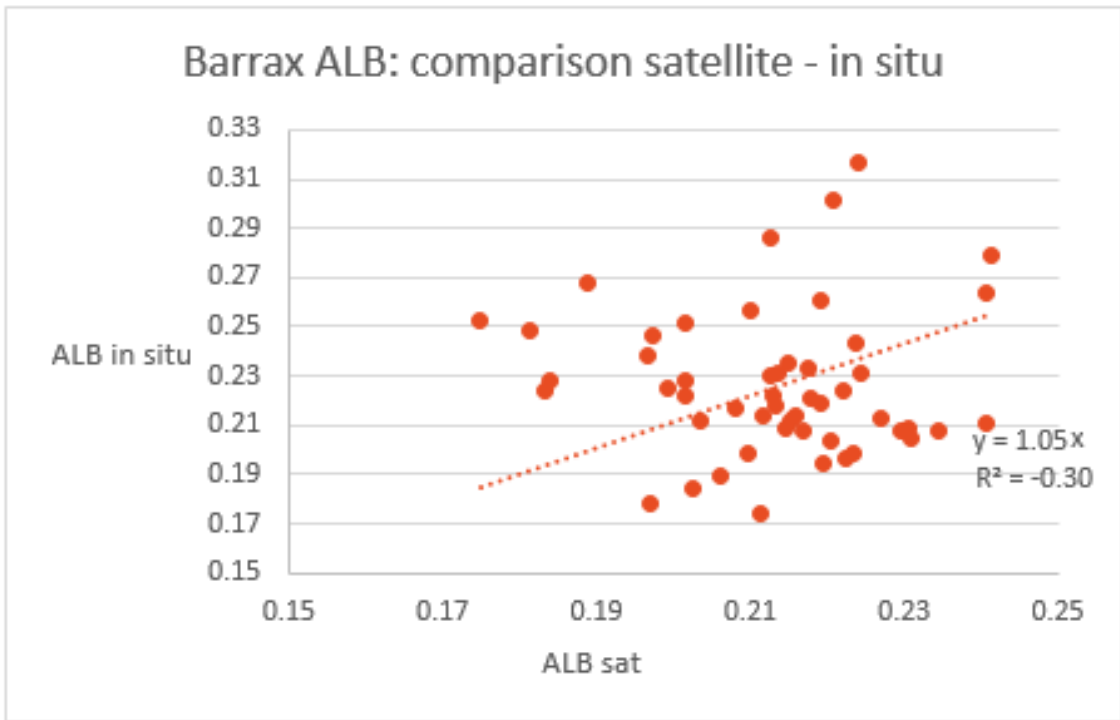


FIGURE 67. BARRAX, PLOT OF THE COMPARISON ALBEDO: LANDSAT WHOLE DATA - EL CRUCE DATA

### 4.3.2 FOGGIA

The parameters considered are Albedo and LST, using two different stations moved in the years in different areas over different crop types. In this way, the analysis has been done in the following coordinates (UTM33N):

- ID a) 551926.26 E, 4578481.39 N
- ID b) 551747.1 E, 4579289.68 N
- ID c) 551754.43 E, 4578473.33 N
- ID d) 553133 E, 4600073 N

ID	Year	JD	LST °C sat	LST °C in situ	ALB sat	ALB In situ	LSTerr[%]	ALBerr[%]
a	2013	362	11.90	11.29	0.13	0.17	0.05	0.23
a	2014	77	27.06	26.52	0.16	0.19	0.02	0.15
a	2014	125	26.01	24.53	0.17	0.16	0.06	0.03
a	2014	141	40.56	33.32	0.18	0.17	0.22	0.05
a	2014	157	44.07	45.74	0.19	0.18	0.04	0.06
a	2014	173	47.00	40.80	0.23	0.21	0.15	0.06
a	2014	197	34.52	36.63	0.18	0.18	0.06	0.03
a	2014	293	26.27	26.70	0.18	0.19	0.02	0.09
a	2014	325	16.23	17.27	0.16	0.21	0.06	0.23
a	2015	8	8.70	10.78	0.18	0.24	0.19	0.25
b	2015	264	20.37	24.12	0.15	0.15	0.16	0.04
c	2016	243	39.76	37.73	0.19	0.17	0.05	0.13
c	2016	227	38.73	33.42	0.19	0.17	0.16	0.12
c	2016	187	42.15	39.14	0.22	0.15	0.08	0.47
c	2016	147	39.17	43.23	0.15	0.12	0.09	0.25
c	2016	139	30.15	31.27	0.14	0.10	0.04	0.48
d	2016	139	28.83	26.70	0.23	0.15	0.08	0.53
d	2016	163	25.27	30.63	0.22	0.17	0.18	0.30
d	2016	187	40.00	37.13	0.22	0.21	0.08	0.02
d	2016	195	36.62	38.46	0.20	0.18	0.05	0.06
d	2016	203	37.08	34.15	0.20	0.18	0.09	0.10

TABLE 29. FOGGIA, COMPARISON LST AND ALBEDO: LANDSAT DATA - IN SITU DATA

The mean error for LST is 0.09, the mean error for Albedo is 0.17.

In the following figures, the comparison between ground and satellite LST are reported. As already seen for Barrax, the angular coefficient is almost 1, with a high  $R^2$  (0.8-0.9).



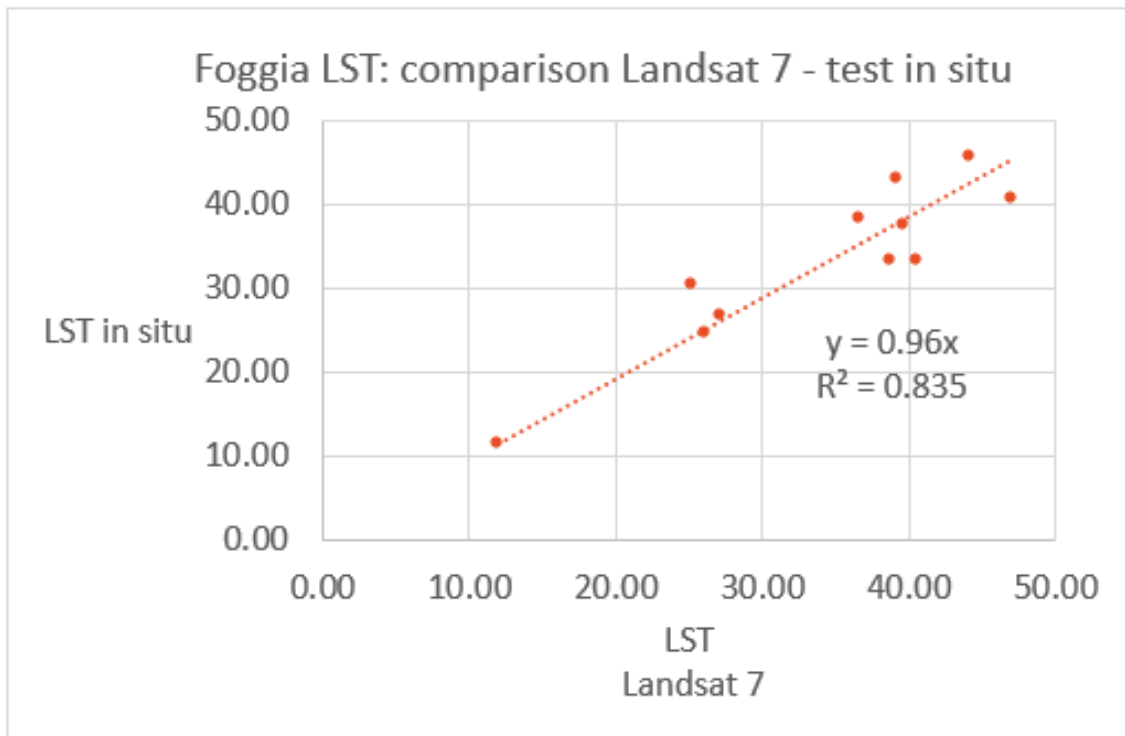


FIGURE 68. FOGGIA, PLOT OF THE COMPARISON LST: L7 DATA - IN SITU DATA

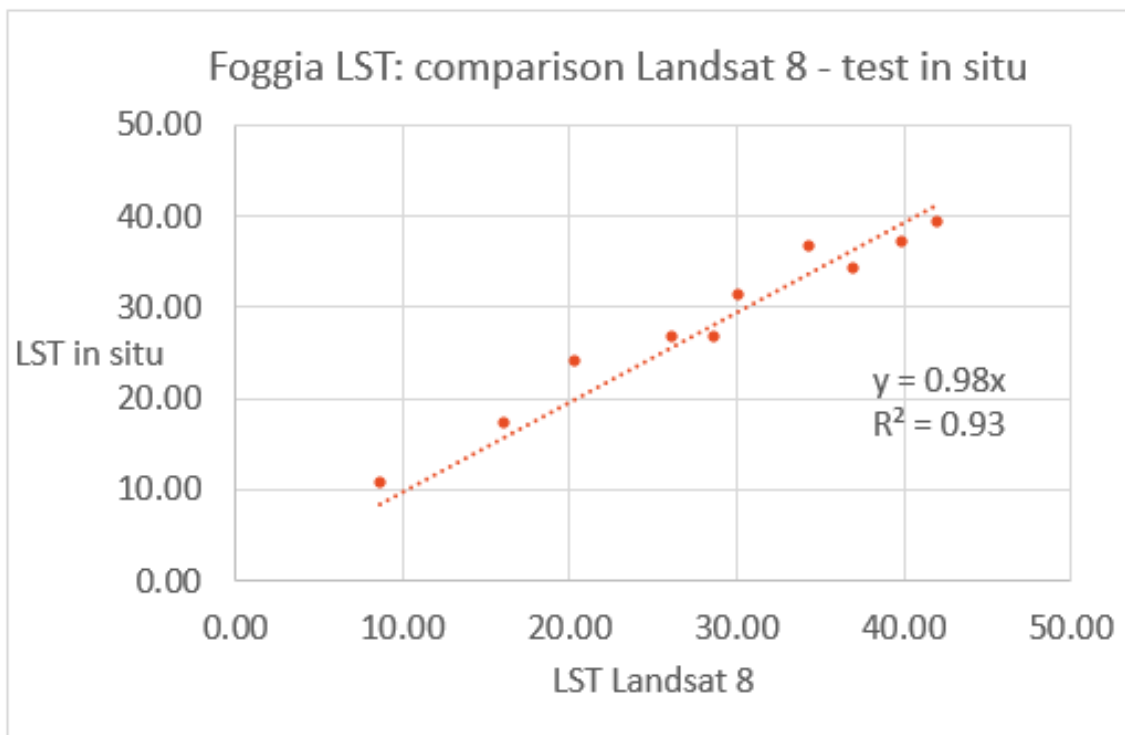


FIGURE 69. FOGGIA, PLOT OF THE COMPARISON LST: L8 DATA - IN SITU DATA

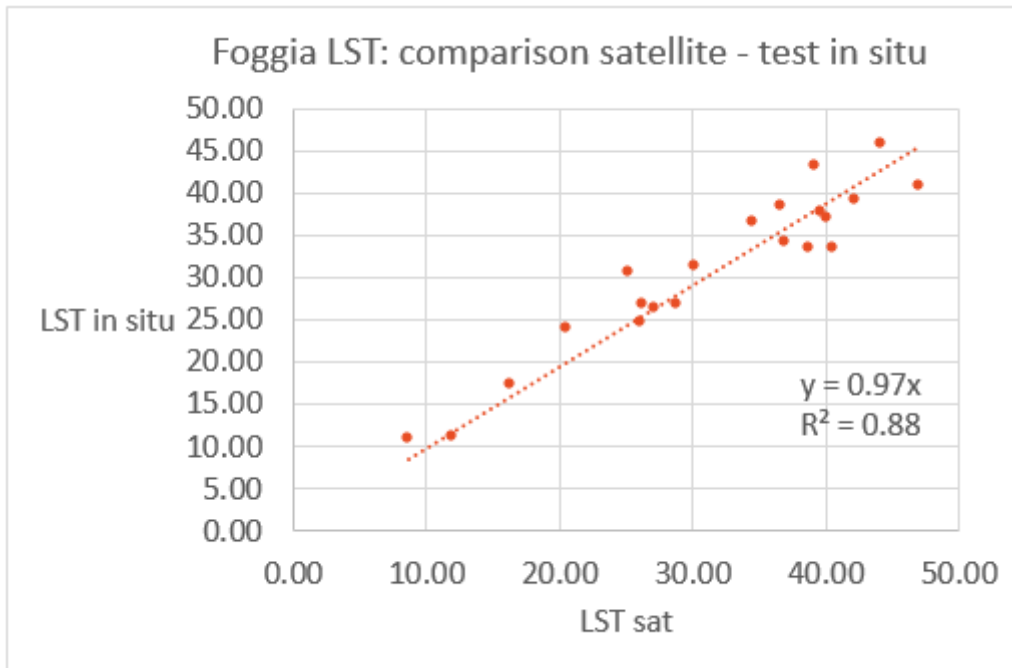


FIGURE 70. FOGGIA, PLOT OF THE COMPARISON LST: LANDSAT WHOLE DATA - IN SITU DATA

The comparison is also reported for ground and satellite albedo, confirming the results of Barrax with low  $R^2$ .

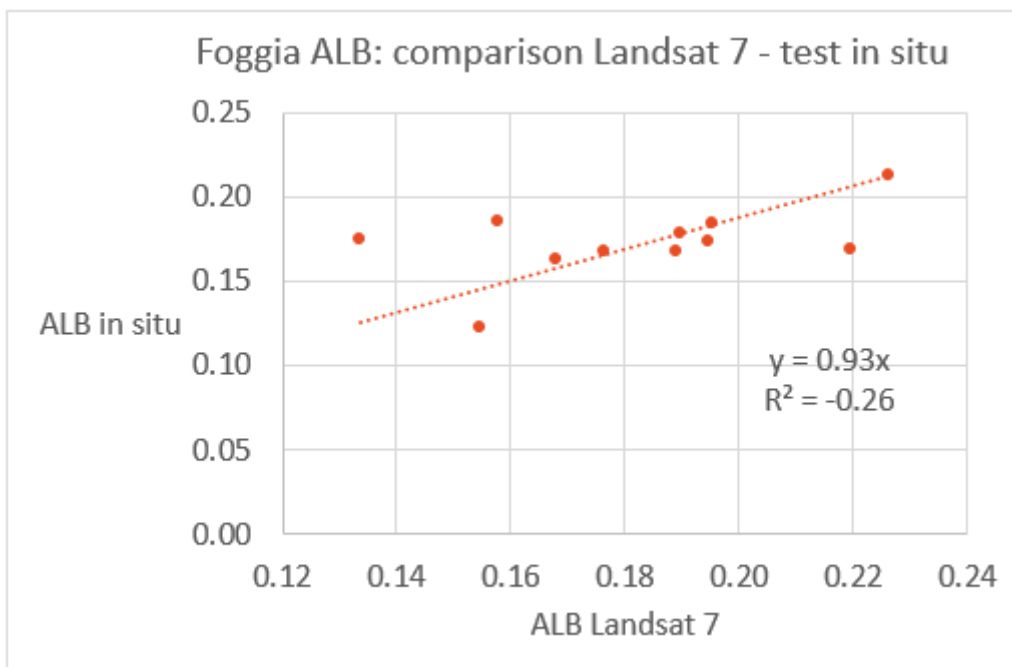


FIGURE 71. FOGGIA, PLOT OF THE COMPARISON ALBEDO: L7 DATA - IN SITU DATA

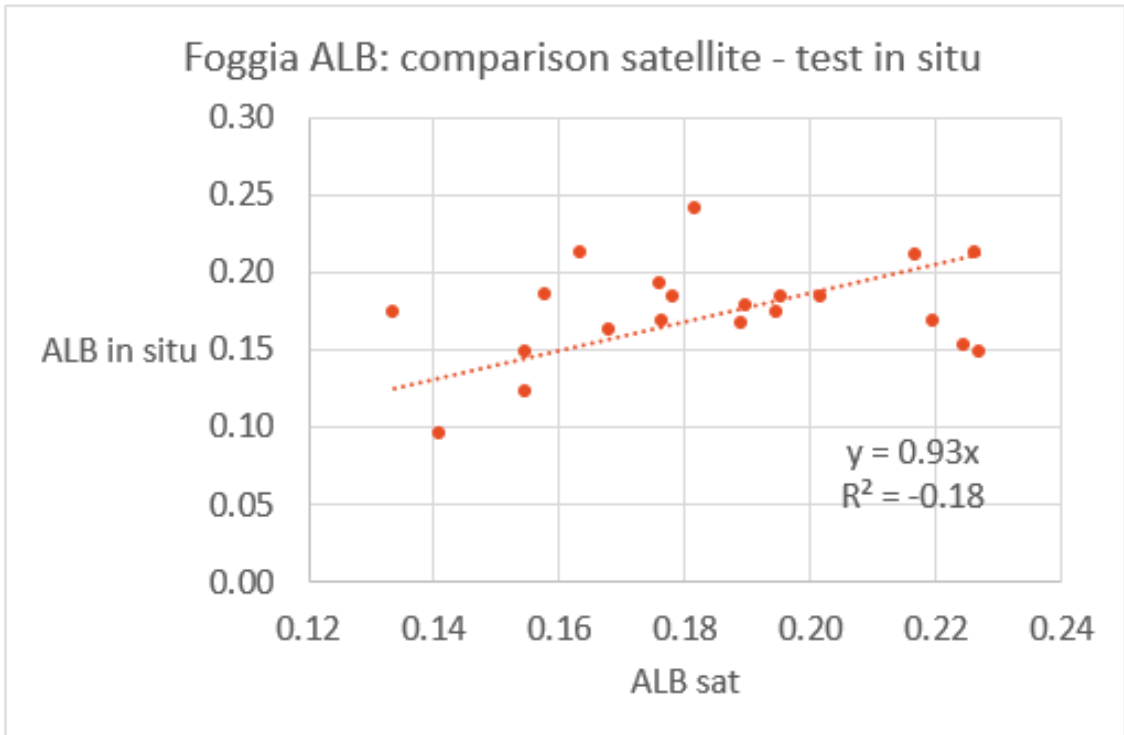


FIGURE 72. FOGGIA, PLOT OF THE COMPARISON ALBEDO: L8 DATA - IN SITU DATA

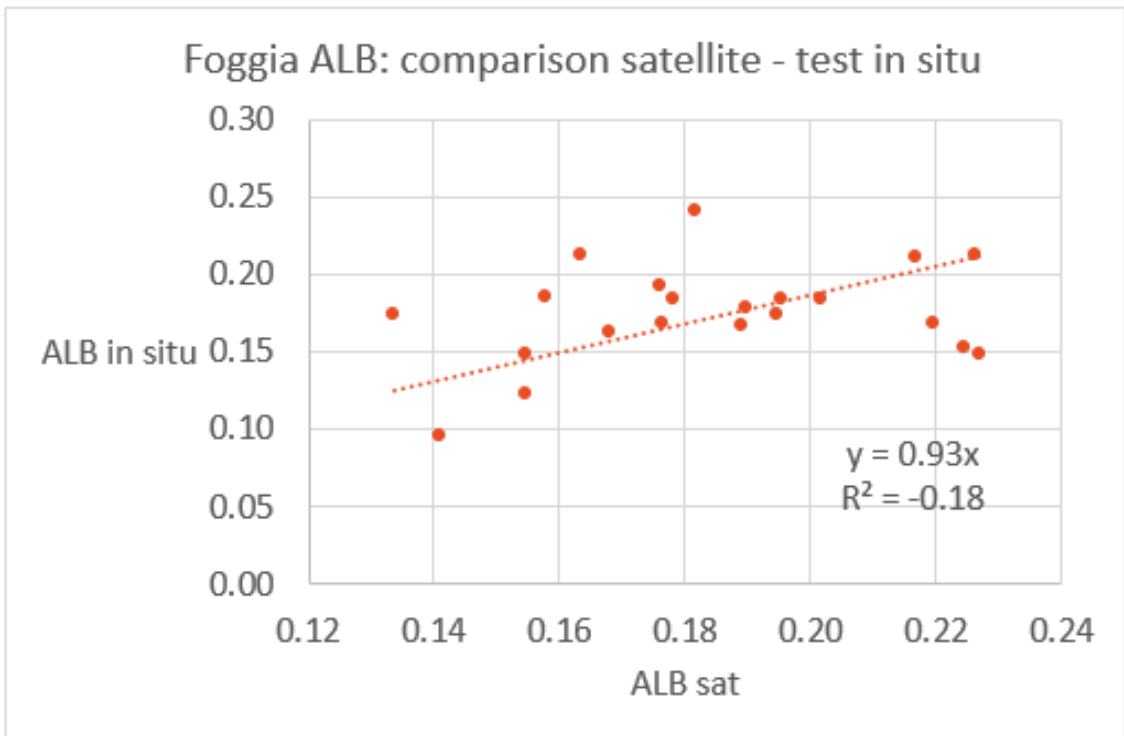


FIGURE 73. FOGGIA, PLOT OF THE COMPARISON ALBEDO LANDSAT WHOLE DATA - IN SITU DATA

## 5 LAND USE CLASSIFICATION

In this chapter the land use classification is presented for the two case studies.

The supervised classification is used, which clusters pixels in a dataset into classes based on user-defined training data, which must be defined before of starting the supervised classification. Once defined, is possible to select the classes to map in the output.

Supervised classification methods presented by ENVI include Maximum likelihood, Minimum distance, Mahalanobis distance, and Spectral Angle Mapper (SAM). If the data used are single-band input data, only Maximum likelihood and Minimum distance are available. (<http://www.harrisgeospatial.com>)

The classification choice is the Maximum Likelihood; this classification assumes that the statistics for each class in each band are normally distributed and calculates the probability that a given pixel belongs to a specific class. Each pixel is assigned to the class that has the highest probability (that is, the maximum likelihood).

Maximum Likelihood classification calculates the following discriminant functions for each pixel in the image:

$$g_i(x) = \ln p(\omega_i) - \frac{1}{2} \ln \left| \sum_i \right| - \frac{1}{2} (x - m_i)^T \sum_i^{-1} (x - m_i)$$

Where  $i$  is the class,  $x$  the  $n$ -dimensional data (where  $n$  is the number of bands),  $p(\omega_i)$  the probability that a class occurs in the image and is assumed the same for all classes,  $\left| \sum_i \right|$  is the determinant of the covariance matrix of the data in a class,  $\sum_i^{-1}$  is the inverse of the covariance matrix of a class and  $m_i$  is the mean vector of a class.

The final classification image is a single-band image that contains the final class assignments. The definition of the training data needs the building of some Regions of Interest (ROIs). Each ROI has an own ID and an assigned characterising colour. The classification is related to a particular period of time; this is very important in an agriculture area where the crops change every season.

## 5.1 BARRAX

The classification in Barrax is done over 3 years: 2012, 2014 and 2015.

### 5.1.1 BARRAX, 28<sup>TH</sup> OF MAY AND 13<sup>TH</sup> OF JUNE 2012

For the period among the end of May 2012 and the beginning of June 2012, the satellite data usable for that period are the Landsat 7 imageries of the Julian Day 149 and 165, the 28<sup>th</sup> of May and the 13<sup>th</sup> of June. About this period the land use information, which are then extended to the whole case study area, are given by this picture (ITAP).

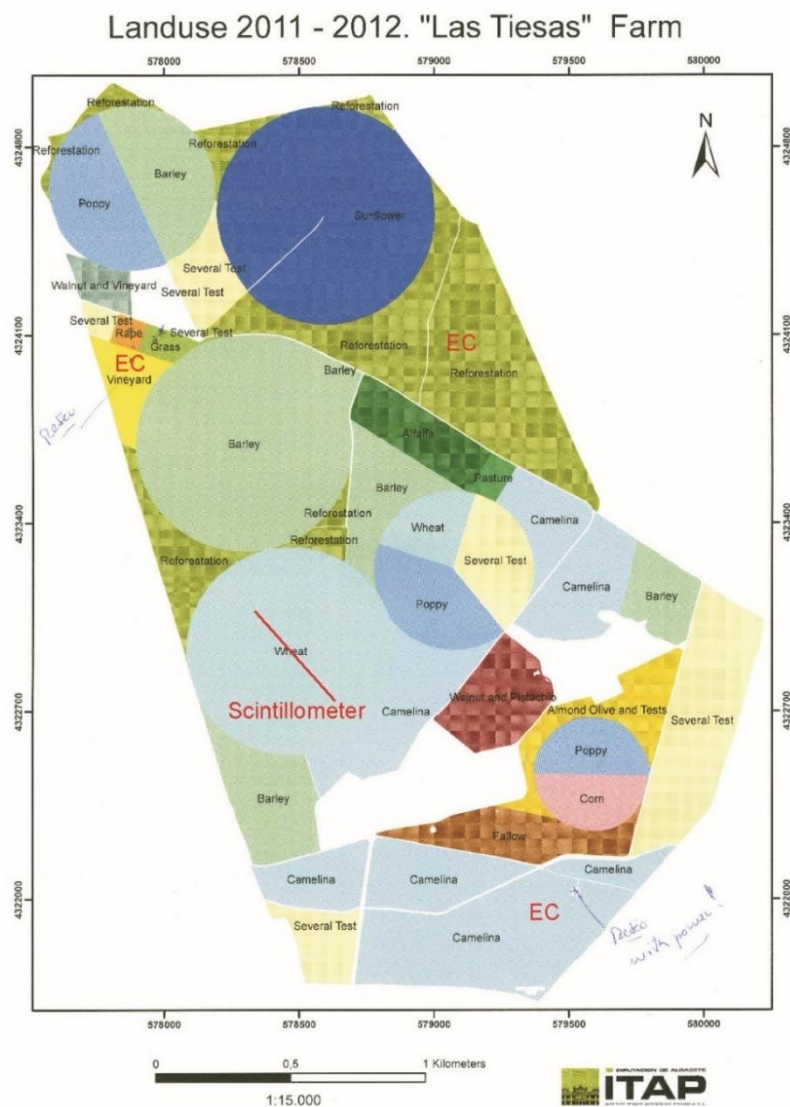


FIGURE 74. BARRAX LANDUSE MAP 2011 -2012 IN LAS TIASAS FARM

Using the land use map, it is possible to identify the training data in ENVI, i.e. the ROIs required to apply the supervised classification tool. In add to the land use ROIs there are ROIs for water, bare soil and urban area. Bare soil and urban have a similar spectrum, sometimes the software has difficulties in distinguish them.

ROI Name	Color	Pixels	ROI Name	Color	Pixels
Poppy	Red	100	Poppy	Red	100
Sunflower	Blue	142	Sunflower	Blue	212
Reforestation	Yellow	245	Reforestation	Yellow	275
Grass	Cyan	9	Walnut and Vineyard	Maroon	16
Test rap	Magenta	12	Camelina	Coral	187
Walnut and Vineyard	Maroon	16	Fallow	Aquamarine	38
Wheat	Sea Green	572	Com	Orchid	36
Walnut and pistachio	Purple	29	Water	Sienna	13
Camelina	Coral	274	Other vegetation type	Chartreuse	258
Fallow	Aquamarine	38	Bare soil	Thistle	131
Com	Orchid	36	Urban	Magenta2	10
Water	Sienna	13	Barley	Green	311
Other vegetation type	Chartreuse	401	Alfalfa	Purple2	9
Bare soil	Thistle	131	Pasture	Orange3	16
Urban	Magenta2	10	Wheat	Sea Green	492
Barley	Green	250	Wainut and Pistachio	Purple	11

TABLE 30. BARRAX ROIs FOR IMAGE OF JD 149 (LEFT) AND JD 165 (RIGHT), BASED ON LANDUSE MAP 2012

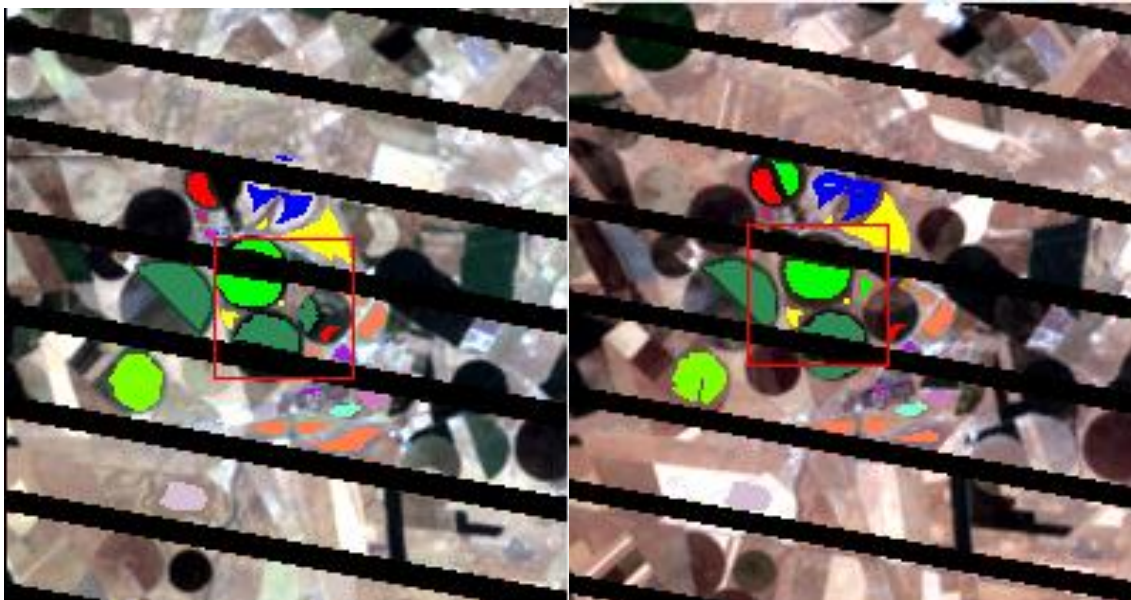


FIGURE 75. BARRAX, TRAINING ROI, JD 149 (LEFT) AND (RIGHT) JD 165, 2012

In this operation, it is necessary to build a ROI for each image, due to the presence of the stripes that occupy different pixels in the images, for this reason some pixels of the first ROI match with NaN pixels of the stripes of the second ROI and it isn't possible to compute the classification.

The following step is to calculate the Maximum Likelihood classification.

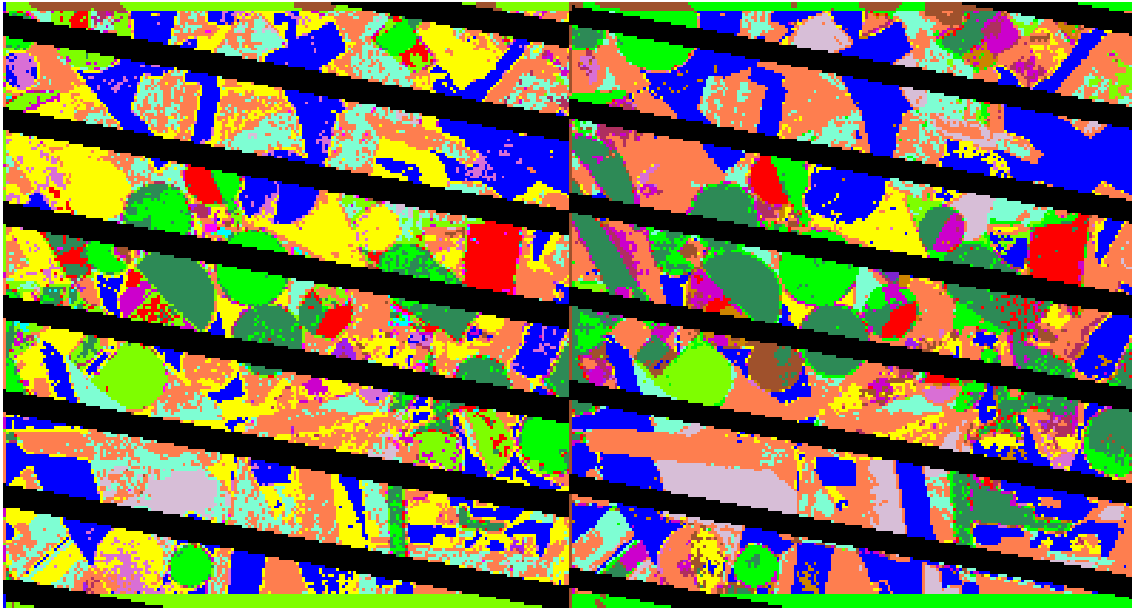


FIGURE 76. BARRAX, CLASSIFIED IMAGE, JD 149 (LEFT) AND (RIGHT) JD 165, 2012

The main difference in the two images is the reforestation. The yellow parts in the first image become coral in the second ones, probably the spectra of camelina and reforestation are both similar to the spectra of those areas, this is why the software has some difficulties working on them.

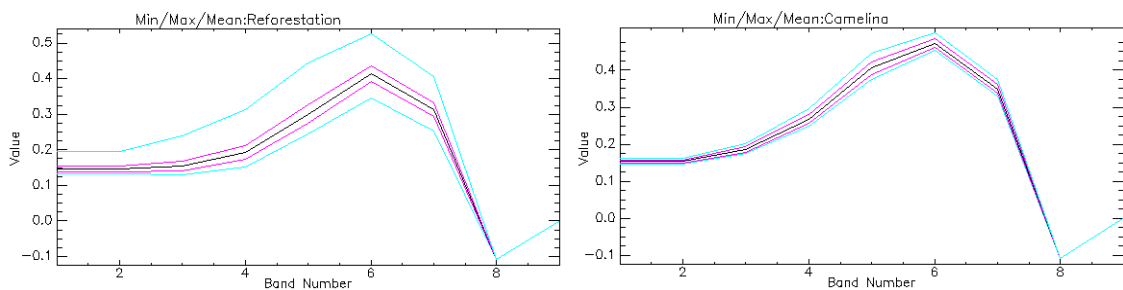


FIGURE 77. BARRAX, SPECTRA OF REFORESTATION AND CAMELINA

### 5.1.2 BARRAX, 4<sup>TH</sup> OF JUNE 2014

For the period among the end of May 2013 and the beginning of June 2014, the classification is done over the images of the 4<sup>th</sup> of June 2014 (JD 155). About this period the land use information, which are then extended to the whole case study area, are given by this picture (ITAP).

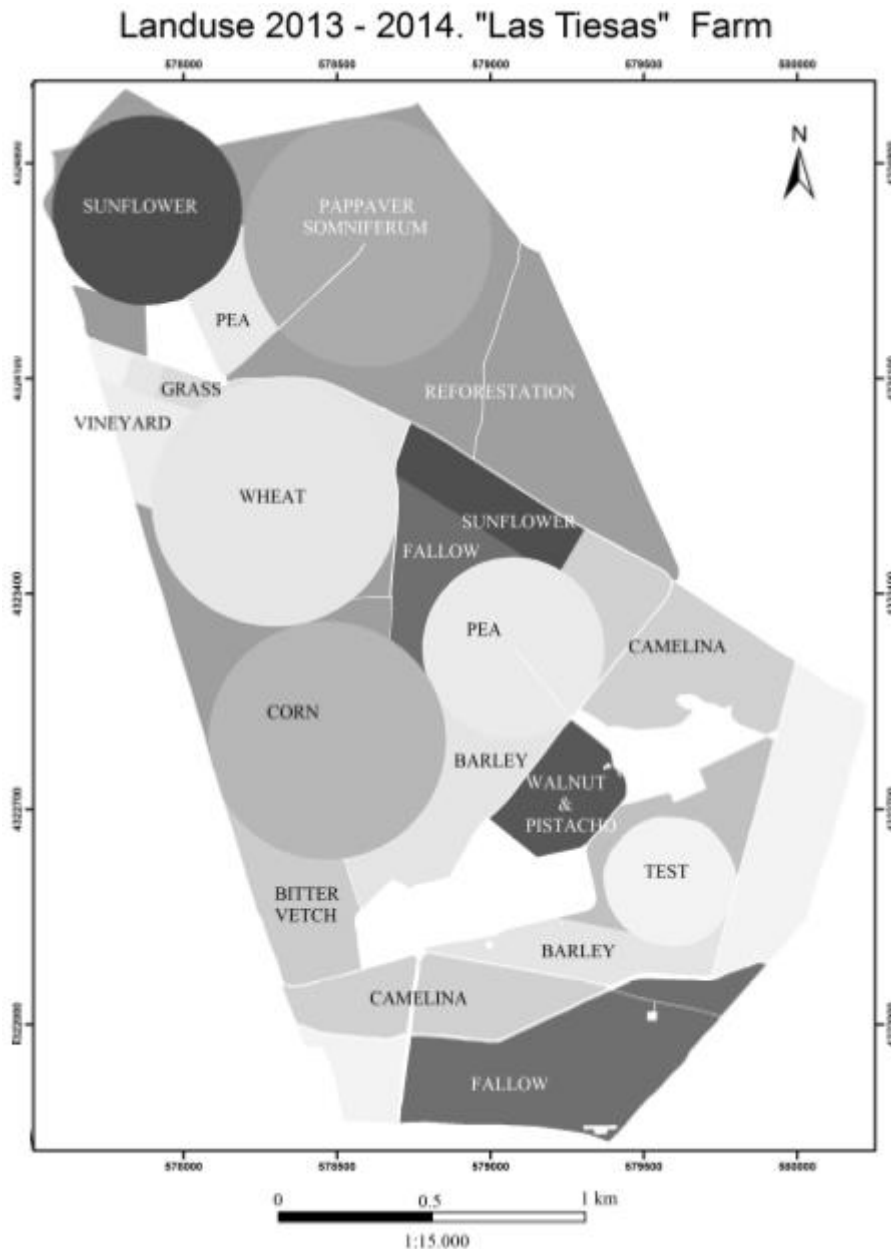


FIGURE 78. BARRAX LANDUSE MAP 2013 -2014 IN LAS TIASAS FARM (C. LATORRE 2014)



ROI Name	Color	Pixels
Sunflower	Red	295
Pappaver somniferum	Green	436
Pea	Blue	246
Wheat	Yellow	420
Reforestation	Cyan	357
Fallow	Magenta	235
Com	Maroon	395
Walnut and pistacho	Sea Green	85
Bitter vetch	Coral	76
Vineyard	Aquamarine	26
Camelina	Orchid	164
Barley	SiennaPurple	111
Water	Chartreuse	9
Urban	Thistle	24

TABLE 31. BARRAX ROIs FOR IMAGE OF JD 155 2014

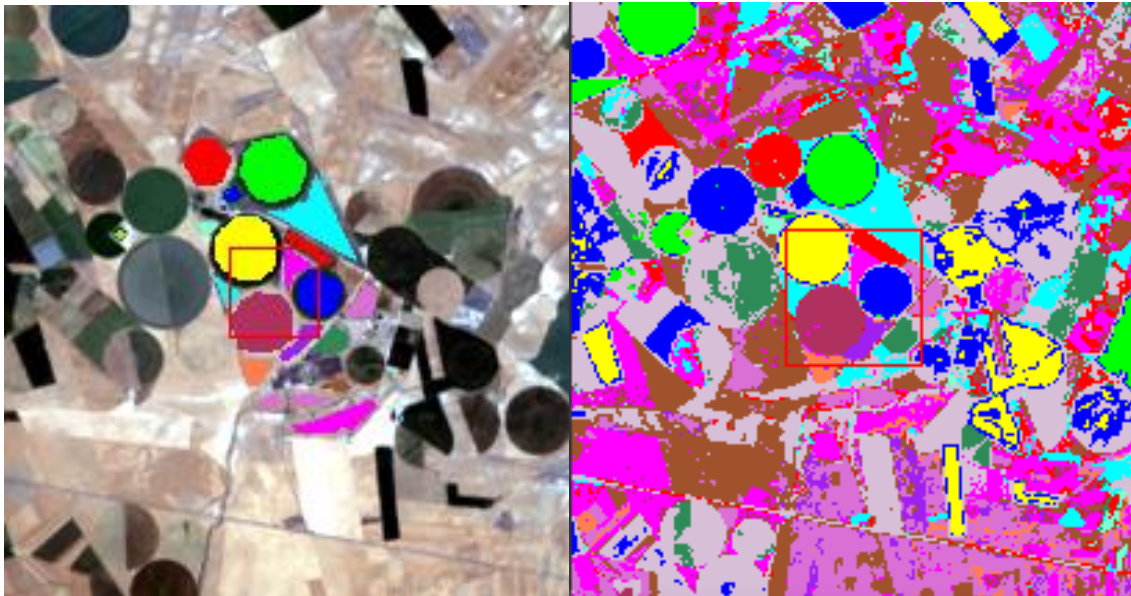
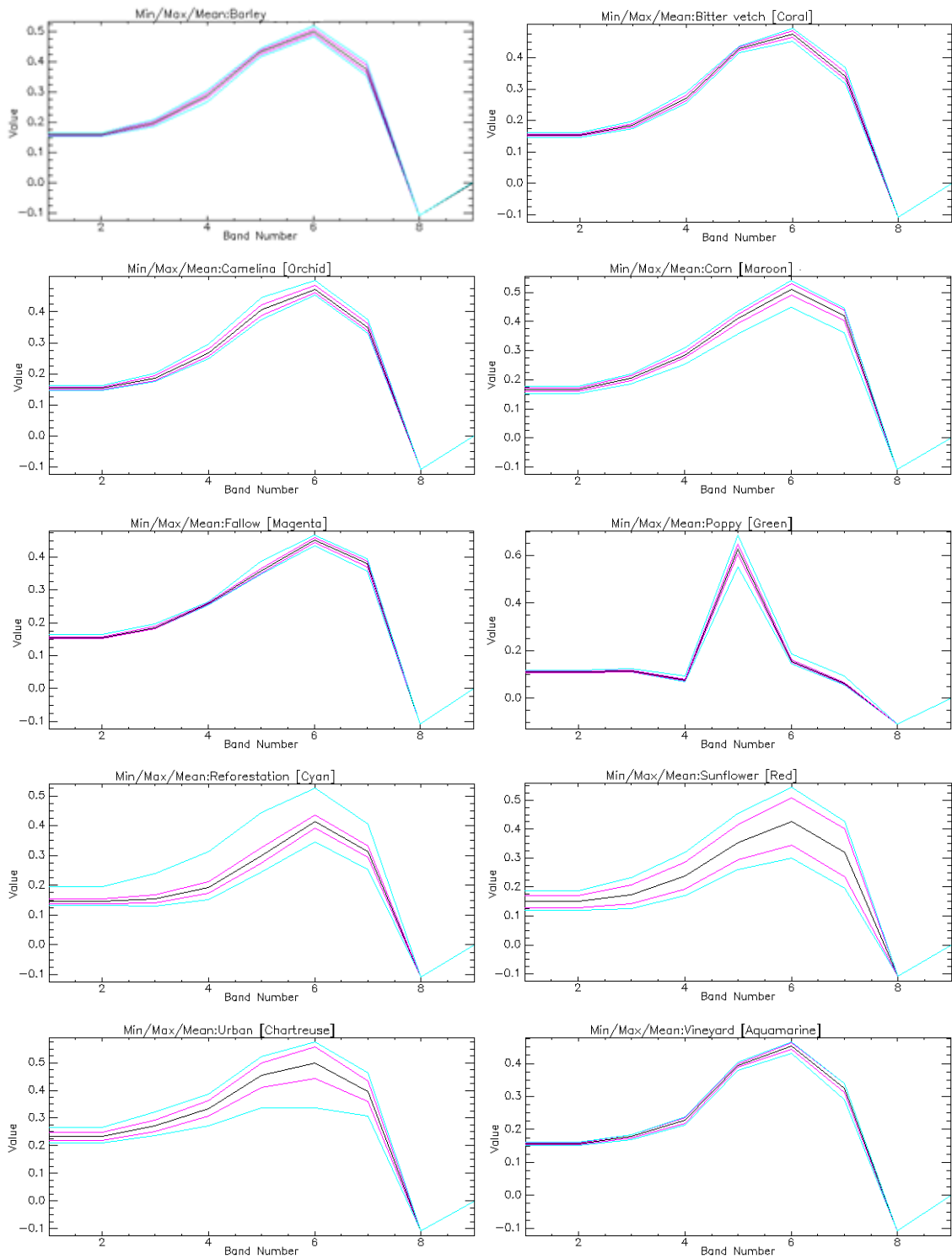


FIGURE 79. BARRAX, TRAINING ROI, JD 155 2014 (LEFT) AND CLASSIFIED IMAGE, JD 155 2014 (RIGHT)

It is possible to notice that the main colours present in the map correspond to fallow (bare soil) and urban where the image in real colour looks like without vegetation.

Otherwise, the pivots present in the rest of the area are classified pretty good.

Following, the entire spectra analysed are represented.



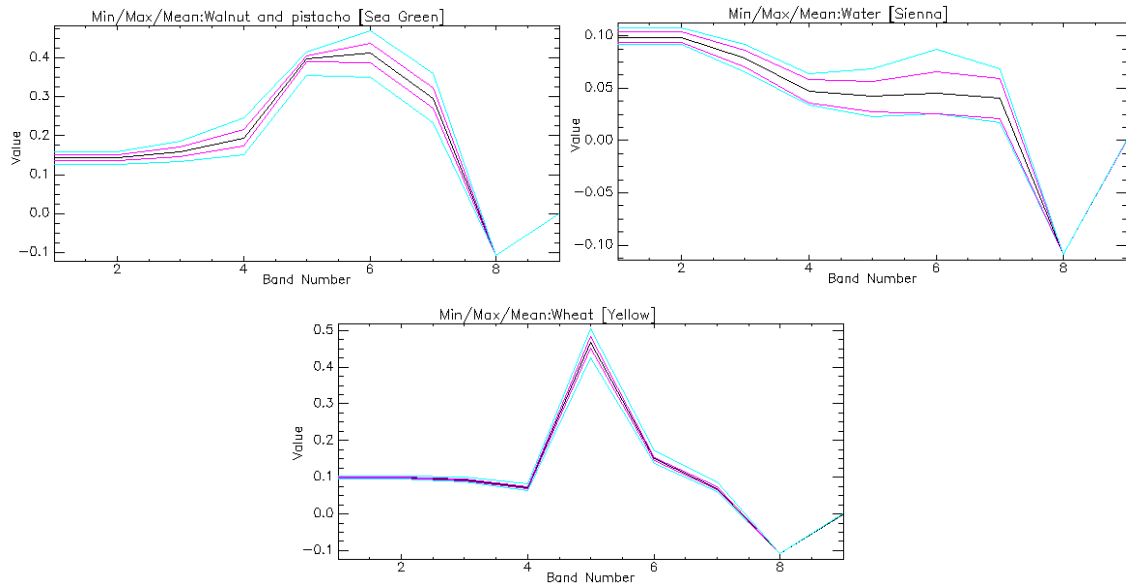


FIGURE 80. BARRAX, SPECTRA OF USED ROIs, JD 155 2014

The spectrum of each ROI changes in the time, from the growing of the plants to the harvest. The spectra similar to the urban or bare soil spectrum, mean that the harvest is already occurred, or that the plants are little and need time to grown up.

From the following images is possible to see the evolution in three months of the poppy spectrum, monitoring the plants the day 19<sup>th</sup> of May (JD 139), the 4<sup>th</sup> of June (JD 155) and the 13<sup>th</sup> of July (JD 194) of the year 2014. During this period the plants are growing, the plants are getting ready for the harvest and finally in July the harvest is already occurred.

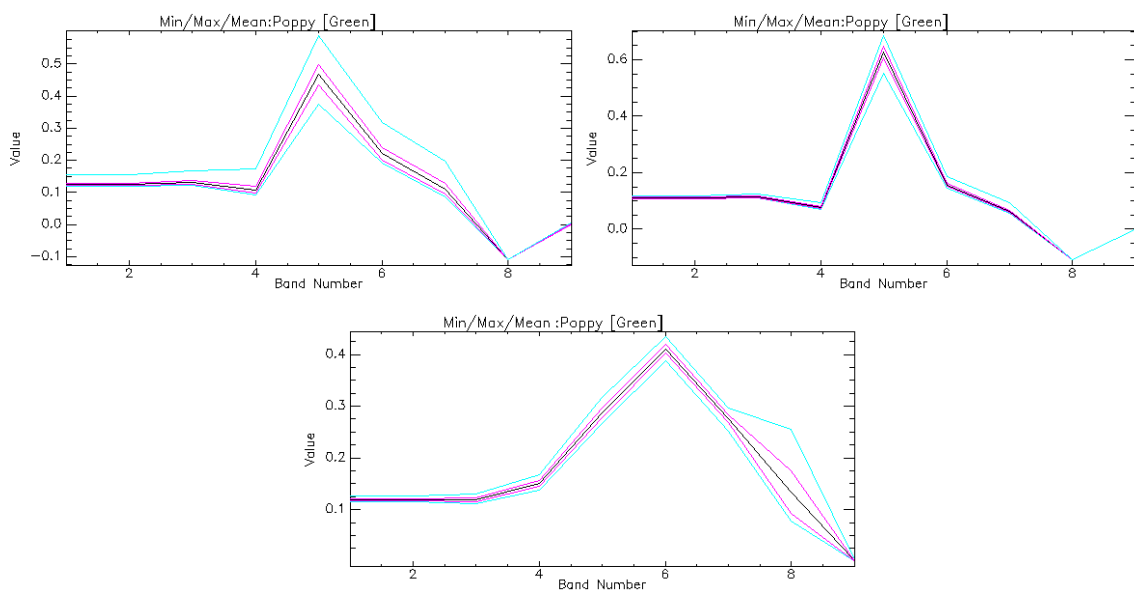


FIGURE 81. BARRAX, SPECTRA OF POPPY ROI, JD 139 (LEFT), 155 (RIGHT) AND 194 (DOWN) 2014

### 5.1.3 BARRAX, 7<sup>TH</sup> OF JUNE 2015

Another classification is done on a different period of time, in the same season but in the year 2015, using obviously the land use map of 2015, and a Landsat 8 image.

This time the main crops are barley but there is a high variability.

The JD 158, 7<sup>th</sup> of June 2015 is classified with the same methodology. ROIs are identified (Figure 83, left) and the classification is performed.

Moreover, having a lot of fields of barley, a validation is done. Not all the ROIs of barley are used for a second classification and checking if the software is able to identify if the ROI not used is a region of barley, and if something changes in the whole processed area.

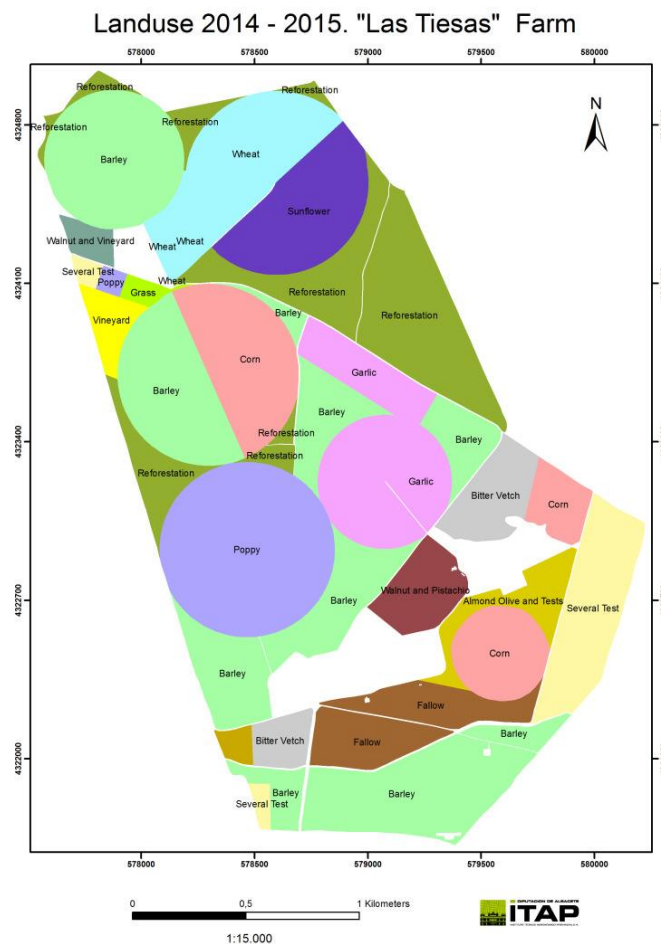


FIGURE 82. BARRAX LANDUSE MAP 2014 -2015 IN LAS TIASAS FARM

ROI Name	Color	Pixels
Barley	Red	956
Wheat	Green	239
Fallow	Yellow	108
Garlic	Cyan	305
Poppy	Magenta	409
Grass	Maroon	9
Bitter Vetch	Sea Green	102
Walnut and Pista	Purple	80
Vineyard	Coral	34
Sunflower	Aquamarine	228
Almond olive and	Orchid	72
Reforestation	Orange1	441
Water	Sienna	13
Urban	Chartreuse	31
Com	Blue	326
Bare soil	Thistle	231
Undefined	Black	0

TABLE 32. BARRAX ROIs FOR IMAGE OF JD 158 2015



FIGURE 83. BARRAX, TRAINING ROI, JD 158 2015. WITH ENTIRE BARLEY ROIs (LEFT), AND WITHOUT A BARLEY ROI(RIGHT)

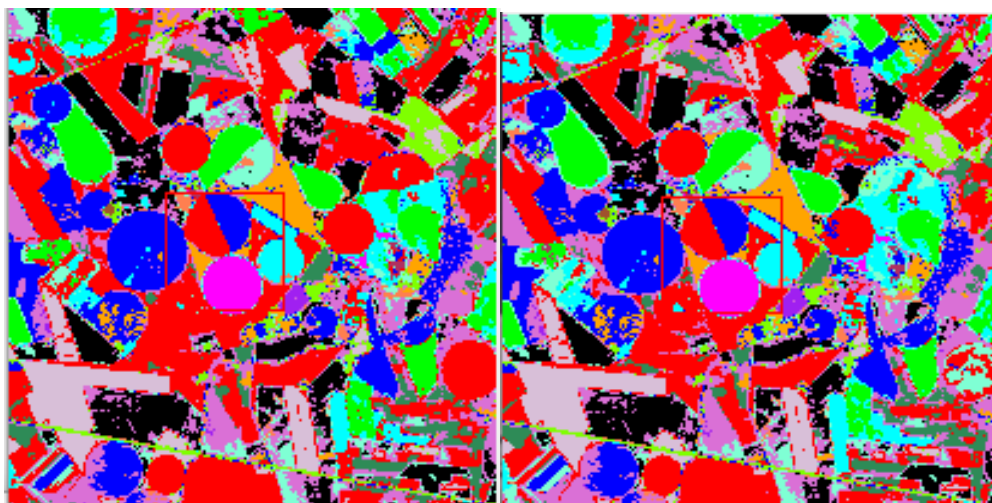


FIGURE 84. BARRAX, CLASSIFIED IMAGE, JD 158 2015. CLASSIFICATION MADE WITH ENTIRE BARLEY ROIs (LEFT), AND WITHOUT A BARLEY ROI(RIGHT)

As notable, the differences among the two images are almost null and the not used ROI is correctly identified. The black regions are created because ENVI is not able to distinguish the difference between two ROI given to classify the imagery, i.e. when the spectra of the ROIs in that region are too similar to both.

In the following the spectra of the different ROIs are reported in the different bands, showing also the homogeneity of the single ROI.

The spectra have different slopes and values for the different crops. NDVI is also computed: highest value is obtained for wheat, while the lowest for bitter vetch and reforestation.

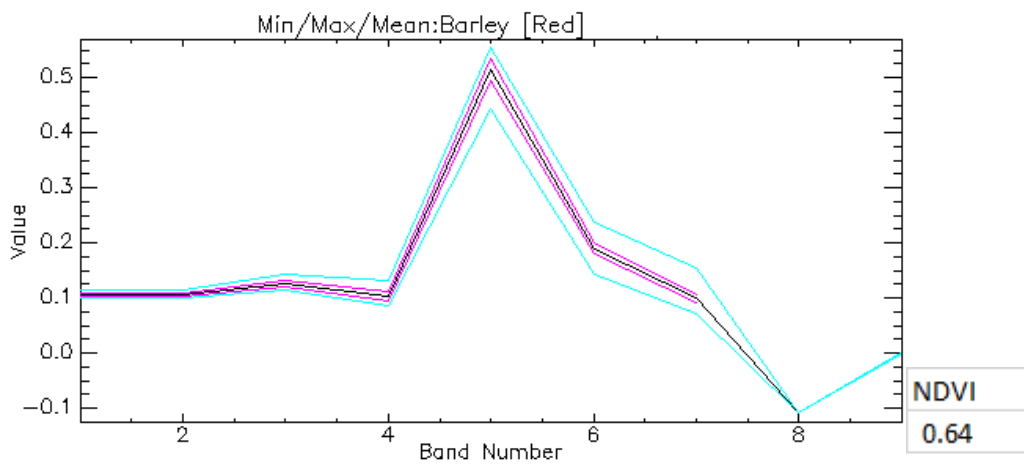


FIGURE 85. BARRAX, SPECTRUM OF BARLEY ROI, JD 158 2015

Band	Min	Max	Mean	Stdev
1	0.10	0.12	0.11	0.00
2	0.10	0.12	0.11	0.00
3	0.11	0.14	0.13	0.01
4	0.09	0.13	0.10	0.01
5	0.44	0.55	0.52	0.02
6	0.14	0.24	0.19	0.01
7	0.07	0.16	0.10	0.01
9	0.00	0.00	0.00	0.00

TABLE 33. BARRAX, STATISTICS OF THE SPECTRUM OF BARLEY ROI, JD 158 2015

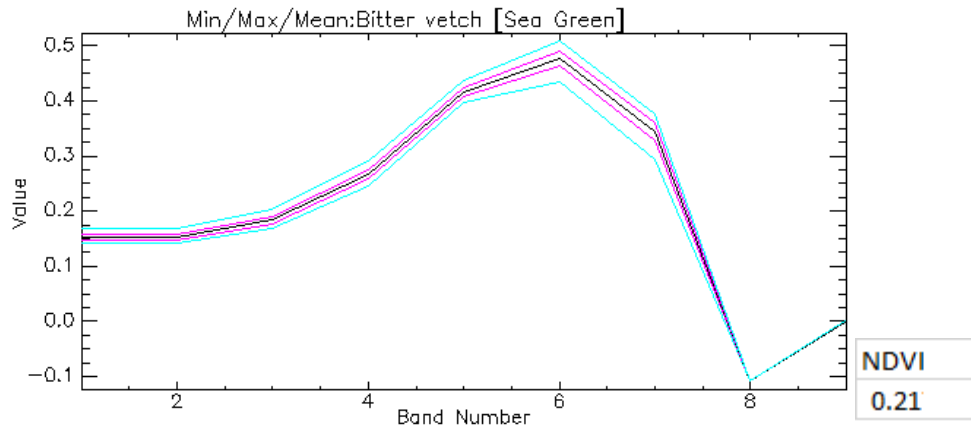


FIGURE 86. BARRAX, SPECTRUM OF BITTER VETCH ROI, JD 158 2015

Band	Min	Max	Mean	Stdev
1	0.14	0.17	0.15	0.00
2	0.14	0.17	0.15	0.00
3	0.17	0.20	0.18	0.01
4	0.25	0.29	0.27	0.01
5	0.40	0.44	0.42	0.01
6	0.43	0.51	0.48	0.01
7	0.29	0.38	0.34	0.01
9	0.00	0.00	0.00	0.00

TABLE 34. BARRAX, STATISTICS OF THE SPECTRUM OF BITTER VETCH ROI, JD 158 2015

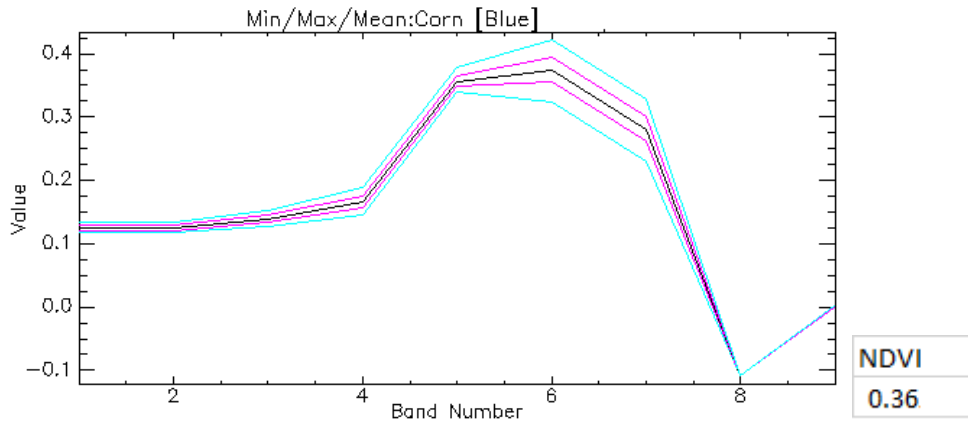


FIGURE 87. BARRAX, SPECTRUM OF CORN ROI, JD 158 2015

Band	Min	Max	Mean	Stdev
1	0.12	0.13	0.12	0.00
2	0.12	0.13	0.12	0.00
3	0.13	0.15	0.14	0.01
4	0.14	0.19	0.17	0.01
5	0.34	0.38	0.36	0.01
6	0.32	0.42	0.37	0.02
7	0.23	0.33	0.28	0.02
9	0.00	0.00	0.00	0.00

TABLE 35. BARRAX, STATISTICS OF THE SPECTRUM OF CORN ROI, JD 158 2015

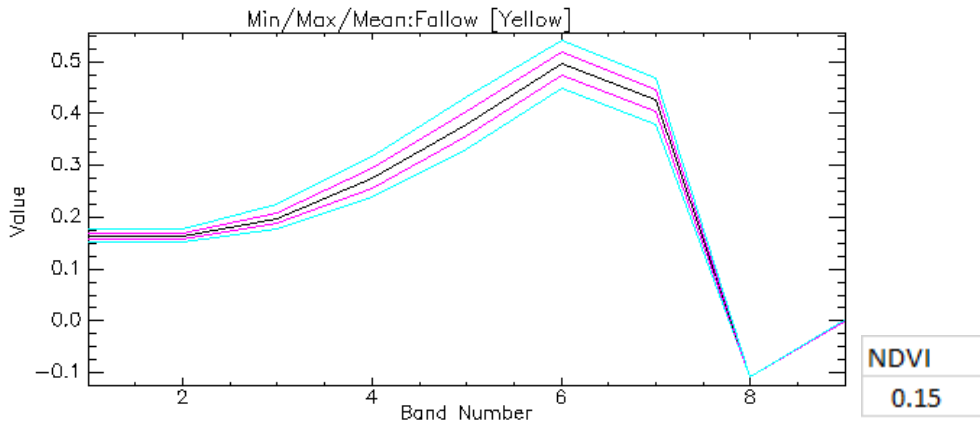


FIGURE 88. BARRAX, SPECTRUM OF FALLOW ROI, JD 158 2015

Band	Min	Max	Mean	Stdev
1	0.15	0.18	0.16	0.01
2	0.15	0.18	0.16	0.01
3	0.18	0.22	0.20	0.01
4	0.24	0.32	0.28	0.02
5	0.33	0.43	0.38	0.02
6	0.45	0.54	0.50	0.02
7	0.38	0.47	0.43	0.02
9	0.00	0.00	0.00	0.00

TABLE 36. BARRAX, STATISTICS OF THE SPECTRUM OF FALLOW ROI, JD 158 2015

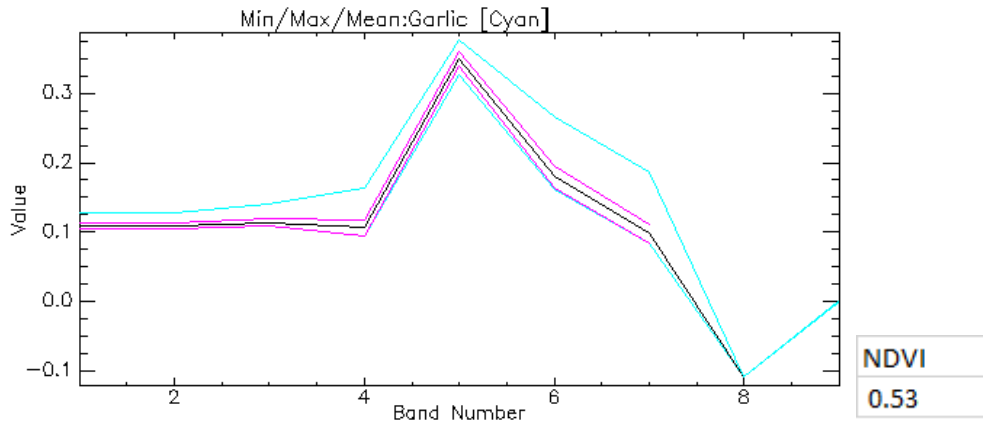


FIGURE 89. BARRAX, SPECTRUM OF GARLIC ROI, JD 158 2015

Band	Min	Max	Mean	Stdev
1	0.11	0.13	0.11	0.00
2	0.11	0.13	0.11	0.00
3	0.11	0.14	0.11	0.01
4	0.09	0.16	0.11	0.01
5	0.33	0.38	0.35	0.01
6	0.16	0.27	0.18	0.02
7	0.08	0.19	0.10	0.01
9	0.00	0.00	0.00	0.00

TABLE 37. BARRAX, STATISTICS OF THE SPECTRUM OF GARLIC ROI, JD 158 2015



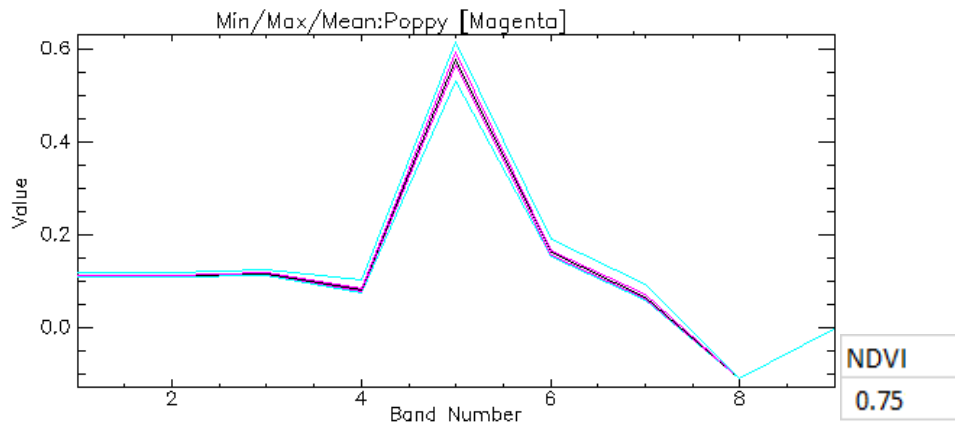


FIGURE 90. BARRAX, SPECTRUM OF POPPY ROI, JD 158 2015

Band	Min	Max	Mean	Stdev
1	0.11	0.12	0.11	0.00
2	0.11	0.12	0.11	0.00
3	0.11	0.13	0.12	0.00
4	0.08	0.10	0.08	0.00
5	0.53	0.62	0.58	0.01
6	0.15	0.19	0.16	0.01
7	0.06	0.09	0.07	0.00
9	0.00	0.00	0.00	0.00

TABLE 38. BARRAX, STATISTICS OF THE SPECTRUM OF POPPY ROI, JD 158 2015

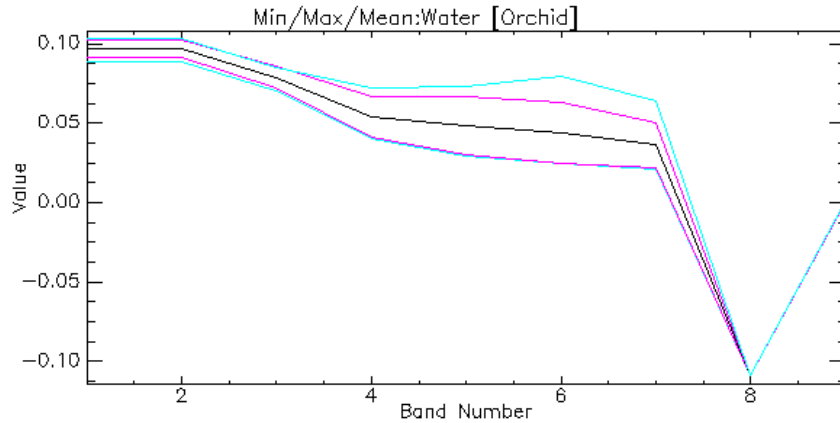


FIGURE 91. BARRAX, SPECTRUM OF BARLEY ROI, JD 158 2015

Band	Min	Max	Mean	Stdev
1	0.09	0.10	0.10	0.01
2	0.09	0.10	0.10	0.01
3	0.07	0.09	0.08	0.01
4	0.04	0.07	0.05	0.01
5	0.03	0.07	0.05	0.02
6	0.02	0.08	0.04	0.02
7	0.21	0.06	0.04	0.01
9	0.00	0.00	0.00	0.00

TABLE 39. BARRAX, STATISTICS OF THE SPECTRUM OF BARLEY ROI, JD 158 2015

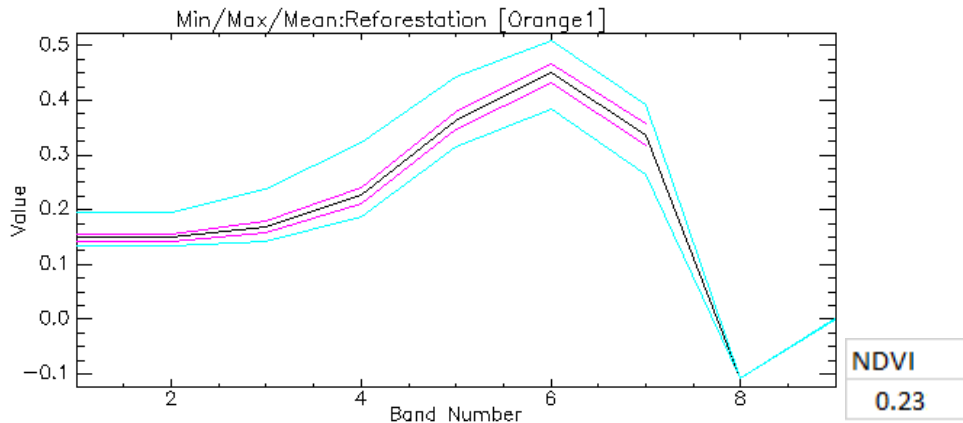


FIGURE 92. BARRAX, SPECTRUM OF REFORESTATION ROI, JD 158 2015

Band	Min	Max	Mean	Stdev
1	0.13	0.20	0.15	0.01
2	0.13	0.20	0.15	0.01
3	0.14	0.24	0.17	0.01
4	0.19	0.32	0.23	0.01
5	0.32	0.44	0.36	0.02
6	0.38	0.51	0.45	0.02
7	0.26	0.39	0.34	0.02
9	0.00	0.00	0.00	0.00

TABLE 40. BARRAX, STATISTICS OF THE SPECTRUM OF REFORESTATION ROI, JD 158 2015

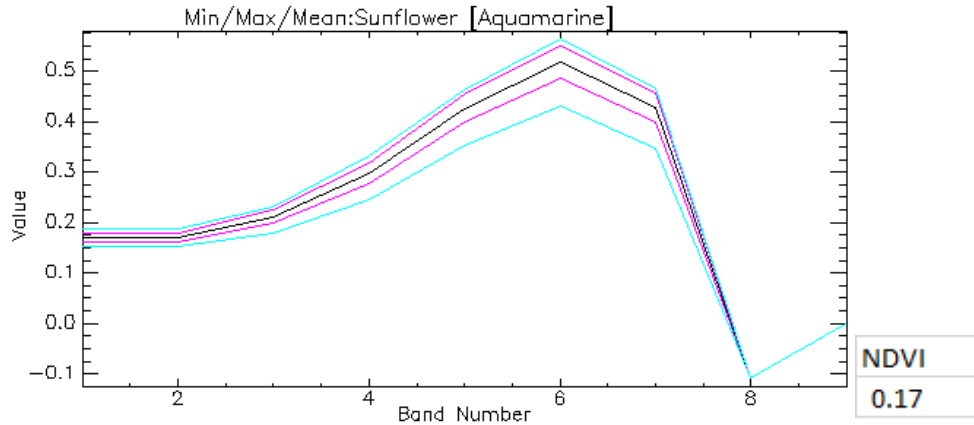


FIGURE 93. BARRAX, SPECTRUM OF SUNFLOWER ROI, JD 158 2015

Band	Min	Max	Mean	Stdev
1	0.15	0.19	0.17	0.01
2	0.15	0.19	0.17	0.01
3	0.18	0.23	0.21	0.01
4	0.24	0.33	0.30	0.02
5	0.35	0.46	0.43	0.03
6	0.43	0.56	0.52	0.03
7	0.35	0.47	0.43	0.03
9	0.00	0.00	0.00	0.00

TABLE 41. BARRAX, STATISTICS OF THE SPECTRUM OF SUNFLOWER ROI, JD 158 2015

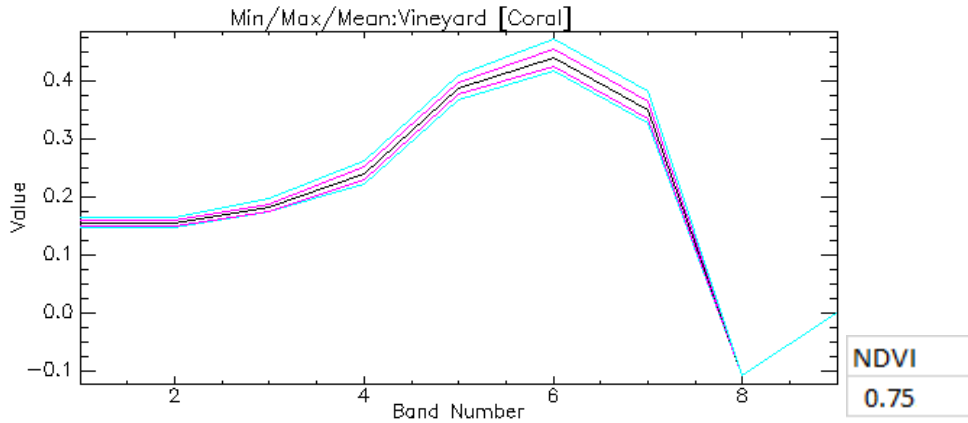


FIGURE 94. BARRAX, SPECTRUM OF VINEYARD ROI, JD 158 2015

Band	Min	Max	Mean	Stdev
1	0.11	0.12	0.11	0.00
2	0.11	0.12	0.11	0.00
3	0.11	0.13	0.12	0.00
4	0.08	0.10	0.08	0.00
5	0.53	0.62	0.58	0.01
6	0.15	0.19	0.16	0.01
7	0.06	0.09	0.07	0.00
9	0.00	0.00	0.00	0.00

TABLE 42. BARRAX, STATISTICS OF THE SPECTRUM OF VINEYARD ROI, JD 158 2015

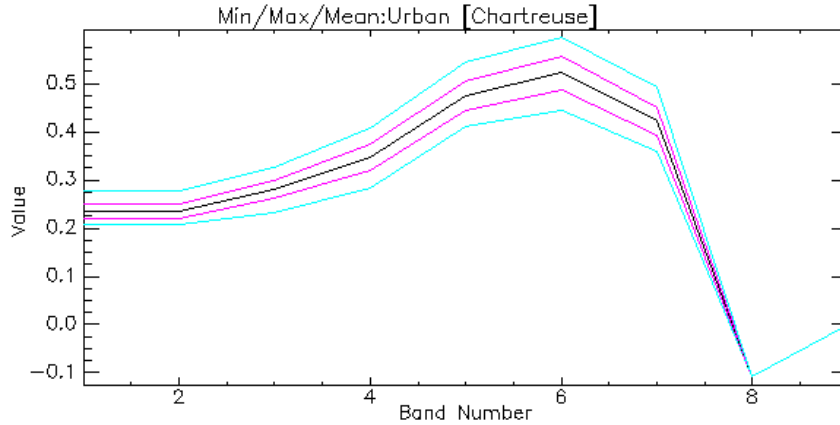


FIGURE 95. BARRAX, SPECTRUM OF URBAN ROI, JD 158 2015

Band	Min	Max	Mean	Stdev
1	0.21	0.28	0.24	0.02
2	0.21	0.28	0.24	0.02
3	0.23	0.32	0.28	0.02
4	0.28	0.41	0.35	0.03
5	0.41	0.54	0.47	0.03
6	0.44	0.60	0.52	0.03
7	0.36	0.49	0.42	0.03
9	0.00	0.00	0.00	0.00

TABLE 43. BARRAX, STATISTICS OF THE SPECTRUM OF URBAN ROI, JD 158 2015

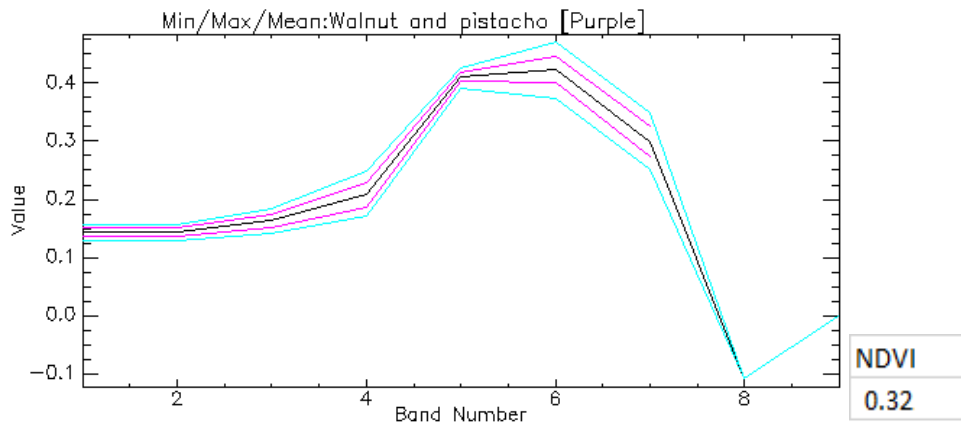


FIGURE 96. BARRAX, SPECTRUM OF WALNUT AND PISTACHO ROI, JD 158 2015

Band	Min	Max	Mean	Stdev
1	0.13	0.16	0.14	0.01
2	0.13	0.16	0.14	0.01
3	0.14	0.18	0.16	0.01
4	0.17	0.25	0.21	0.02
5	0.39	0.43	0.41	0.01
6	0.37	0.47	0.42	0.02
7	0.25	0.35	0.30	0.03
9	0.00	0.00	0.00	0.00

TABLE 44. BARRAX, STATISTICS OF THE SPECTRUM OF WALNUT AND PISTACHO ROI, JD 158 2015

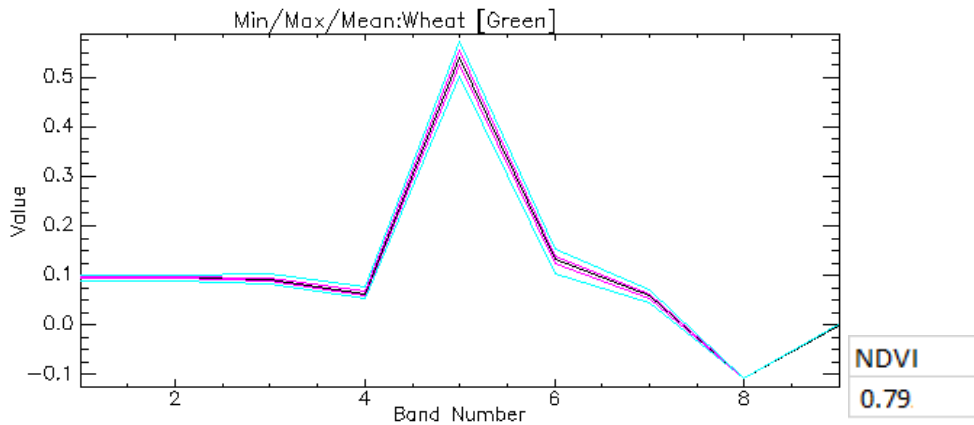


FIGURE 97. BARRAX, STATISTICS OF THE SPECTRUM OF WHEAT ROI, JD 158 2015

Band	Min	Max	Mean	Stdev
1	0.09	0.10	0.10	0.00
2	0.09	0.10	0.10	0.00
3	0.08	0.10	0.09	0.00
4	0.05	0.08	0.06	0.00
5	0.50	0.57	0.54	0.01
6	0.10	0.15	0.13	0.01
7	0.04	0.07	0.06	0.00
9	0.00	0.00	0.00	0.00

TABLE 45. BARRAX, STATISTICS OF THE SPECTRUM OF WHEAT ROI, JD 158 2015

## 5.2 FOGGIA

The supervised classification in Foggia is done in two different seasons, in winter and in summer, according to the seasonal crops. The winter classification is done using Landsat 8 images on the 27<sup>th</sup> of January 2016, the summer one on the 19<sup>th</sup> of May 2016. In winter the fields have mainly green vegetables, in summer mainly tomatoes and wheat.

The ROIs are retrieved from a farmer of the Consorzio della Capitanata.

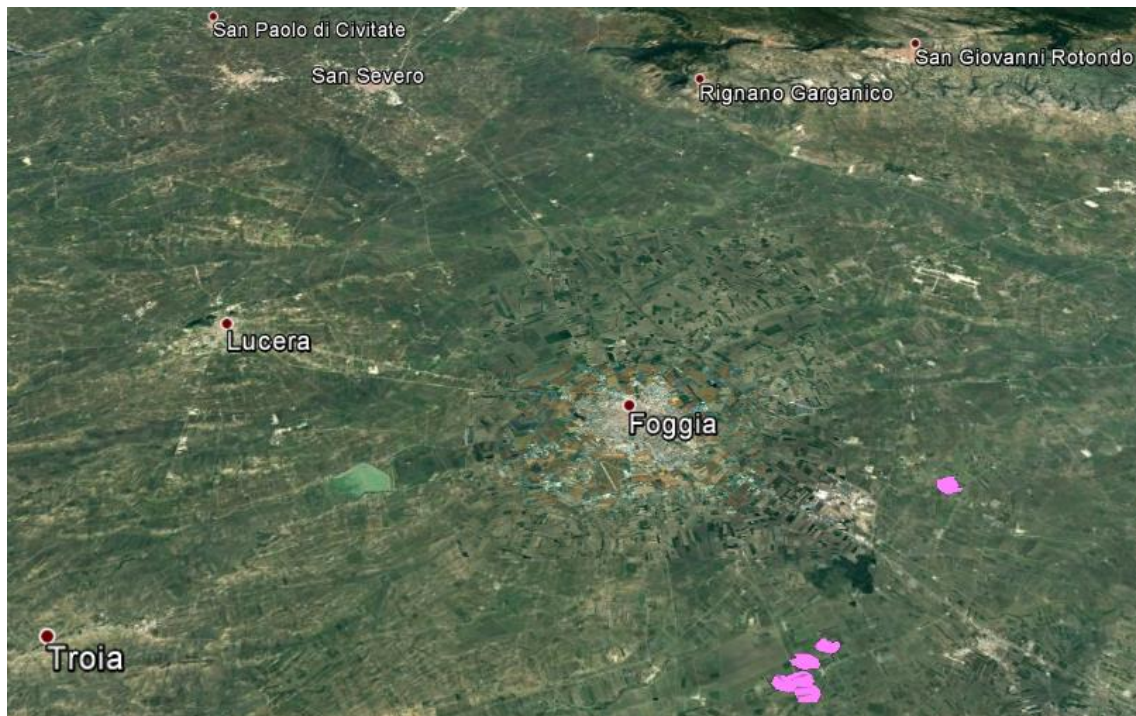


FIGURE 98. FOGGIA, SHAPE FILE CONTAINING 2016 LANDUSE INFORMATION, PLOTTED ON GOOGLE EARTH IMAGE

### 5.2.1 FOGGIA, 27<sup>TH</sup> OF JANUARY 2016

In the processed areas, there are some clouds, but it is possible to apply the classification because the clouds are on the border of the images out of the area of Capitanata consortium.

It is important to identify the urban area that has a similar spectrum response to the bare soil and clouds, due to the high reflectance.

ROI Name	Color	Pixels
Cavolo	Red	142
Spinaci	Green	737
Rucola	Blue	6
Erbette	Yellow	464
Pak choi	Cyan	159
Coste	Sea Green	106
Cavolo nero	Orchid	67
Finocchi	Red1	117
Asparagi	Blue1	647
Prezzemolo	Orange 1	89
Verze	Orange3	157
Cima di rapa	Chartreuse	59
Water	Magenta	2,095
Urban	Maroon	5,044
Vigna	Purple	24
Ulivi	Coral	17
Parco Naturale	Aquamarine	1,180
Bare Soil	Sienna	1,250

TABLE 46. FOGGIA ROIs, BASED ON INFORMATIONAL SHAPE FILE, JD 027. WHERE CAVOLO=CABBAGE, SPINACI=SPINACH, RUCOLA=ROCKET SALAD, ERBETTE=LEAF BEET, COSTE=SWISS CHARD, CAVOLO NERO=BLACK CABBAGE, FINOCCHI=FENNEL, ASPARAGI=ASPARAGUS, PREZZEMOLO=PARSLEY, VERZE=SAVOY CABBAGE, CIME DI RAPA=TURNIP GREENS, VIGNA=VINEYARDS, ULIVI=OLIVE GROVES, PARCO NATURALE=NATURAL PARK, IS A WOODLAND.

Here some spectra of the biggest ROI analysed:

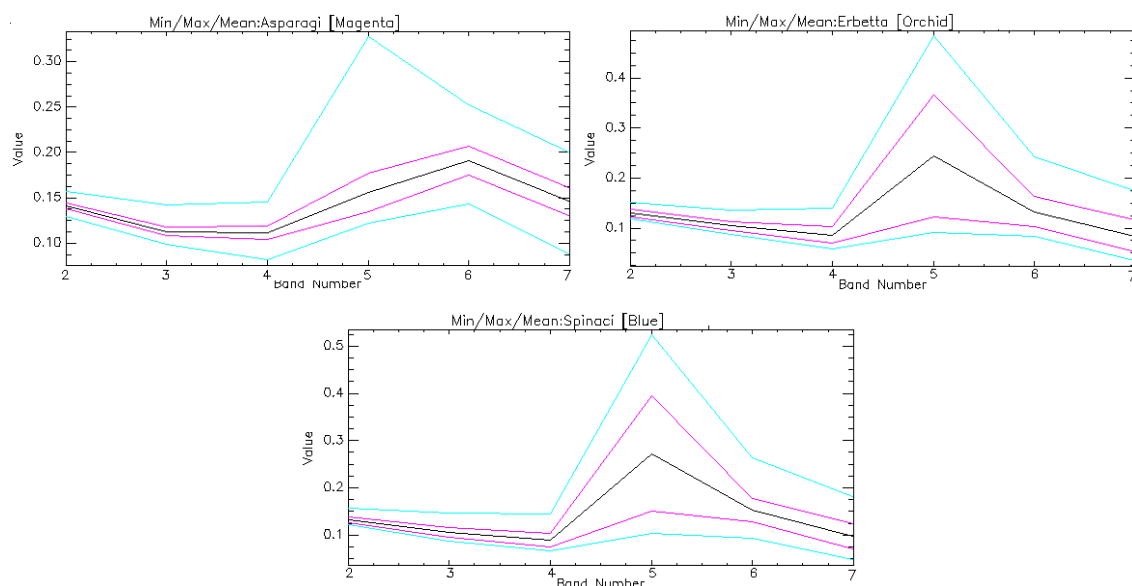


FIGURE 99. FOGGIA, SPECTRA OF ASPARAGUS, LEAF BEET AND SPINACH

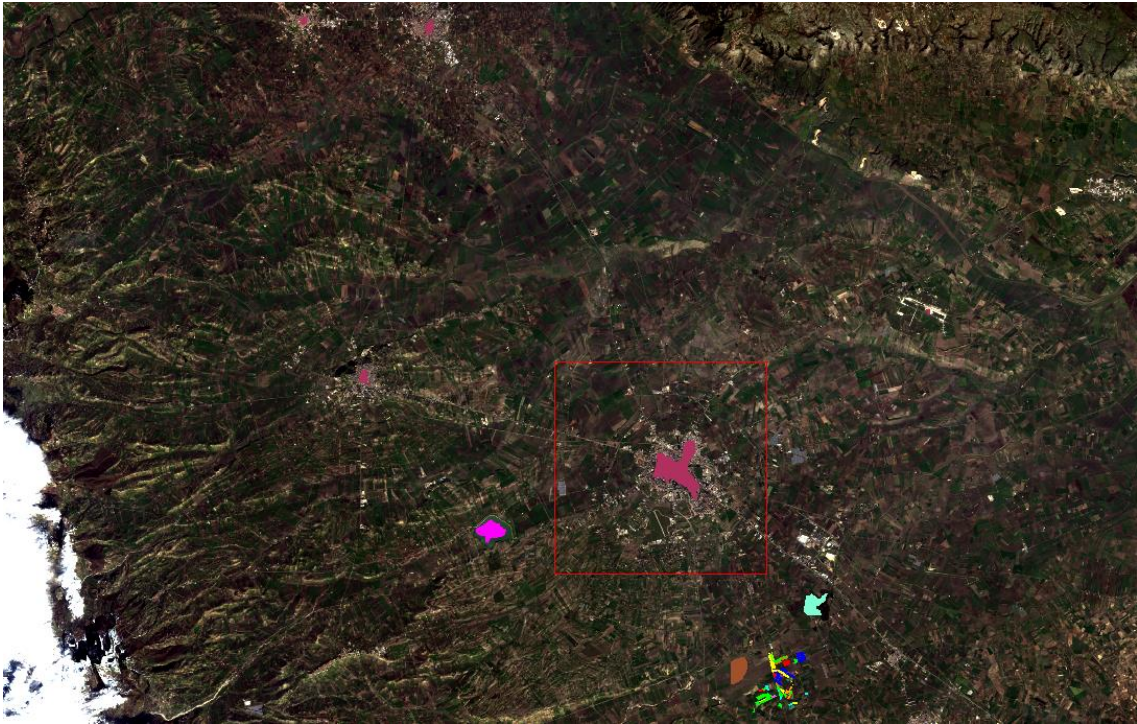


FIGURE 100. FOGGIA, TRAINING ROIs, JD 027



FIGURE 101. FOGGIA, ZOOM ON TRAINING ROIs, JD 027

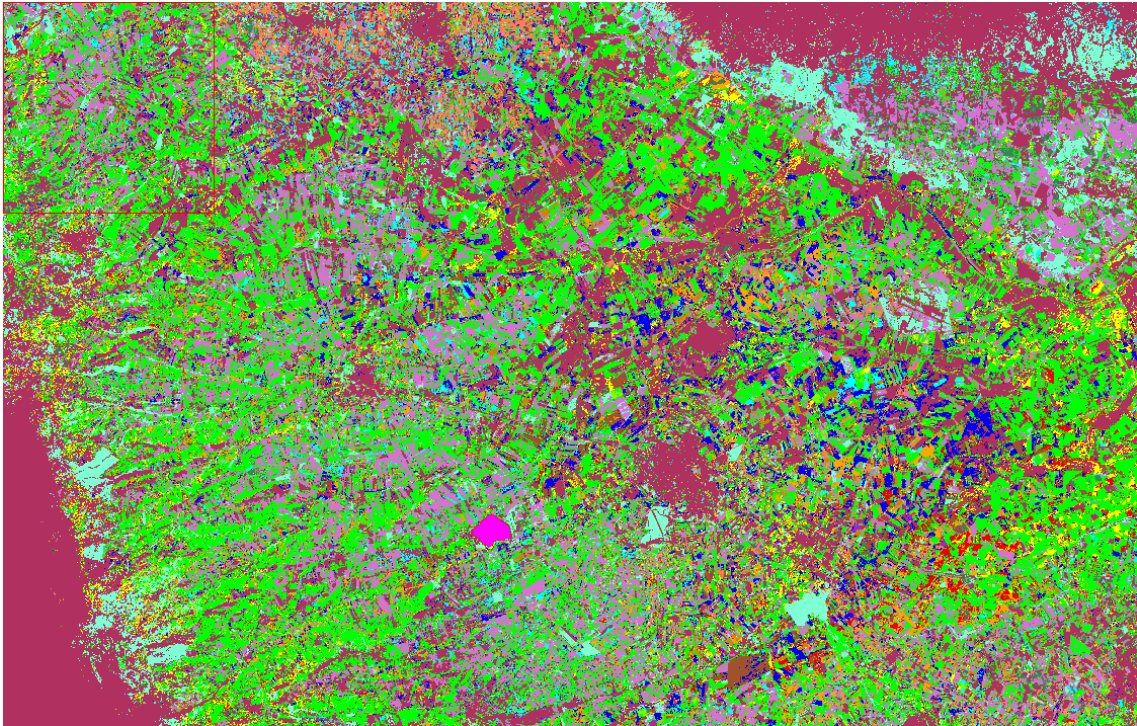


FIGURE 102. FOGGIA, CLASSIFIED IMAGE JD 027

As expected, the classification presents a large area of green vegetables fields, and urban area that sometimes is comparable to bare soil cause the difficulty in differentiating the spectra.

### 5.2.2 FOGGIA, 19<sup>TH</sup> OF MAY 2016

The second classification is done on the 19<sup>th</sup> of May 2016. The ROIs are retrieved from a farmer of the Consorzio della Capitanata.

ROI Name	Color	Pixels
Parco Naturale	Red	810
Pomodoro	Green	352
Asparagi	Blue	647
Water	Yellow	1,315
Ulivo	Cyan	9
Grano	Magenta	2,659
Vigna	Maroon	18
Bare soil	Sea Green	481
Urban	Purple	134

TABLE 47. FOGGIA ROIs, BASED ON INFORMATIONAL SHAPE FILE, JD 139. WHERE POMODORO=TOMATOES, ASPARAGI=ASPARAGUS, VIGNA=VINEYARDS, ULIVI=OLIVE GROVES, GRANO=WHEAT, PARCO NATURALE=NATURAL PARK, IS A WOODLAND.



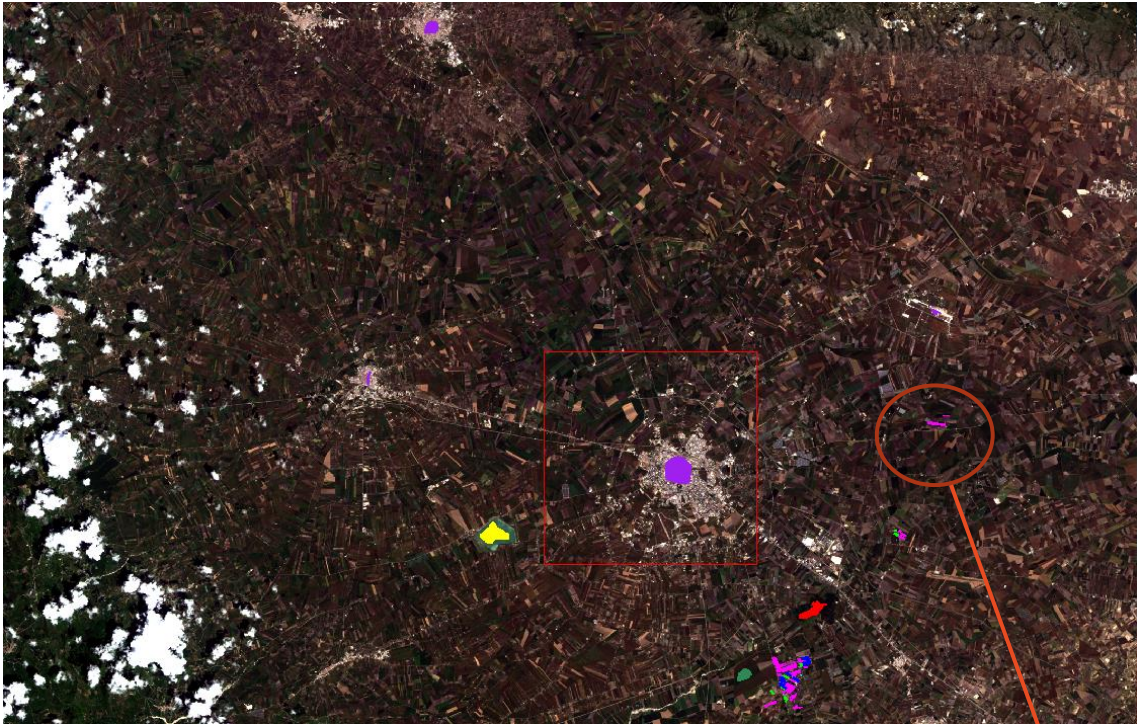


FIGURE 103. FOGGIA, TRAINING ROIs, JD 139

ROI USED FOR  
VALIDATION

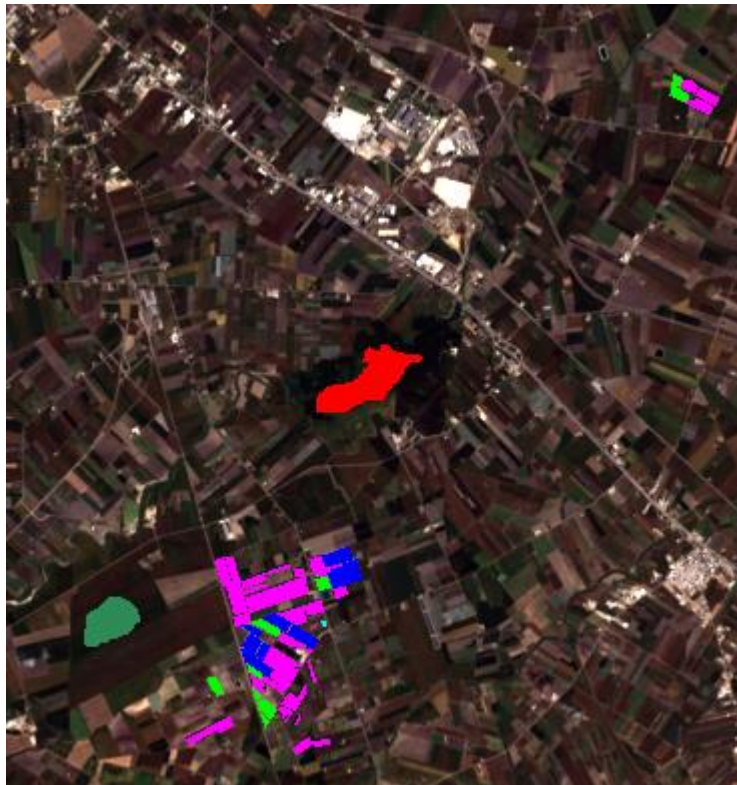


FIGURE 104. FOGGIA, ZOOM ON TRAINING ROIs, JD 139

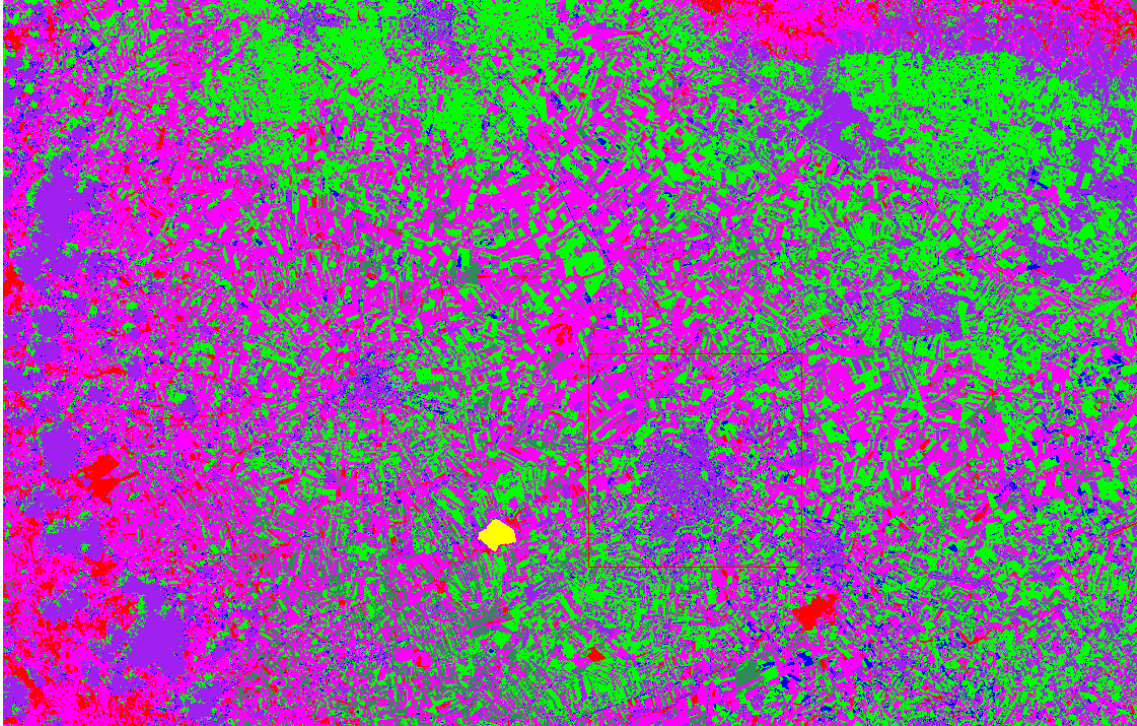


FIGURE 105. FOGGIA, CLASSIFIED IMAGE, JD 139.

It is possible to notice that the main part of the image is magenta and green, i.e. the colours of wheat and tomatoes, as desirable knowing that those are the mainly crops in this season.

As we can see in Figure 203, on the right side of the image there is a ROI of wheat (magenta colour); in order to validate the classification, this ROI is cancelled and is built a new classification, checking if, in those fields, the software is able to recognize the wheat and if, in a larger scale, something changes.

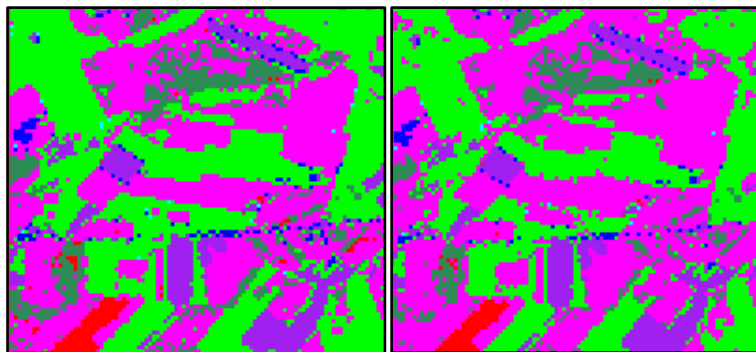


FIGURE 106. FOGGIA VALIDATION, ZOOM ON THE CLASSIFIED IMAGE AREA WITHOUT PART OF WHEAT ROI (LEFT) AND THE CLASSIFIED AREA WITH ENTIRE ROI (RIGHT), JD 139 2016

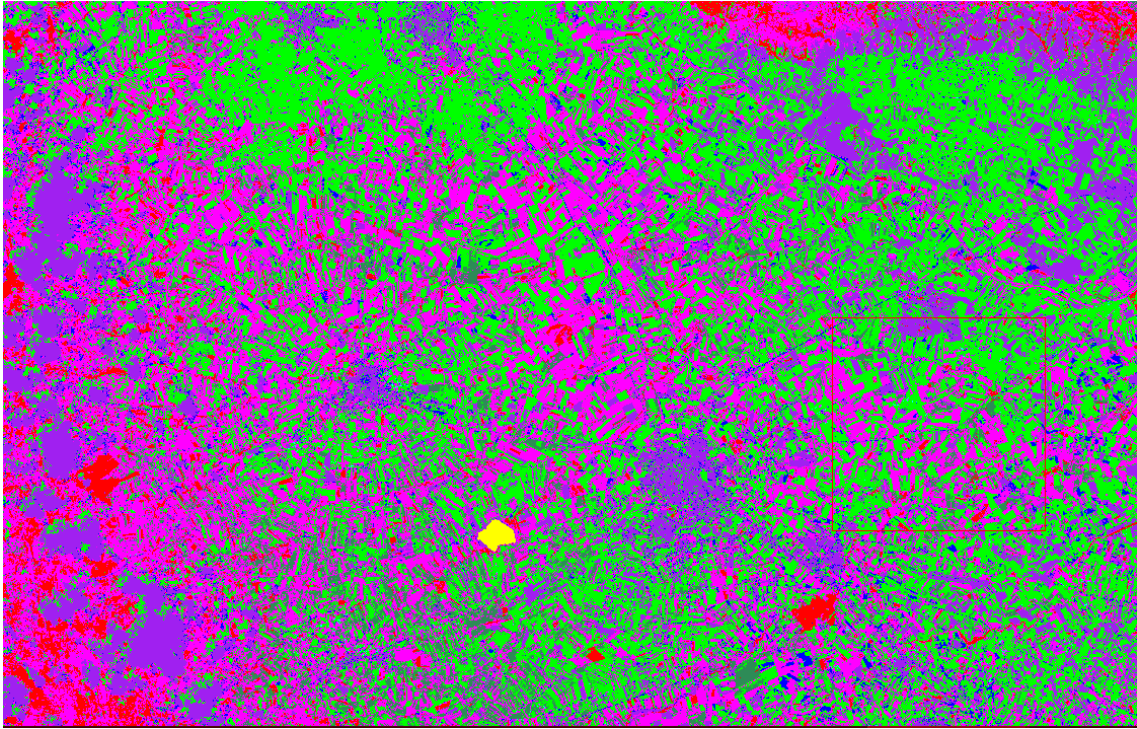


FIGURE 107. FOGGIA VALIDATION, CLASSIFIED IMAGE WITHOUT PART OF WHEAT ROI, JD 139 2016

The result of the validation is good: the differences among the calibrations are few.

## 6 MODELLING: WATER AND ENERGY FLUXES (BARRAX)

The objective of this chapter is to understand how the errors are propagated into the hydrological model. In particular, the effect of input parameters (FVC, LAI, Albedo), from different satellites and dates, will be analysed on FEST-EWB estimates of LST and latent heat flux. This is achieved with the idea of using Landsat 5, 7, 8 and Sentinel 2 and 3 data.

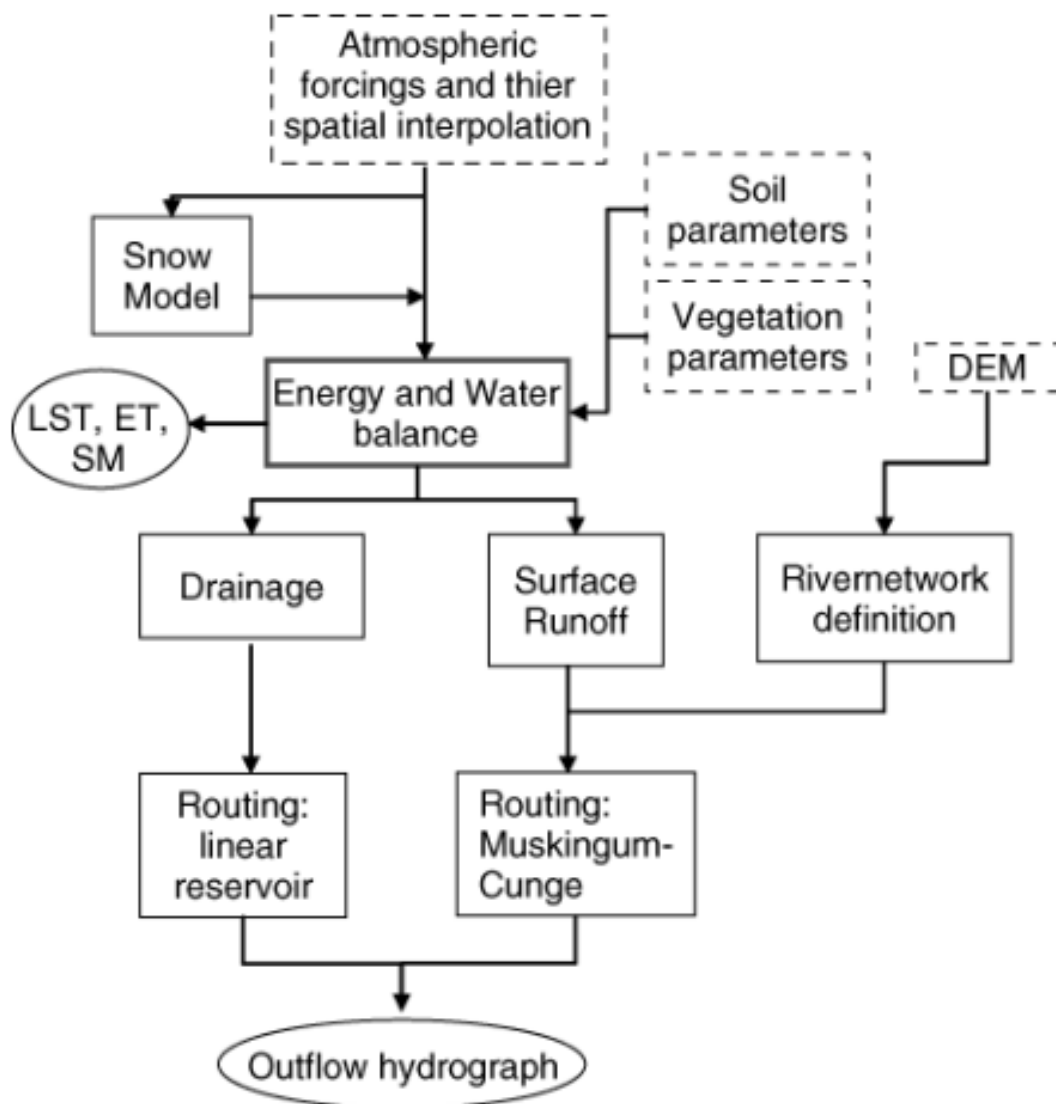


FIGURE 108. FEST-EWB PROCESS

## 6.1 INTRODUCTION TO FEST-EWB HYDROLOGICAL MODEL

FEST-EWB (Flash-flood Event-based Spatially distributed rainfall-runoff Transformation-Energy Water Balance) is a distributed hydrological energy water balance model and it is developed starting from the FEST-WB (Mancini 1990). This model is thought for a synergic use of hydrological model with remote sensing data. FEST-EWB computes the main processes of the hydrological cycle: ET, infiltration, surface runoff, flow routing, subsurface flow and snow dynamics (Corbari C 2009). In the FEST-EWB, the energy balance module is introduced, it computes energy and water balance equations to compute soil moisture dynamic. In particular, the energy balance is solved looking for the land surface temperature that closes the balance. So, the latent and sensible heat fluxes are function of LST, as also soil moisture. The model is distributed so that the computation domain is discretized with a mesh of regular square cells in which every parameter is defined or calculated (Chiara Corbari 2011).

## 6.2 INPUT PARAMETERS

The input parameters of the system are:

1. meteorological data related to a defined temporal window, which are data of rain, air temperature, humidity, velocity of the wind and solar radiation.
2. Digital Elevation Model
3. Soil parameters
4. Vegetation parameters

The first three point are taken from Corbari et al 2015 (CORBARI 2015).

Albedo, FVC and LAI retrieved from remote sensing data in chapter 4.

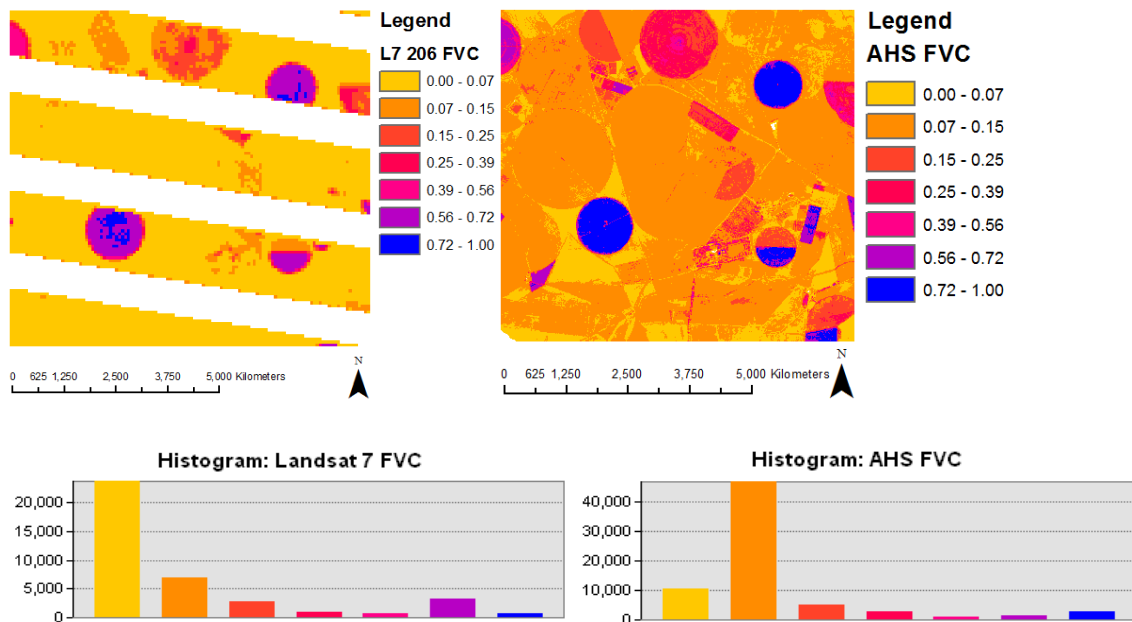
The meteorological data are available from 18<sup>th</sup> of July 2012 till the 27<sup>th</sup> of July 2012, when the usable Landsat images are only the Landsat 7 ones. In order to provide to the model images without stripes, the images are corrected in two different ways named Gapfill and Likelihood. Gapfill data are corrected with the Gapfill add in for ENVI, which makes an interpolation of the data of the nearby pixels, meanwhile the data called Likelihood are

manually filled using the values of the same fields which were available. The FEST model is run 7 times with different input data, using the configurations shown by the table:

Configurations	LAI	FVC	ALB
L5 Gapfill	L5	L5	L7 213 Gapfill
L5 Likelihood	L5	L5	L7 213 Likelihood
L7 213 Gapfill	L7 213 Gapfill	L7 213 Gapfill	L7 213 Gapfill
L7 213 Likelihood	L7 213 Likelihood	L7 213 Likelihood	L7 213 Likelihood
L7 206 Gapfill	L7 206 Gapfill	L7 206 Gapfill	L7 206 Gapfill
L7 206 Likelihood	L7 206 Likelihood	L7 206 Likelihood	L7 206 Likelihood
AHS sim	AHS	AHS	AHS

TABLE 48. CONFIGURATIONS OF THE SIMULATIONS

Where 206 and 213 indicate the Julian Day from which are taken the data and AHS data are retrieved by the Airborne Hyperspectral Scanner during the flight campaign of the 25<sup>th</sup> and 26<sup>th</sup> of July. In the following the comparison between the maps retrieved from Landsat 7 in the JD 206 (24<sup>th</sup> of July) and AHS images retrieved the JD 207 (25<sup>th</sup> of July), and all the others inputs. Moreover, are plotted the histograms of the maps, with classes on x axis and count on y axis.



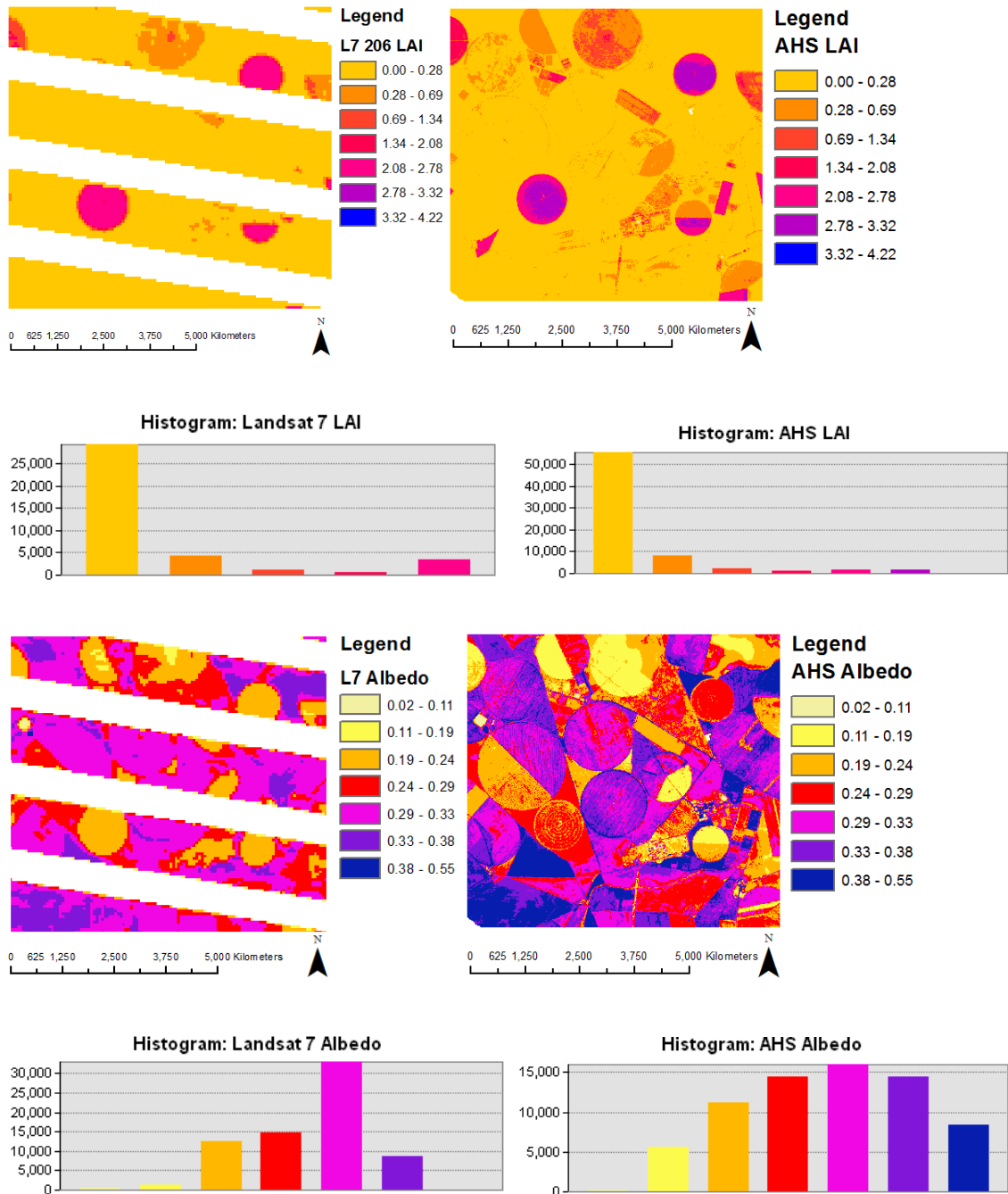
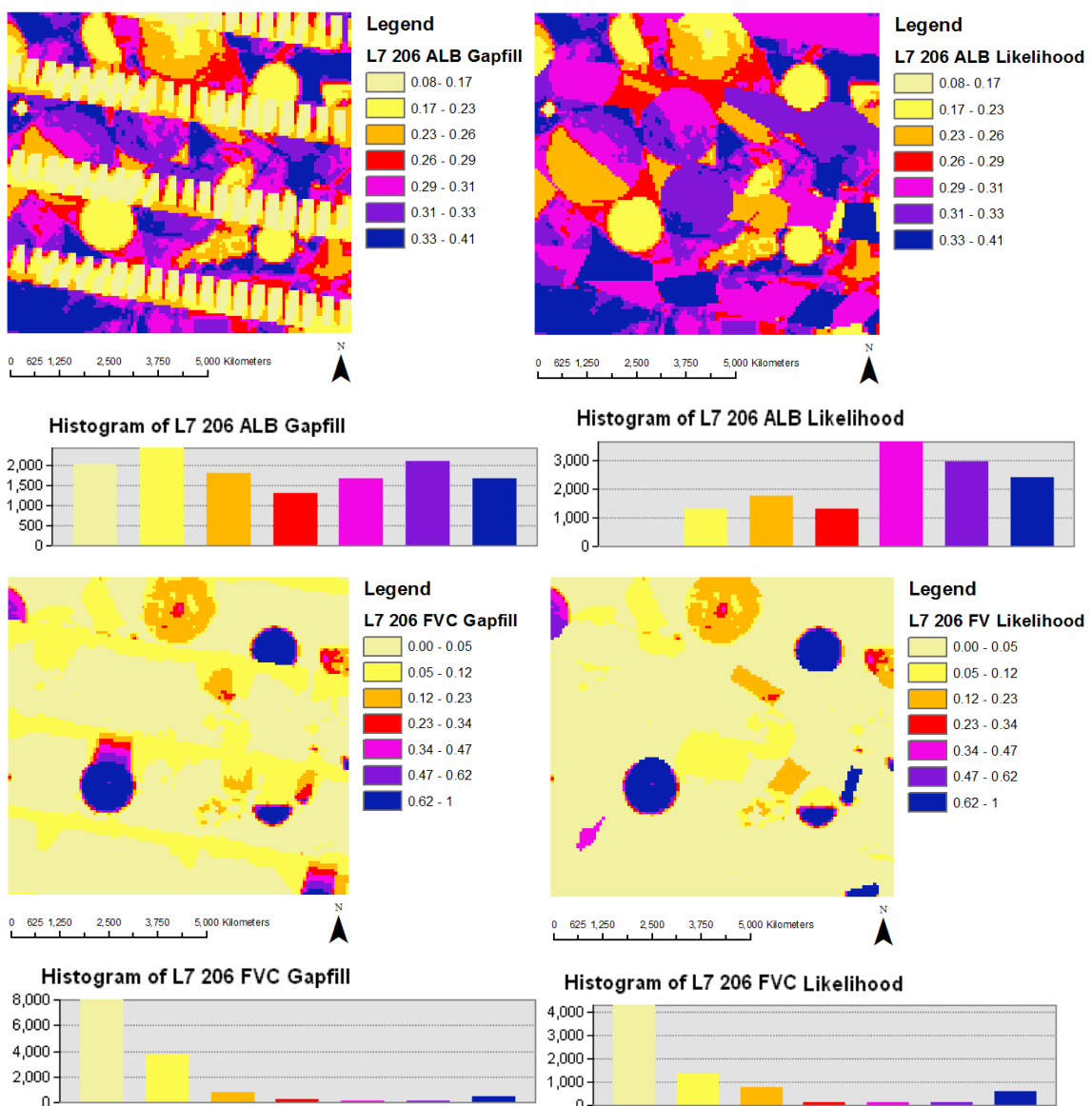


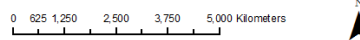
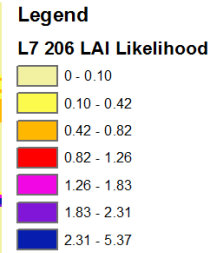
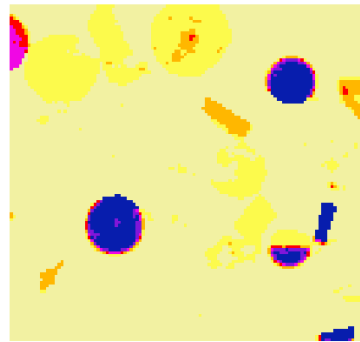
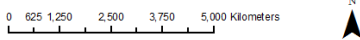
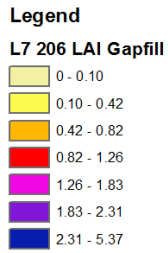
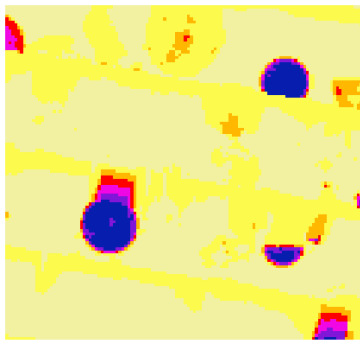
FIGURE 109. COMPARISON AMONG L7 206-AHS 207 RETRIEVED DATA

Landsat stat	FVC	LAI	ALB	AHS stat	FVC	LAI	ALB
min	0.00	0.00	0.01	min	0	0	0.03
max	0.75	2.73	0.41	max	0.81	3.34	0.55
mean	0.13	0.38	0.29	mean	0.15	0.38	0.3
Stdev	0.20	0.71	0.05	Stdev	0.16	0.6	0.07

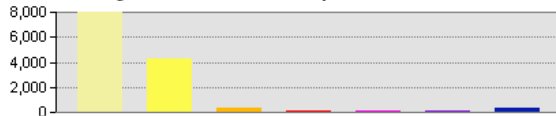
TABLE 49. STATISTICAL COMPARISON AMONG L7 206-AHS 207 RETRIEVED DATA



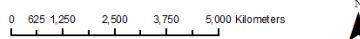
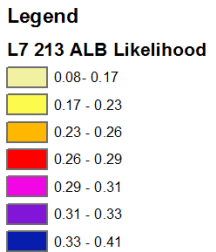
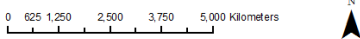
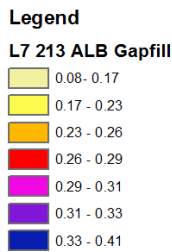
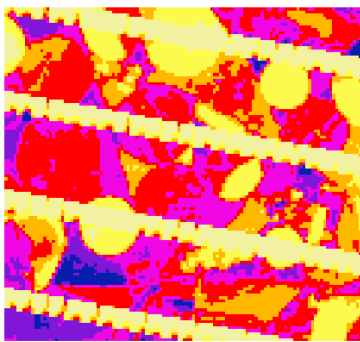
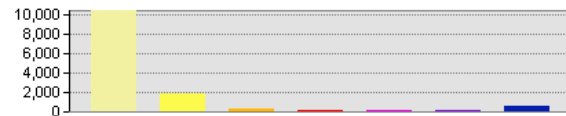




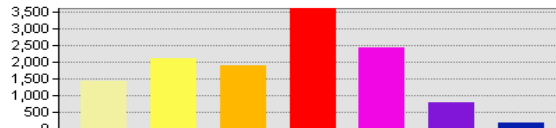
**Histogram of L7 206 LAI Gapfill**



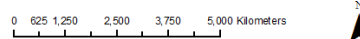
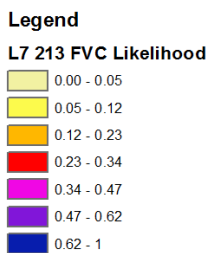
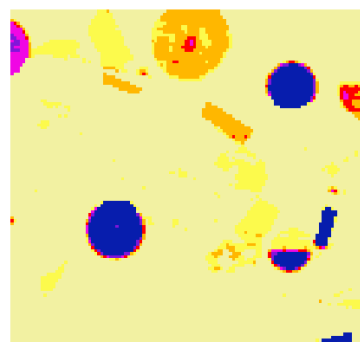
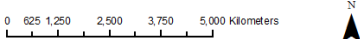
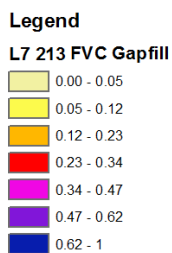
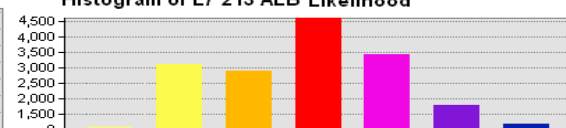
**Histogram of L7 206 LAI Likelihood**



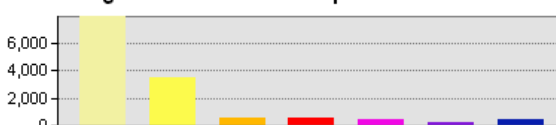
**Histogram of L7 213 ALB Gapfill**



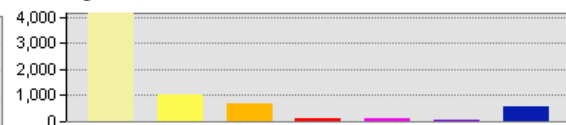
**Histogram of L7 213 ALB Likelihood**



**Histogram of L7 213 FVC Gapfill**



**Histogram of L7 213 FVC Likelihood**



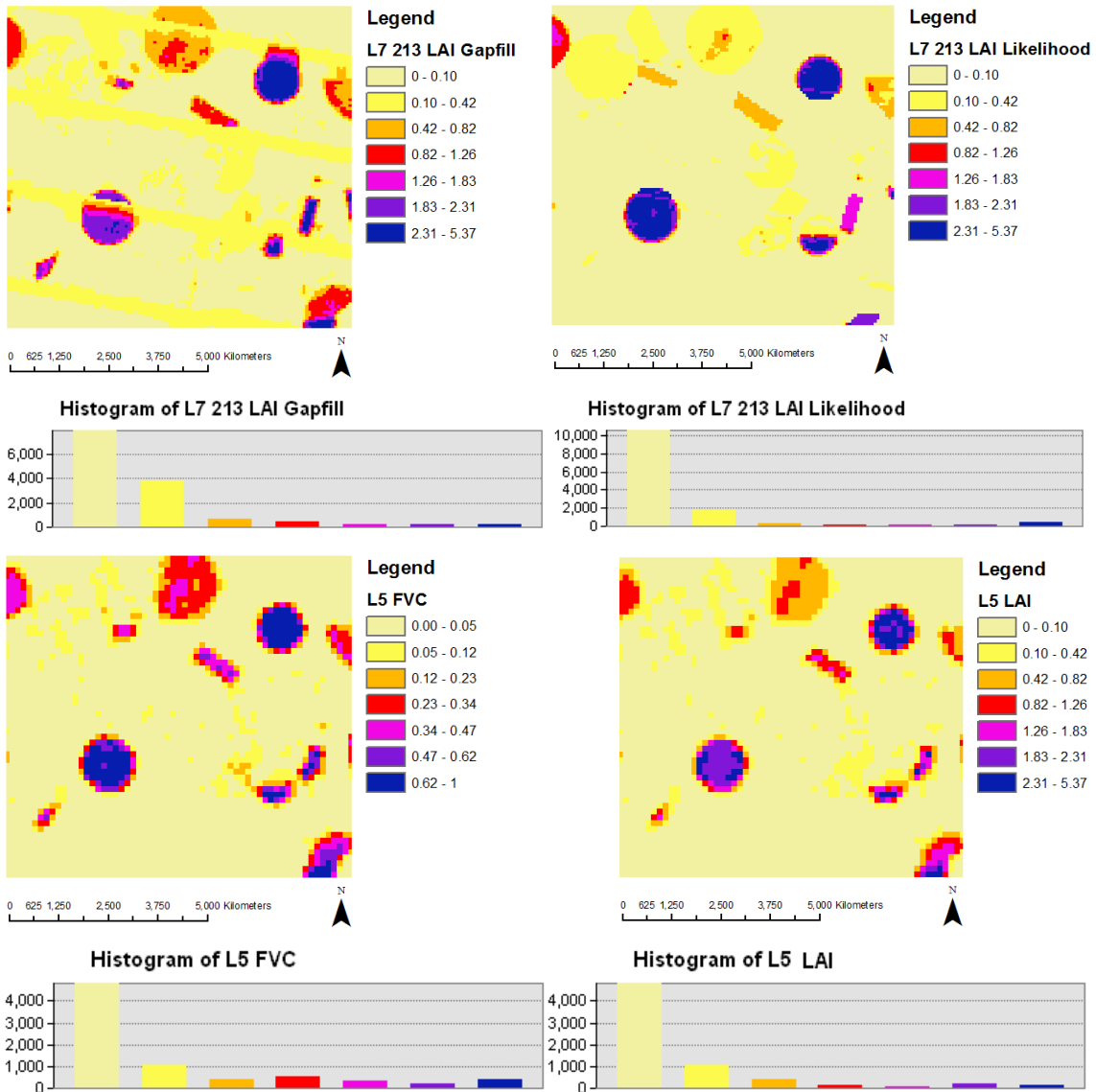


FIGURE 110. INPUT COMPARISON

The FVC mean values are all closer to 0.06, the higher values come from the Gapfill configurations. The LAI mean values are the more variables as we can see from the highest standard deviation values, among 0.16 and 0.23. Albedo values have the smallest standard deviation considering all the parameters.

It is possible to see all the estimated values thank to the following table, in which are reported the basic statistical values; in order to know the committed errors, input Root Mean Square Errors can be find in the subchapter 6.4.2.

206 Likelihood	FVC	LAI	ALB
<b>min</b>	0.00	0.00	0.09
<b>max</b>	0.75	2.73	0.41
<b>mean</b>	0.06	0.19	0.30
<b>Stdev</b>	0.16	0.52	0.04

213 Likelihood	FVC	LAI	ALB
<b>min</b>	0.00	0.00	0.03
<b>max</b>	0.75	2.73	0.40
<b>mean</b>	0.06	0.17	0.27
<b>Stdev</b>	0.15	0.50	0.04

206 Gapfill	FVC	LAI	ALB
<b>min</b>	0.00	0.00	0.01
<b>max</b>	0.75	2.73	0.41
<b>mean</b>	0.08	0.21	0.25
<b>Stdev</b>	0.14	0.48	0.08

213 Gapfill	FVC	LAI	ALB
<b>min</b>	0.00	0.00	0.00
<b>max</b>	1.00	4.42	0.40
<b>mean</b>	0.09	0.23	0.24
<b>Stdev</b>	0.15	0.46	0.07

L5	FVC	LAI
<b>min</b>	0.00	0.00
<b>max</b>	0.80	3.24
<b>mean</b>	0.06	0.16
<b>Stdev</b>	0.16	0.48

TABLE 50. INPUT STATISTICAL COMPARISON

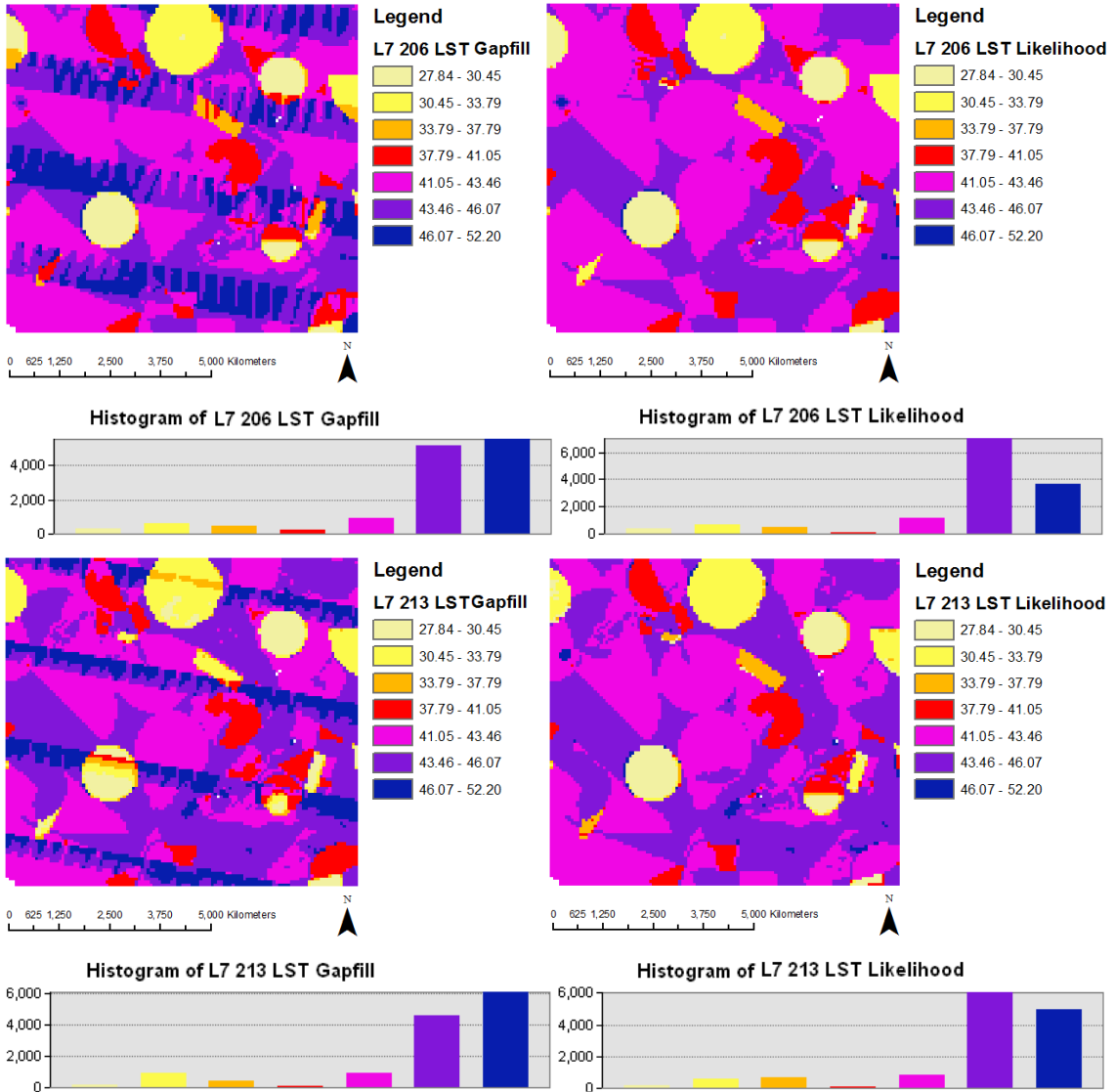
### 6.3 OUTPUT PARAMETERS

The main output parameters are net radiation, evapotranspiration, ground heat flux ( $g$ ), sensible heat ( $h$ ), shortwave incoming radiation, soil moisture, LST, latent heat ( $le$ ) and it is possible to assess the shortwave outgoing radiation ( $Rsout$ ) as product of albedo and shortwave incoming radiation.

It is possible to see an example of the output of LST and  $le$  referred to the days 24<sup>th</sup> of July and for the 25<sup>th</sup> of July. Each map is the result of a simulation done using in input the configurations already shown. Under the word “Legend” there is the name of the configuration used.

LST values are expressed in °C,  $le$  values are W/m<sup>2</sup>.

### 6.3.1 COMPARISON LST OUTPUT, 24<sup>TH</sup> OF JULY



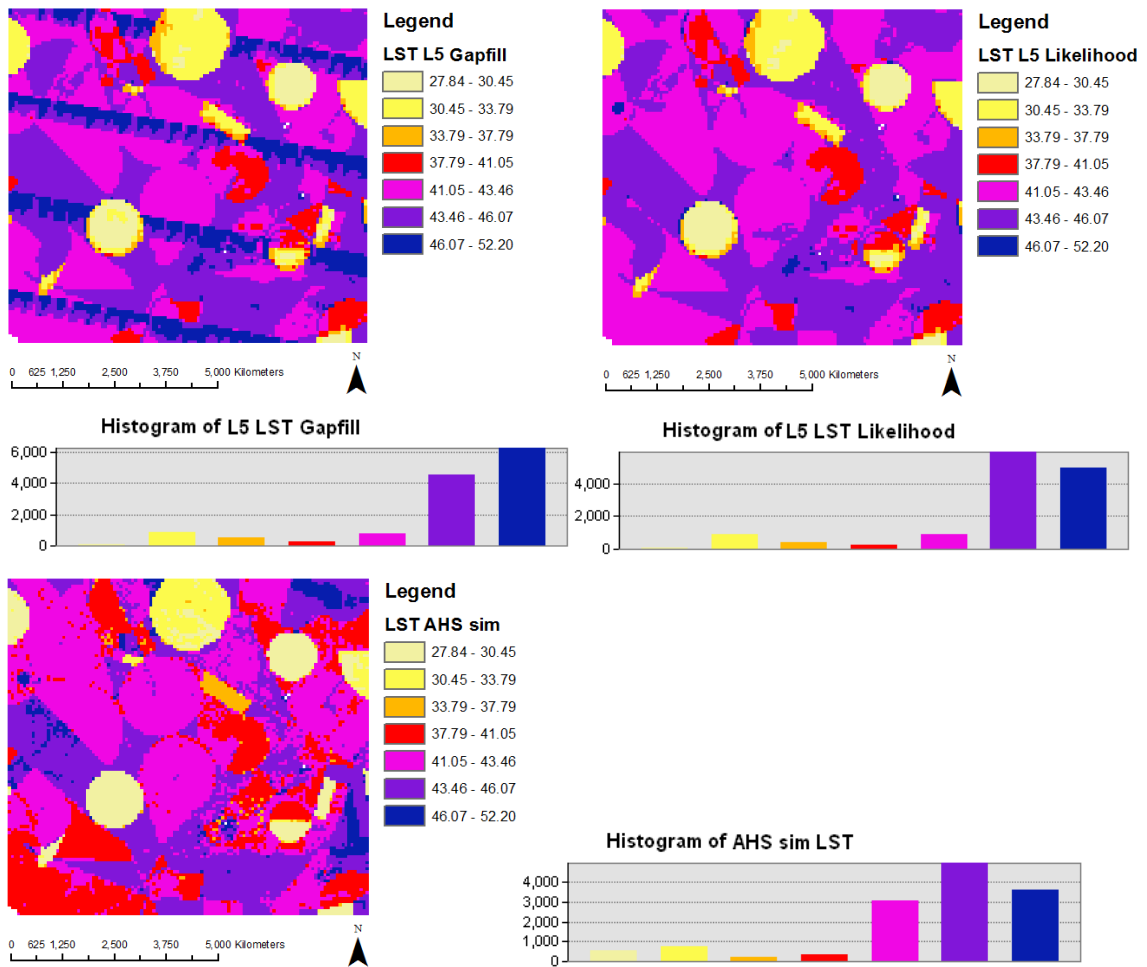


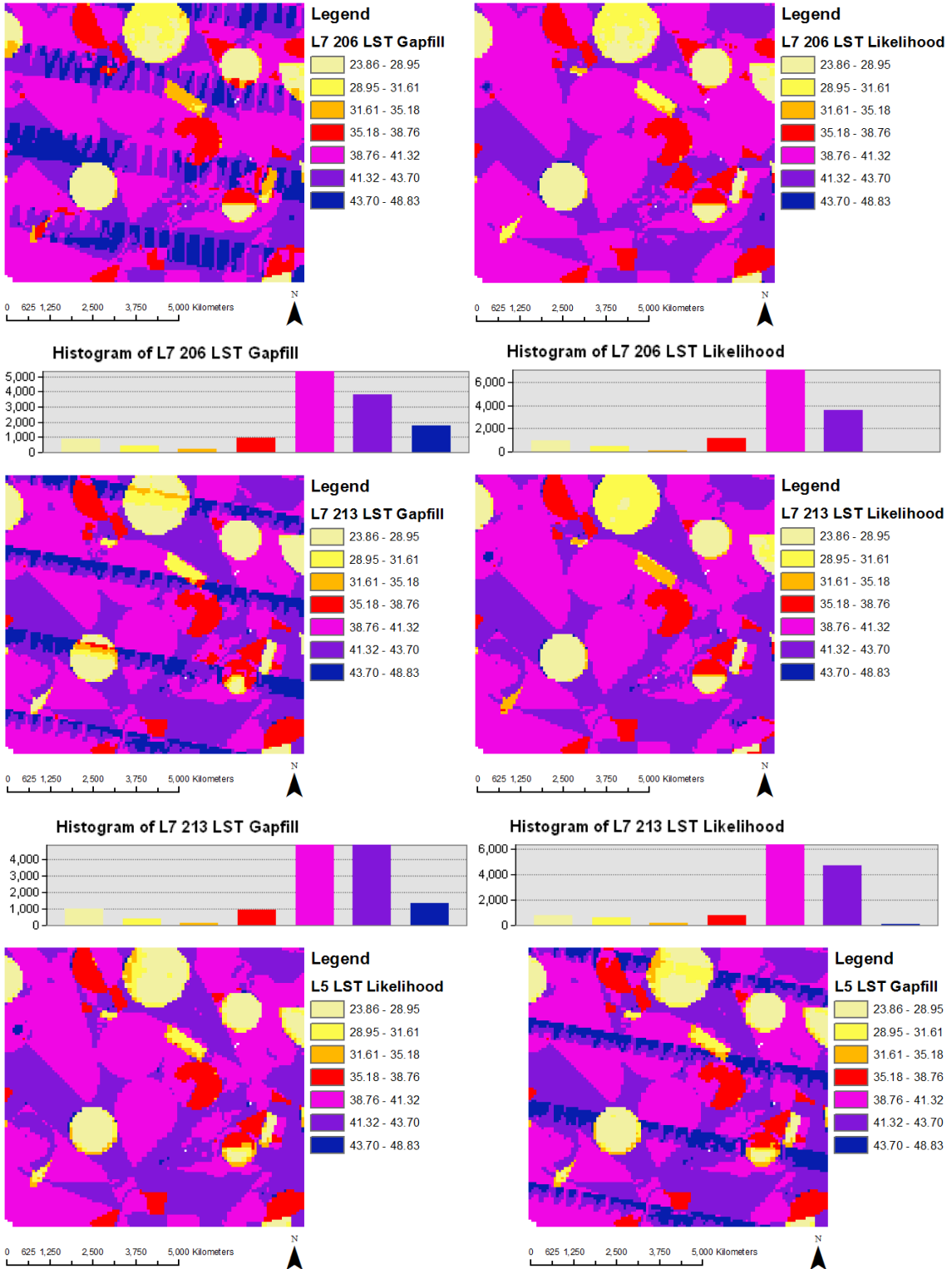
FIGURE 111. COMPARISON LST OUTPUT, 24<sup>TH</sup> OF JULY

LST 24th July [°C]	mean	Stdev
L5 Gapfill	42.64	4.46
L5 Likelihood	42.01	4.13
AHS sim	41.10	4.61
L7 206 Gapfill	42.48	4.49
L7 206 Likelihood	41.50	4.13
L7 213 Gapfill	42.56	4.50
L7 213 Likelihood	42.03	4.15

TABLE 51. OUTPUT STATISTICAL COMPARISON LST 24<sup>TH</sup> OF JULY

The maximum mean difference is between L5 Gapfill and AHS sim, it is 1.54 °C.

### 6.3.2 COMPARISON LST OUTPUT, 25<sup>TH</sup> OF JULY



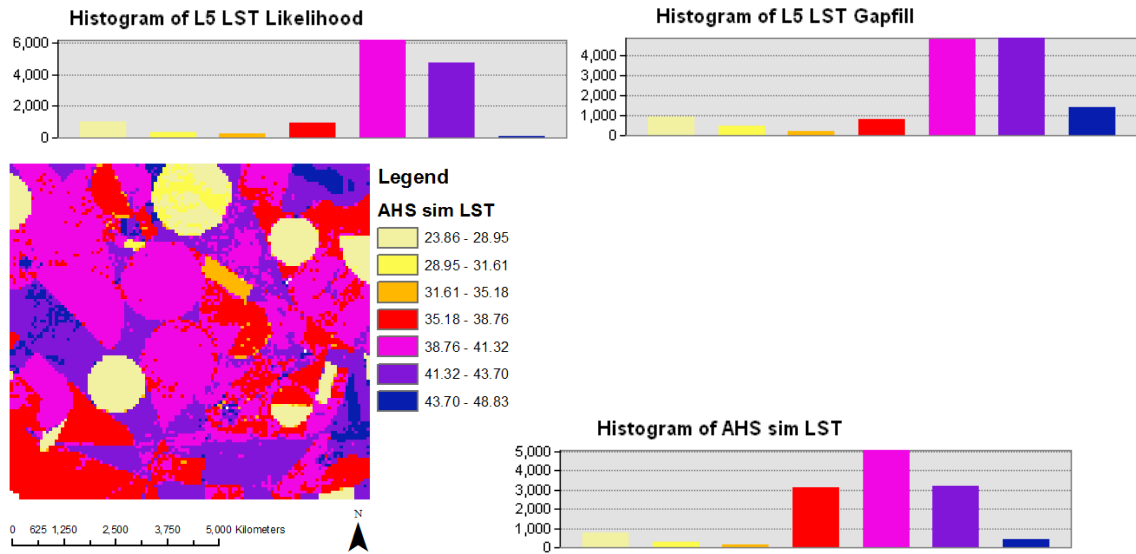


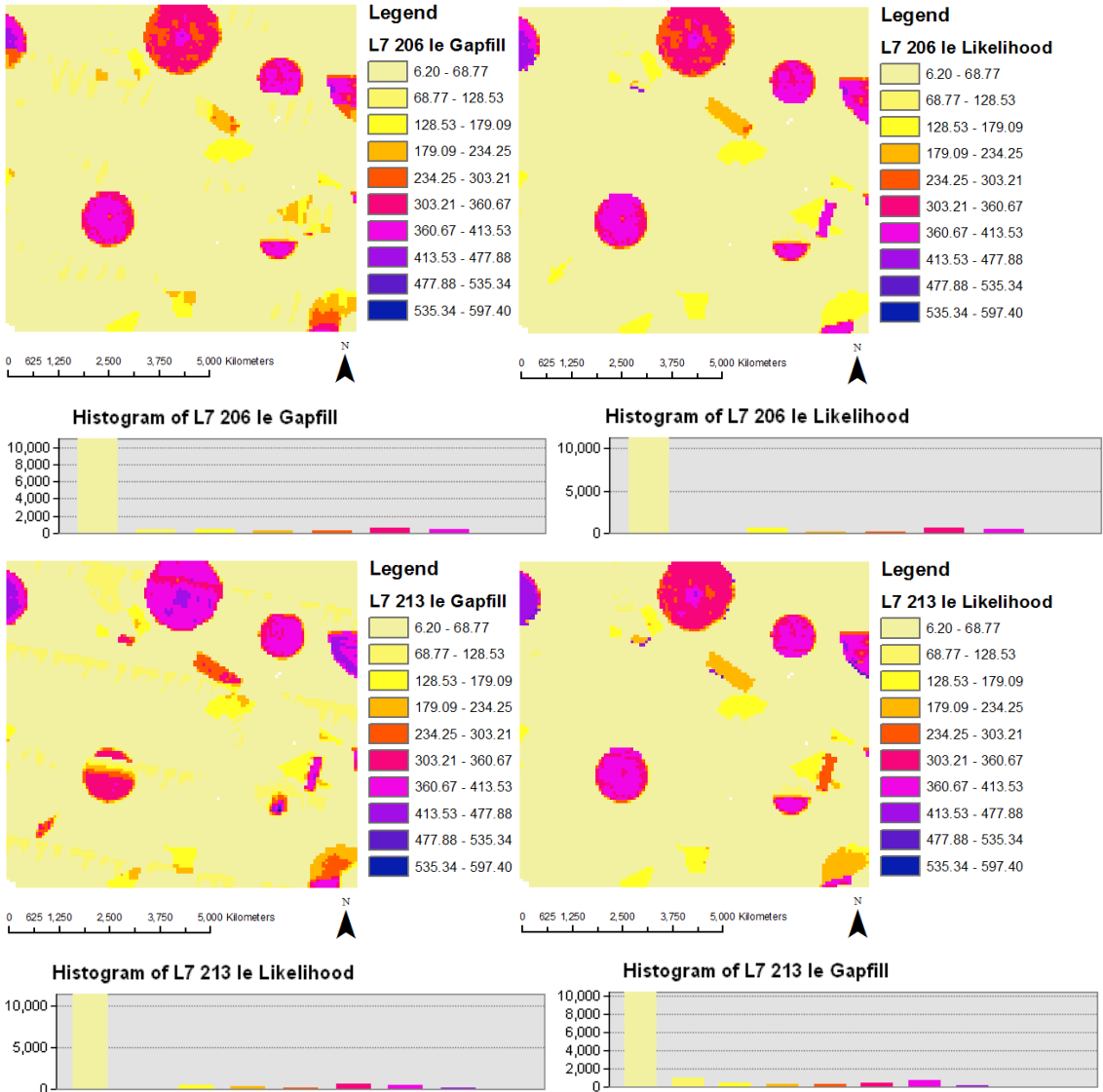
FIGURE 112. COMPARISON LST OUTPUT, 25<sup>TH</sup> OF JULY

LST 25th July [°C]	mean	Stdev
L5 Gapfill	40.04	4.46
L5 Likelihood	39.44	4.16
AHS sim	38.62	4.63
L7 206 Gapfill	39.88	4.54
L7 206 Likelihood	38.96	4.19
L7 213 Gapfill	39.98	4.49
L7 213 Likelihood	39.45	4.20

TABLE 52. OUTPUT STATISTICAL COMPARISON LST 25<sup>TH</sup> OF JULY

The maximum mean difference is between L5 Gapfill and AHS sim, it is 1.42 °C.

### 6.3.3 COMPARISON LE OUTPUT, 24<sup>TH</sup> OF JULY





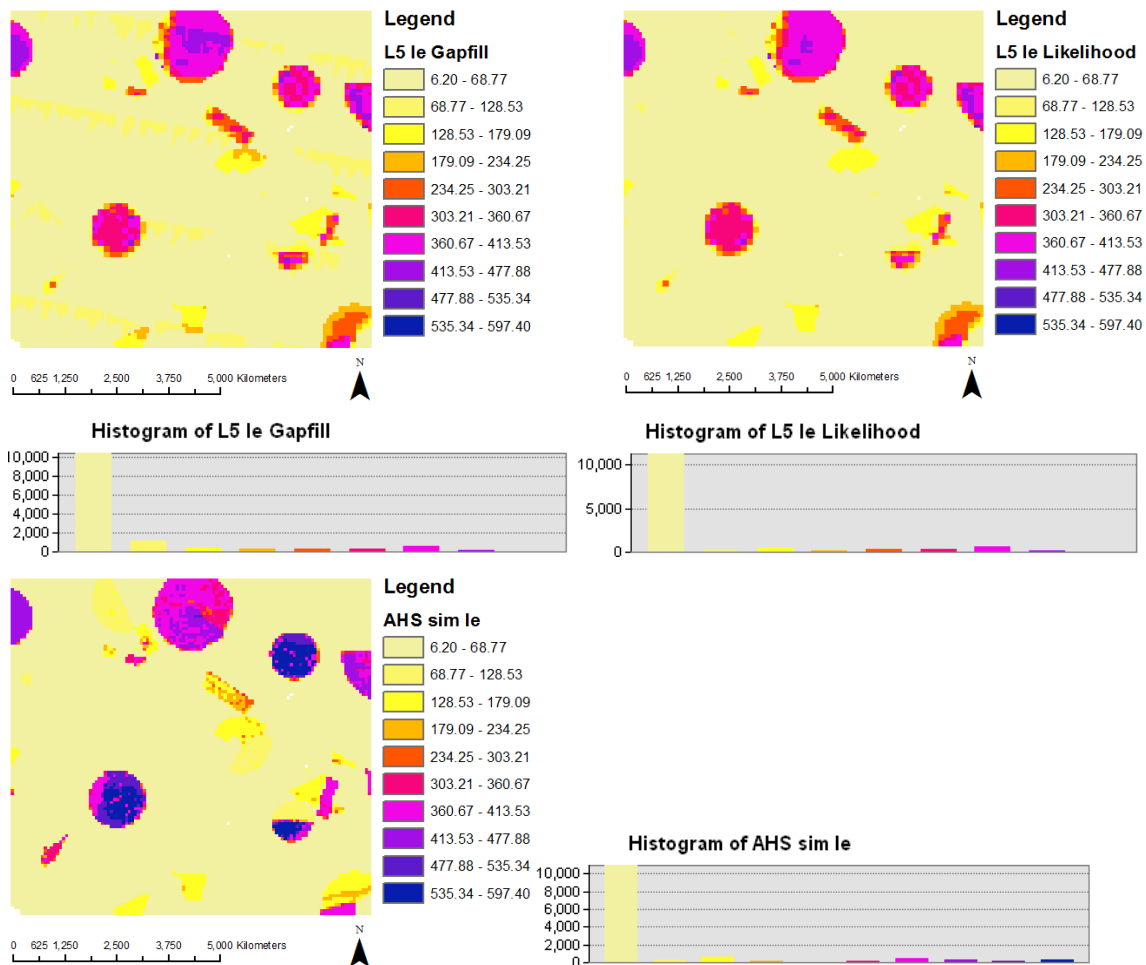


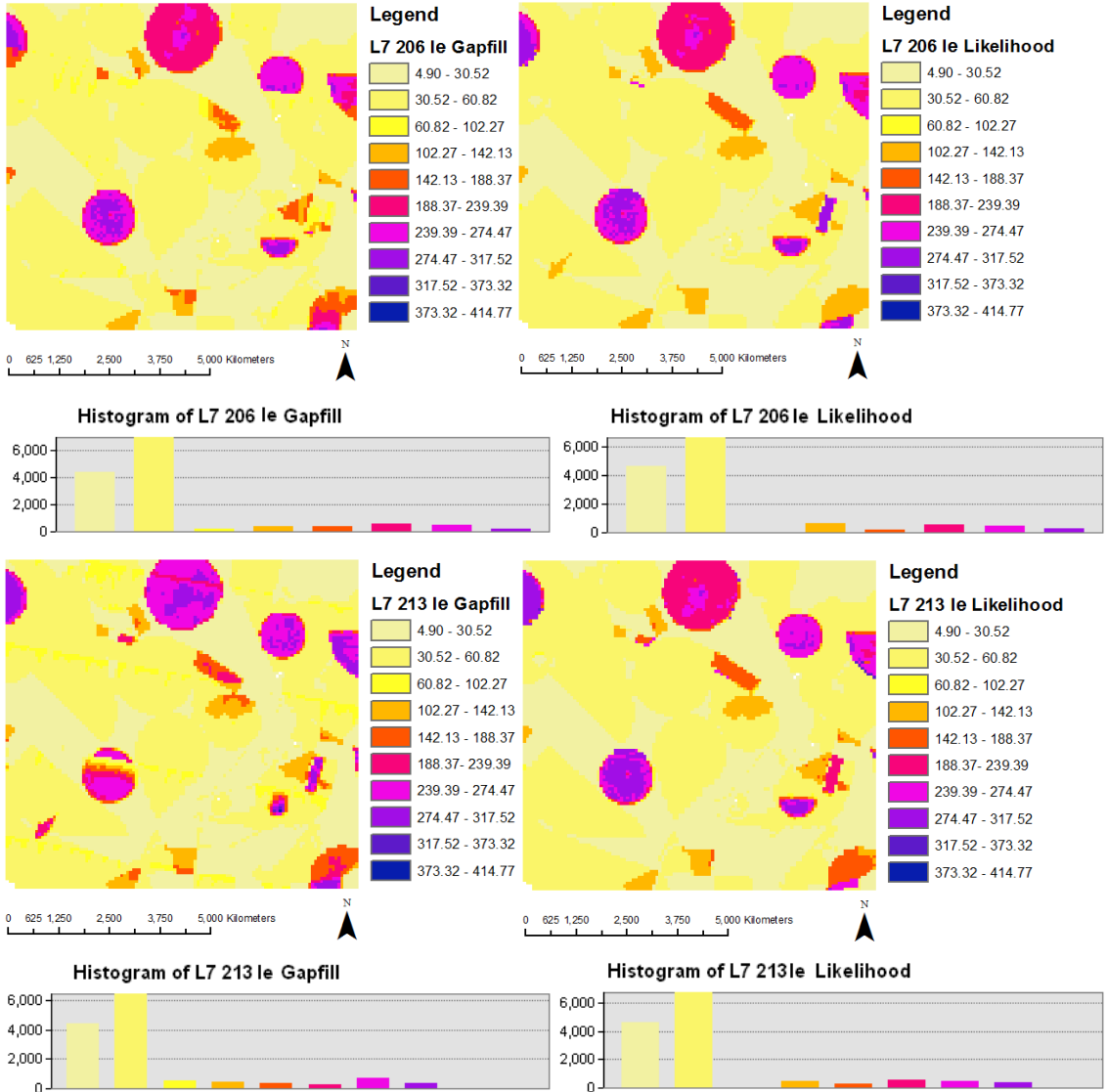
FIGURE 113. COMPARISON *LE* OUTPUT, 24<sup>TH</sup> OF JULY

le 24th July [W/m <sup>2</sup> ]	mean	Stdev
L5 Gapfill	83.54	98.80
L5 Likelihood	80.92	97.14
AHS sim	91.11	126.44
L7 206 Gapfill	79.17	90.42
L7 206 Likelihood	79.45	95.59
L7 213 Gapfill	84.47	99.89
L7 213 Likelihood	81.32	97.04

TABLE 53. OUTPUT STATISTICAL COMPARISON *LE* 24<sup>TH</sup> OF JULY

The highest values is founded in AHS simulations, which presents the highest standard deviation. The minimum value is the one given by L7 206 Gapfill simulation, which presents the minimum standard deviation.

### 6.3.4 COMPARISON LE OUTPUT, 25<sup>TH</sup> OF JULY



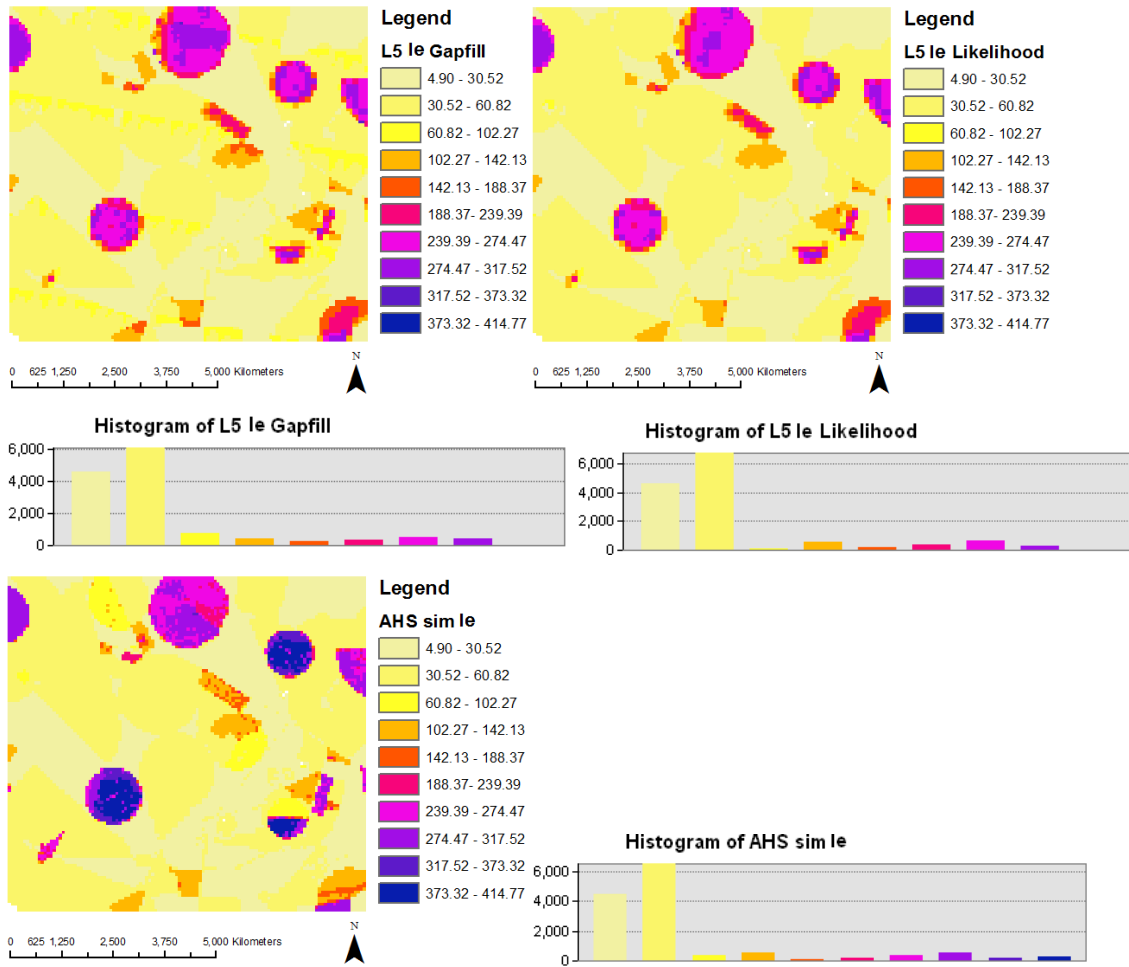


FIGURE 114. COMPARISON *le* OUTPUT, 25<sup>TH</sup> OF JULY

<b>le 25th July [W/m<sup>2</sup>]</b>	<b>mean</b>	<b>Stdev</b>
<b>L5 Gapfill</b>	65.28	68.71
<b>L5 Likelihood</b>	63.16	67.42
<b>AHS sim</b>	69.47	86.30
<b>L7 206 Gapfill</b>	62.33	63.85
<b>L7 206 Likelihood</b>	62.11	67.11
<b>L7 213 Gapfill</b>	65.85	69.20
<b>L7 213 Likelihood</b>	63.60	68.05

TABLE 54. OUTPUT STATISTICAL COMPARISON *le* 25<sup>TH</sup> OF JULY

The highest mean value is the AHS simulated one, in comparison to the analysed day before the values are lower of about 20 W/m<sup>2</sup>.

The results achieved for both the days about the 2 parameters analysed are good, and the differences among them are few. Meanwhile using LST Gapfill the stripes are evident, in *le* maps the stripes disappear.

### 6.3.5 OUTPUT COMPARISON WITH PUNCTUAL DATA

Another analysis on the output is carried out on data retrieved from three in field stations. The stations are called vineyard (V), reforestation (R) and camelina (C), due to their position on the corresponding fields. The coordinates (X,Y) are:

- C: 579406, 4321737
- R: 578986, 4323804
- V: 577796, 4323787

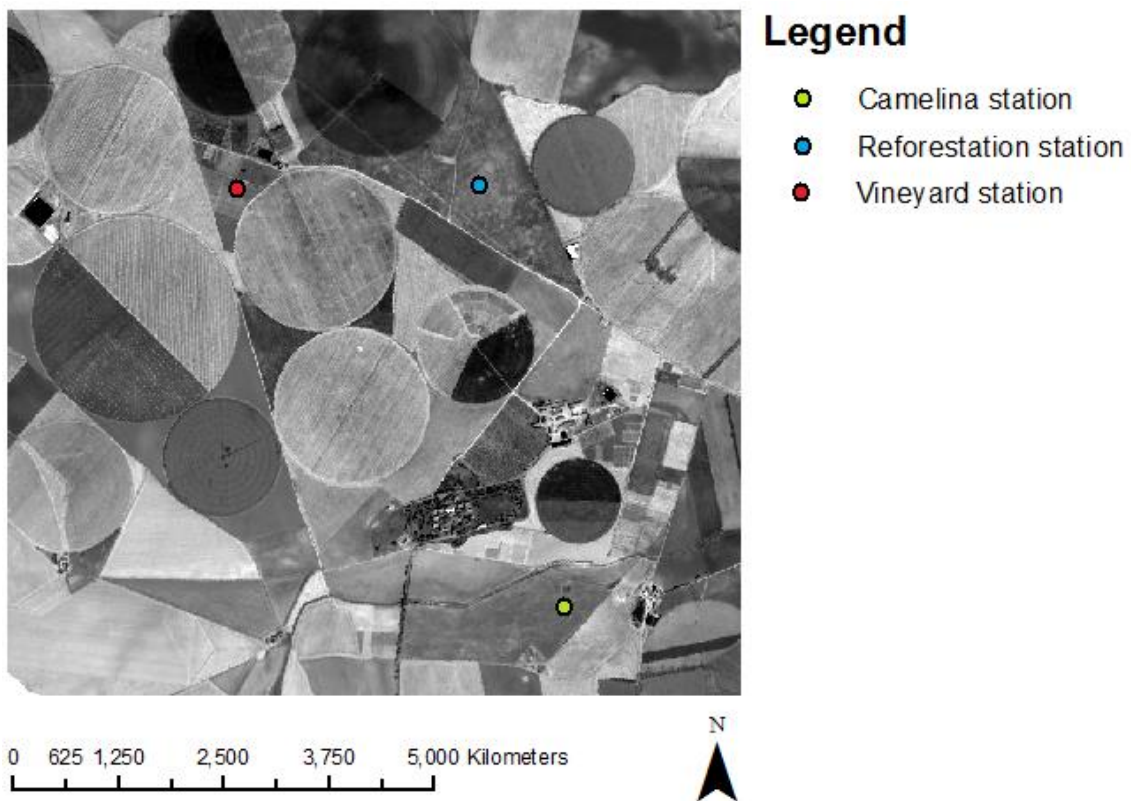
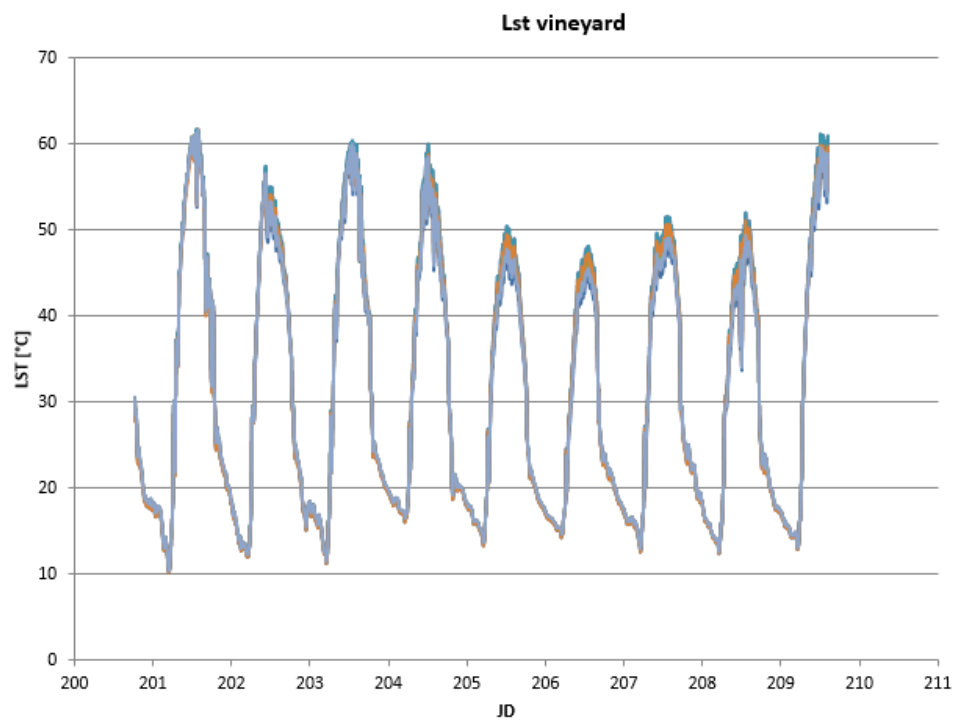
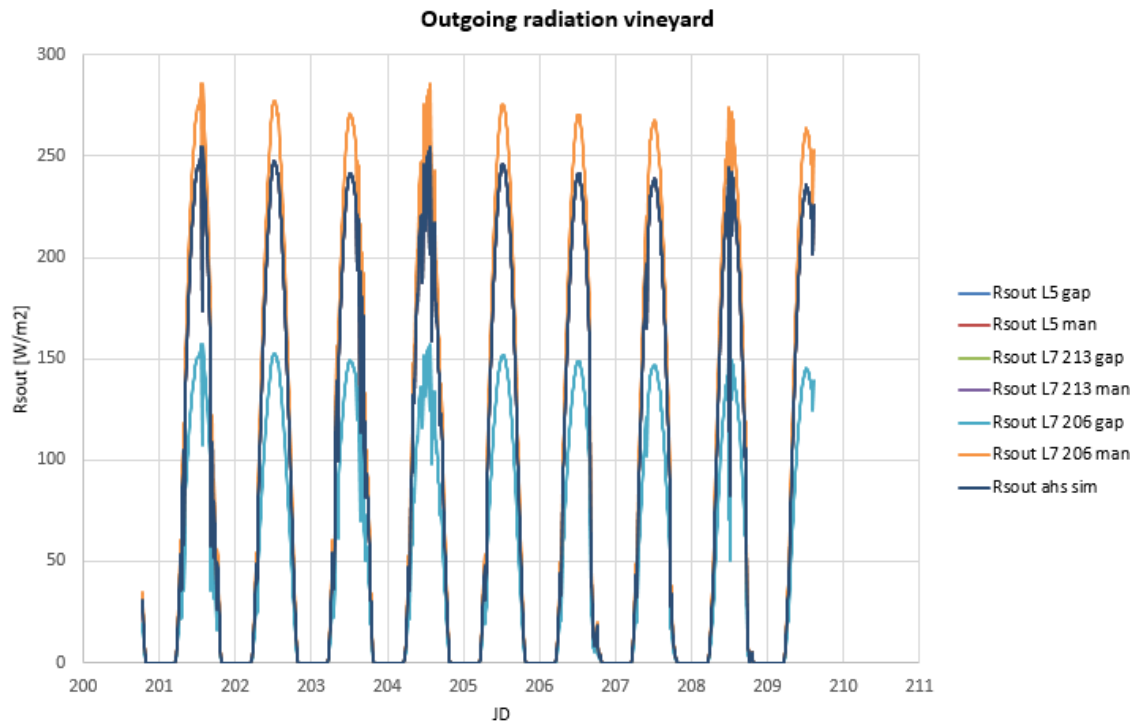


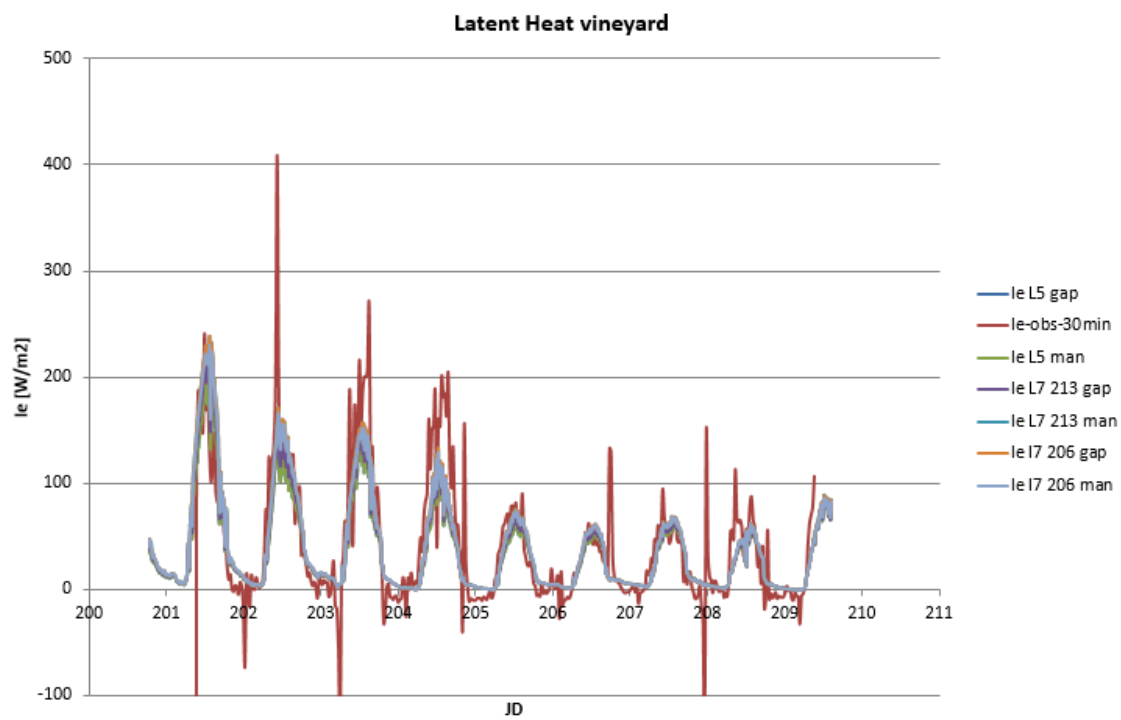
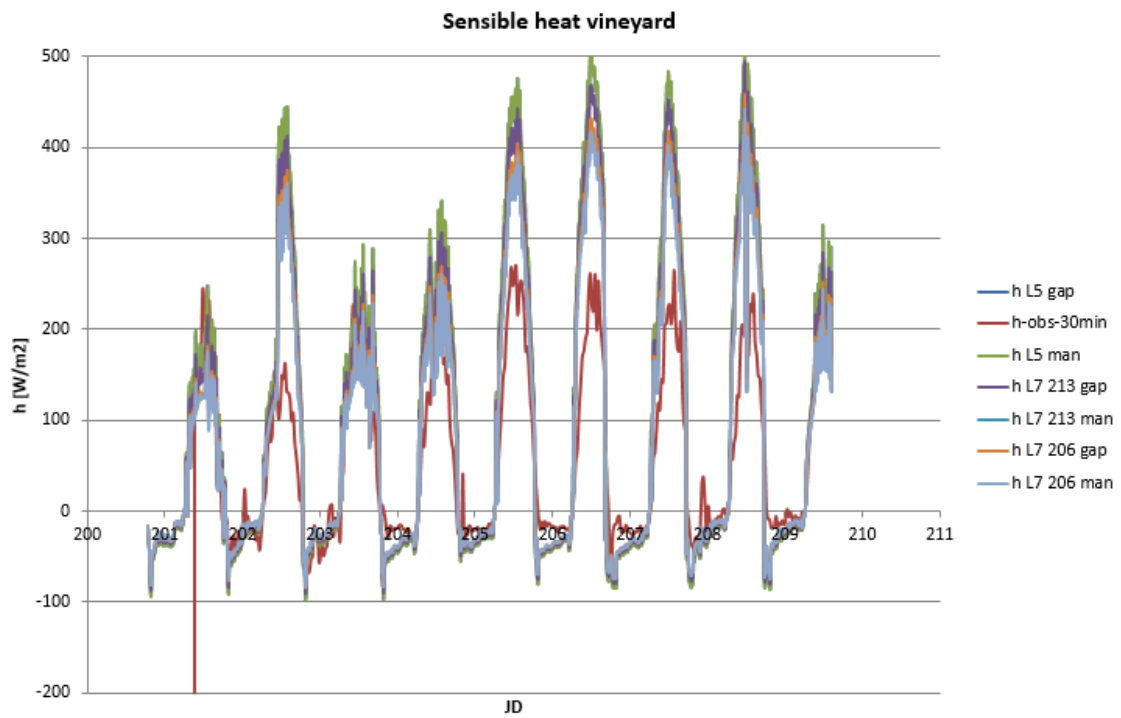
FIGURE 115. MAP OF THE STATIONS USED FOR OUTPUT COMPARISONS

The stations retrieved data in the same period of the simulations; in the following are plotted the simulated  $le$ ,  $h$ ,  $g$ , LST and  $Rs_{out}$  over the entire simulated period of time in the three pixels where three stations collected punctual data, and the observed station data.

Sometimes in the plotted graphics is not possible distinguish a series from the others due to the strict similarity. It is possible to find the Root Mean Square Errors of the data in the subchapter 6.4.

### 6.3.5.1 VINEYARD PUNCTUAL OUTPUT DATA





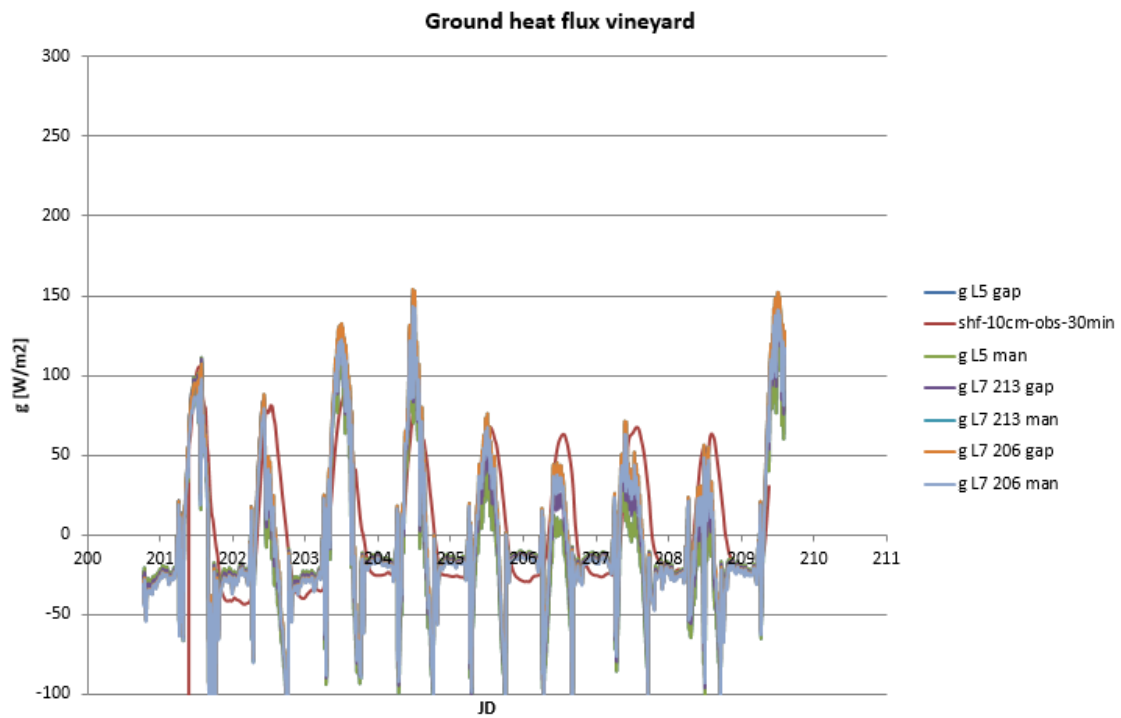
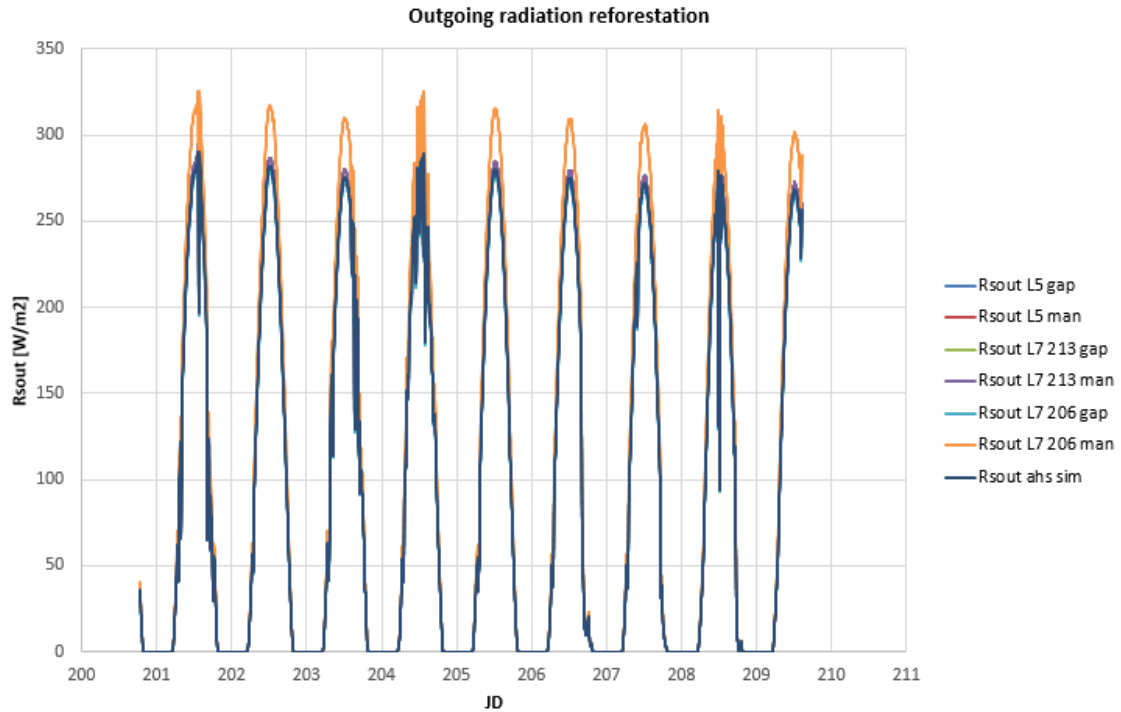
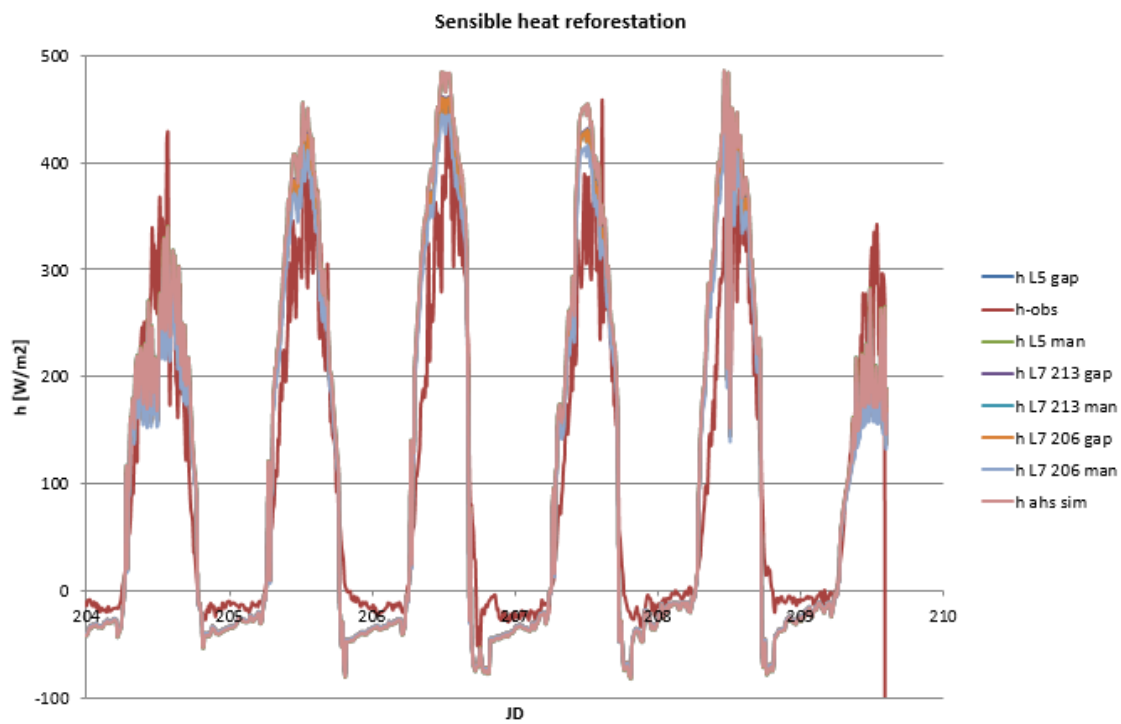
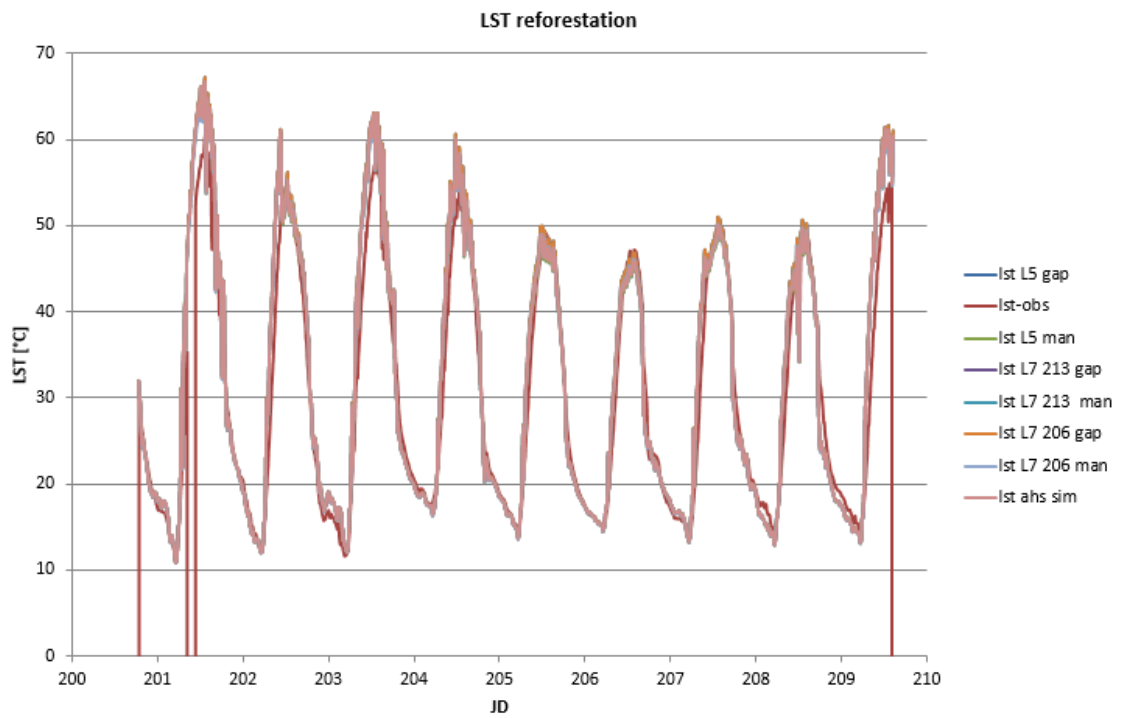


FIGURE 116. VINEYARD, PUNCTUAL OUTPUT GRAPHICS

### 6.3.5.2 REFORESTATION PUNCTUAL OUTPUT DATA







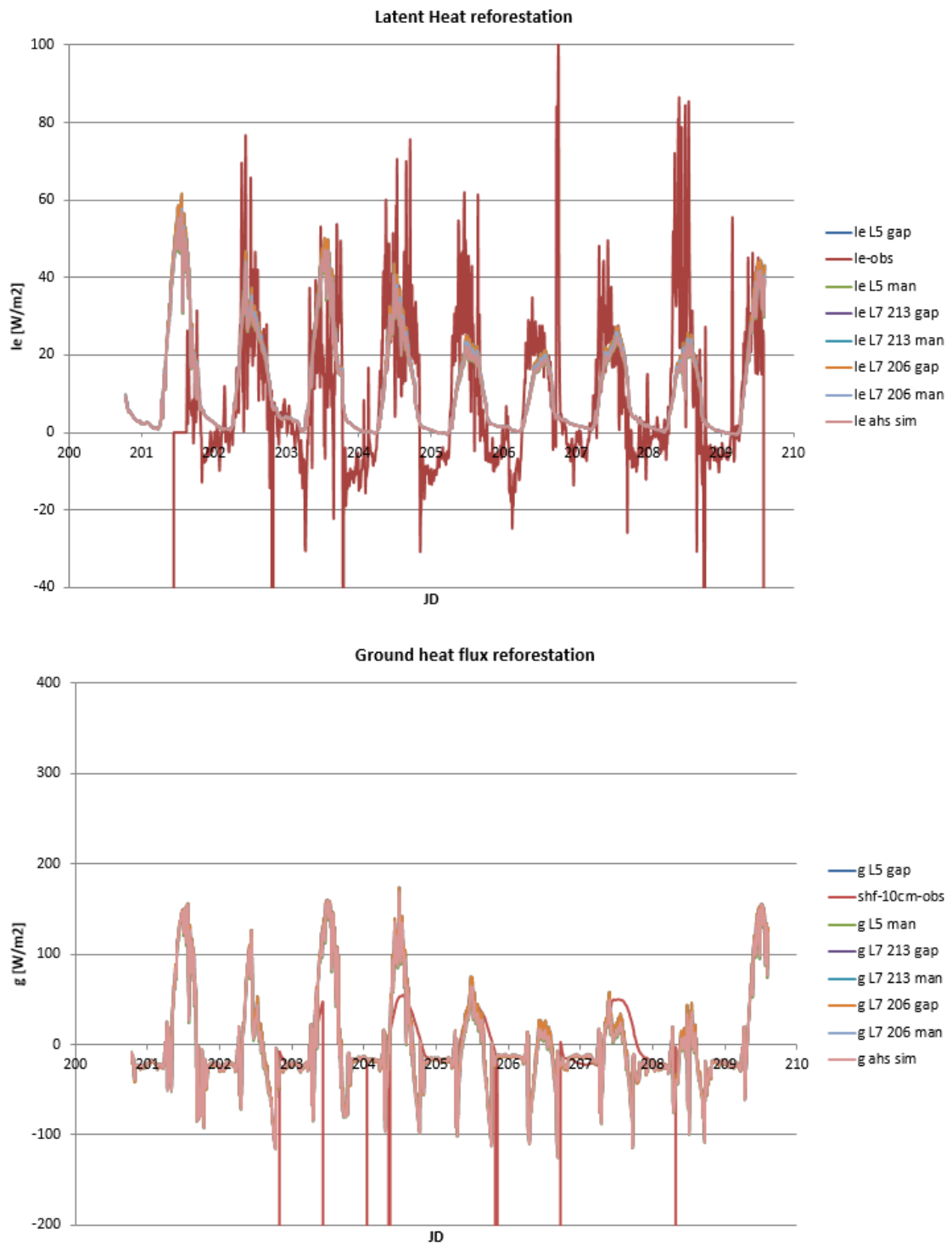
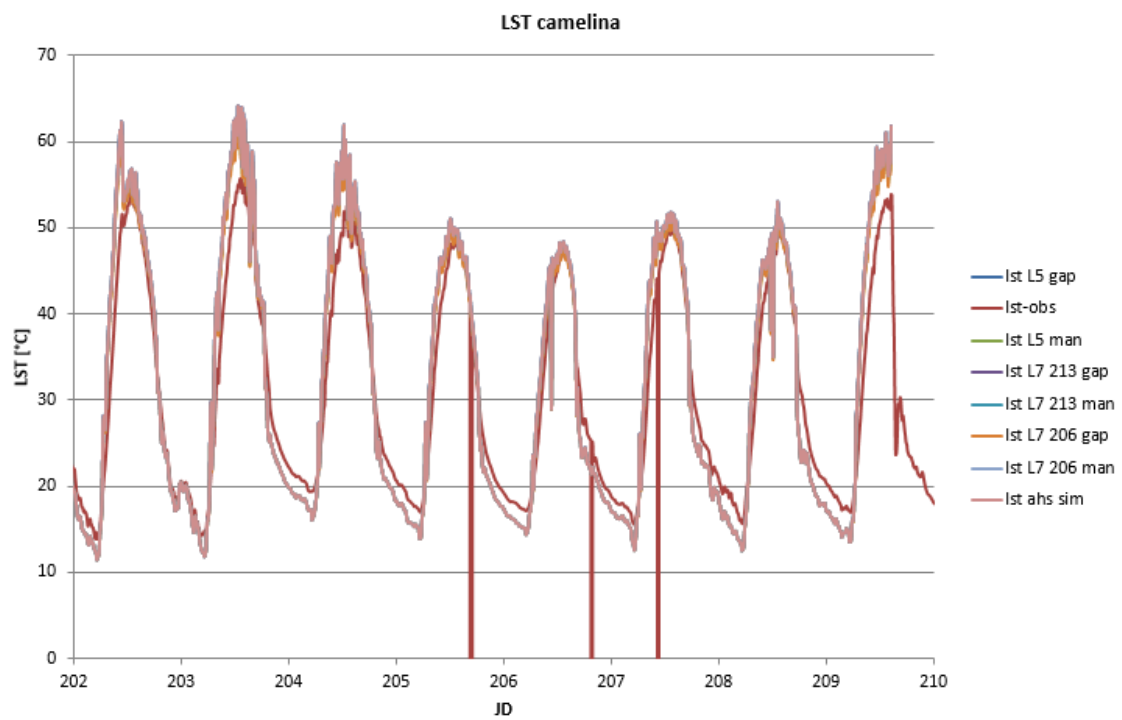
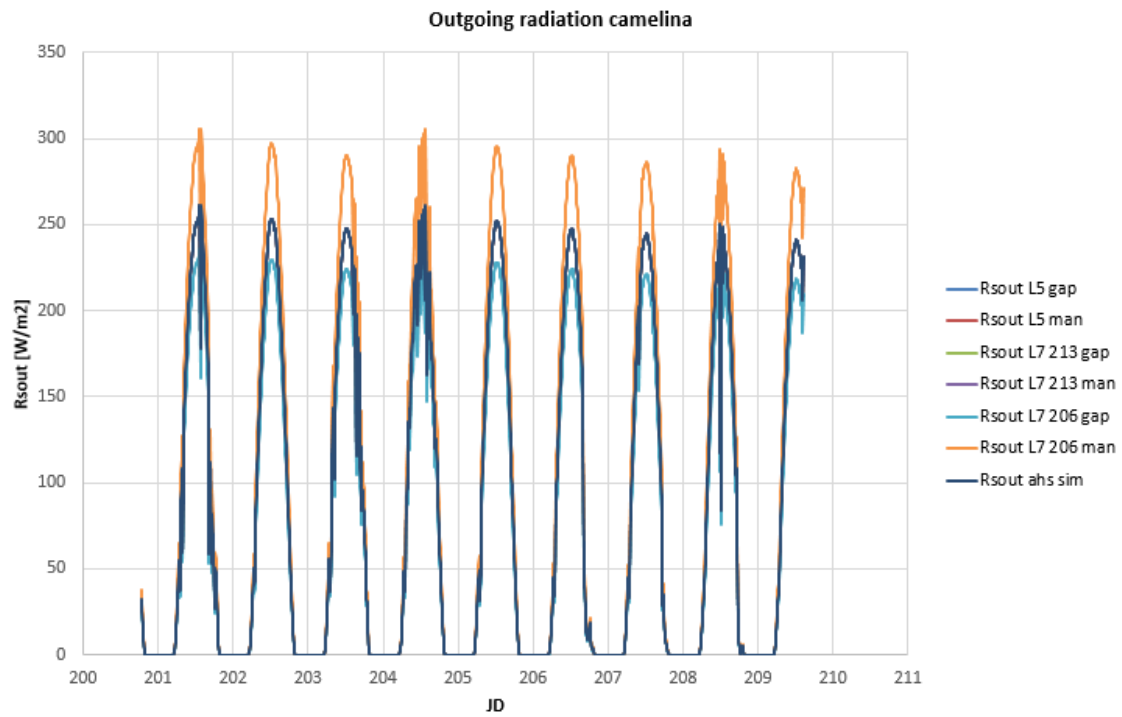
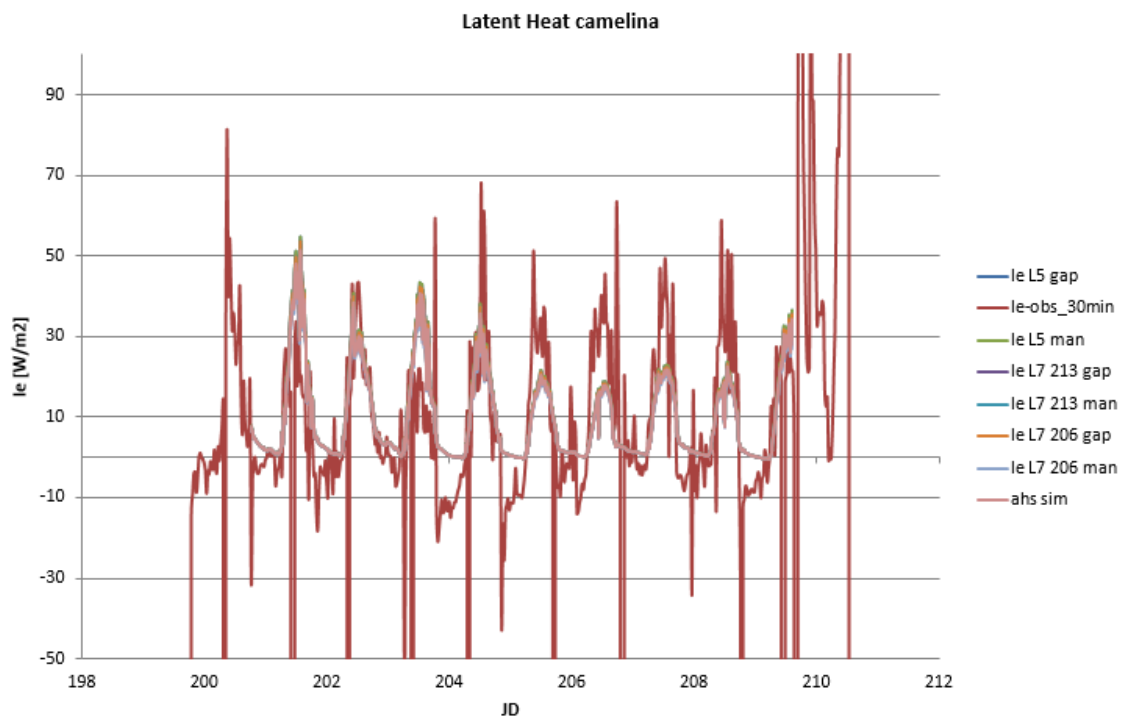
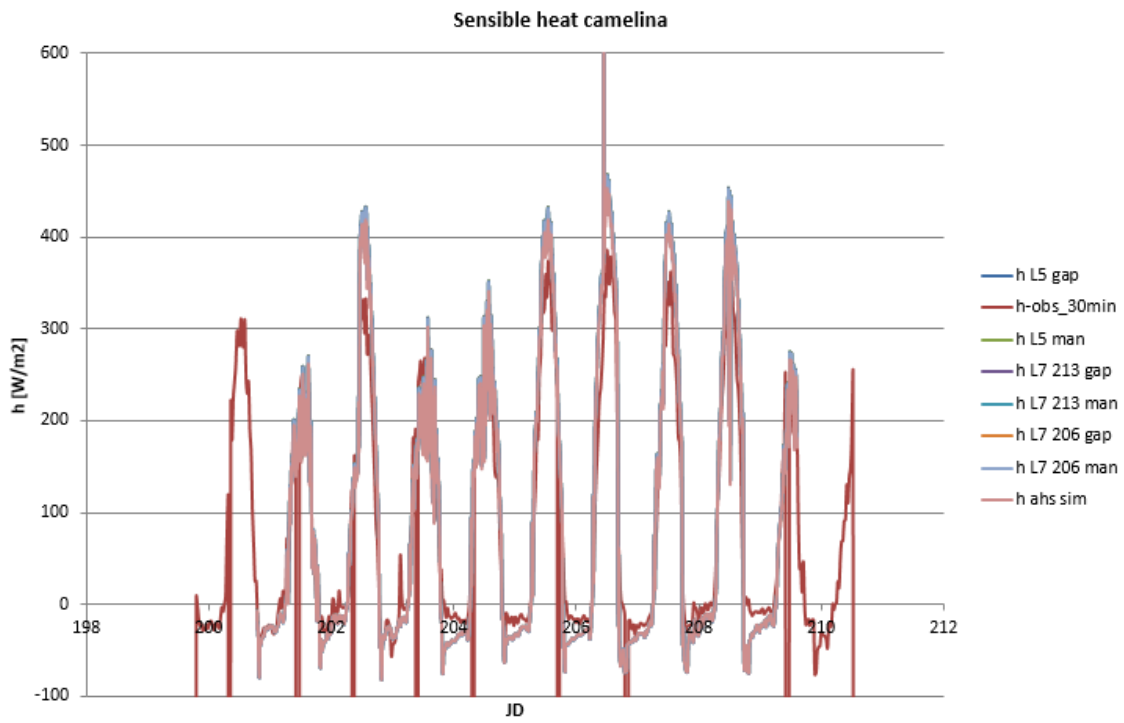


FIGURE 117. REFORESTATION, PUNCTUAL OUTPUT GRAPHICS

### 6.3.5.3 CAMELINA PUNCTUAL OUTPUT DATA





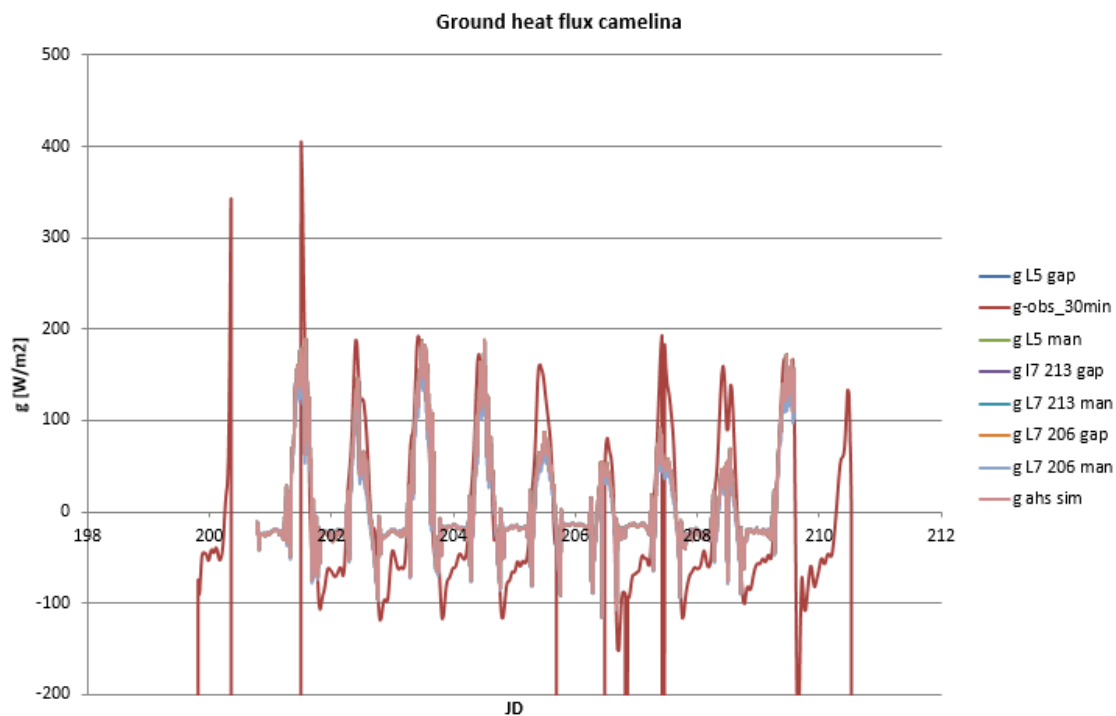


FIGURE 118. CAMELINA, PUNCTUAL OUTPUT GRAPHICS

Not all the graphics present the observed series, because not all the stations worked in the same way. All the simulations have a similar trend to the observed ones and are really similar each other.

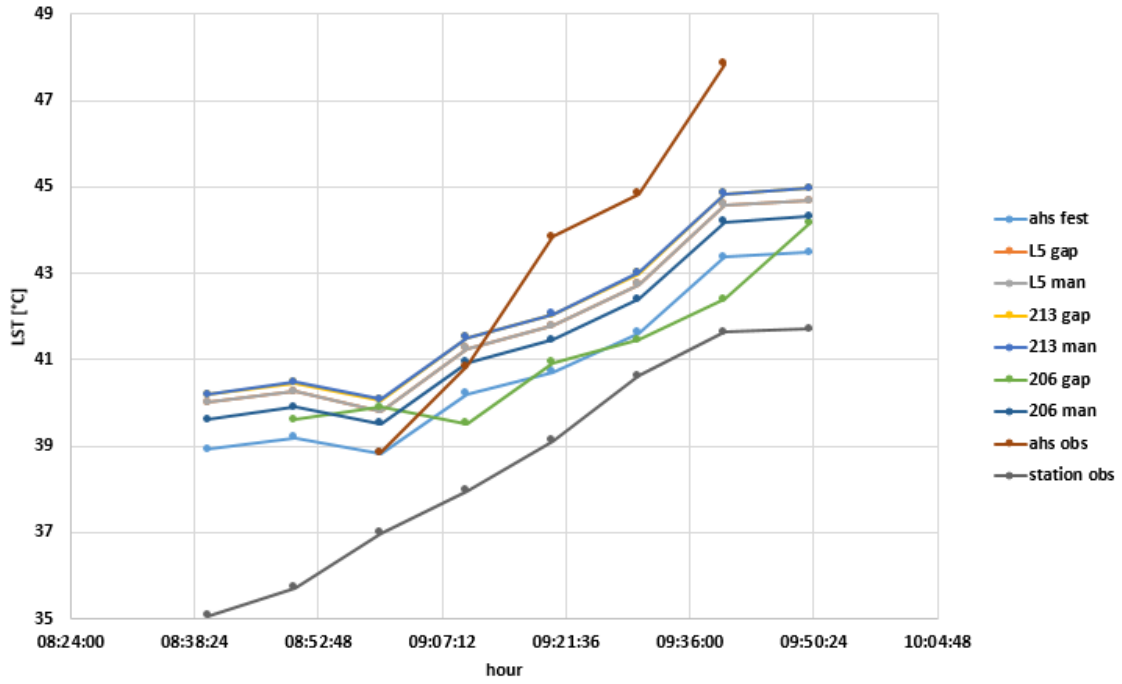
#### 6.3.5.4 AHS - SIMULATIONS PUNCTUAL COMPARISON ON 25<sup>TH</sup> AND 26<sup>TH</sup> OF JULY

With the aim of study in deep the behaviour of the series in the day 25<sup>th</sup> and 26<sup>th</sup> of July, are analysed the retrieved data assessed from the UTC hour 8.40 till UTC hour 9.50 with a step of 10 minutes and the data are compared with the ones retrieved by the Airborne Hyperspectral Scanner during a flight campaign effected in that period (Corbari, 2012).

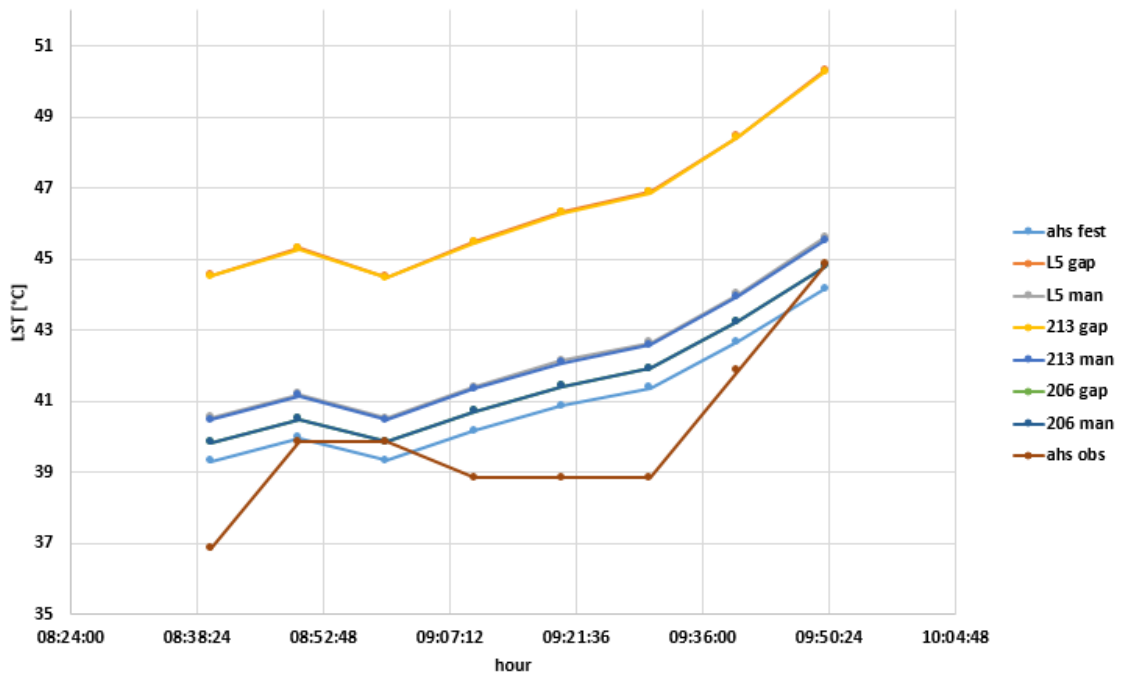
In this comparison, the difference among the values of the station reforestation is notable. This station is located in a particular place, where the variability between bare soil and plants is high and this high variability could be the reason of the differences recorded among the sensors.

Are plotted the graphics of the two days considered in the analysis:

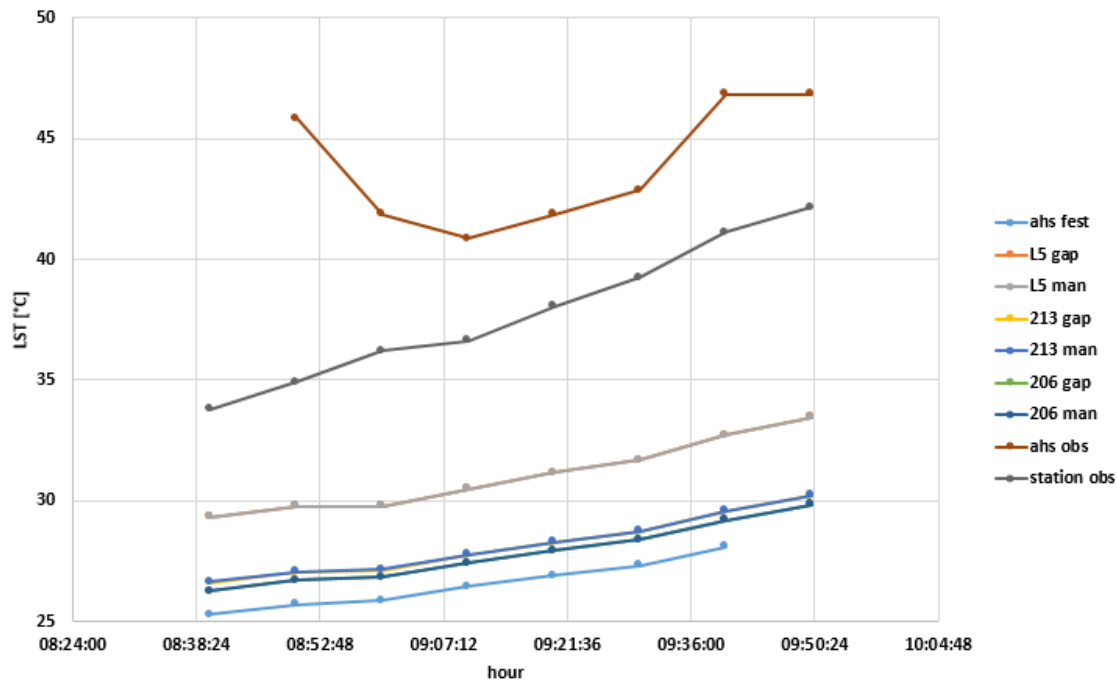
LST camelina 25th of July 2012



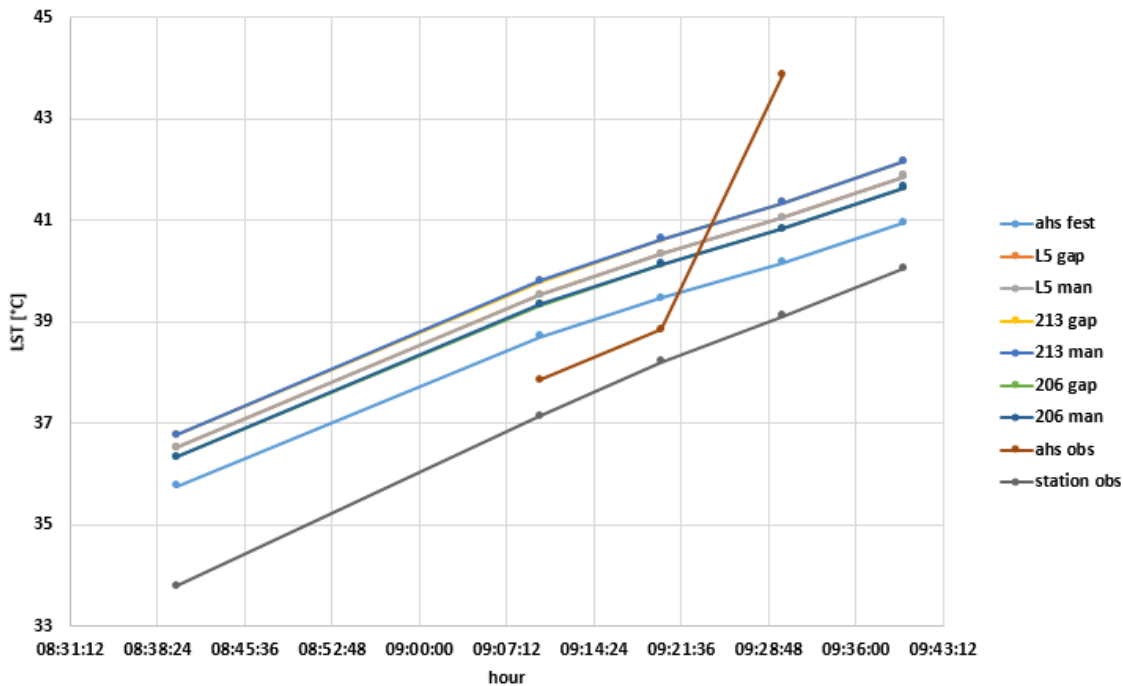
LST vineyard 25th of July 2012



LST reforestation 25th of July 2012



LST camelina 26th July 2012



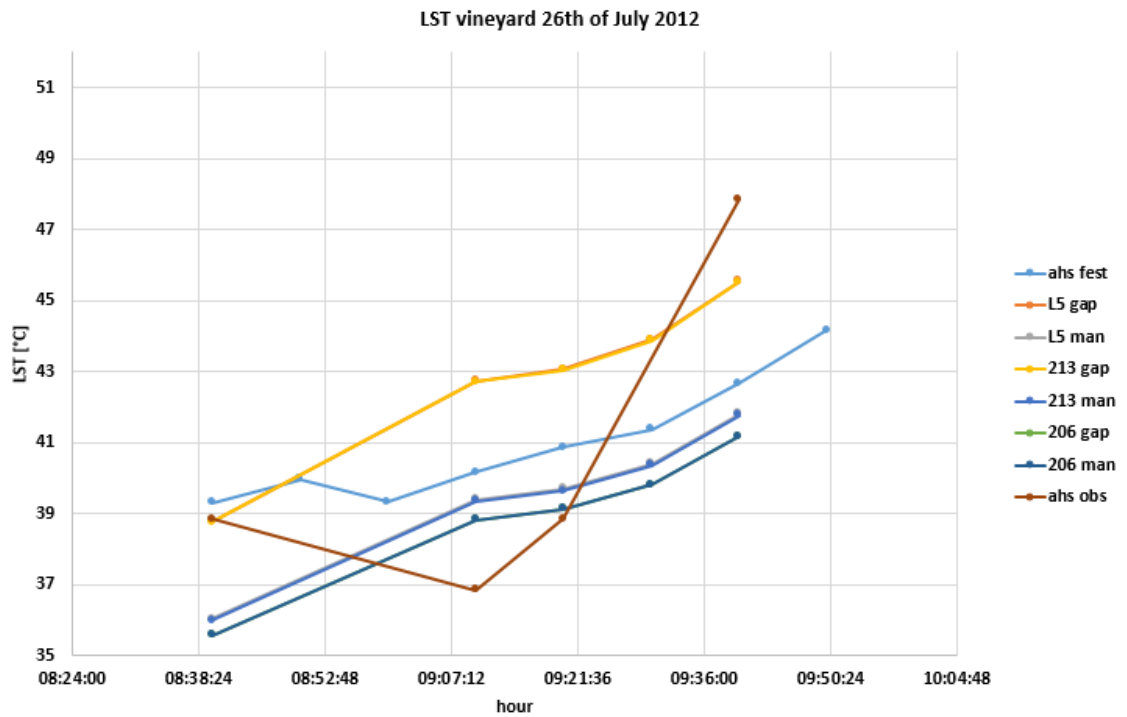
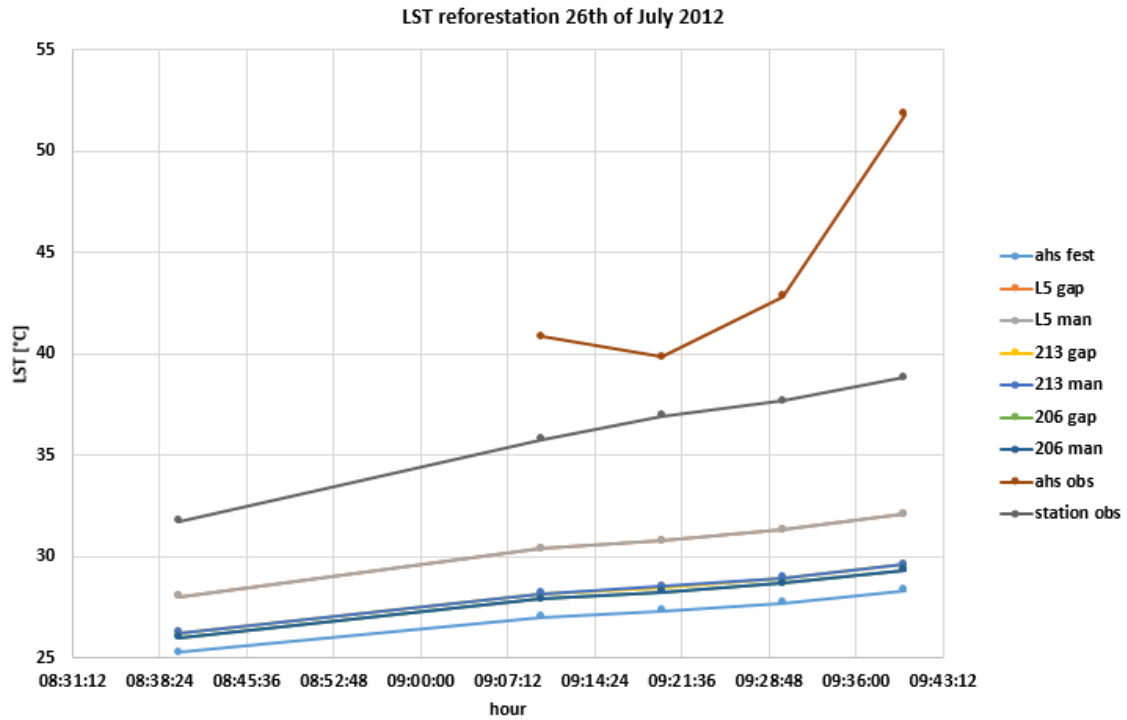


FIGURE 119. AHS-SIMULATIONS PUNCTUAL COMPARISON ON 25<sup>TH</sup> AND 26<sup>TH</sup> OF JULY

It is possible to notice that in the plotted graphs, often is not possible to see all the series, this is because the configuration Gapfill and Likelihood are overlaid each other.

## 6.4 ROOT MEAN SQUARE ERROR (RMSE)

RMSE is a measure of the differences between values predicted by a model and the values observed. The RMSE serves to aggregate the magnitudes of the errors in predictions for various times into a single measure of predictive power. The RMSE is used, in this case, to estimate the error committed and committable by the simulations of the model. All the input parameters are dimensionless.

$$RMSE = \sqrt{E(\hat{\theta} - \theta)^2}$$

Where  $\hat{\theta}$  represents the simulated/estimated data,  $\theta$  is the observed and E is the operator mean.

### 6.4.1 RMSE INPUT

The following tables describe, for each station (R, C, V), the RSME committed by each simulation about each input parameter, referred to the AHS sample values supposed without errors.

<b>R</b>	<b>L5 GAP</b>	<b>L5 MAN</b>	<b>213 GAP</b>	<b>213 MAN</b>	<b>206 GAP</b>	<b>206 MAN</b>
<b>LAI</b>	0.03	0.03	0.18	0.16	0.02	0.11
<b>FVC</b>	0.01	0.01	0.09	0.09	0.01	0.08
<b>Albedo</b>	0.00	0.00	0.00	0.00	0.00	0.04

<b>V</b>	<b>L5 GAP</b>	<b>L5 MAN</b>	<b>213 GAP</b>	<b>213 MAN</b>	<b>206 GAP</b>	<b>206 MAN</b>
<b>LAI</b>	0.21	0.21	0.17	0.42	0.37	0.37
<b>FVC</b>	0.08	0.08	0.07	0.20	0.16	0.20
<b>Albedo</b>	0.00	0.00	0.00	0.00	0.10	0.03

<b>C</b>	<b>L5 GAP</b>	<b>L5 MAN</b>	<b>213 GAP</b>	<b>213 MAN</b>	<b>206 GAP</b>	<b>206 MAN</b>
<b>LAI</b>	0.04	0.04	0.09	0.19	0.05	0.19
<b>FVC</b>	0.02	0.02	0.05	0.09	0.02	0.09
<b>Albedo</b>	0.03	0.03	0.03	0.03	0.05	0.02

The highest values are detectable in the LAI measurements in the vineyard stations, but in the other measurements the differences are few.



### 6.4.2 RMSE OUTPUT

The following tables describe, for each station (R, C, V), the RSME committed by each simulation about each input parameter, referred to the sample values observed by the stations supposed without errors. The RSME obtained is the mean of the RSMEs of all the comparable data over the entire simulation period.

<b>R</b>	<b>L5 GAP</b>	<b>L5 MAN</b>	<b>AHS</b>	<b>213 GAP</b>	<b>213 MAN</b>	<b>206 GAP</b>	<b>206 MAN</b>
<b>RMSE (le) W/m2</b>	12.97	12.99	13.10	13.77	13.84	13.84	13.31
<b>RMSE (h) W/m2</b>	48.84	48.84	48.80	47.39	47.33	47.33	46.83
<b>RMSE (g) W/m2</b>	17.70	17.70	18.03	18.79	18.86	18.86	17.23
<b>RMSE (LST) °C</b>	3.02	3.02	3.08	3.21	3.22	3.22	2.95

<b>V</b>	<b>L5 GAP</b>	<b>L5 MAN</b>	<b>AHS</b>	<b>213 GAP</b>	<b>213 MAN</b>	<b>206 GAP</b>	<b>206 MAN</b>
<b>RMSE (le) W/m2</b>	26.60	26.83	26.52	26.19	25.97	25.95	25.98
<b>RMSE (h) W/m2</b>	66.35	66.35	61.57	58.08	49.99	50.04	47.39
<b>RMSE (g) W/m2</b>	48.99	48.99	47.58	46.07	43.38	43.54	44.27

<b>C</b>	<b>L5 GAP</b>	<b>L5 MAN</b>	<b>AHS</b>	<b>213 GAP</b>	<b>213 MAN</b>	<b>206 GAP</b>	<b>206 MAN</b>
<b>RMSE (le) W/m2</b>	90.88	90.68	91.05	90.93	90.84	90.84	91.27
<b>RMSE (h) W/m2</b>	115.19	115.19	111.83	115.02	114.80	114.80	114.80
<b>RMSE (g) W/m2</b>	152.21	152.21	153.67	152.06	152.02	152.02	154.55
<b>RMSE (LST) °C</b>	3.79	3.53	3.53	3.81	3.82	3.38	3.82

In output the highest values of RMSE are present in camelina station where the ground heat flux reaches 154.55 W/m<sup>2</sup> of RMSE. The difference among the Likelihood and Gapfill configuration, on a mean analysis on the entire time period are few, it is impossible to say which one works better, but the differences on punctual data are notable on LST output mapped comparisons in 6.3 subchapter, where Likelihood configuration demonstrate to be better than Gapfill, and the mean difference about those dates among these two configurations is 0.5-1 °C, the higher values are all coming from Gapfill configuration. It is almost the same for *le*, the difference are not strong in the maps, where the stripes seems smoothed, and the difference among Gapfill and Likelihood is 2-3 W/m<sup>2</sup>, the higher values are all coming from Gapfill configuration. Gapfill high mean values are contaminated by the stripes, which contains the highest values.

## CONCLUSIONS

In this thesis, we have analyzed a large amount of satellites data of Landsat 7 and Landsat 8. The analyses done clarify how is actually preferable working with Landsat 8, due to the failure of Landsat 7 SLC, which affects the measures and often it makes impossible working on comparisons with punctual analysis data collected *in situ*, because is not possible to know which part of the images won't be retrieved from the sensor: the black stripes always change their position. Nevertheless, about the analyzed pixels, there's no difference among the performances of the two satellites, the quality of data is very good in both the satellites for LST, albedo, FVC, LAI data. How it is possible to notice from the graphics and from the low values of the errors in the comparison with in field campaigns, the algorithms used play a great role in the analyses and the obtained results are excellent. The Foggia surrounding territory, often presents cloudy images during the winter months, in fact the analyzed imageries in those periods are few, but thanks to the combination Landsat 7 and Landsat 8, the processable images since 2014 can be more.

The land use classification works well, especially if supported by good detailed land use maps for specific period of time. The best training ROIs, are those which have few spectral dispersion and that are composed by a great number of pixels, allowing, in this way, a good classification. In order to optimize the classification, it is necessary to provide any type of spectrum present in the area, without forgetting water, bare soil and urban (bare soil and urban have similar spectra, due to the high reflectance).

Promising results are obtained by the hydrological model FEST-EWB. The simulations show that is possible to work with Landsat 7 corrected images, and that those images can be utilizable in input and validation of the model. Moreover, the RSME of Gapfill input and Likelihood input is almost the same, in output the differences are not strong; in the same way, it is possible to say that the combinations using Landsat 5 are good as well. It is difficult to choose which simulation worked better, the differences among the configurations used are minimal. For future uses, Landsat 7 and Landsat 8 retrieved images can be really helpful in calibration and validation of hydrological models, on field studies, to individuate water stress and analyse the health of the plants and recognize and classify the different spectra of the areas.

## BIBLIOGRAPHY

- A. Beck, G. P. Anderson, P. K. Acharya, J. H. Chetwynd, L. S. Bernstein, E. P. Shettle, M. W. Matthew, and S. M. Adler-Golden, *MODTRAN4 User's Manual*. Hanscom AFB, MA, USA: Air Force Res. Lab., 1999.
- al, Corbari et. “Intercomparison of Surface Energy Fluxes Estimates from the FEST-EWB and TSEB Models over the Heterogeneous REFLEX 2012 Site (Barrax, Spain).” 2012.
- Ana ANDREU, Wim J. TIMMERMANS, Drazen SKOKOVIC and Maria P. GONZALEZ-DUGO. 2015.
- C. Latorre, F. Camacho, F. de la Cruz, R. Lacaze, M. Weiss, F. Baret. *Seasonal monitoring of FAPAR over the Barrax cropland site in Spain, in support of the validation of PROBA-V products at 333 m.* . 2014.
- Chiara Corbari, Giovanni Ravazzani and Marco Mancini. “A distributed thermodynamic model for energy and mass balance computation: FEST–EWB.” 2011.
- Corbari C, Ravazzani G, Martinelli J, Mancini M. “Elevation based correction of snow coverage retrieved from satellite images to improve model calibration.” *Hydrology and Earth System Sciences*, 2009.
- Corbari, Josè A. Sobrino, Marco Mancini & Victoria Hidalgo. “Mass and energy flux estimates at different spatial resolutions in a heterogeneous area through a distributed energy–water balance model and remote-sensing data.” 2012.
- CORBARI, TIMMERMANS, ANDREU. “Intercomparison of Surface Energy Fluxes Estimates from the FEST-EWB and TSEB Models over the Heterogeneous REFLEX 2012 Site (Barrax, Spain).” *Acta Geophysica*, 2015.
- Google. <https://www.google.it/maps>. .
- <http://consorzio.fg.it/>. <http://consorzio.fg.it/>. .

<http://www.harrisgeospatial.com>.

ITAP. <http://www.itap.es/>

J. C. Jiménez-Muñoz, J. Cristóbal, J. A. Sobrino, G. Sòria, M. Ninyerola, X. Pons.  
*Revision of the single-channel algorithm for land surface*. IEEE Trans.Geosci.  
Remote Sens., Jan. 2009.

Jiménez-Muñoz, José Sobrino. “Land surface temperature derived from airborne  
hyperspectral scanner thermal infrared data.” 2006.

Juan C. Jiménez-Muñoz, José A. Sobrino \*, Cristian Mattar, Belen  
Franchez-Muñoz, José A. Sobrino \*, Cristian Mattar, Belen Franch.  
*Atmospheric correction of optical imagery from MODIS and Reanalysis*.  
Valencia, Spain, 2010.

Juan C. Jiménez-Muñoz, José A. Sobrino, Leonardo Paolini. *Land surface temperature  
retrieval from LANDSAT TM 5*. 2004.

Muhammad Ali, Carsten Montzka , Anja Stadler, Gunter Menz, Frank Thonfeld, and  
Harry Vereecken. *Estimation and Validation of RapidEye-Based Time-Series of  
Leaf Area Index for Winter Wheat in the Rur Catchment* . Bonn, Germany:  
Clement Atzberger and Prasad S. Thenkabail , 2015 .

NASA. <http://atmcorr.gsfc.nasa.gov/>. <http://atmcorr.gsfc.nasa.gov/>.

Rabuffetti D, Ravazzani G, Corbari C, Mancini M. “Verification of operational  
Quantitative Discharge Forecast (QDF) for a regional warning system.” *Natural  
Hazards and Earth System Sciences*, 2008.

T.N. Carlson, G. Petropoulos, M.J. Wooster and S. Islam. *A review of Ts/VI remote  
sensing based methods for the retrieval of land surface energy fluxes and soil  
surface moisture* . 2009.

USGS. <http://earthexplorer.usgs.gov/> .

USGS. [http://landsat.usgs.gov/Landsat8\\_Using\\_Product.php](http://landsat.usgs.gov/Landsat8_Using_Product.php).

Wikipedia. <https://it.wikipedia.org>.

Yinghai Ke, Jungho Im<sup>2</sup>, Seonyoung Park and Huili Gong. *Downscaling of MODIS One Kilometer Evapotranspiration Using Landsat-8 Data and Machine Learning Approaches*. Richard Gloaguen and Prasad S. Thenkabail, 2016 .

## ACKNOWLEDGMENTS

This thesis is the result and conclusion of five years of significant learning, during which I got to learn a lot from teachers and classmates, from the academic point of view and not.

First of all, I would like to thank the engineer Corbari who coached me, assisted, supported and guided in the work and in the writing of this paper with professionalism, patience and dedication. Thanks prof.

And thanks to my supervisor, Marco Mancini.

I also thank Professor Sobrino and his team, who welcomed me warmly in Valencia; particularly thanks to Drazen, who, from the first moment, treated me like a friend, helping me in learning the skills necessary to kick off this thesis, and also the Spanish language, with long conversations on the way to Barrax: I think I've ever thanked properly, this looks like a good occasion to do it: gracias de todo corazón.

A huge thank you to my family, which allowed me to start and continue the studies that I loved, always supporting me. I will never stop to thank you.

Thanks to old friends, on whom I can always trust, and thanks to Ariel Jr friends. A hug to all my classmates, thank you for every smile you gave me, thank you for gave me the pleasure of dining with you, thanks for the pats on the back after a rejection, thanks for having celebrated with me after a successful, thanks for supported me, thank you for having had the patience to study and prepare for an exam with me, to explain something when I did not understand, thanks to you I have reached this goal, after a journey that has seen, above all, two constants, two true teammates called Igor and Federico, who have provided me the assist for this victory, so far the most important victory of my life, our victory.

Were five wonderful years, thank you.

## RINGRAZIAMENTI

Questo lavoro è frutto e conclusione di 5 significativi anni di apprendimento, durante i quali ho avuto modo di imparare moltissimo da egregi professori e compagni di corso, dal punto di vista accademico e non.

In primis, vorrei ringraziare l'ingegner Corbari che mi ha istruito, assistito, supportato e guidato nel lavoro e nella stesura di questo elaborato con professionalità, pazienza e dedizione. Grazie Prof. Così come ringrazio il professor Mancini, per avermi dato l'opportunità di poter svolgere un elaborato di tesi in questo affascinante ambito scientifico. Ringrazio inoltre caldamente il professor Sobrino e il suo team, che mi hanno accolto calorosamente a Valencia, in particolar modo grazie a Drazen, che fin dal primo momento mi ha trattato come un amico, aiutandomi nell'apprendimento delle nozioni necessarie per dare il via a questo elaborato, e della lingua spagnola, con le lunghe chiacchierate in viaggio verso Barrax: penso di non avervi mai ringraziato a dovere, questa mi sembra l'occasione giusta, *gracias de todo corazón*.

Un immenso grazie alla mia famiglia, che mi ha permesso di intraprendere e proseguire gli studi che in questi anni mi hanno appassionato, senza farmi mai mancare nulla, assecondandomi nelle scelte e correggendomi quando necessario, sostenendomi in tutto e per tutto. Non finirò mai di ringraziarvi.

Grazie agli amici di sempre, quelli veri, su cui posso contare in ogni momento, quelli che anche se non li vedi per mesi, quando li ritrovi sembra siano passati solo un paio di giorni dall'ultima volta. Grazie agli amici di Ariel Jr, le risate con voi sono state un vero e proprio antistress scacciapensieri anche in periodo esami.

Infine, cadendo nel mai banale *last but not least*, un abbraccio a tutti i miei compagni di corso e ai colleghi tesisti, mia seconda famiglia degli ultimi mesi in questo ateneo; grazie per aver avuto la pazienza di studiare e preparare un esame con me, di spiegarmi e rispiegarmi qualcosa quando non la capivo, grazie per le pacche sulle spalle dopo una bocciatura, grazie per aver gioito con me dopo un successo, grazie per avermi regalato il piacere di pranzare insieme a voi, grazie per avermi supportato e sopportato, grazie per ogni sorriso che mi avete strappato, grazie le risate che mi avete rubato.

Grazie a tutti voi ho raggiunto questo traguardo, dopo un percorso che ha visto, sopra tutte, 2 costanti, 2 veri compagni di squadra di nome Igor e Federico, che mi hanno fornito l'assist per questo goal, finora il più importante della mia vita, un goal che sa di vittoria. Una vittoria nostra, e sarei un bugiardo se la rivendicassi solo mia. Grazie ragazzi, grazie mille.

Grazie a tutti coloro che mi hanno regalato un sorriso. Sono stati 5 anni meravigliosi.

Grazie.